

1. Report No. CR 179513	2. Government Accession No.	3. Recipient's Catalog No.	
4. Title and Subtitle FURTHER DEVELOPMENT OF THE DYNAMIC GAS TEMPERATURE MEASUREMENT SYSTEM Volume I — Technical Efforts		5. Report Date August 1986	
		6. Performing Organization Code	
7. Author(s) D. L. Elmore, W. W. Robinson, and W. B. Watkins		8. Performing Organization Report No. P&W/GPD FR-19381	
		10. Work Unit No.	
9. Performing Organization Name and Address Pratt & Whitney Government Products Division P. O. Box 109600, West Palm Beach, FL 33410-9600		11. Contract or Grant No. NAS3-24228	
		13. Type of Report and Period Covered Draft Final Report	
12. Sponsoring Agency Name and Address National Aeronautics and Space Administration NASA-Lewis Research Center Cleveland, Ohio 44135		14. Sponsoring Agency Code	
		15. Supplementary Notes Project Manager, G. C. Fralick, Instrumentation and Fluid Mechanics Division, NASA-Lewis Research Center, Cleveland, Ohio 44135	
16. Abstract A compensated dynamic gas temperature thermocouple measurement method was experimentally verified. Dynamic gas temperature signals from a flow passing through a chopped-wheel signal generator and an atmospheric pressure laboratory burner were measured by the dynamic temperature sensor and other fast-response sensors. Compensated data from dynamic temperature sensor thermoelements were compared with fast-response sensors. Results from the two experiments are presented as time-dependent waveforms and spectral plots. Comparisons between compensated dynamic temperature sensor spectra and a commercially available optical fiber thermometer compensated spectra were made for the atmospheric burner experiment. Increases in precision of the measurement method require optimization of several factors, and directions for further work are identified.			
17. Key Words (Suggested by Author(s))		18. Distribution Statement Unclassified - unlimited	
19. Security Classif. (of this report) Unclassified	20. Security Classif. (of this page) Unclassified	21. No. of Pages 153	22. Price*

*For sale by the National Technical Information Service, Springfield, Virginia 22161

FOREWORD

During identification and evaluation of the concepts for experimental verification of the dynamic gas temperature sensors, assistance and consultation was provided by Dr. Robert Moffat, a recognized authority in temperature measurements. Dr. R. R. Dils of Accufiber, Inc. provided valuable information on the operation and characteristics of the optical fiber thermometer.

PRECEDING PAGE BLANK NOT FILMED

TABLE OF CONTENTS

<i>Section</i>	<i>Page</i>
SUMMARY	1
INTRODUCTION	2
TECHNICAL DISCUSSION	4
Task 1a — Identification of Methods	4
Task 1b — Analysis and Selection of Methods	14
Task 1d — Fabrication, Testing, and Analysis	19
Task 1e — Additional Data Analysis	97
Task II — Reduction of Execution Time of the Dynamic Gas Temperature Measurement Data Reduction Package	125
Task III — Reprogramming of Dynamic Gas Temperature Measurement System Data Package into FORTRAN IV	138
Task IV — Data Acquisition	142
DISCUSSION OF RESULTS	143
Rotating Wheel Experiment	143
Subscale Combustor Experiment	143
Computer Programming Efforts	144
Recommendations	144
CONCLUSIONS	146
LIST OF SYMBOLS	147
REFERENCES	150
BIBLIOGRAPHY	151

PRECEDING PAGE BLANK NOT FILMED

SUMMARY

The objectives of this contract were to experimentally verify the accuracy of the dynamic gas temperature measurement system, and to optimize the compensation software for execution speed by reprogramming into FORTRAN IV. This work represents a continuation of the technical work performed under contract NAS3-23154, Dynamic Gas Temperature Measurement System (Reference 1). Objectives of the previous contract were to develop a high frequency-response gas temperature measurement system for use in a gas turbine combustor.

Task I involved experimental verification of the dynamic gas temperature measurement system, including identification of experiments, analysis and selection of two experiments, hardware fabrication, testing and data analysis. A rotating wheel experiment which alternately directed hot and cold gas streams onto the sensors was specified by the contract. The second experiment used an atmospheric pressure burner. Dynamic temperature sensors were designed for each experiment. Reference sensors used were compensated fine-wire resistance thermometers. In addition, an optical fiber thermometer was evaluated for dynamic response in the burner test. In the rotating wheel test, it was found that the compensated dynamic temperature sensor amplitude at 250 Hz was 23 percent lower than the compensated fine-wire resistance thermometer. Peak-to-peak (p-p) temperature variation of this test point was 154K (277°F). In the burner test, it was found that compensated dynamic temperature sensor amplitudes of the frequency components varied between 18 and 48 percent higher than compensated fine-wire resistance thermometer. The burner, however, is a broadband source and relative differences (48 percent, for instance) are small in absolute magnitude (48 percent of 10 rms K/ $\sqrt{\text{Hz}}$, i.e., 4.8 rms K/ $\sqrt{\text{Hz}}$). The compensated optical fiber thermometer read between 30 percent lower and 200 percent higher than the compensated dynamic temperature sensor over the 4 Hz to 1 kHz bandwidth. As with the previous comparison, however, relative differences are small in absolute magnitude because of the broadband character of the source.

Tasks II and III involved reprogramming of the dynamic temperature sensor compensation software into FORTRAN IV and streamlining the code for minimal execution time. The software was written under Contract NAS3-23154, and was implemented in Hewlett Packard (HP) 5451C Fourier Analyzer for efficiency of the Fourier routines in the development process. Execution times were approximately one hour per case. In the present effort, all software has been implemented on an IBM computer, and execution time has been demonstrated to be less than four minutes per case.

The remaining tasks involved on-site assistance at NASA with transferring software and experimental data acquisition briefings and reports.

INTRODUCTION

Increases in durability and performance of gas turbine engines require detailed knowledge of component operating environments. This is especially true in the engine hot section, where temperatures and heat fluxes imposed by the high temperature, high pressure combustor exhaust gases require substantial cooling of turbine blades and vanes. Condition of combustor exit flows can be highly turbulent with wide excursions in temperature at frequencies extending into the kHz regime. These conditions can have a significant impact on heat transfer rates to the turbine components and have established the need for dynamic gas temperature measurements at high frequencies. However, the environment is especially severe for measurement probes used for development purposes, requiring rugged sensors and structural designs adequate for steady state and vibratory loads at operational temperatures without compromise to sensor response and accuracy.

The objectives of this work were to: 1) experimentally verify a dynamic gas temperature measurement system in laboratory experiments, and 2) to reprogram compensation software into FORTRAN IV and optimize for execution speed. In previous work (Reference 1), a measurement system was developed for gas turbine combustor exhausts, with special emphasis placed on dynamic response to enable determination of fluctuating components. The measurement probes were demonstrated to have greater than one hour life in a jet engine combustor, and very long (greater than 5 hours) life in an atmospheric burner. Under the current program, the measurement and compensation methods were verified by comparing the results obtained by the compensated dynamic sensors with those of fine-wire resistance thermometers of intrinsically high frequency response.

Two sources of dynamic temperature signals were used. The first was a rotating wheel which alternately introduced hot and cold air to the sensors. At a constant rotation rate, this signal generator output approximated a square wave, narrowband frequency source. The second was an atmospheric pressure laboratory burner which had been used in the previous development effort. Dynamic signal content was broadband and relatively low amplitude.

The technical effort was organized into four major tasks with Task I further subdivided into five subtasks.

Task I: Frequency Response Experiment Verification

- Task Ia: Identification of Methods
- Task Ib: Analysis and Selection of Methods
- Task Ic: Review
- Task Id: Fabrication, Testing, and Analysis
- Task Ie: Additional Data Analysis

Task II: Reduction of Execution Time of the Dynamic Gas Temperature Measurement System Data Reduction Package

Task III: Reprogramming of Dynamic Gas Temperature Measurement System Data Package into FORTRAN IV

Task IV: Data Acquisition

Task I accomplished the frequency response experimental verification including screening and selection of experimental methods, fabrication, testing, and analysis of the data. Tasks II and III were concerned with refinement of the data compensation software by reducing execution

time and reprogramming the software into FORTRAN IV for execution on generally available computers. Task IV was a level-of-effort on-site technical assistance task to be provided at NASA.

TECHNICAL DISCUSSION

Task 1a — Identification of Methods

Summary. — Candidate concepts for generating known dynamic temperature signals were identified through surveys of technical literature and consultation with recognized experts in the field of temperature measurement. These concepts defined different types of experiments that could be used to evaluate the frequency response of the dynamic gas temperature measurement system of Reference 1. The experiments identified fall into two general categories: the first involves using an atmospheric pressure laboratory-scale combustor, and the second involves using any number of mechanical techniques for generating periodic or step-impulse signals.

Concept Identification. — Literature surveys were performed using the NASA Recon, Lockheed Dialog, and Defense Technical Information Center computerized survey systems to identify candidate experimental techniques. In attempts to minimize duplication and identify new information, literature surveys listed in NASA Report CR-16827 (Reference 1) were used as a starting point, and keyword combinations were modified for the current surveys. In addition, Dr. Robert Moffat of Stanford University was consulted for potential experimental methods. In addition to the references used in the NASA report, 36 additional sources were identified. These are listed in the Bibliography.

Methods identified fall into two general categories. The first category uses an atmospheric pressure combustor of approximately 454 gm/sec (1 lbm/sec) flowrate. In this combustor, as in the gas turbine combustor, turbulent entrainment of ambient temperature air into the combustion stream produces the dynamic temperature signal. Velocity fluctuations about the mean have been previously shown (Reference 2) to be weakly (less than 10 percent) correlated with temperature fluctuations. The laboratory burner or combustor concepts (shown in Figure 1) include the following:

- **Impulse Actuated Two-Wire Probe** — Two gas streams would be established having the desired high and low temperature. The probe would be moved from one to the other stream by a mechanical actuator. A small fine wire or other temperature standard would be used with the two-wire probe. It is recognized that it would be difficult to attain the required 250 Hz frequency response due to the actuator speed limitations.
- **Two-Wire Probe and Aspirating Hot Film Probe** — In this concept, the natural frequency fluctuations of the laboratory burner would be the only source of fluctuations. A reference probe of high frequency response, such as an aspirating probe (Thermo-Systems, Inc. (TSI) Model 1735) (Figure 2) would be used as the standard measurement of the gas temperature fluctuations. The referenced TSI probe has a frequency response of up to 100 kHz and is capable of operation at 3500°C (6330°F), 152 meters per second (500 feet per second), and 1 atmosphere. However, the accuracy of this probe would be limited due to conduction errors from the water cooler probe housing.
- **Two-Wire Probe and Anemometer Probe** — In this concept, the temperature standard would be a hot wire anemometer probe replacing the previously discussed aspirating hot film probe. The anemometer would be a high temperature probe such as a TSI Series A4 probe (Figure 3) operated as a constant current resistance thermometer.

- **Three-Wire Probe** — In this concept, again the natural frequency fluctuations occurring in the combustor would be the source. An additional third thermocouple element would be added to the two-wire probe. This thermocouple element would provide additional verification by compensating data in three combinations: very small-small, very small-large, and small-large. Previous test experience (Reference 1) suggests that very small wires (25 μm or less) will survive for many minutes in this environment.
- **Oscillating Splitter Plate and Two-Wire Probe** — This concept is similar to the previously described test where a splitter plate having two different temperature gas streams is used in the combustor. However, instead of moving the probe from the cold to the hot stream, the splitter plate would be oscillated mechanically to divert the streams over a stationary probe assembly and temperature standard. The principal difficulties in this concept are in making certain that the flow stays attached to both faces of the splitter plate and in the complex mechanical system required.

The second category of verification experiments involves hardware configurations which use air as the working fluid and which suggest an obvious temperature variation. The configurations are as follows:

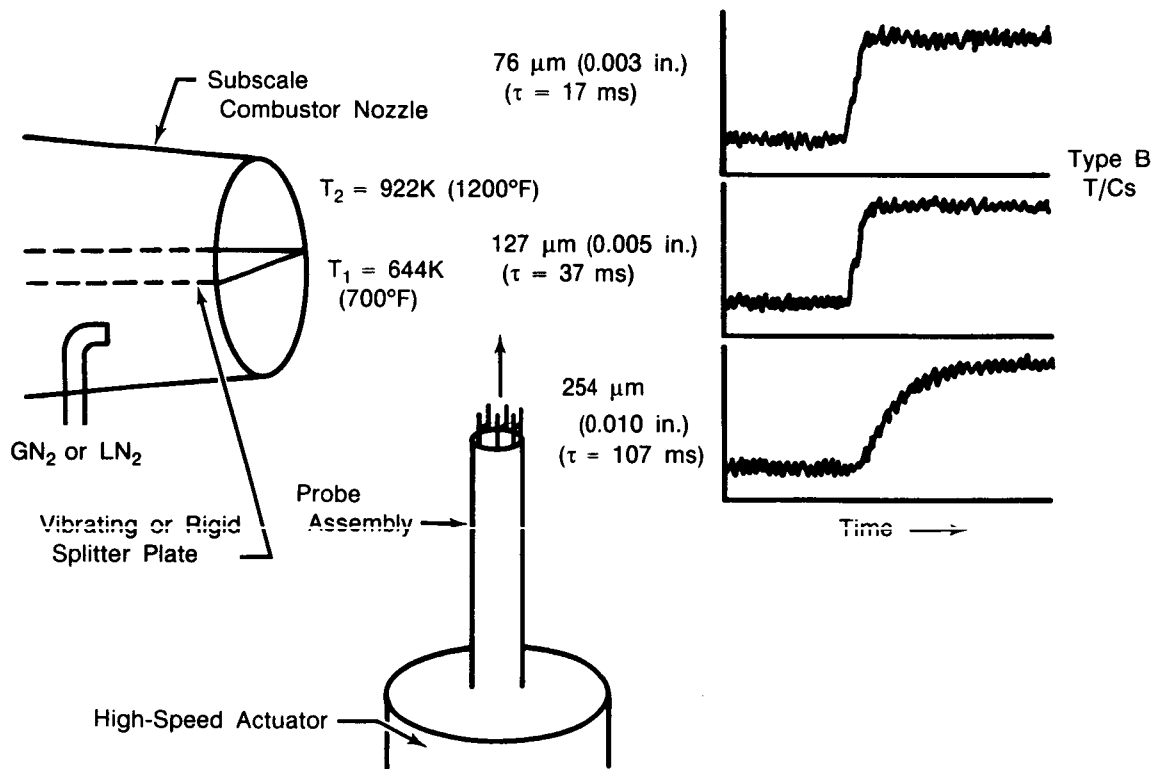
- **Rotating Wheel** — The original rotating wheel experiment has been tested at Pratt & Whitney, as shown in Figure 4. It consists of two rotating wheels having circles of holes which turn the hot and cold airflows on and off. The hole patterns are phased to alternately heat and cool the test probe which is positioned between the wheels. Phasing of the two-hole patterns suggests a temperature variation. For example, if the holes in pattern A are out of phase with the holes in pattern B, an approximate square-wave temperature variation will result as the wheels are rotated. The primary frequency is the number of holes in one pattern multiplied by the rotation rate. Peak-to-peak variation in temperature is the difference in stream temperatures. Figure 5 presents typical test data for the temperature and velocity profiles generated using the original rotating wheel apparatus.
- **Modified Rotating Wheels** — One of the drawbacks to the previously described rotating wheel is that the streams flow in opposite directions. Based on recommendations from Dr. Robert Moffat, the rotating wheel experiment was modified (Figure 6) to use a collector/transition duct which blends the two gas streams through a single nozzle at the probe. Using a screen in the transition duct and proper design of the phasing of the holes should make it possible to achieve a nearly sinusoidal temperature waveform, which is preferred.
- **Blowdown Tube** — This concept (Figure 7) would use a burst diaphragm and a capacitive heater to provide a step input. The disadvantages to this system are: (1) problems with probe damage due to particles from the burst diaphragm, and (2) inaccuracy resulting from not generating a sharp instantaneous step function.
- **Pulsatile Pressure System** — This system, shown in Figure 8, consists of a flow channel with two orifices. The first orifice is operated critically so the flow is constant. The second orifice would be periodically occluded by a rotating disk valve which would cause the pressure in the volume between

the orifices to fluctuate. Isentropic compression results in temperature fluctuations. The primary disadvantage is the large variations in flow required to produce the temperature fluctuations.

- **Piston in Cylinder** — This system, shown in Figure 9, again uses two orifices but uses a piston to compress the gas between the orifices and thus obtain a temperature fluctuation. This system still has a flow variation. However, it is smaller than the pulsatile system.
- **Sprinkler Head** — This concept, shown in Figure 10, consists of a wheel made from two halves containing milled passages. The passages are curved so that the air flow will provide the momentum to rotate the assembly. The passages would also be canted slightly in the axial direction so that the flow from each stream would impinge on the test probe located near the wheel. This configuration has the advantage of providing temperature fluctuations with a relatively uniform and constant velocity. The primary disadvantages would be associated with the large amount of air required and the complexity of designing the rotating seals and bearings.
- **Fluidic Oscillator** — This concept, shown in Figure 11, is based on a modification of a fluidic switch to oscillate two streams (hot and cold). Switching of the two flow streams (hot and cold) would be achieved by alternately applying pressure pulses to the control ports. The pressure pulses could be supplied by a rotating valve assembly. The probe would be positioned in the area shown in Figure 11.

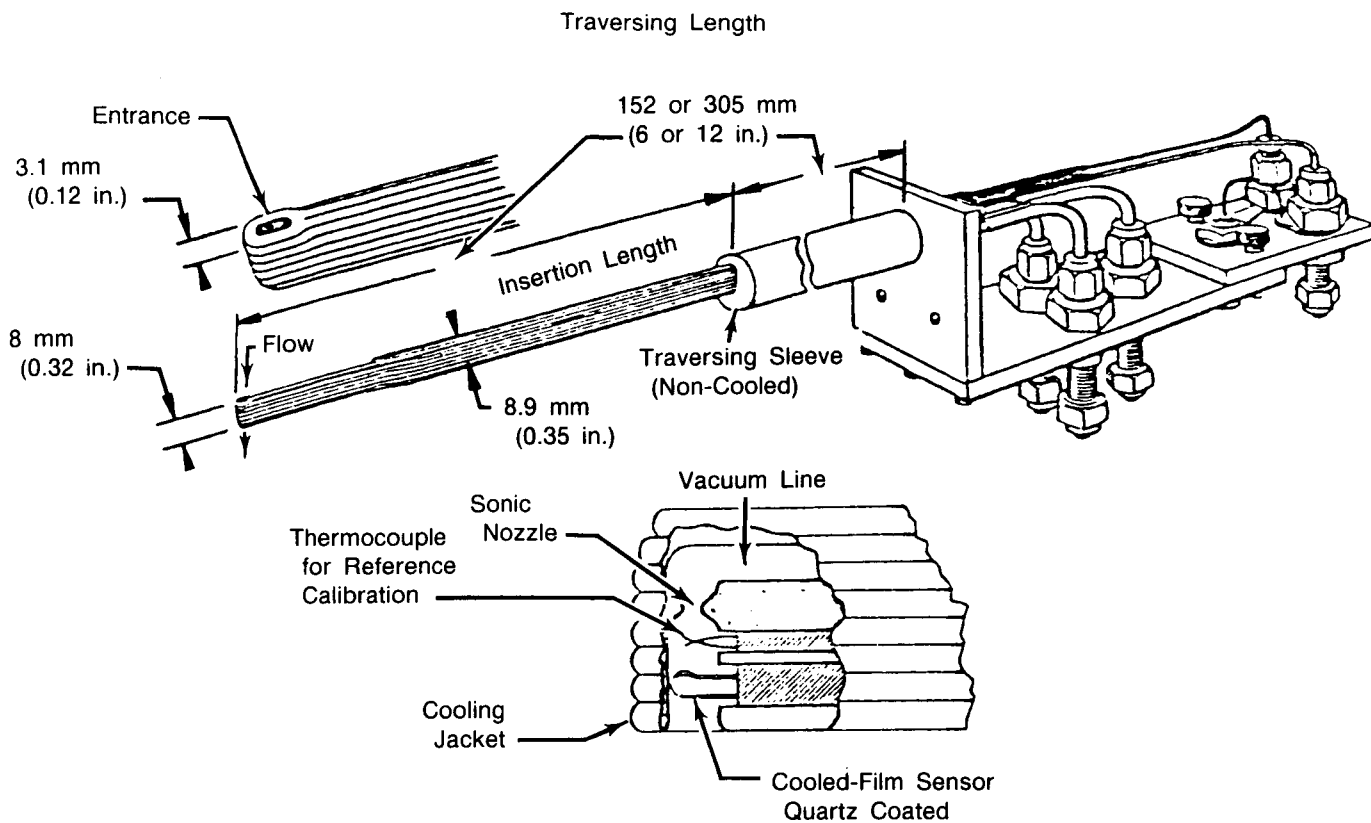
This principal difficulty with the above methods concerns the degree of correlation between velocity fluctuations and temperature fluctuations, and consequent applicability of the compensation method.

- Impulse Actuated 2-Wire Probe and Anemometer Probe
- 2-Wire Probe and TSI Aspirating Probe
- 2-Wire Probe and Anemometer Probe
- 3-Wire Probe and Anemometer Probe (Dual Data Compensation)
- Oscillating Splitter and 2-Wire Probe



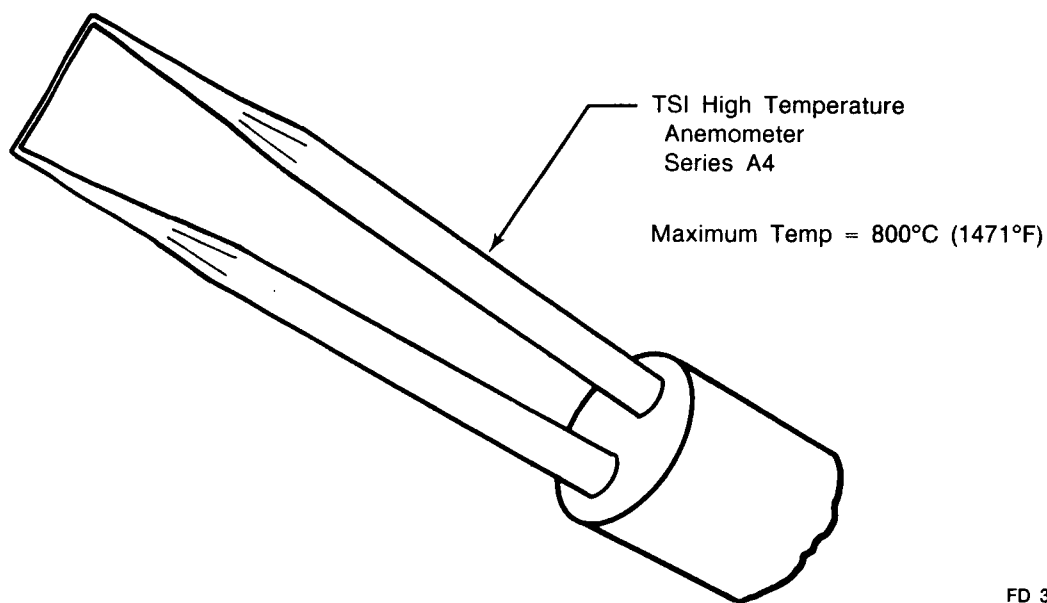
FD 312788

Figure 1. Laboratory Burner Concepts



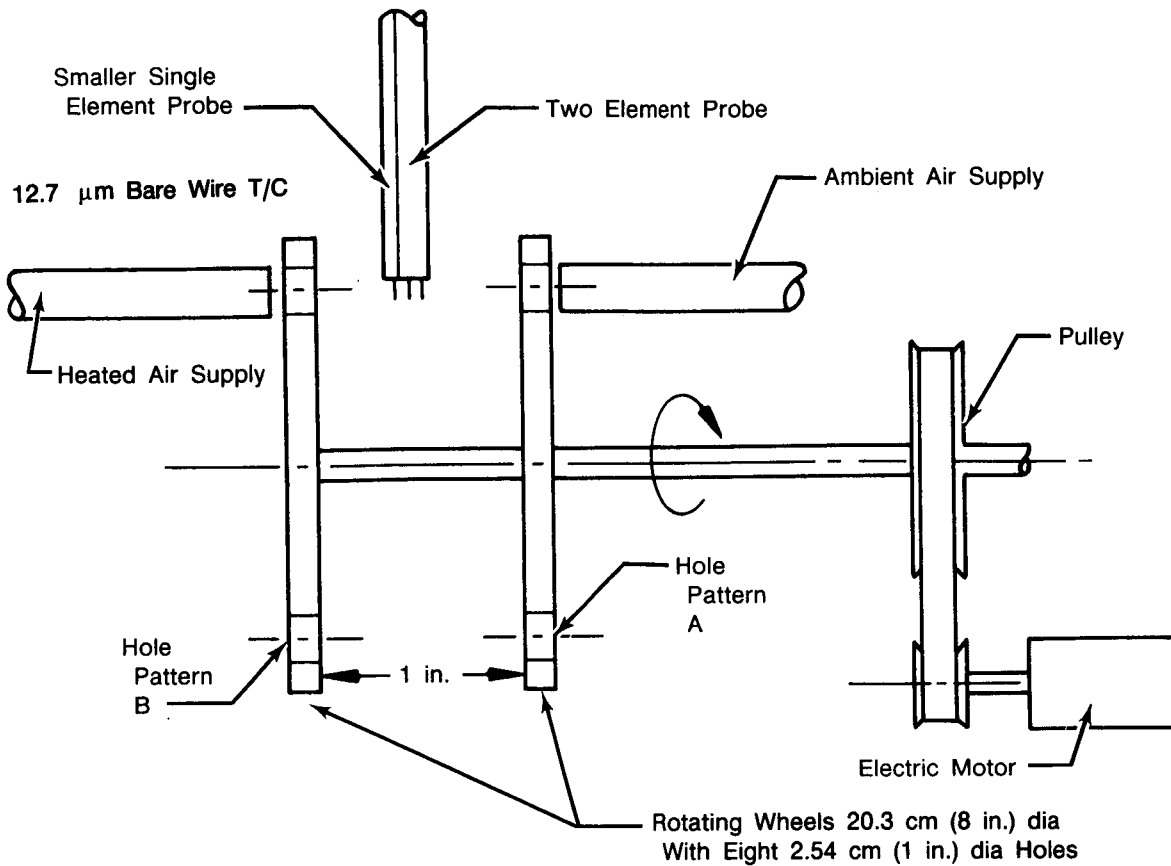
FD 312789

Figure 2. TSI Aspirating Probe



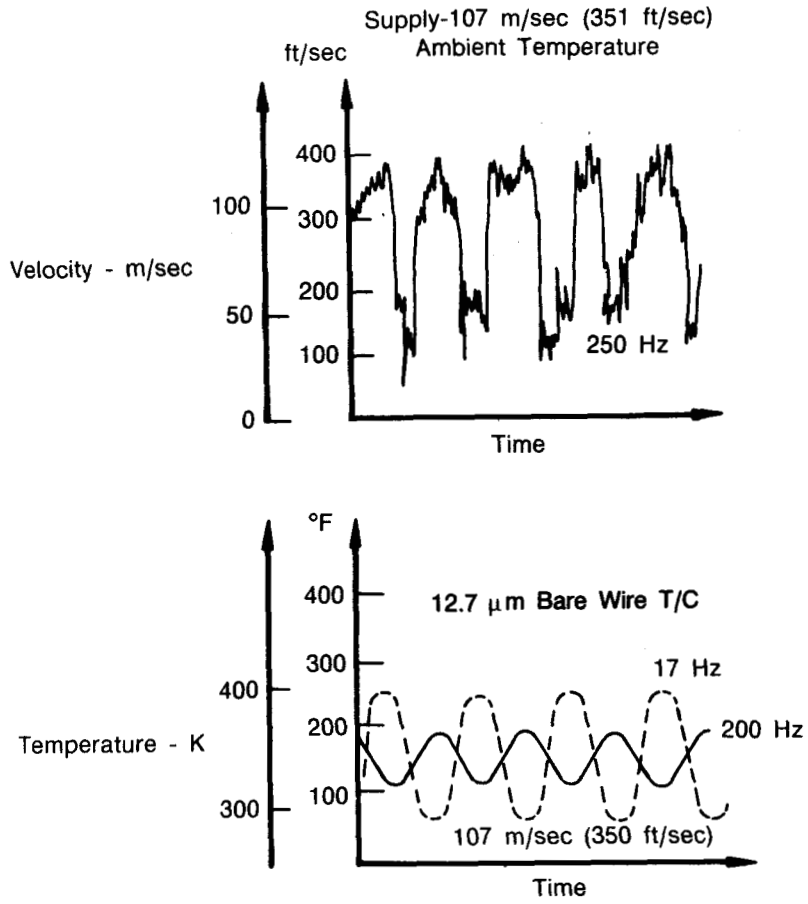
FD 312790

Figure 3. High Temperature Anemometer (Resistance Thermometer) Probe



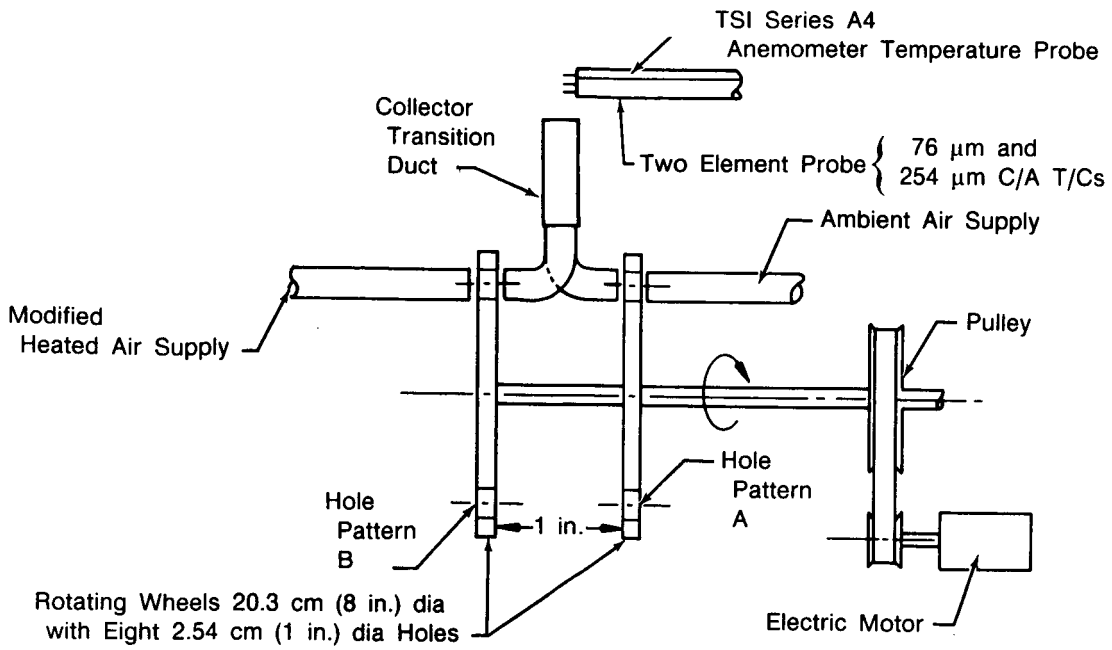
FD 312791

Figure 4. Existing Rotating Wheel Schematic



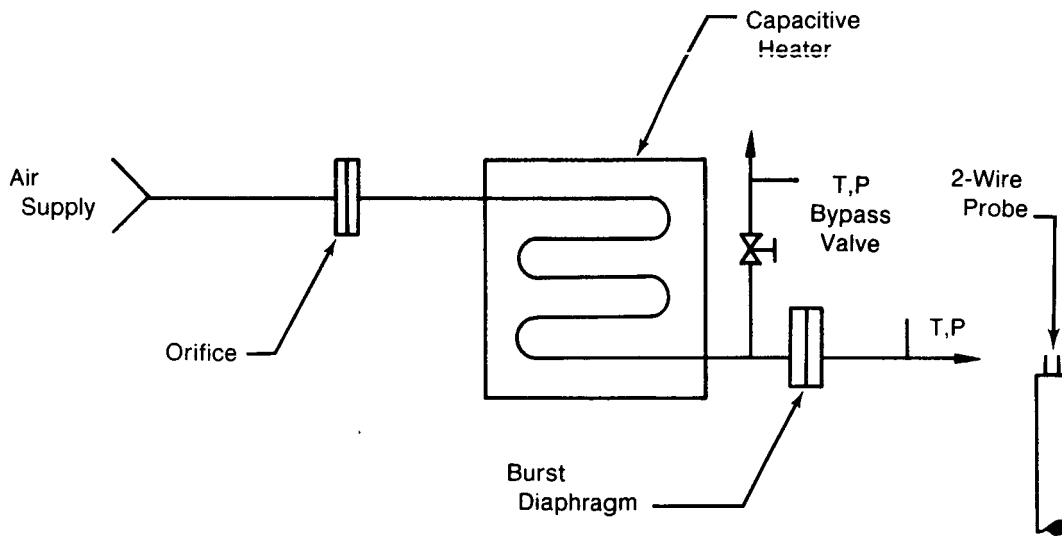
FD 312792

Figure 5. Typical Rotating Wheel Test Data



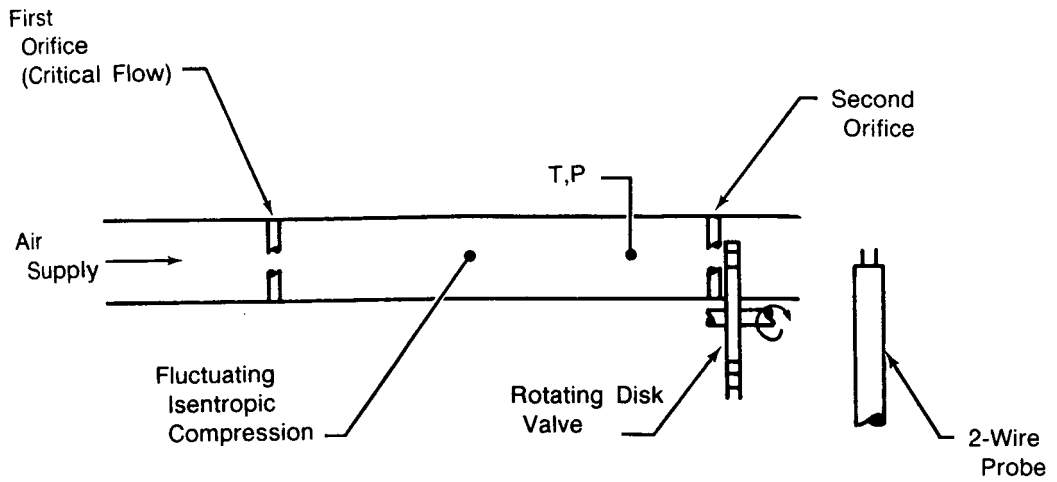
FD 312793

Figure 6. Modified Rotating Wheel Schematic



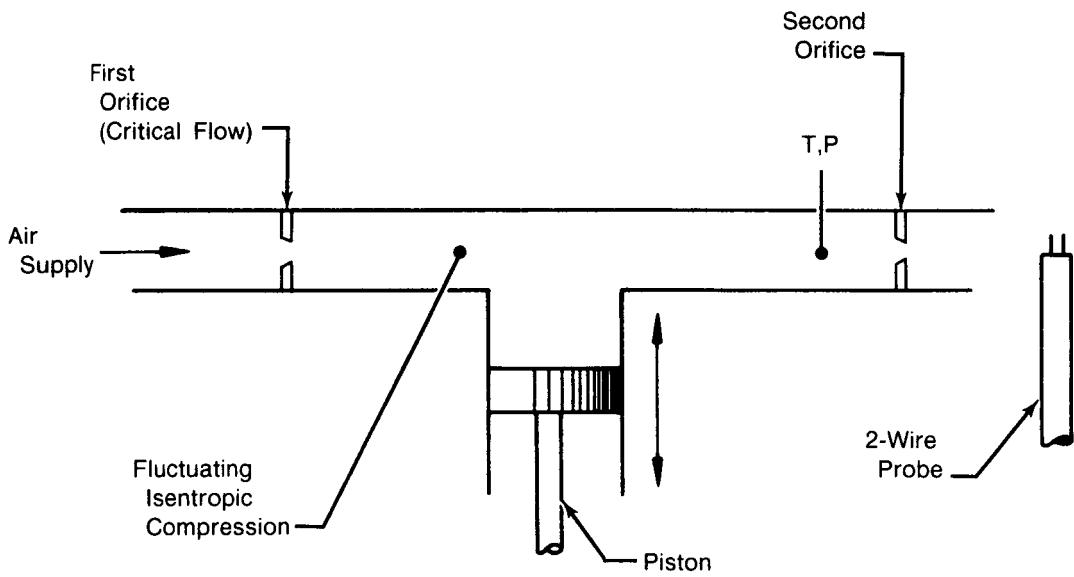
FD 312794

Figure 7. Blowdown Tube Concept



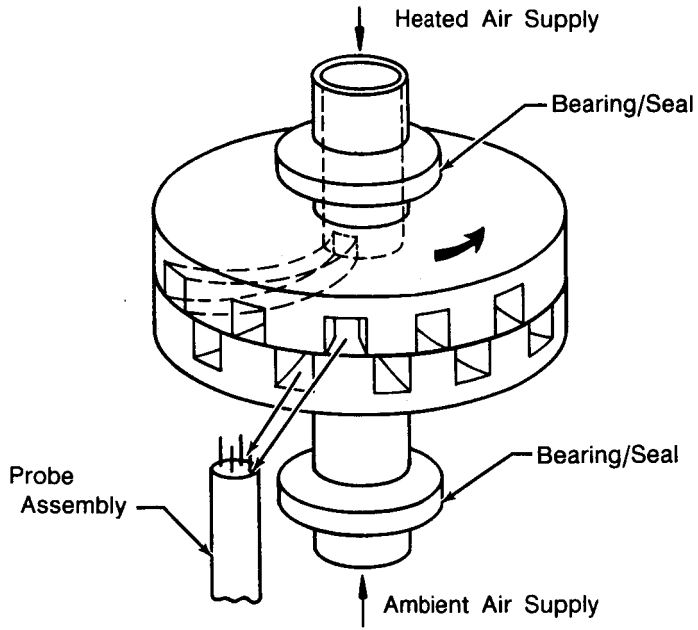
FD 312795

Figure 8. Pulsatile Pressure System Concept



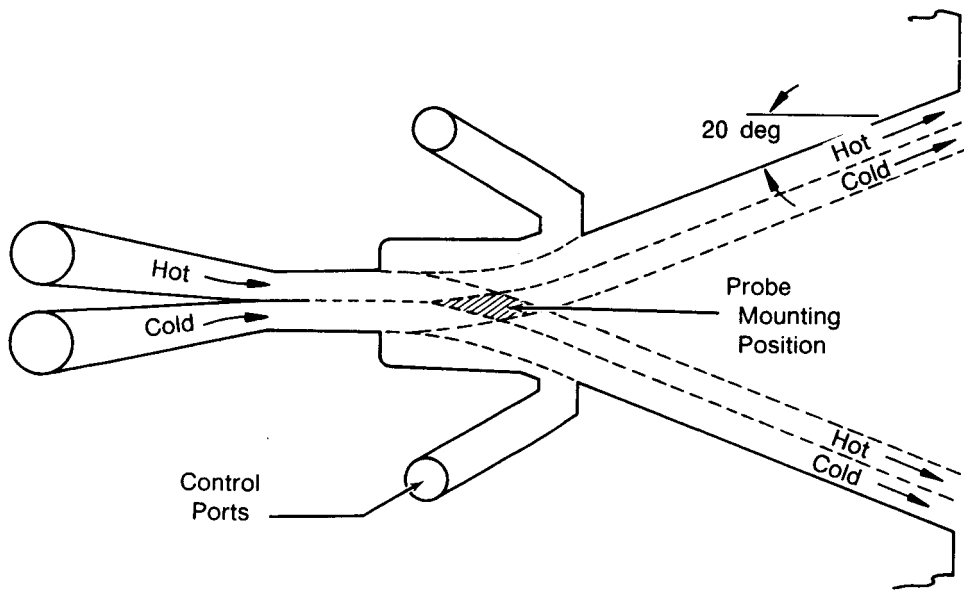
FD 312796

Figure 9. Piston in Cylinder Concept



FD 312797

Figure 10. Sprinkler Head Concept



FD 312798

Figure 11. Fluidic Oscillator Concept

Task 1b — Analysis and Selection of Methods

Summary. — The concepts identified in Task 1a were analyzed and reviewed for frequency content, temperature fluctuation amplitude, pressure, velocity, and relative cost. Mechanical, structural, thermal, and data acquisitive/reduction analyses were conducted as required. Each concept was then ranked for the previously mentioned criteria and the final selections were made. The first experiment selected corresponds to the contract statement of work (SOW) requirement for a rotating wheel concept. The rotating wheel, which alternately supplies hot and cold streams, was designed and was based on modifying an existing apparatus. The second experiment selected used an atmospheric burner to test a three-wire probe with dual-data compensation. Both experiments were conducted using a commercially available TSI model anemometer probe operating as a resistance thermometer as a gas temperature measurement standard.

Concept Evaluation and Selection. — The concepts identified in Task 1a were reviewed in terms of meeting the following experimental test conditions specified in the contract SOW:

- Frequency Response: 250 Hz (minimum)
- Temperature fluctuations: 278K (500°F) peak-to-peak (minimum)
- Pressure: Atmospheric or greater
- Flow Rate: Mach 0.1 (minimum)
- Gas Composition: Air acceptable.

Mechanical, thermal, and data acquisition/reduction analyses were conducted where necessary. All concepts were ranked and selections made as summarized in Table 1. The first test selected, as specified in the SOW, is the rotating wheel concept. Based on recommendations from Dr. Moffat, the existing rotating wheel experiment was modified. The second experiment selected was the laboratory burner rig test using a three-wire probe with dual-data compensation and the use of a TSI anemometer probe as a gas temperature standard. A brief discussion of each concept, the analyses performed, and the final ranking is presented in the following paragraphs.

The modified rotating wheel experiment (Figure 6) incorporates a transition duct that allows turning and directing the alternating flows at the test probe. It is also based on modifying the heated air supply to increase its output to obtain the required 278K (500°F) temperature fluctuations. The two sensors designed for these tests are shown in Figure 12. They are based on using 76 μm (0.003 inch) and 254 μm (0.010 inch) diameter Chromel-Alumel thermocouple wire material. This material was required to achieve a large enough output at the lower temperatures of this test. A structural analysis performed on the wires included evaluating stresses due to air loading and vibration and indicated high safety margins.

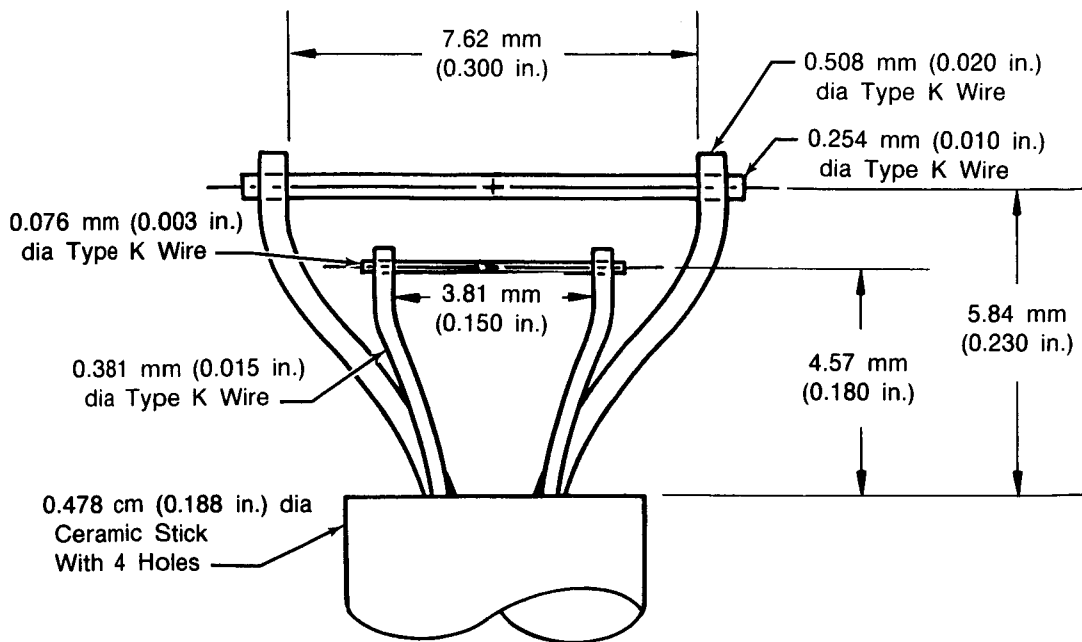
These tests would also be conducted using a TSI high temperature anemometer probe for a gas temperature measurement standard. This probe (shown in Figure 3) would be operated as a resistance thermometer (constant current). A structural and thermal analysis showed that the probe would survive the temperature and velocities and the first order frequency response would be approximately 406 Hz which would provide to accurate measurements (less than 1 percent error) up to 100 Hz. It was also planned to extend the sensors response by using an inverse function RC element circuit (Figure 13). The anemometer resistance element was also analyzed for conduction errors to the support wires for the rotating wheel conditions of:

Sinusoidal Temperature Fluctuations = 278K (500°F) p-p
Velocity = 76.2 m/sec (250 ft/sec)
Frequency = 250 Hz.

TABLE 1. — RANKING SELECTION

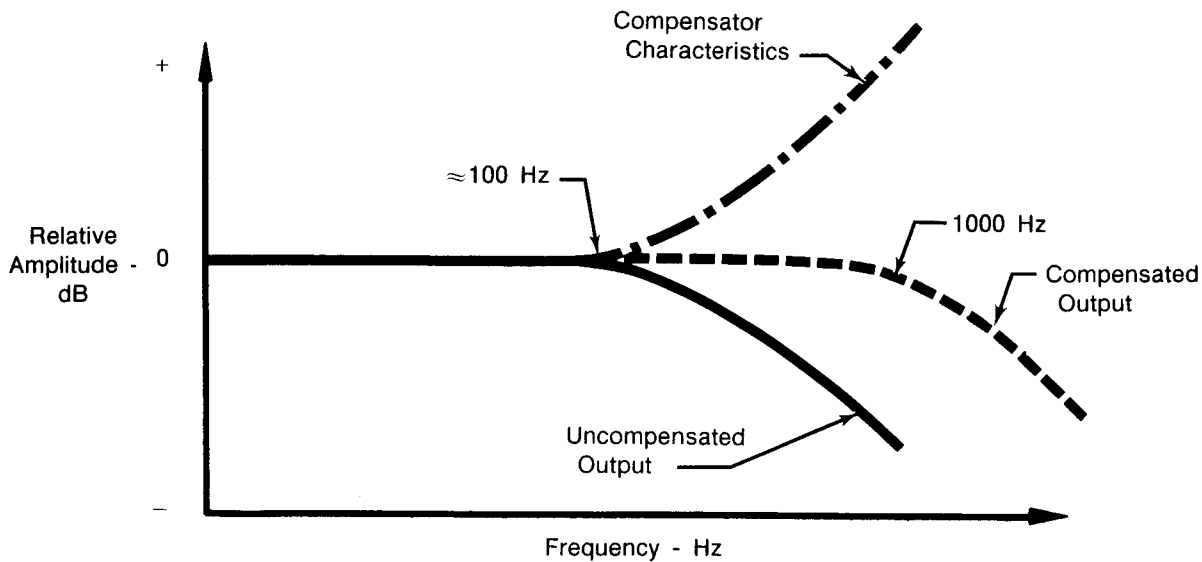
Concept	Known Frequency Content > 250 Hz	Temperature Fluctuations > 500°F	Pressure P-P ≥ 1 ATM	Gas Velocity > 0.1 Mn.	Relative Cost (Fabricability/Operability)	Totals
Existing Rotating Wheel	4	4	4	2	4	18
*Modified Rotating Wheel	4	4	4	4	4	20
Lab Burner — Impulse Actuated 2-Wire Probe and Anemometer	1	3	4	4	4	16
Lab Burner — 2-Wire Probe and Anemometer Std	3	3	4	4	4	18
Lab Burner — 2-Wire Probe and Aspirating Probe Std	4	1	4	4	4	17
*Lab Burner — 3-Wire Probe and Anemometer Std	4	3	4	4	4	19
Oscillating Splitter	3	3	4	2	1	13
Blowdown Tube	1	3	4	3	2	13
Pulsatile System	3	3	2	1	1	10
Piston in Cylinder	3	3	2	2	1	11
Laser Heating	2	3	3	4	2	14
Sprinkler Head	4	4	4	3	1	16
Fluidic Oscillator	3	2	4	3	2	14
Legend						
4 — Superior						
3 — Good						
2 — Average						
1 — Below average						
0 — Inferior						
*Final selections						

6745C



FD 312799

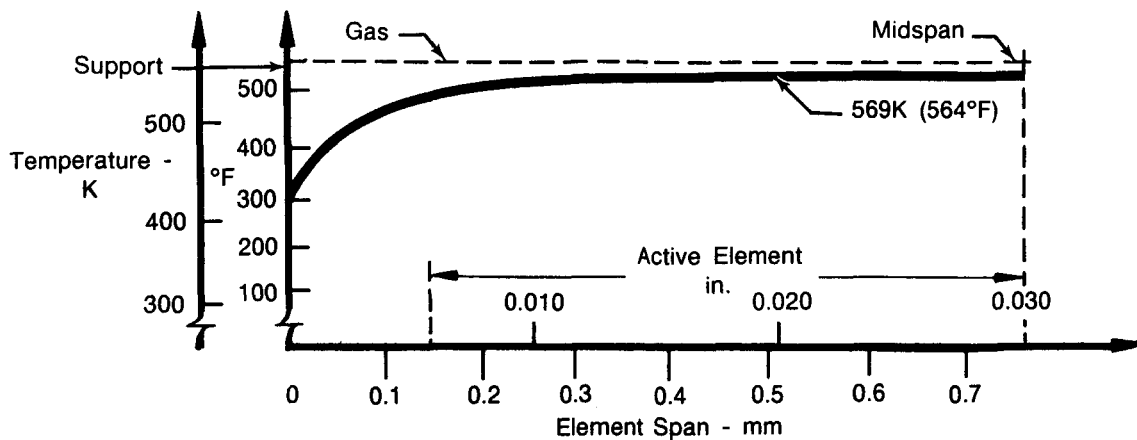
Figure 12. Rotating Wheel Two-Wire Thermocouple Proposed Geometry



FD 312800

Figure 13. Resistance Thermometer Temperature Probe Compensation

The predicted temperature profile for the resistance element is shown in Figure 14. An analysis of these profiles reveals that the maximum errors would occur at the peak temperature of the gas of 569K (564°F). The indicated temperature of the element would be 562K (552°F) or a maximum error of -7K (-12°F), which corresponds to about a 2.0 percent error which is negligible.



FD 312801

Figure 14. Resistance Thermometer Temperature Probe Predicted Conduction Errors

A TSI aspirating probe (shown in Figure 2) was also proposed as a temperature measurement standard since it is designed to operate at very high frequencies and temperatures. However, it has a water-cooled housing which would induce large conduction errors. A review of the delicate construction and specifications revealed this probe would be an expensive and operationally difficult probe to use.

The use of a linearly actuated probe between hot and cold streams, such as in the laboratory burner concept shown in Figure 1, was rated low due to its frequency limitations. Linear speeds required to achieve a sharp, well defined function would be very high. Actuation times of less than 1 millisecond (ms) were required and no commercially obtainable actuators could be found.

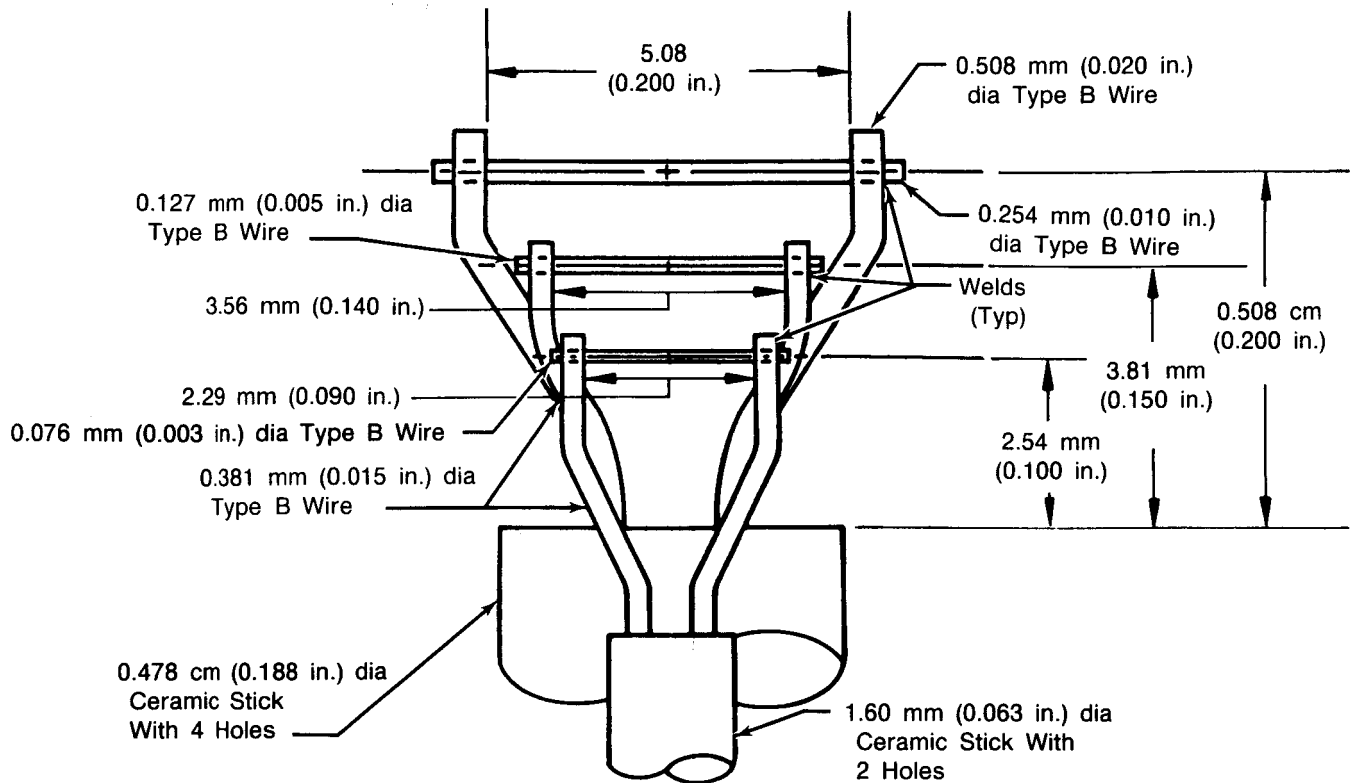
The atmospheric pressure laboratory burner (combustor experiment) was also proposed as a temperature source using existing temperature fluctuations generated by the combustion process. These fluctuations have been measured previously and are of the magnitude required for the test conditions (Reference 1). Concepts using a two- or three-wire test probe and a temperature standard probe (aspirating or anemometer) were considered. The three-wire probe ranked higher than the other concepts and was selected.

The three-wire concept uses three different size wires so that data compensation of different two-wire combinations would provide additional verification to the gas temperature measurement standard. The gas temperature standard was again the TSI high temperature anemometer operated as a resistance thermometer. Thermal and structural analyses of the TSI probe revealed it would be acceptable at the minimum operating conditions of the laboratory burner previously tested in Reference 1. These conditions are:

- Temperature = 1050K (1430°F)
- Pressure = 1 atmosphere
- Velocity = 104 meters per second (340 feet per second).

Based on a review of the data previously reported in Reference 1, the anticipated temperature fluctuations occurring at these conditions should be 278K (500°F) peak-to-peak. The predicted first order frequency response of the TSI probe was 493 Hz and would again require the use of an inverse function resistance-capacitance (RC) circuit to extend its response.

The geometry of the proposed three-wire probe is shown in Figure 15. A two-wire probe using 127 μm (0.005 inch) and 254 μm (0.010 inch) diameter elements would be constructed. The third element would be made up in a separate housing using a two-hole ceramic stick and would have a 76 μm (0.003 inch) diameter element. The wire would be Type B thermocouple material which was used previously in Reference 1. The sizes selected were based on a review of the laser butt weld limitations which necessitated limiting the smallest diameter to 76 μm . A review of previous analyses performed on the 76 μm /254 μm combinations reported in Reference 1 indicates acceptable accuracy over the reduced frequency range of 250 Hz. The remaining concepts shown in Table 1 ranked lower due to a variety of reasons.



FD 312802

Figure 15. Combustor Experiment Three-Wire Thermocouple Sensor Geometry

The oscillating splitter plate concept would use a mechanical actuated plate between the flow streams in a laboratory burner or similar device. The primary disadvantages are making certain the flows remain attached, the complex mechanical system, and the required mechanical speeds and resulting forces.

The blowdown tube in Figure 7 rated low on frequency content since it is hard to obtain a very fast step function that also would be stable during the time it was flowing. The mechanical problems associated with the impulse loading of the probe elements was also severe. The possibility of structural damage of the probe elements due to fragments from the burst diaphragm must also be considered.

The pulsatile pressure system (Figure 8) and the piston in a cylinder concept (Figure 9) both depend upon isentropic compression of air to produce the required temperature fluctuations. Both concepts, however, have flows which must have varying velocities along with the

temperature fluctuations. This introduces another unknown into the experiment. Dr. Moffat wrote computer programs to analyze both of these systems. The results indicated that the piston in a cylinder concept would produce smaller velocity fluctuations than the pulsatile system. However, both fluctuation magnitudes are unacceptable.

The sprinkler head concept, shown in Figure 10, provides uniform temperature fluctuations at a uniform and constant velocity. As previously stated, however, it would be a complicated and costly system to design and supply with heated air.

The fluidic oscillator is another concept that is promising for future applications. Mr. G. Fraclik at NASA-Lewis Research Center built and tested a model of the oscillator to demonstrate its capabilities. The results of these tests indicate the switching speed to be less than anticipated and additional design and testing would be required to meet the present frequency requirement.

Task 1d — Fabrication, Testing, and Analysis

Summary. — The designs for the rotating wheel and combustor (laboratory burner) experiments were completed and drawings for the test hardware were generated. The test hardware, including thermocouple probes, resistance thermometer (anemometer) probes, flow manifold, and miscellaneous hardware, was fabricated or procured. Each experiment was set up, checked out, and conducted successfully with the acquisition of dynamic temperature on frequency modulation (FM) tape. The data were then played back and digitized in a HP Fourier Analyzer to produce a digital tape. The data were processed on the IBM computer and program developed in Task III.

Overview of Data Acquisition and Processing. — During rig tests, data were collected on an FM magnetic tape recorder. These data were reproduced post-test in an off-line data processing center to produce a digital tape for input to a mainframe IBM computer. The data analysis routines were executed in the IBM computer.

Tables 2, 3, and 4 list specific equipment used in the data acquisition of the rotating wheel experiment, combustor experiment, and the post-test data playback and digitization process respectively. An IBM model 3090 computer system was used for execution of the data analysis routines. Figures 16 and 17 depict the test configurations for the dual thermocouple and resistance thermometer setups used on the rotating wheel and combustor experiments respectively. Figure 18 depicts the data acquisition setup for the high temperature optical fiber thermometer used on the subscale combustor experiment.

TABLE 2. — EQUIPMENT LIST FOR ROTATING WHEEL EXPERIMENT

<i>Item</i>	<i>Comments</i>
Precision Instrument Model 2114 FM Tape Recorder	IRIG FM intermediate band 30 ips 27 kHz center of frequency (CF); 1/2v rms and 1v rms full scale record amplifier settings
Encore Electronics Model 610 Strain Gage Amplifier	EMF mode; 5 kHz filter settings for dynamic signals and 10 Hz for dc signal
Thermo-Systems Inc. (TSI) Model 1053A Constant Temperature Anemometer with Model 1226 Sensors	Temperature mode, referred to as resistance thermometer throughout report
General Purpose Oscilloscope (Hewlett Packard Model 1200B)	For monitoring data and calibration signals
Hewlett Packard Model 3456A Digital Voltmeter	For use in system calibration (ac and dc)
Pratt & Whitney General Purpose Precision dc Voltage Source	For calibrating Encore amplifiers
Hewlett Packard Model 200CD Oscillator (or Equivalent)	For inputting ac calibration signals on FM tape recorder.

6745C

TABLE 3. — EQUIPMENT LIST FOR COMBUSTOR RIG EXPERIMENT

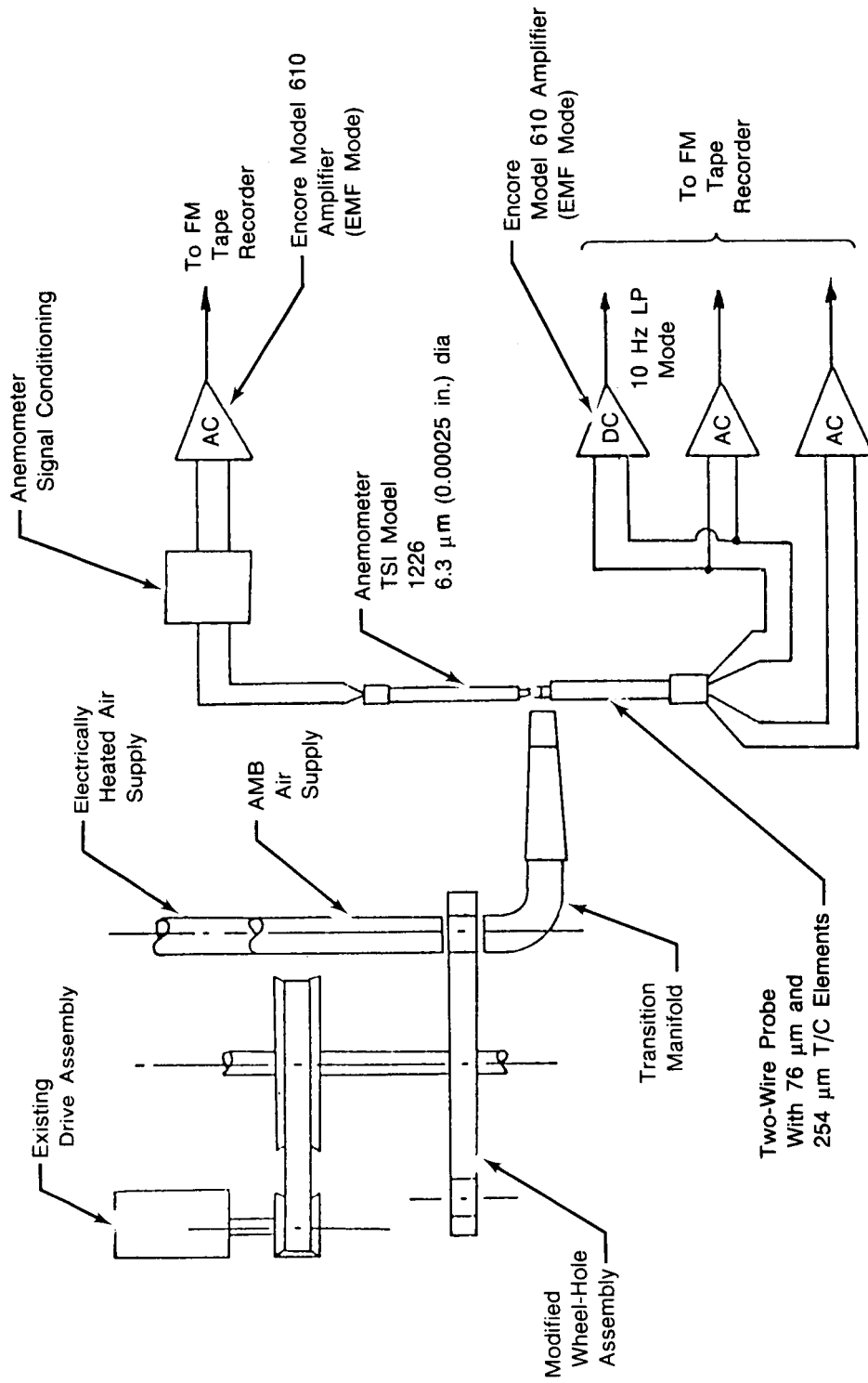
<i>Item</i>	<i>Comments</i>
Honeywell Model 101 FM Tape Recorder	IRIG FM medium band; 54 kHz CF, 30 ips; 1/2v and 1v rms full scale record amplifier settings
Encore Electronics Model 610 Strain Gage Amplifier	EMF mode; 5 kHz filter setting for dynamic signals and 10 Hz for dc signal
Thermo-Systems Inc. Model 1053 A Constant Temperature Anemometer with Model 1226 Sensor	Temperature mode
General Purpose Oscilloscope Hewlett Packard Model 1200 B	For monitoring data and calibration signals
Hewlett Packard Model 3456A Digital Voltmeter	For use in system calibration (ac and dc)
Moxon Inc. Model 3564 dc Power Supply with an External Voltage Attenuator Circuit	For calibrating Encore amplifiers
Wavetek Model 134 Function Generator	For inputting ac calibration signals on FM tape recording.

6745C

TABLE 4. — EQUIPMENT LIST FOR DATA PLAYBACK AND DIGITIZATION

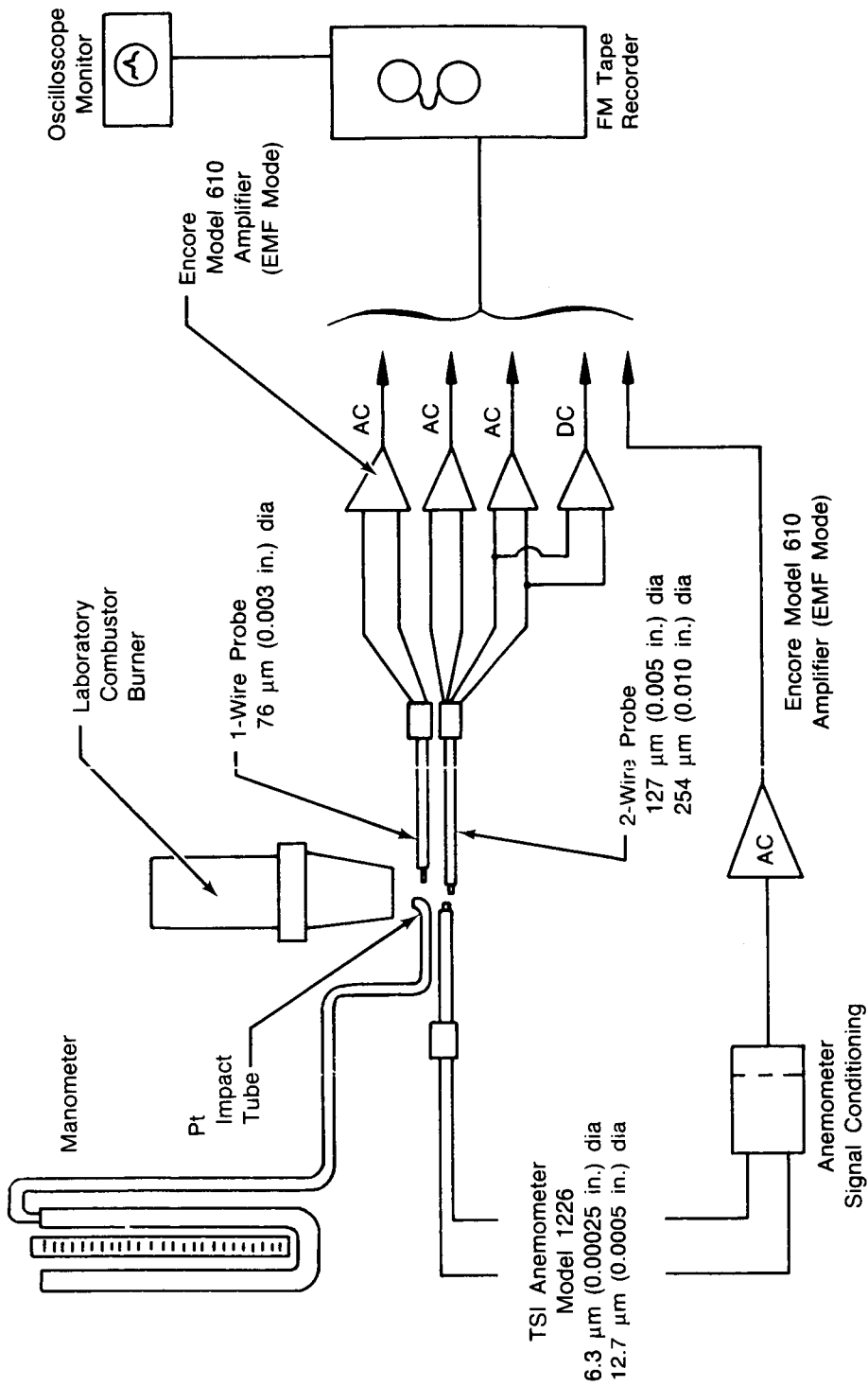
<i>Item</i>	<i>Comments</i>
Honeywell Model 96 Tape Transport with FM IRIG Reproduce Amplifier	Reproduce electronics set to match those used in data recording
Hewlett Packard Model 54440A Low Pass Multi-Pole Elliptical Anti-Aliasing Filters	Corner frequency set to 1250 Hz
Hewlett Packard Model 5451C Fourier Analyzer System with Model HP7970E 1600 characters per inch (cpi) Digital Magnetic Tape Recorder	12 bit ADC; set to 4096 Hz sampling rate; digital tape is ADC thruput file
Nonlinear Systems Series X-2 Digital Voltmeter	For calibration of reproduce system (gain and zero)
Rockland Model 1022F Low Pass Multipole Filter	Lowpass filter set to 0.2 Hz for additional filtering of 254 μ m thermocouple dc data
Pratt & Whitney Model E2657-1 Thermocouple Compensation Amplifier	For compensation of resistance thermometer data; time constants modified to match system tau at each specific test point
Hewlett Packard Model 1200B Oscilloscope	For general purpose signal monitoring

6745C



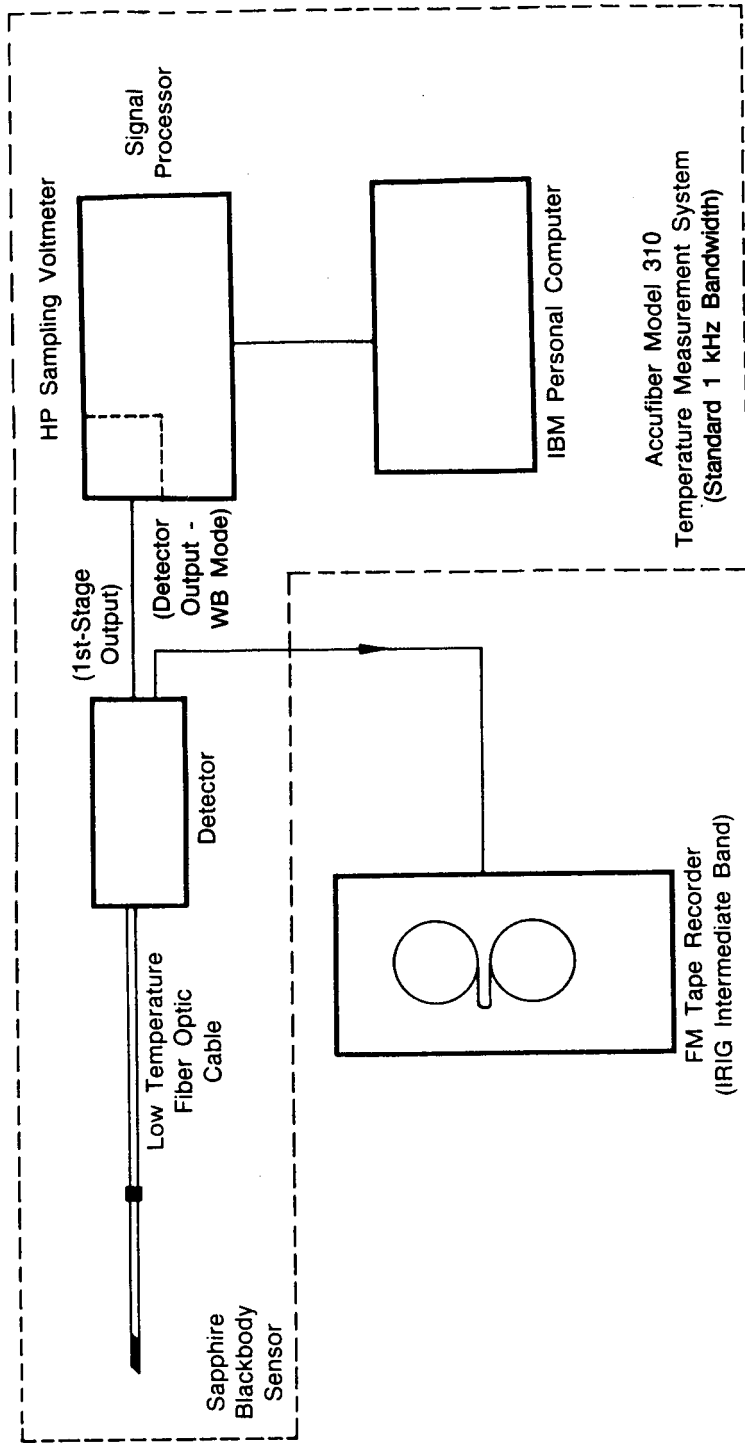
FD 312803

Figure 16. Rotating Wheel Experiment Test Schematic



FD 312804

Figure 17. Combustor Experiment Test Schematic



FD 312805

Figure 18. Optical Fiber Thermometer System Schematic for Combustor Experiment

FM magnetic tape recordings were made of the dynamic alternating current (ac) signals from the large and small thermocouple elements for the dual thermocouple probes and the direct current (dc) (low pass filtered) signal from the large thermocouple element. In the subscale combustor experiment where 76 μm (0.003 inch), 127 μm (0.005 inch), and 254 μm (0.010 inch) thermocouple elements were used, the dc signal from the 254 μm (0.010 inch) was used for measuring the mean gas path temperature. Only the dynamic portions of the resistance thermometer and the optical fiber thermometer signals were recorded on FM tape.

Data presented in this report were not corrected for radiation losses. It was shown in the original report (Reference 1) that radiation heat losses in the dynamic portion of the temperature waveform are insignificant under the worst-case environmental conditions of the original contract statement of work. If desired, mean temperature measurements can be corrected for radiation losses post-test in a conventional manner.

The first order frequency bandwidth of the FM magnetic tape recorders was dc to 10 kHz (-3 dB) minimum. The Encore amplifiers used for conditioning and extracting the dynamic signals from the data were operated in the ac coupled mode (-3 dB at about 5 Hz). The low pass multi-pole output filter on the Encore amplifiers were set to 5 kHz for the dynamic signals and 10 Hz for dc thermocouple signals.

The Encore amplifiers used for signal conditioning were operated in the "fixed" gain mode. Prior to test, each amplifier was calibrated (dc coupled mode) at various fixed gain settings using a laboratory working standard voltmeter and a precision dc calibration voltage source. During rig testing, the amplifier gains (fixed ranges) were set at each test point to provide optimum signal levels for FM tape recording. The specific gain settings were recorded and used to establish system calibration at each test point. Calibration signals applied directly to the FM tape recorder inputs were used to calibrate the FM tape reproduce system. Thermocouple data were converted from calibrated voltages to temperature using NBS calibration curve coefficients. The resistance thermometers were calibrated in an oven using a thermocouple to establish a linear voltage to temperature sensitivity factor. Rig test data were converted to temperature using the linear sensitivity factors. Optical fiber thermometer dynamic data were scaled using system gain settings and curve fits of sample black body look up tables provided by the manufacturer.

Data were digitized, three channels at a time, at a sampling rate of 4096 Hz per channel. Multiple pole elliptical anti-aliasing filters set at 1250 Hz (-3 dB) were used. The digitizers were dc coupled. Additional low pass filtering (4 pole Butterworth) was employed on the dc thermocouple to ensure that the digitized signal represented the mean temperature. The dc thermocouple signals were used in scaling the dynamic (ac) thermocouple signals as well as providing a measurement of the mean gas path temperature.

The dual thermocouple (Dynamic Gas Temperature Measurement System) data were processed using the software developed under previous NASA contract (Reference 1) and implemented in the mainframe IBM computer under the current contract. Processed data were typically presented in the frequency domain as log power spectral density (PSD) and/or narrowband frequency spectrum plots with and without frequency compensation. Additionally, some data were presented in linear power spectral density format. Instantaneous time records were also plotted with and without frequency compensation. Ensemble averaged compensated frequency domain plots were computed over the entire range of the frequency analysis (i.e., to one-half of the sampling frequency). All frequency domain data presented in this report are plotted over the full 2048 Hz bandwidth of the analysis. Data beyond 1000 Hz are attenuated by the anti-aliasing filters and are included only to provide insight into the system noise floors. Dynamic temperature time records were compensated over approximately 1250 Hz bandwidth via the "threshold" parameter in the data compensation software. The values were determined by operator examination of the uncompensated PSD plots. The threshold values used are specified on the data plots.

Plots are captioned by experiment, type of analysis, and test point. Additionally, some plots contain a "data point" designator. The data point designates the specific digitization session within the steady-state test point. Thus, plots of corresponding data points are precisely time correlated.

Following the test, an IRIG-time code signal was recorded over a spare track on the subscale combustor rig FM data tape. Attempts to record a post-test time code signal on the rotating wheel FM data tape were unsuccessful. The 76 μm (0.003 inch) thermocouple data were compared to the resistance thermometer, the 127 μm (0.005 inch) thermocouple, and the optical fiber thermometer. Precise time correlation was obtained by simultaneously digitizing each of these signals with the 76 μm (0.003 inch) thermocouple data in multiple sessions. Temporary utility software routines were written to scale and merge resistance thermometer and optical fiber thermometer data into the dual thermocouple data analysis routines in the mainframe IBM computer for processing, thus, ensuring commonality of many of the analysis routines.

Dual thermocouple data were compensated with the Dynamic Gas Temperature Measurement System software implemented on the IBM mainframe computer under the current contract. The compensation method is based on comparing measured and predicted responses of two different diameter thermocouples to the fluctuating gas temperature field in a finite differences model of the thermocouples to measure an aerodynamic parameter, Γ , containing the thermocouple time response. Thus, the time response of the thermocouple is measured in situ. The measured time response parameter is then used in the finite differences model to derive a compensation frequency response spectrum for data correction. The above process is executed digitally in the IBM computer and involves extensive use of Fast Fourier Transforms. All data compensation was done off-line, post-test. The aerodynamic parameter, Γ , is related to the time constant, τ , of a thermocouple by the expression:

$$\tau = \frac{D^{3/2}}{4\Gamma} \quad (1)$$

Where: D = Thermocouple element diameter.

The resistance thermometer data were compensated off-line, post-test using an existing in-house design analog compensation amplifier. The amplifier provided a first order inverse of the resistance thermometer frequency response function (gain and phase). The resistance thermometer corner frequency was determined by relating the first order thermal time constant of the sensor as a cylinder in cross flow, the probe geometry, and the probe material properties:

$$\tau = \frac{\rho_w C_{pw} D}{4h_g} = \frac{1}{2\pi f_c} \quad (2)$$

Thus, the time responses of the resistance thermometers were estimated, not measured. However, due to their inherently high response (the corner frequencies ranged from 195 to 508 Hz in these experiments) errors in the estimation of the corner frequencies were not as significant as any error in the measurement of the response of the dual thermocouple. Corner frequencies of the thermocouples were less than 13.5 Hz. Capacitive elements in the analog compensation amplifier were modified to obtain an amplification versus frequency characteristic shown in Figure 13, thereby extending the frequency response to greater than 1 kHz. The modified frequency response of the compensation amplifier was verified by measurement to be within ± 0.16 dB and ± 1.5 degrees phase of the desired response over the dc to 1 kHz bandwidth. The compensation amplifier contained a low pass single pole filter with a corner frequency of about 3 kHz to limit system noise.

Errors in temperature measurements were presented as percent of reading computed as:

$$\text{Error} = \left[\frac{\text{sensor A reading}}{\text{reference sensor reading}} \right] - 1 \times 100\% \quad (3)$$

For errors derived from log PSD plots, the ratio of sensor reading to the reference sensor reading (Equation 3) was computed as:

$$\frac{\text{sensor A reading}}{\text{reference sensor reading}} = \text{antilog}_{10} \left[\frac{\text{sensor A reading (dB)} - \text{reference sensor reading (dB)}}{20} \right] \quad (4)$$

Where dB are readings from the power spectral density plots which were computed as:

$$\text{dB} = 10 \log_{10} \left[\frac{\text{sensor reading in } K^2/\text{Hz}}{1K^2/\text{Hz}} \right] \quad (5)$$

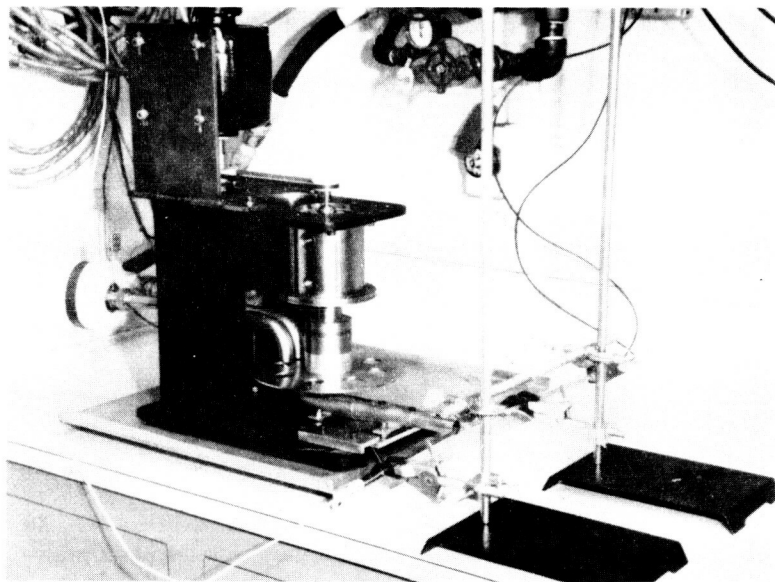
In the frequency domain, error was evaluated as a function of frequency. In some instances, results were presented at specific frequencies and, in others, over a band of frequencies. Errors specified over a frequency band were the largest encountered within that band (ignoring obvious power line harmonics). In the time domain, errors were based on comparisons of the measured rms values and the peak-to-peak values. To aid in eliminating spurious noise spikes, the five highest positive peaks and the five highest negative peaks were arbitrarily ignored in establishing the peak-to-peak fluctuations in the time waveforms. This is a practice commonly used at Pratt & Whitney in processing dynamic strain gage data. Both digital printouts and readings scaled from plots were used in computing the errors. Results based on data scaled from plots are identified in the summary tables and the effect of the plot readability is indicated.

In general, all data comparisons in Task 1d were presented as a percent of reading of the dynamic component errors. This inherently entailed computing errors based on very small values of temperature fluctuations (typically less than 4K rms/ $\sqrt{\text{Hz}}$ at 1000 Hz). For the rotating wheel experiment, data errors were also presented as percent of absolute temperature reading with the mean temperature added to the dynamic component measurements. Since only the dynamic temperature components were measured from the resistance thermometer, the mean gas path temperature measured from the 254 μm (0.010 inch) thermocouple was used for determining the absolute temperature for the resistance thermometer data. Additionally, rotating wheel experiment errors were presented as the difference in temperature readings.

The question of how best to present errors is a complex issue and beyond the scope of the current contract. The magnitude is highly dependent upon the method used in the calculation of the error. The percent of reading dynamic component errors presented in this report would not necessarily be representative of a high frequency component of significantly higher amplitude since it would inherently have a higher signal to noise ratio. However, any portion of the error due to an error in the determination of the compensation spectrum would be directly applicable to the error in a higher amplitude frequency component.

Rotating Wheel Experiment. — The modified rotating wheel experiment defined in Tasks 1a and 1b was tested using existing hardware at Pratt & Whitney that was modified to meet the test conditions required.

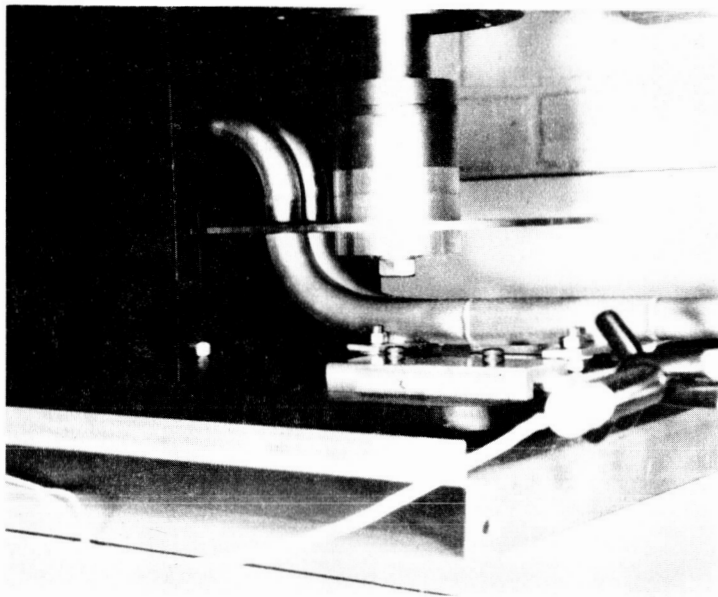
(1) **Hardware and Test Configuration:** The final test configuration of the rotating wheel experiment is shown schematically in Figure 16. An existing drive assembly consisting of an electric motor and shaft was used to rotate a wheel plate which had 8 holes mounted on a 20.32 cm (8 inch) bolt circle diameter. Heated and ambient temperature air was supplied to two tubes mounted close together on one side of the rotating wheel and in-line with the holes bolt circle diameter. The heated air supply was obtained by using electrical heaters. As the wheel rotated, the holes passed the two air supply tubes and allowed hot and cold air pulses to flow. A special manifold was placed on the opposite side of the rotating wheel and had two elbows placed in-line with the supply tubes. These elbows collected the hot and cold pulses. The elbows were formed into a transition section which became a single circular tube. Hot and cold air pulses were thereby delivered to the sensors mounted immediately downstream of the single circular tube. The actual test hardware is shown in Figures 19, 20, and 21.



FD 312806

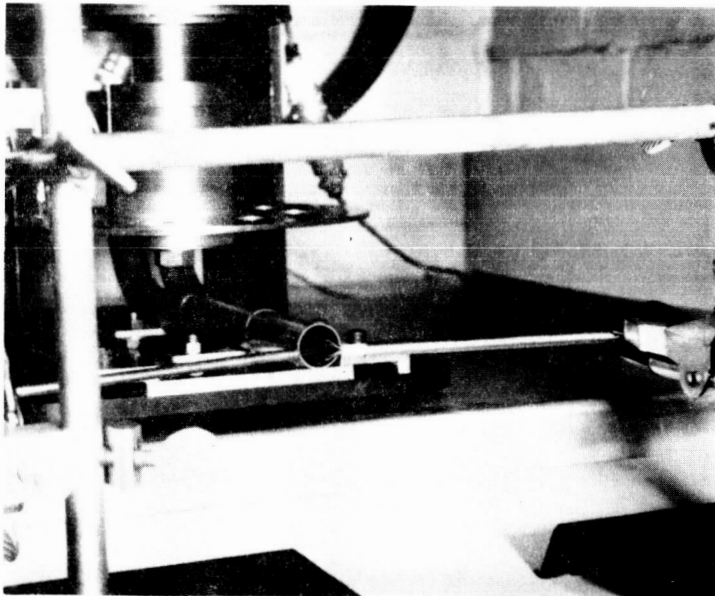
Figure 19. Overall View of Rotating Wheel Experiment

ORIGINAL PAGE IS
OF POOR QUALITY



FD 312807

Figure 20. Wheel/Manifold Detail for the Rotating Wheel Experiment

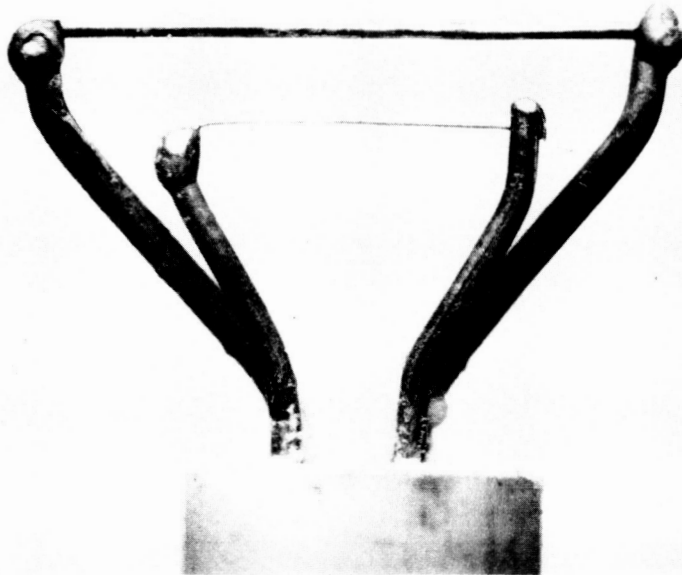


FD 316119

Figure 21. Probe Detail of Rotating Wheel Experiment

The two wire thermocouple probes were fabricated from the design shown in Figure 12. These were fabricated using Chromel-Alumel (C/A) thermocouple alloy wire instead of the previously used Type B alloy wire which is used in combustor tests. The C/A type wire provides a higher emf output signal down to ambient temperatures whereas Type B has no output below 339K (150°F). A considerable amount of time and effort was involved in fabricating the

thermocouple junctions due to the differences in the properties and welding characteristics of the C/A and the previously used Type B alloy. The butt welded uniform diameter junctions of $76\ \mu\text{m}$ (0.003 inch) and $254\ \mu\text{m}$ (0.020 inch) were finally fabricated and assembled into the probe shown in Figure 22. The probe shown was actually used in testing the rotating wheel. The probe was also pre-test inspected to define all of the dimensions. The results, along with the print dimensions, are shown in Figure 23. The inspection was made by taking calibrated photographs through a microscope and measuring the dimensions from the photographs.



FD 316120

Figure 22. Thermocouple Probe for the Rotating Wheel Experiment

The temperature standard probe was a commercially available TSI Model 1226 anemometer. This probe consisted of a $6.35\ \mu\text{m}$ (0.00025 inch) platinum-iridium resistance element. The probe was used as a resistance thermometer.

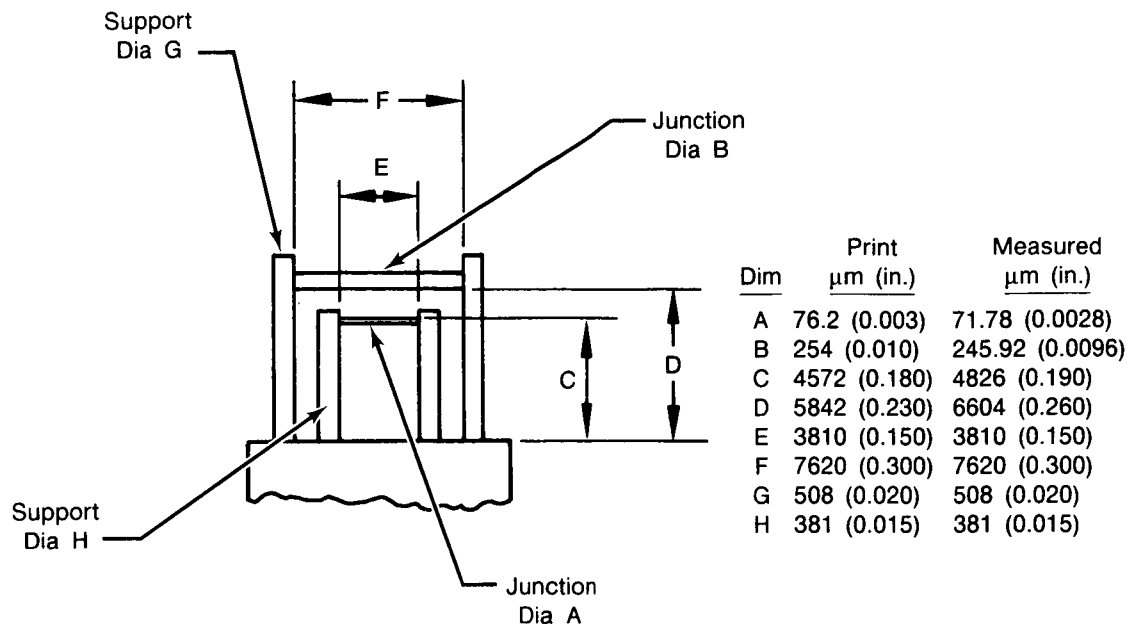
The data acquisition system shown in Figure 16 consisted of the FM type record system previously developed in Reference 1. In addition, TSI equipment was used and the signal recorded on FM tape along with the thermocouple signals.

(2) *Test Program:* The TSI Model 1226 resistance thermometers were checked out and calibrated. The test apparatus was then set up, and the facility and hot and cold air supplies were checked out and characterized. The system was flowed and set up to provide the nominal flow conditions of:

$$\bar{V} = 107\ \text{m/sec}\ (351\ \text{ft/sec})$$

$$T_{\text{hot}} = 567\text{K}\ (560^\circ\text{F})$$

$$T_{\text{cold}} = 289\text{K}\ (60^\circ\text{F})$$



FD 312808

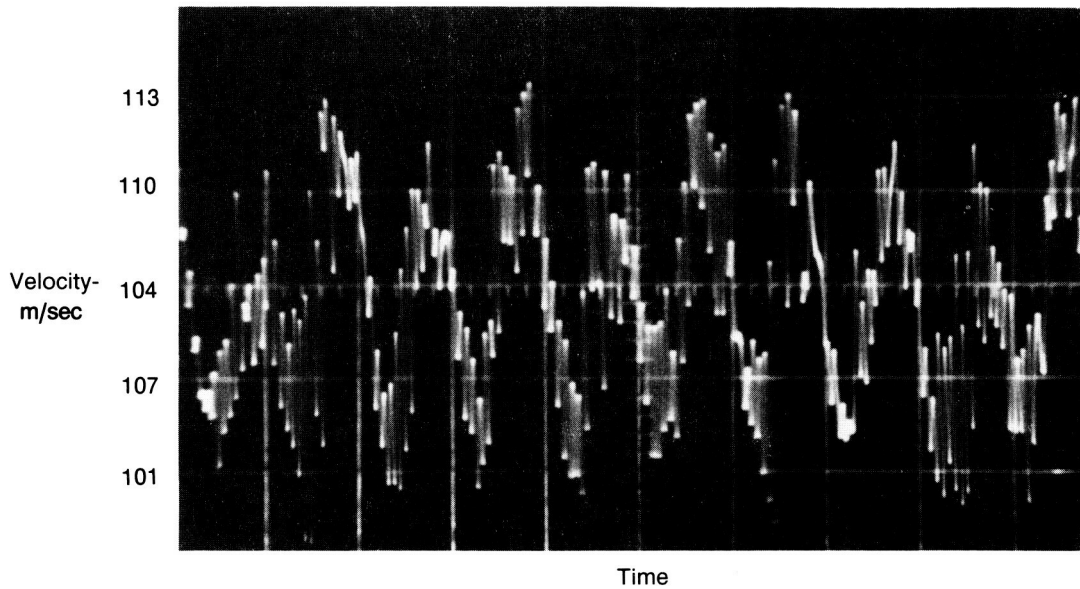
Figure 23. Rotating Wheel Experiment Thermocouple Probe Pre-Test Inspection Summary

Velocity measurements were run on both air sources at ambient temperature and nozzle velocities set using the same $\Delta P/P$ corresponding to the velocities during hot tests. The velocities were measured at the same location that the test probes were located using a TSI Model 1227 hot wire anemometer. This probe had a $9 \mu\text{m}$ (0.00035 inch) tungsten element. Measurements were made at varying rotating wheel speeds corresponding to fundamental frequencies of 20, 88, 150, 200, and 250 Hz. Figure 24 presents an actual oscilloscope trace of the velocity versus time for the 250 Hz test point.

The resistance thermometer temperature standard probe and the two-wire thermocouple probe were mounted downstream of the transition duct exit. The test program conducted consisted of 11 tests described in Table 5. The first test was with zero air flow to record probe ambient background noise levels on FM tape. Test 2 was an attempt to run a 250 Hz point; however, the resistance thermometer failed prior to recording data. Test 3 was a repeat of Test 2 and 1 minute of data were recorded before the resistance thermometer again failed. Additional $6.4 \mu\text{m}$ (0.00025 inch) resistance thermometers were not available so the remaining tests were run, as shown in Table 5, at varying frequency and flow conditions. Tests 10 and 11 were attempts to obtain more smooth sinusoidal temperature waveforms by installing a wire mesh in the transition duct; however, it did not affect the waveforms appreciably.

(3) **Data Analysis:** Table 5 lists test points recorded on FM tape. Test point 3 was selected to be the primary analysis point. It was the singular high frequency point where $6.4 \mu\text{m}$ (0.00025 inch) diameter resistance thermometer data were obtained.

Data comparisons were made between the $76 \mu\text{m}$ thermocouple and the $6.4 \mu\text{m}$ resistance thermometer. The $254 \mu\text{m}$ thermocouple was only used in determining the compensation spectrum of the $76 \mu\text{m}$ thermocouple.



FD 312809

Figure 24. Plot of Velocity Versus Time at 250 Hz for the Rotating Wheel Experiment

The 6.4 μm resistance thermometer used in this test had the highest inherent frequency response characteristics (-3 dB at 508 Hz) of all sensors used in the experiment. Test point 1 (ambient background) was used to establish data signal to noise ratios. Ultimately, test point 4 (20 Hz) was used to establish the compensation spectrum for the thermocouple response correction. Test points 6 and 9 were partially processed (9 μm diameter resistance thermometer data only) to document the temperature profile of the rig at low (20 Hz) and high (250 Hz) frequencies.

A determination of Γ from the fundamental 250 Hz frequency component at test point 3 could not be made because the measured ratio of thermocouple responses did not fall within the range of values predicted by the compensation software. A measured value of Γ is necessary to produce the compensation spectrum. Investigation into the sensitivity of the ratio of the large to the small thermocouple responses (i.e., their transfer function) as a function of frequency and Γ showed (Figure 25) that at frequencies higher than the corner frequency (-3 dB) of the smaller diameter thermocouple, the sensitivity decreases dramatically.

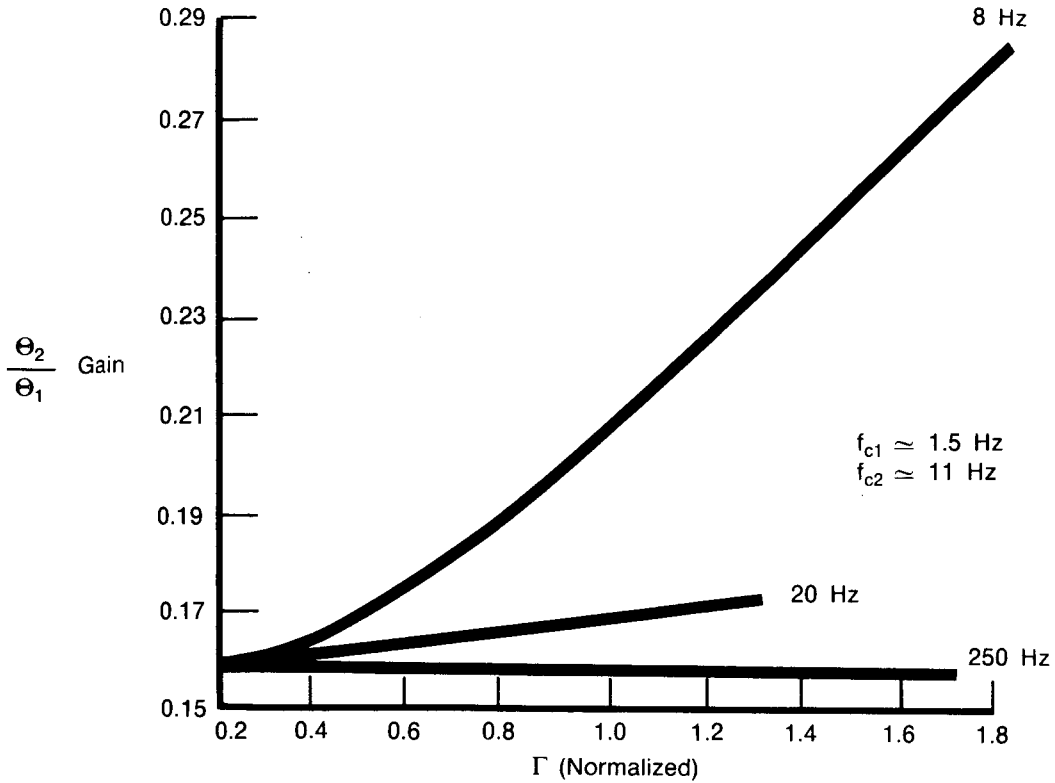
The same effect would also be expected for frequencies lower than the corner frequency of the larger thermocouple. For this experiment, Figure 25 shows that the transfer function between the two thermocouples is essentially a constant for the predicted range of normalized Γ at the 250 Hz test point. A slight error in the measurement of the transfer function from the test data would result in a value which would not yield a measurement of Γ . In fact, the measured transfer function at 250 Hz was slightly low and did not yield a measured Γ . At 20 Hz, the sensitivity is improved but slight errors in the measured value of the transfer function will produce noticeable errors in Γ . There appears to be approximately a one-to-one relationship between the percent error in Γ and the percent error in the amplitude of the frequency compensation spectrum (see Task III). The 8 Hz component produced reasonable sensitivity. This frequency (8 Hz) lies between the predicted corner frequencies of the large and small thermocouple. No attempt was made to determine the specific frequency which would produce optimum sensitivity.

TABLE 5. — ROTATING WHEEL EXPERIMENT TEST CONDITIONS SUMMARY

<i>Test No.</i>	<i>Test Description</i>
1	Gas path conditions - No flow Recorded two-wire thermocouple and resistance thermometer ambient background noise
2	Gas path conditions - 250 Hz, 107 m/sec (350 ft/sec), and 568K (562°F)/289K (60°F) 6.4 μm (0.00025 in.) resistance thermometer (S/N 43379) failed at insertion but recorded two minutes of dual thermocouple data
3	Gas path conditions - 250 Hz, 107 m/sec (350 ft/sec), and 568K (563°F)/289K (60°F) Recorded one minute of 6.4 μm (0.00025 in.) resistance thermometer data before failure. Continued recording two-wire thermocouple data to obtain total of two minutes
4	Gas path conditions - 20 Hz, 107 m/sec (350 ft/sec), and 568K (563°F)/289K (60°F)
5	Same as Test 4 except run at 147 Hz
6	Gas path conditions - 250 Hz, 107 m/sec (350 ft/sec), and 566K (558°F)/289K (60°F) Recorded two minutes of data for 9 μm (0.00035 in.) tungsten resistance thermometer and two-wire thermocouple
7	Same as Test 6 except gas path conditions were 200 Hz, 107 m/sec (350 ft/sec), and 571K (564°F)/289K (60°F)
8	Same as Test 6 except gas path conditions were 150 Hz, 107 m/sec (350 ft/sec), and 571K (568°F)/289K (60°F)
9	Same as Test 6 except run at 20 Hz
10	Gas path conditions - 21 Hz, 113 m/sec (370 ft/sec), and 514K (465°F)/291K (64°F) Installed new 9 μm (00035 in.) S/N 2 Pt plated tungsten thermometer and wire mesh screen, recorded two minutes of data
11	Gas path conditions - 21 Hz, 113 m/sec (370 ft/sec), and 555K (539°F)/288K (58°F) Extended nozzle and added more wire mesh, recorded two minutes of data
Notes: 1) All tests run with Type K dual wire 76.2 μm (0.003 in.)/254 μm (0.010 in.) elements probe S/N A.	
2) Purpose of wire mesh and nozzle extension in Tests 10 and 11 was to obtain a sinusoidal temperature waveform.	

6745C

Table 6 summarizes the values of Γ determined from the experimental data. The value obtained from the 20 Hz point ($9.356 \times 10^{-6} \text{ m}^{1.5}/\text{sec}$) was used for compensating the rotating wheel data presented in this report. The 8 Hz frequency was contained in a random background temperature fluctuation present whenever the rig was running. The source of the random temperature fluctuations (about 0.3K rms/ $\sqrt{\text{Hz}}$) was believed to be entrainment of ambient air around the rotating disk and duct interface. Measurement of Γ from the 8 Hz component present in the 20 Hz test point and the 250 Hz test point yielded values of Γ of 6.479×10^{-6} and $4.039 \times 10^{-6} \text{ m}^{1.5}/\text{sec}$ respectively.



FD 312810

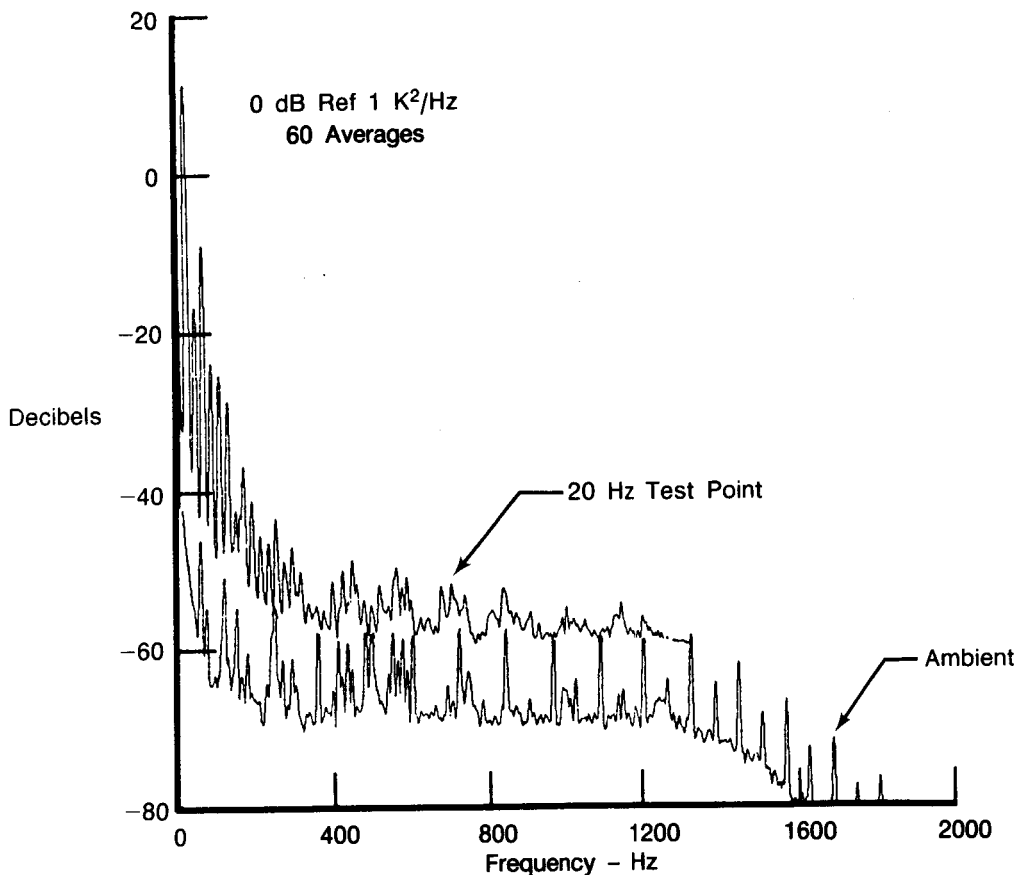
Figure 25. Transfer Function of the Large Thermocouple to the Small Thermocouple for Normalized Γ at Various Frequencies for the Rotating Wheel Experiment

TABLE 6. — SUMMARY OF Γ VALUES MEASURED FOR ROTATING WHEEL RIG

Test Point	Freq. Range Analyzed	Γ
250 Hz	250 Hz	—
250 Hz	\approx 8 Hz Random	$4.039 \times 10^{-6} \text{ m}^{1.5}/\text{sec}$
20 Hz	20 Hz	$9.356 \times 10^{-6} \text{ m}^{1.5}/\text{sec}$
20 Hz	\approx 8 Hz Random	$6.479 \times 10^{-6} \text{ m}^{1.5}/\text{sec}$

6745C

Figure 26 depicts the uncompensated 76 μm (0.003 inch) thermocouple PSD plots for the 20-Hz test point and the ambient background noise. The signal to noise ratio (SNR) at any specific frequency is the difference (in decibels) between the two curves at the specific frequency. The SNR was about 22 dB for the small amplitude 8 Hz random background temperature fluctuation and 55 dB for the 20 Hz fundamental frequency.



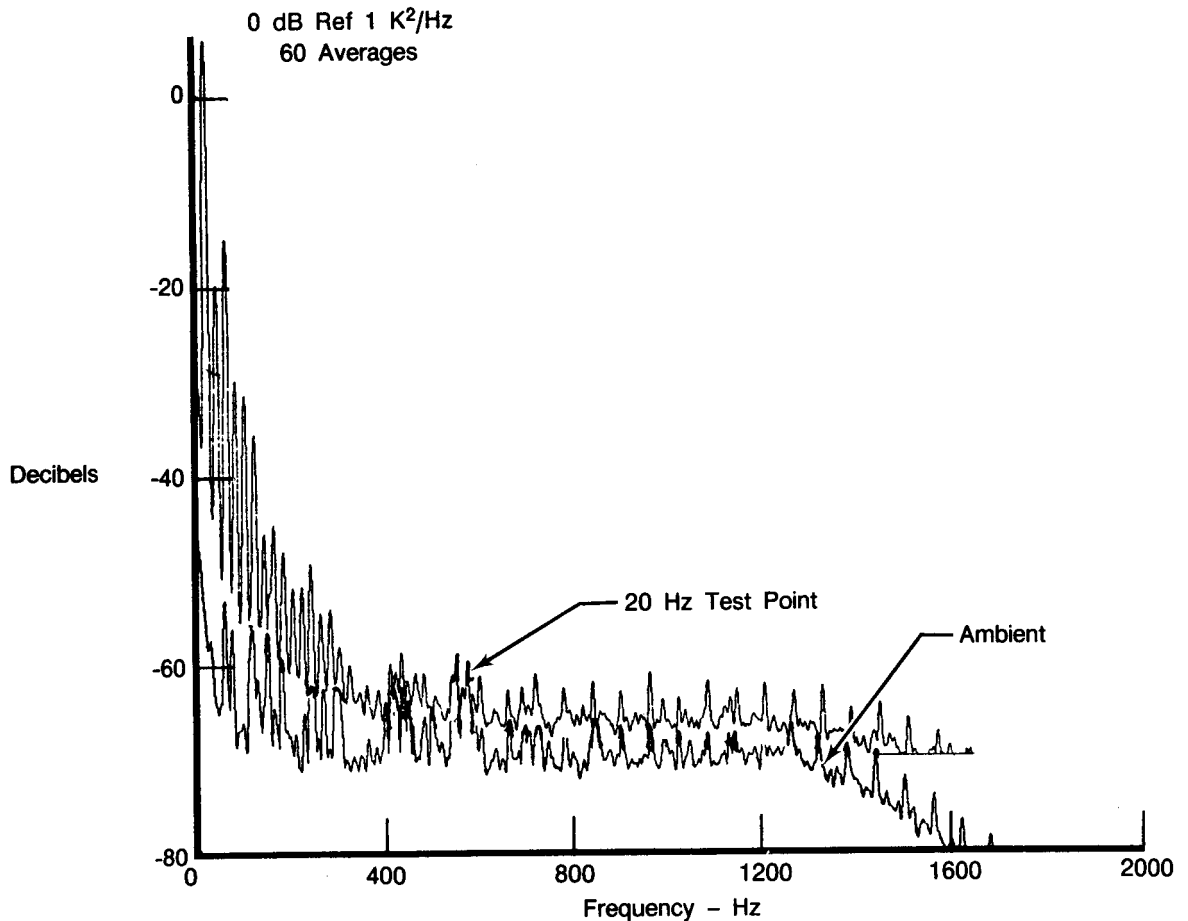
FD 312811

Figure 26. Rotating Wheel Experiment: Power Spectral Density Plots for the Uncompensated 76 μm (0.003 Inch) Thermocouple for the 20 Hz Test Point and Ambient

The SNR for the uncompensated 254 μm (0.010 inch) thermocouple can be determined from Figure 27. At 20 Hz, the SNR was about 60 dB and at 8 Hz the SNR was about 20 dB. The 254 μm (0.010 inch) thermocouple was only used (in conjunction with the 76 μm thermocouple) for the measurement of Γ . In general, the SNR of the data were considered excellent for the computation of the measured Γ .

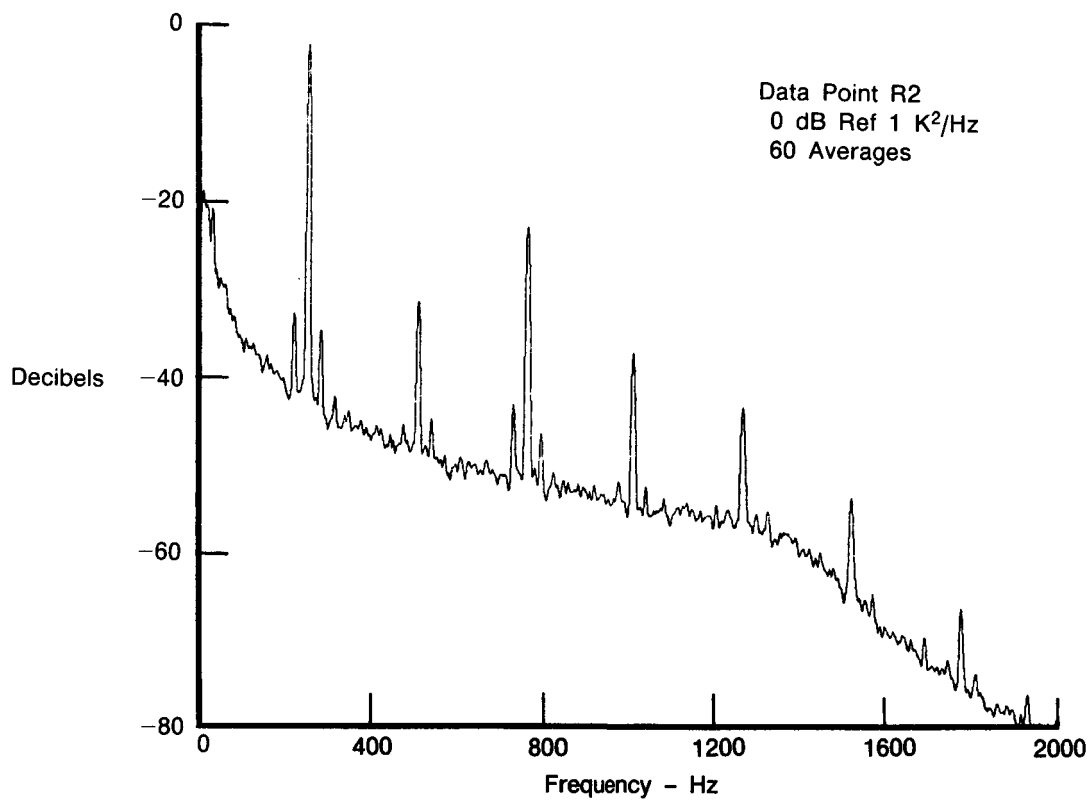
Figures 28 and 29 are the PSD plots of the uncompensated 76 μm (0.003 inch) thermocouple and the 6.4 μm (0.00025 inch) resistance thermometer respectively at the 250 Hz test point. The corner frequency (-3 dB) of the resistance thermometer was 508 Hz. The amplitudes of the 250 Hz component and its harmonics were typically 25 to 30 dB lower than obtained with the resistance thermometer. Following compensation, the 76 μm (0.003 inch) thermocouple (Figure 30) and the compensated 6.4 μm resistance thermometer (Figure 31) PSD plots are very similar. The fundamental 250 Hz component with an amplitude of about 66K rms was the primary frequency for data comparisons. The harmonics at 500 Hz, 750 Hz, and 1000 Hz and the wideband temperature fluctuations were of smaller amplitudes and thus more influenced by noise signal levels. The SNR of the uncompensated 76 μm thermocouple was about 50 dB at 250 Hz, 22 dB at 500 Hz, 38 dB at 750 Hz, and 25 dB at 1000 Hz (Figure 32 compared to the ambient background curve depicted in Figure 33). The SNR of the compensated 6.4 μm

resistance thermocouple (compared to its compensated ambient background noise) was about 67 dB at 250 Hz, 45 dB at 500 Hz, 51 dB at 750 Hz, and 41 dB at 1000 Hz (Figure 34). Figures 35 and 36 depict the narrowband frequency spectra for the compensated 76 μm thermocouple and the 6.4 μm resistance thermometer respectively. A narrowband frequency spectrum is the proper analysis for the rotating wheel data which is predominantly composed of discrete (i.e., narrowband) frequency components. However, the log PSD plot was selected to be the primary mode of data presentation because of its inherently larger dynamic range which permits measurement of both large and small amplitude components without loss of readability from the same data plot. As seen in Figure 36, the fundamental frequency (250 Hz) was the predominant dynamic temperature component and its amplitude was about 66K rms (187K p-p).



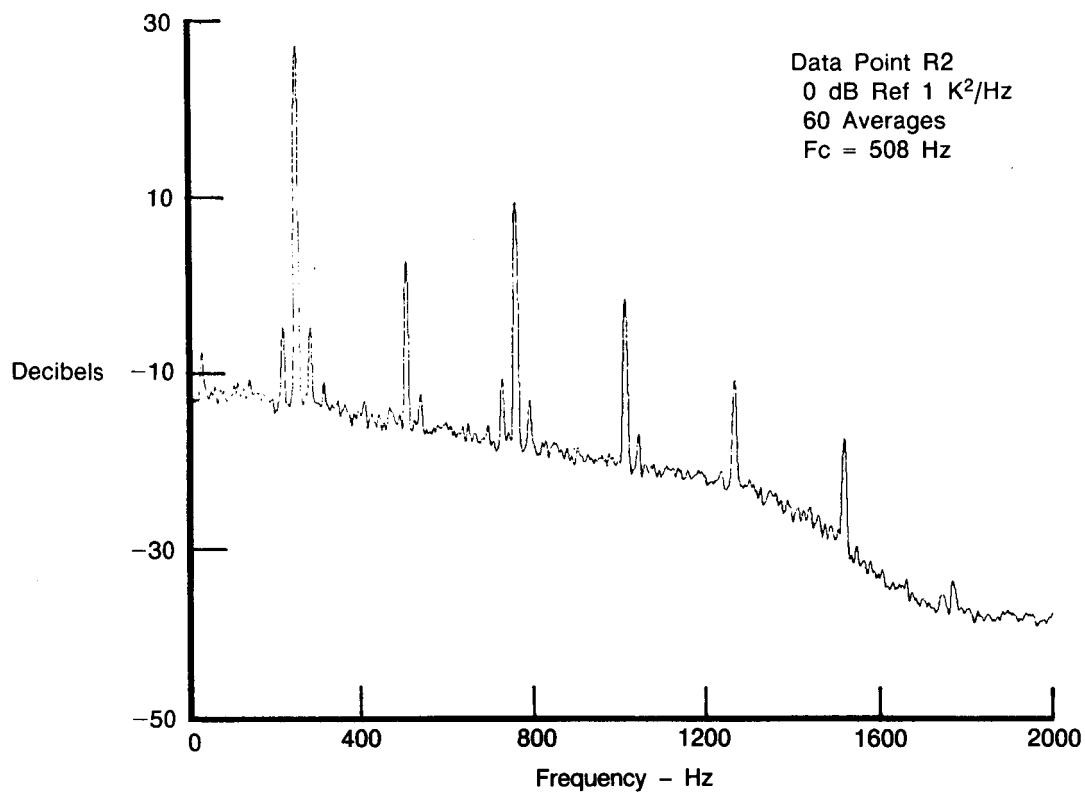
FD 312812

Figure 27. Rotating Wheel Experiment: Power Spectral Density Plots for the Uncompensated 254 μm (0.010 Inch) Thermocouple for the 20 Hz Test Point and Ambient



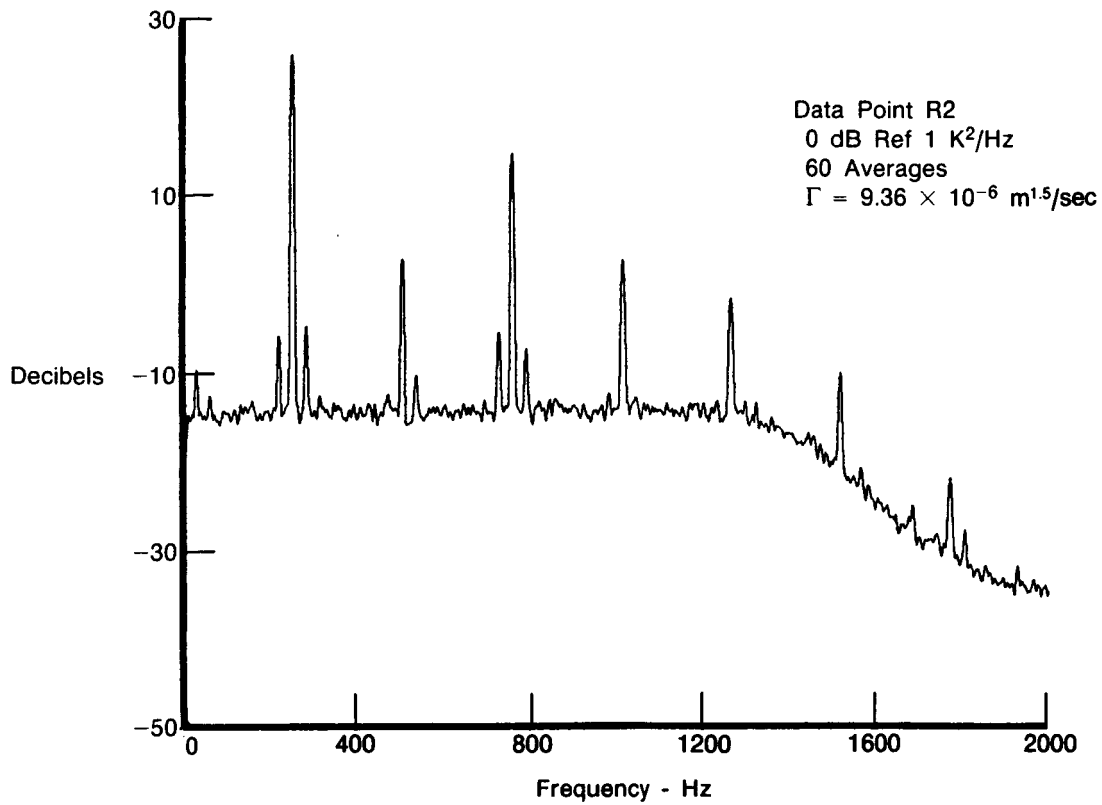
FD 312813

Figure 28. *Rotating Wheel Experiment: Power Spectral Density Plot for the Uncompensated 76 μ m (0.003 Inch) Thermocouple for the 250 Hz Test Point*



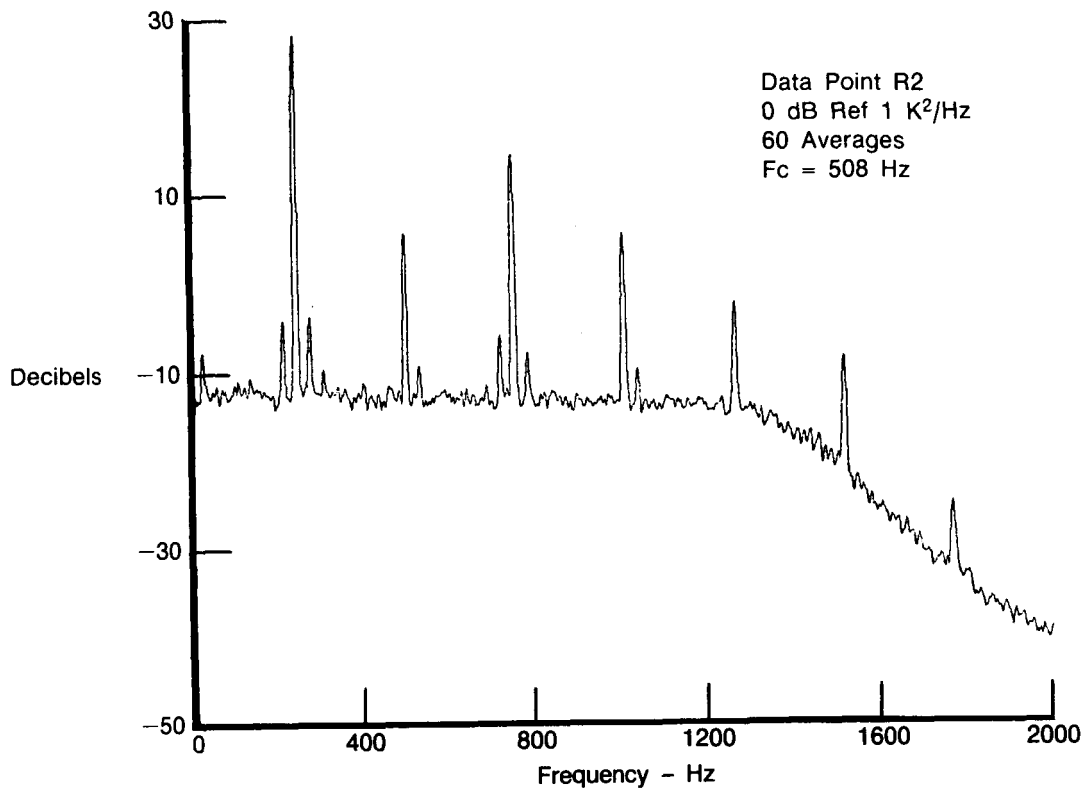
FD 312814

Figure 29. Rotating Wheel Experiment: Power Spectral Density Plot for the Uncompensated 6.4 μm (0.00025 Inch) Resistance Thermometer for the 250 Hz Test Point



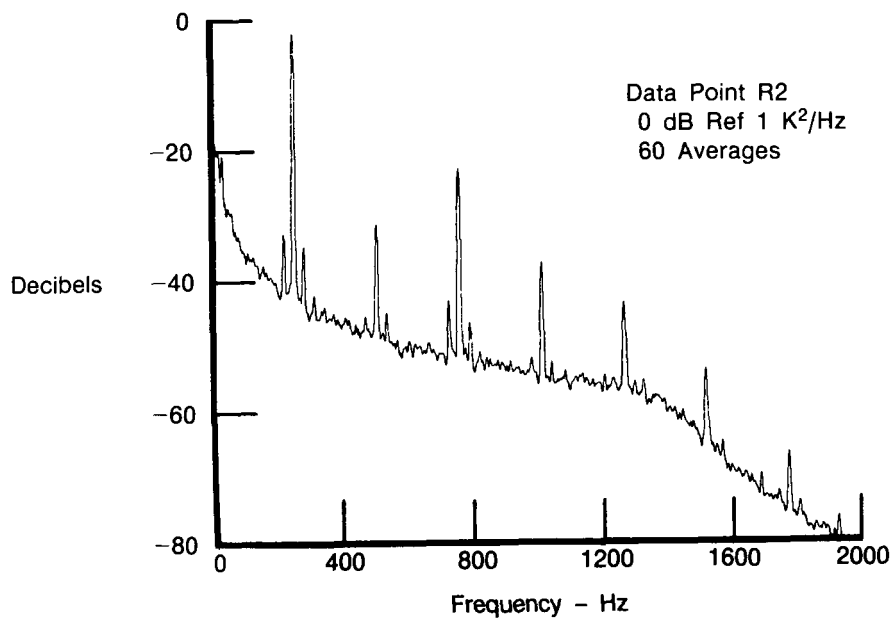
FD 312815

Figure 30. Rotating Wheel Experiment: Power Spectral Density Plot for the Compensated 76 μm (0.003 Inch) Thermocouple for the 250 Hz Test Point



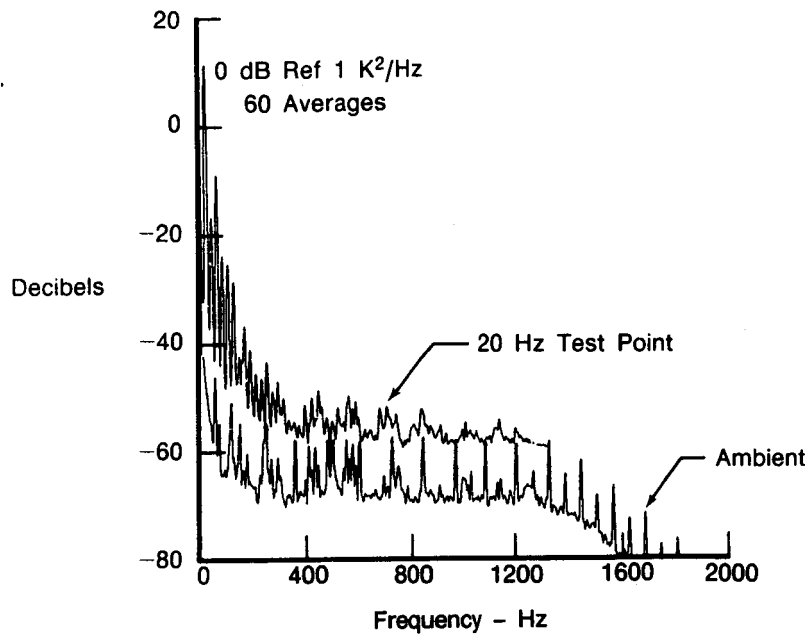
FD 312816

Figure 31. Rotating Wheel Experiment: Power Spectral Density Plot for the Compensated 6.4 μm (0.00025 Inch) Resistance Thermometer for the 250 Hz Test Point



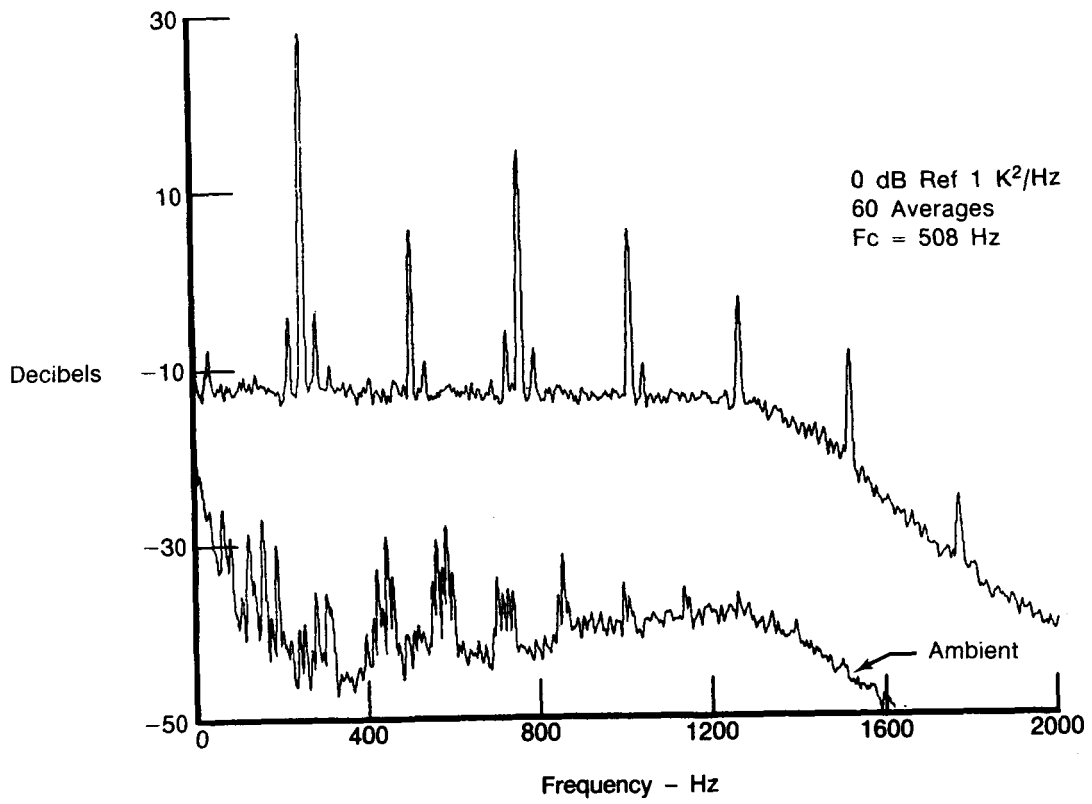
FD 316150

Figure 32. Rotating Wheel Experiment: Power Spectral Density Plot for the Uncompensated 76 μm (0.003 Inch) Thermocouple for the 250 Hz Test Point



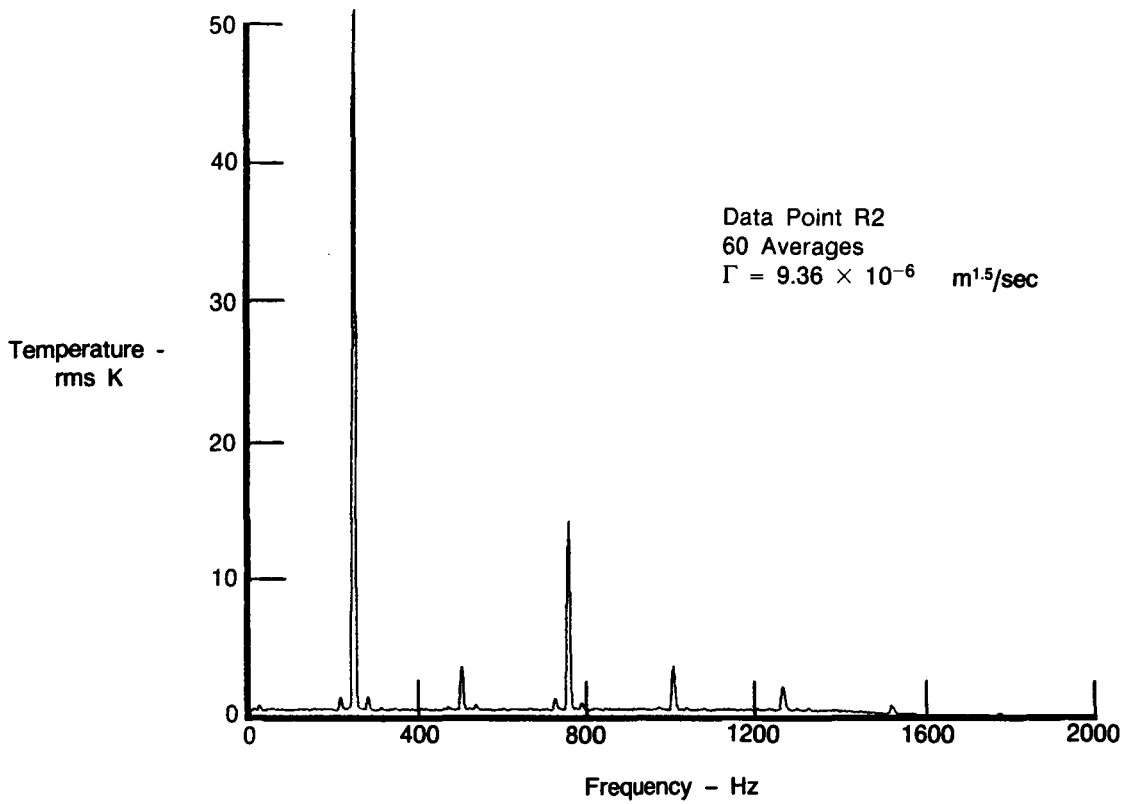
FD 316151

Figure 33. Rotating Wheel Experiment: Power Spectral Density Plots for the Uncompensated 76 μm (0.003 Inch) Thermocouple for the 20 Hz Test Point and Ambient



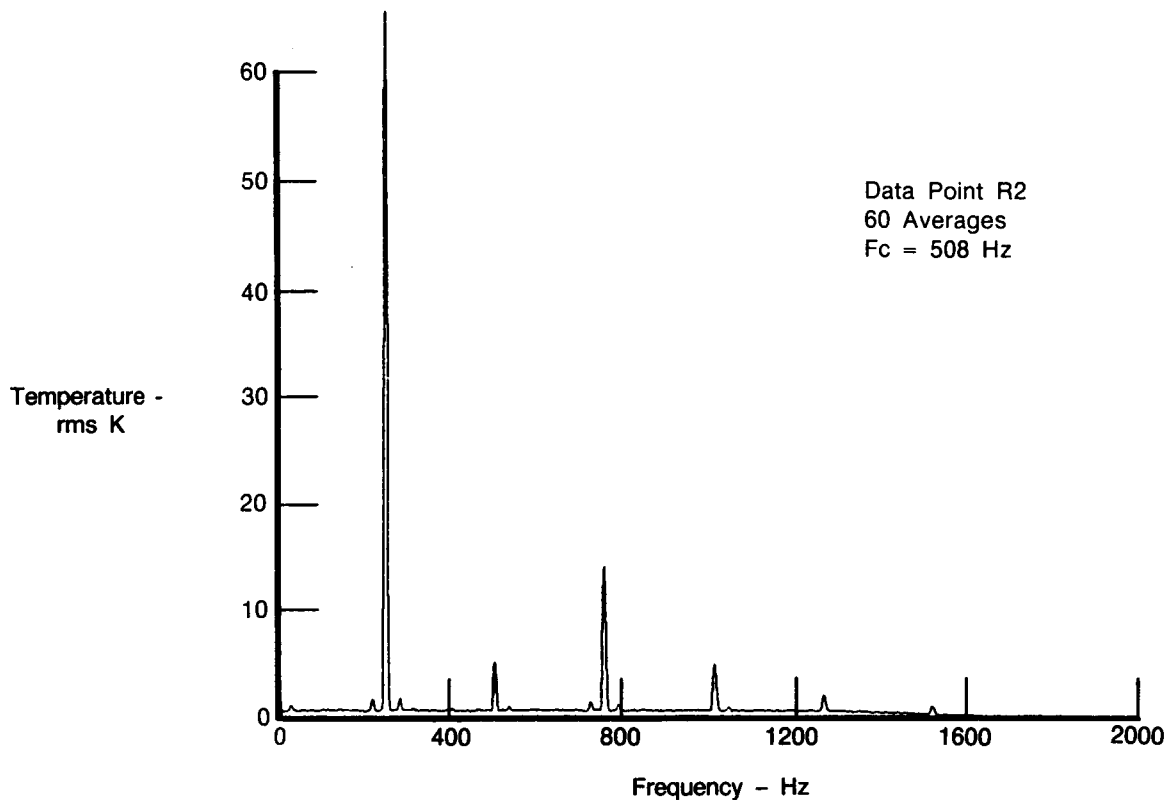
FD 312831

Figure 34. *Rotating Wheel Experiment: Power Spectral Density Plots for the Compensated 6.4 μm (0.0025 Inch) Resistance Thermometer and Ambient*



FD 312832

Figure 35. Rotating Wheel Experiment: Narrow Band Frequency Spectrum for the Compensated 76 μm (0.003 Inch) Thermocouple at 250 Hz Test Point



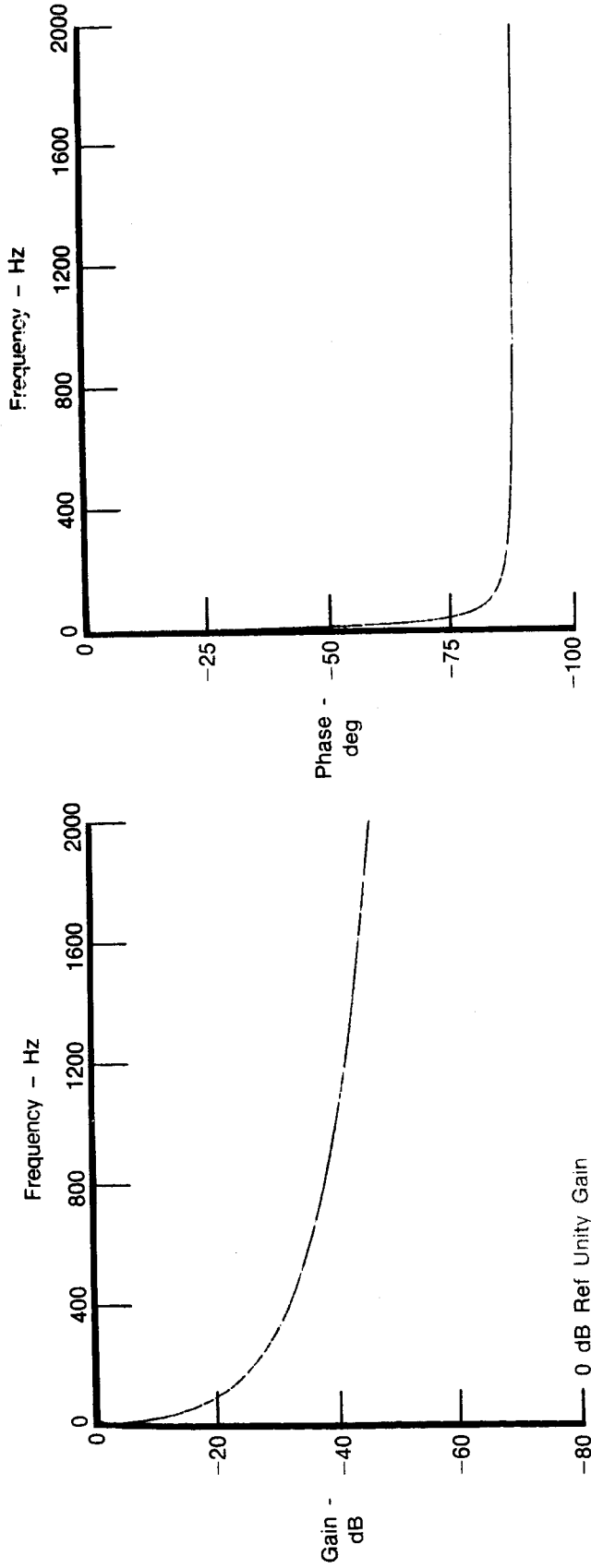
FD 312833

Figure 36. *Rotating Wheel Experiment: Narrow Band Frequency Spectrum for the Compensated 6.4 μm (0.00025 Inch) Resistance Thermometer at 250 Hz Test Point*

Figure 37 depicts the compensation spectrum of the 76 μm thermocouple used for correcting data at the 250 Hz test point. About 28 dB of signal compensation is required at 250 Hz and 40 dB at 1000 Hz. The resistance thermometer, with a corner frequency of 508 Hz, only requires about 0.9 dB of compensation at 250 Hz and 6.9 dB at 1000 Hz.

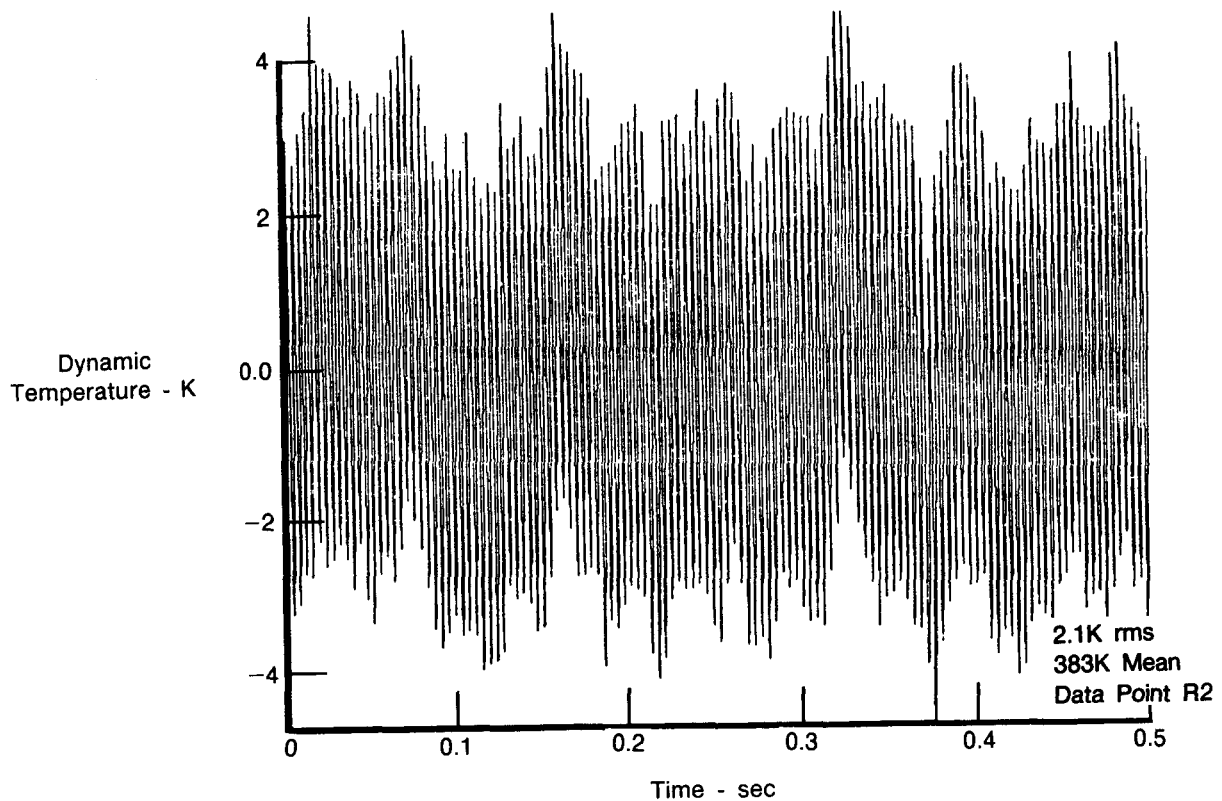
Figures 38 and 39 depict the instantaneous time waveforms of the uncompensated 76 μm thermocouple and the uncompensated 6.4 μm resistance thermometer respectively over a 0.5 second time period at the 250 Hz test point. The 76 μm thermocouple, with its inherently low response, only indicates about an 8K p-p (2.1K rms) overall temperature fluctuation at a mean temperature of 383K. The low level background wideband random temperature fluctuation is a major portion of the overall signal. Although the random fluctuation is only a fractional part of the actual gas temperature dynamics, the thermocouple response at 250 Hz is so poor that the lower frequency band components in the random signal (where the thermocouple is more responsive) contribute significantly to the overall signal. The amplitude of the wideband random signal was about 0.3 rms/ $\sqrt{\text{Hz}}$ over the entire 1000 Hz bandwidth. The 250 Hz component was about 66K rms. The higher response uncompensated 6.4 μm resistance thermometer measured temperature fluctuations of about 174K p-p (63K rms). Note that the random component is only a small portion of the overall signal (Figure 39).

$$\Gamma = 9.36 \times 10^{-6} \text{ m}^{1.5}/\text{sec}$$



FD 312834

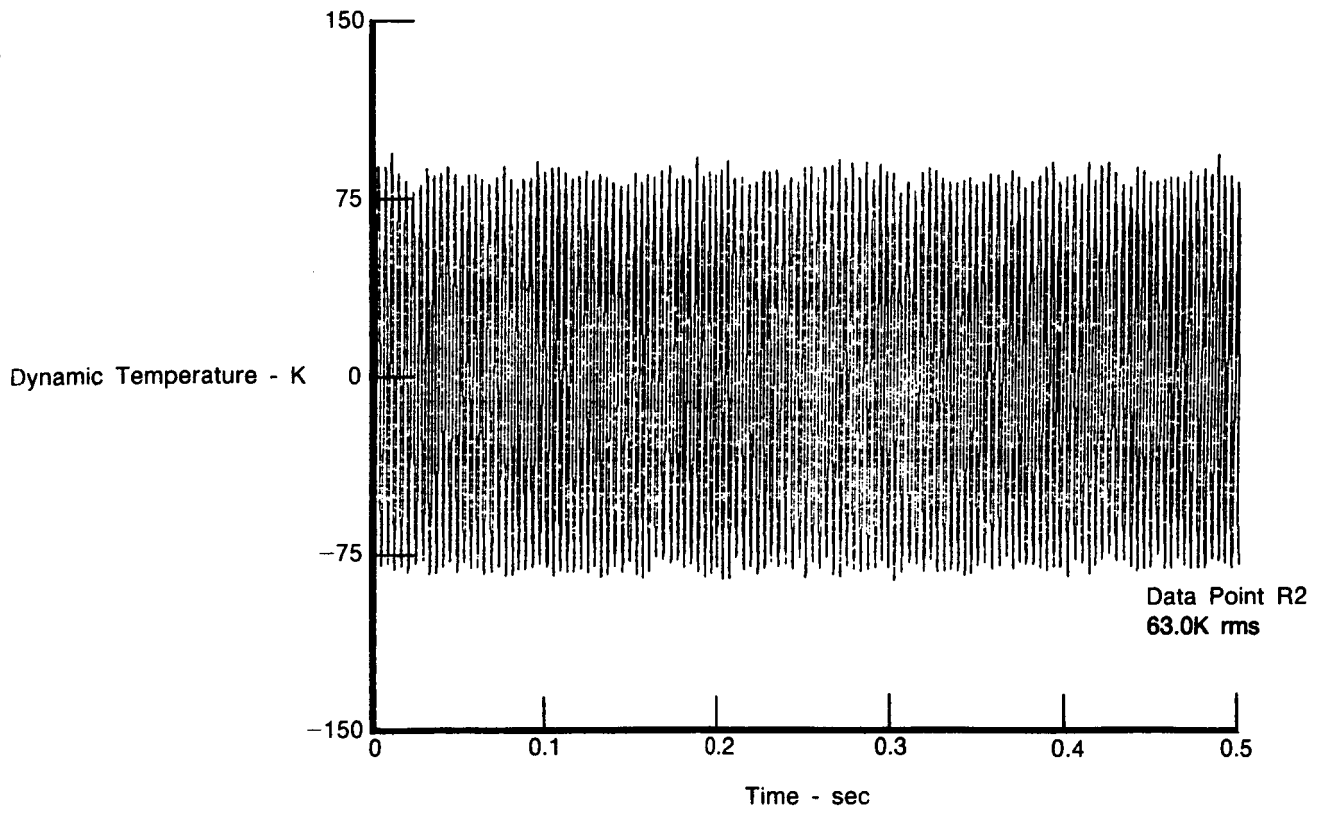
Figure 37. Rotating Wheel Experiment: Compensation Spectrum for the 76 μm (0.003 Inch) Thermocouple Measured at 20 Hz Test Point



FD 312835

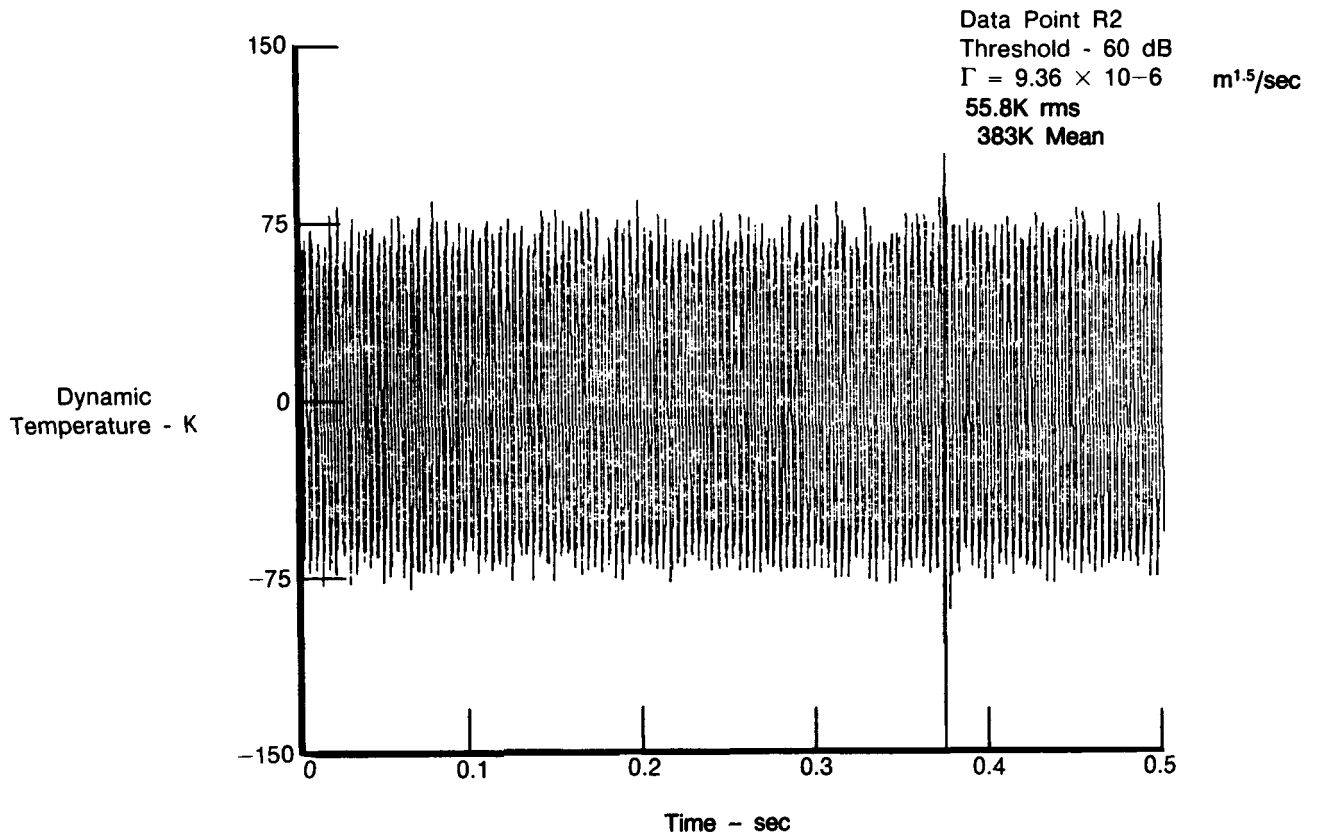
Figure 38. Rotating Wheel Experiment: Uncompensated 76 μm (0.003 Inch) Thermocouple Time Record for the 250 Hz Test Point

The compensated time waveform for the 76 μm thermocouple is shown in Figure 40 and that of the compensated 6.4 μm resistance thermometer in Figure 41. The spike in the compensated thermocouple data which occurs approximately 0.37 second into the record (Figure 40) is an anomaly. Noise spikes of this type can be caused by such events as temporary data file manipulations made to use the dual thermocouple program for processing the resistance thermometer data. Time zero in the compensated thermometer time record corresponds to 0.125 second into the uncompensated resistance thermometer data record. This is inherent in the process used to obtain the compensated thermocouple time record. The compensated thermocouple and compensated resistance thermometer data results are very close considering the magnitude of the compensation employed. The resistance thermometer showed around 194K p-p (71.8 rms) overall which was about 22 percent larger than the thermocouple reading. The wave shape and phasing of the two signals are almost identical (Figures 42 and 43).



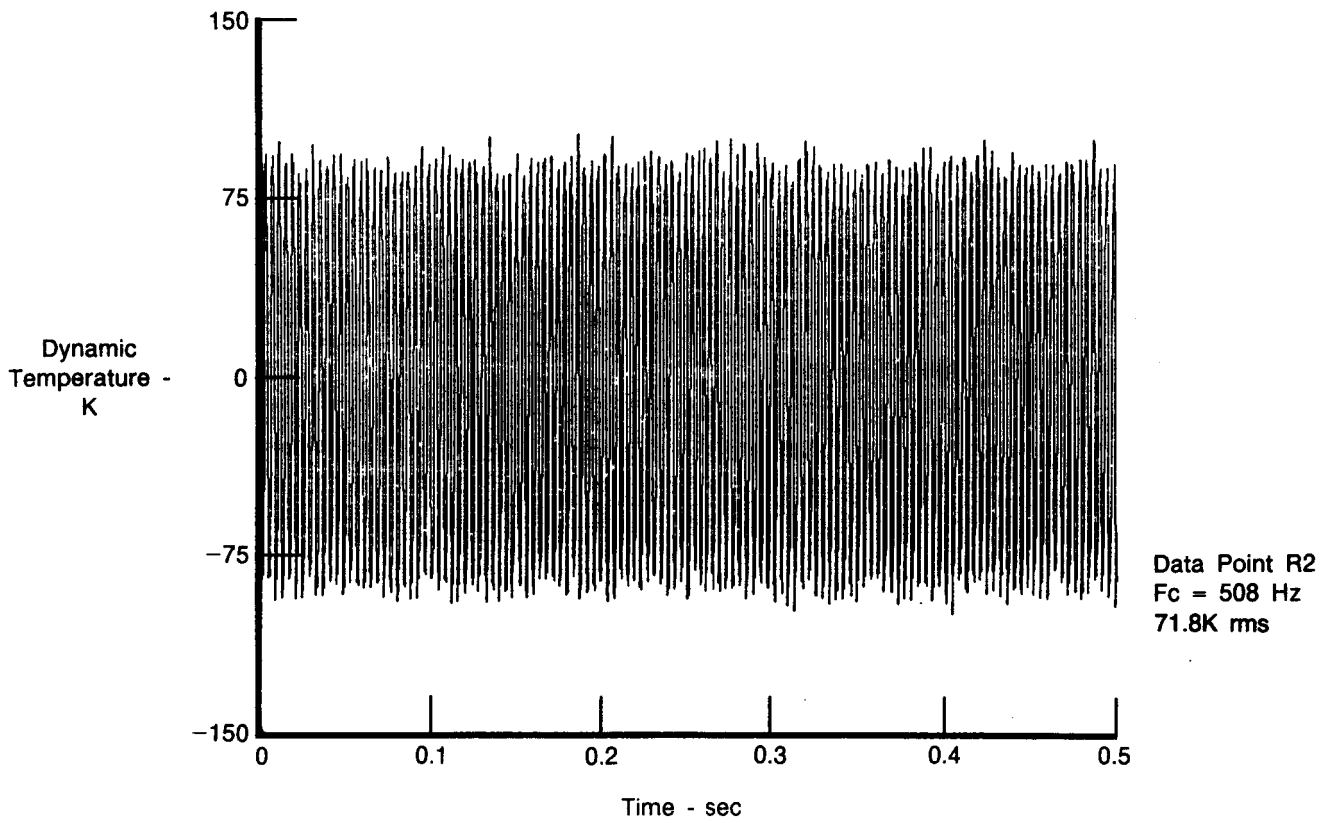
FD 312836

Figure 39. Rotating Wheel Experiment: Uncompensated 6.4 μm (0.00025 Inch) Resistance Thermometer Time Record for the 250 Hz Test Point



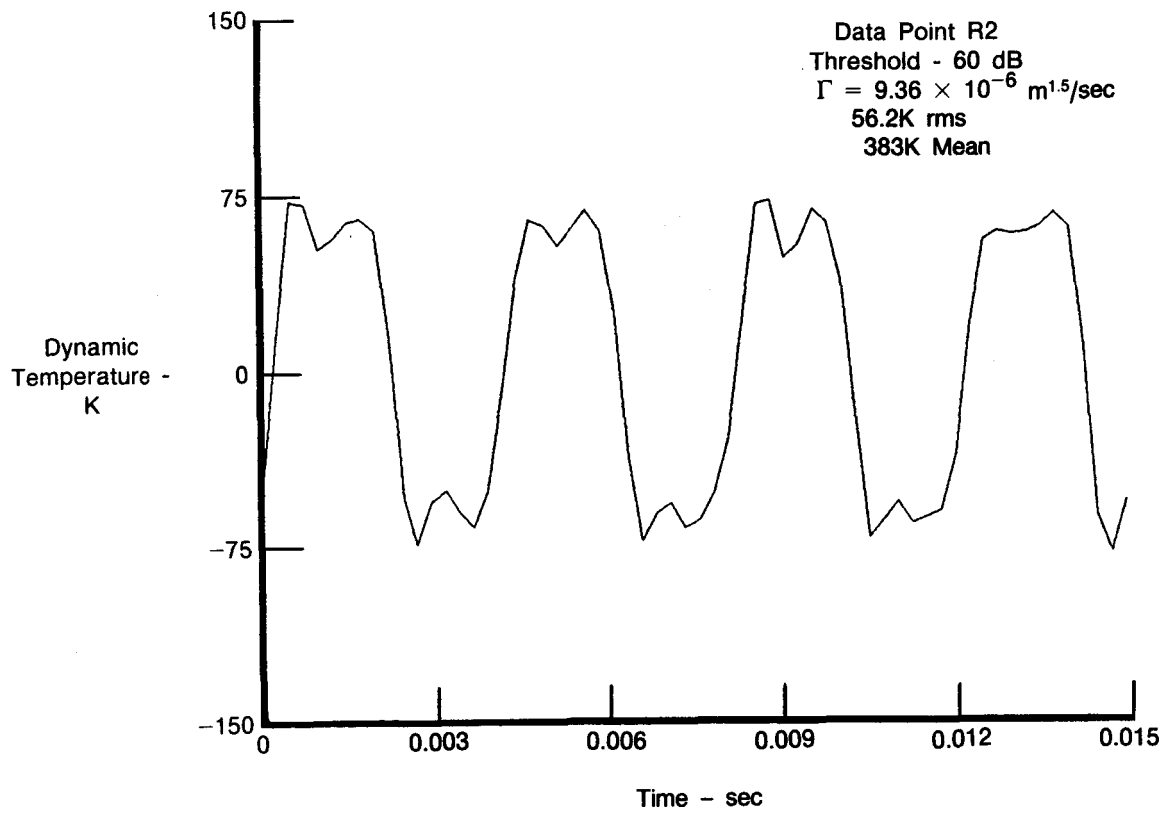
FD 312837

Figure 40. Rotating Wheel Experiment: Compensated 76 μm (0.003 Inch) Thermocouple Time Record for the 250 Hz Test Point



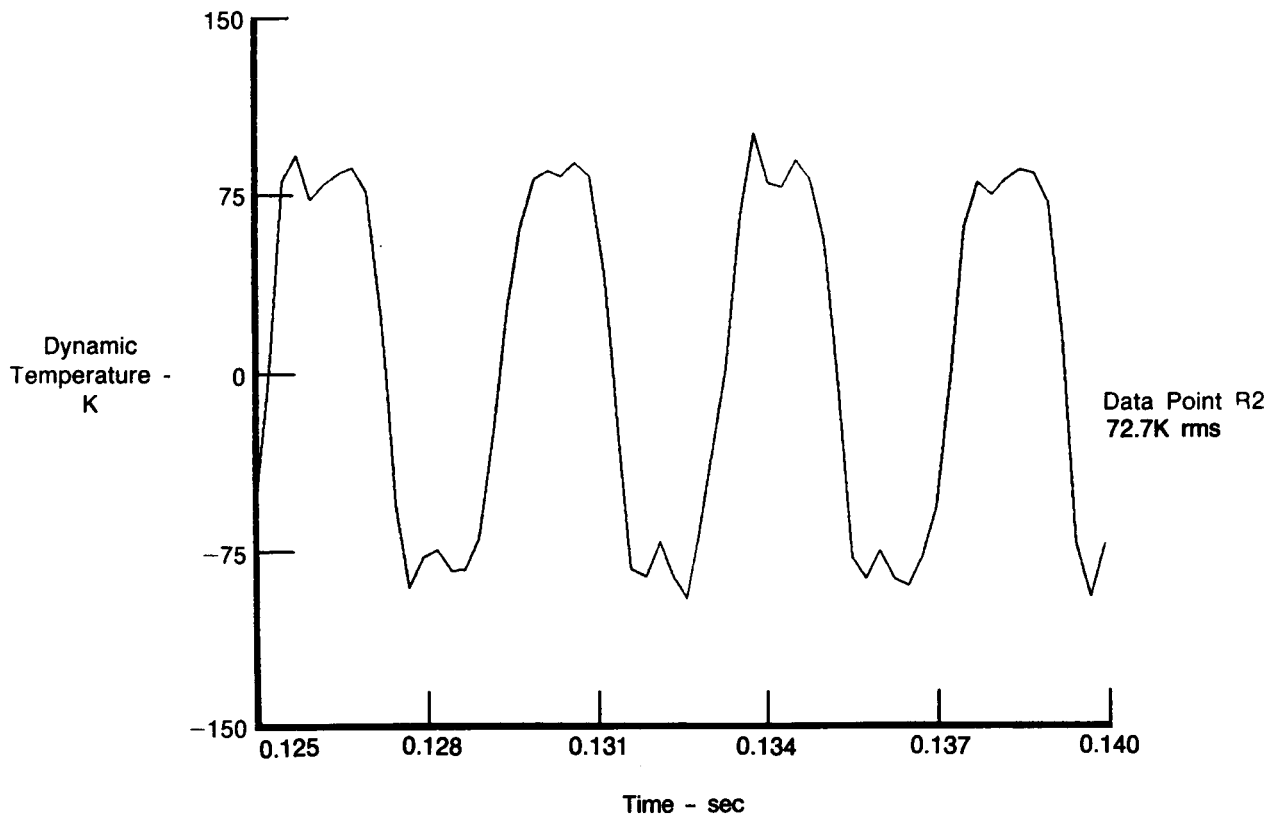
FD 312838

Figure 41. Rotating Wheel Experiment: Compensated 6.4 μm (0.00025 Inch) Resistance Thermometer Time Record for the 250 Hz Test Point



FD 312839

Figure 42. Rotating Wheel Experiment: Compensated 76 μm (0.003 Inch) Thermocouple Partial Time Record for the 250 Hz Test Point



FD 312840

Figure 43. Rotating Wheel Experiment: Compensated $6.4 \mu\text{m}$ (0.00025 Inch) Resistance Thermometer Partial Time Record for the 250 Hz Test Point

Tables 7, 8, and 9 contain detailed comparisons of the errors of the compensated $76 \mu\text{m}$ thermocouple referenced to the compensated $6.4 \mu\text{m}$ resistance thermocouple. Evaluations were made at 250, 500, 750, and 1000 Hz in the frequency domain. In the time domain, rms and peak-to-peak levels were compared. Table 7 lists dynamic component errors in percent of reading. Typically, the thermocouple data were 23 to 28 percent low in both the frequency and time domains. Note that at frequencies other than 250 Hz, the actual gas path temperature fluctuations were quite small (5K to 14K rms). When the mean temperature is included in the error calculation (Table 8), the thermocouple error in percent of absolute temperature reading is typically less than 3.5 percent low in both the frequency and time domains. Presenting results in terms of temperature differences (Table 9) the thermocouple was 15K low at the 250 Hz major frequency component and the overall (1000 Hz bandwidth) rms in the time domain was 16K low. Note that at the low amplitude harmonics (500, 750, and 1000 Hz), the dynamic error in percent of reading was between 28 percent and 3 percent but the error expressed as temperature difference was less than 1.4K rms.

TABLE 7. — ROTATING WHEEL TEST DATA ERROR COMPARISON

Test Point	Sensor	Reference	Dynamic Component Error (% of Reading)					
			Frequency Domain			Time Domain		
			250 Hz	*500 Hz	*750 Hz	*1000 Hz	RMS	P-P
250 Hz "Square Wave"	Compensated 76 μ m (0.003 in.) T/C	Compensated 6.4 μ m (0.00025 in.) Resistance Thermometer	-23%	-28% (± 1)	+3% (± 1)	-28% (± 1)	-22%	-19% (± 1)
*Harmonics of Fundamental Temperature Waveform Repetition Rate								
Note: (1) Gas stream temperature fluctuations were: ~ 66K rms at 250 Hz ~ 5K rms at 500 Hz ~ 14K rms at 750 Hz ~ 5K rms at 1 kHz (2) ($\pm n$) = Readability of scaled plots - applicable where indicated								

6745C

TABLE 8. -- ROTATING WHEEL TEST DATA ERROR COMPARISON

Test Point	Sensor	Reference	Absolute Temperature Error (% of Reading)					
			Frequency Domain			Time Domain		
			250 Hz	*500 Hz	*750 Hz	*1000 Hz	RMS	P-P
250 Hz "Square Wave"	Compensated 76 μm (0.003 in.) T/C	Compensated 6.4 μm (0.00025 in.) Resistance Thermometer	-3.3%	-0.4%	+0.1%	-0.7%	-3.5%	-6.2%
*Harmonics of Fundamental Temperature Waveform Repetition Rate								
Note: (1) Gas stream temperature fluctuations were: ~ 66K rms at 250 Hz ~ 5K rms at 500 Hz ~ 14K rms at 750 Hz ~ 5K rms at 1 kHz (2) Mean temperature was 383K								

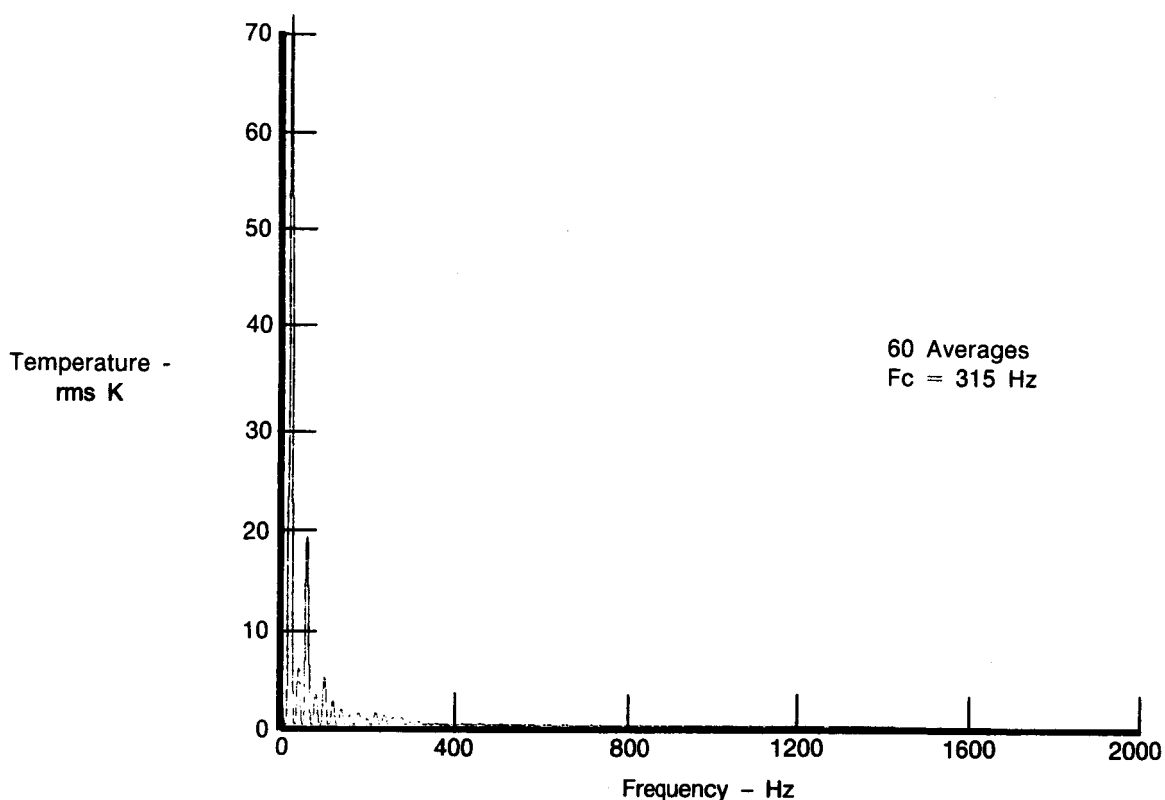
6745C

TABLE 9. — ROTATING WHEEL TEST DATA ERROR COMPARISON

Test Point	Sensor	Reference	Temperature Difference					
			250 Hz	*500 Hz	*750 Hz	*1000 Hz	Time Domain RMS P-P	
250 Hz "Square Wave"	Compensated 76 μ m (0.003 in.) T/C	Compensated 6.4 μ m (0.00025 in.) Resistance Thermometer	-15K rms	-1.4K rms	+0.4K rms	-1.4K rms	-16K rms	-36K
*Harmonics of Fundamental Temperature Waveform Repetition Rate								
Note: Gas stream temperature fluctuations were:								
~ 66K rms at 250 Hz								
~ 5K rms at 500 Hz								
~ 14K rms at 750 Hz								
~ 5K rms at 1 kHz								

6745C

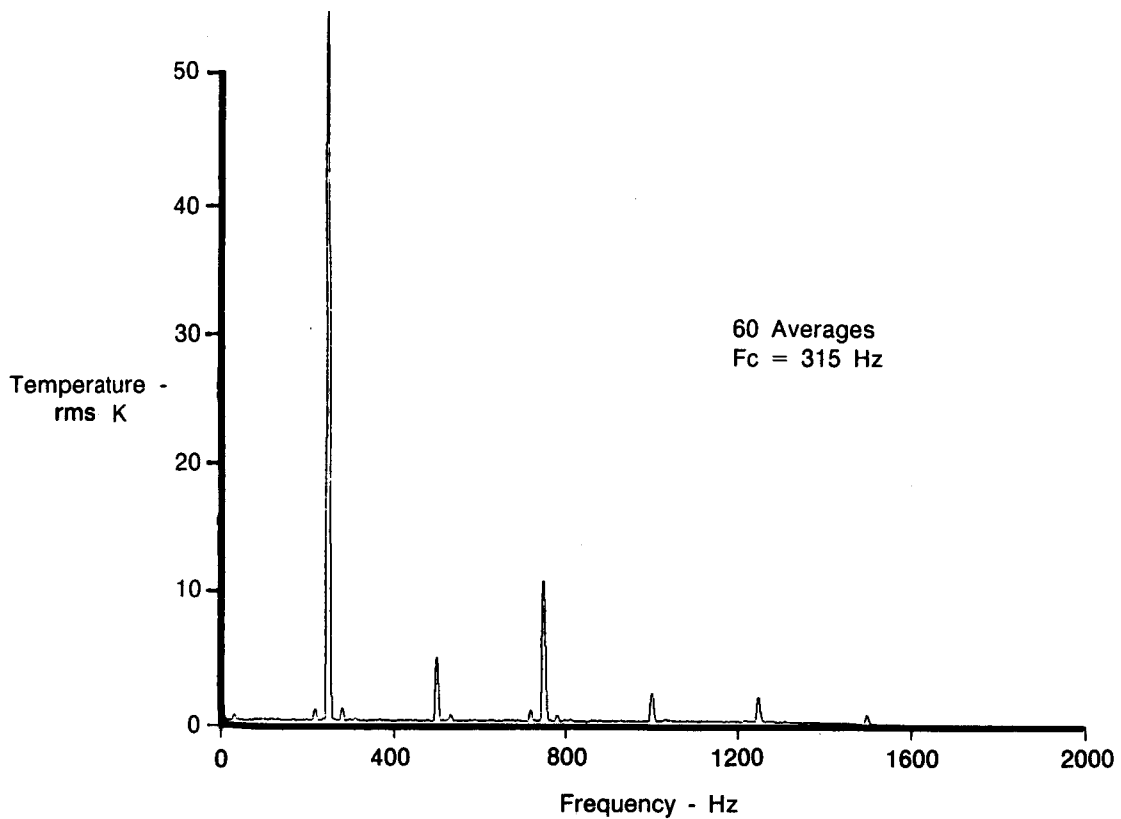
Following failure of the available quantity of 6.4 μm resistance thermometers on the first test point (250 Hz), a 9 μm resistance thermometer was used to provide backup data in conjunction with the dual thermocouple probe. Data were acquired at a variety of test points at fundamental frequencies from 20 to 250 Hz. The 9 μm resistance thermometer data were processed at the 20 and 250 Hz test points. These data were used to evaluate the validity of using a compensation spectrum for the 76 μm thermocouple derived from the 20 Hz test point to correct data at the 250 Hz test point. As seen in Figures 44 and 45, the amplitude of the fundamental frequency at 250 Hz was about 54.5K rms and at 20 Hz it was about 70.9K rms. This represents about a 23 percent change in the level of temperature fluctuations. Figures 24 and 46 depict the instantaneous velocity fluctuations measured with a hot wire anemometer. The velocity fluctuations were about 13.5 m/sec p-p at the 20 Hz and 10.5 m/sec at the 250 Hz test point about a mean velocity of approximately 107 $\mu\text{m}/\text{sec}$ (both test points).



FD 312841

Figure 44. Rotating Wheel Experiment: Narrow Band Frequency Spectrum for the Compensated 9 μm (0.00035 Inch) Resistance Thermometer at the 20 Hz Test Point

The differences in the test conditions at 20 Hz and 250 Hz are probably of little consequence in the test results. However, the inability to measure the compensation spectrum from the 250 Hz test point data is considered to be a drawback in this experiment.



FD 312842

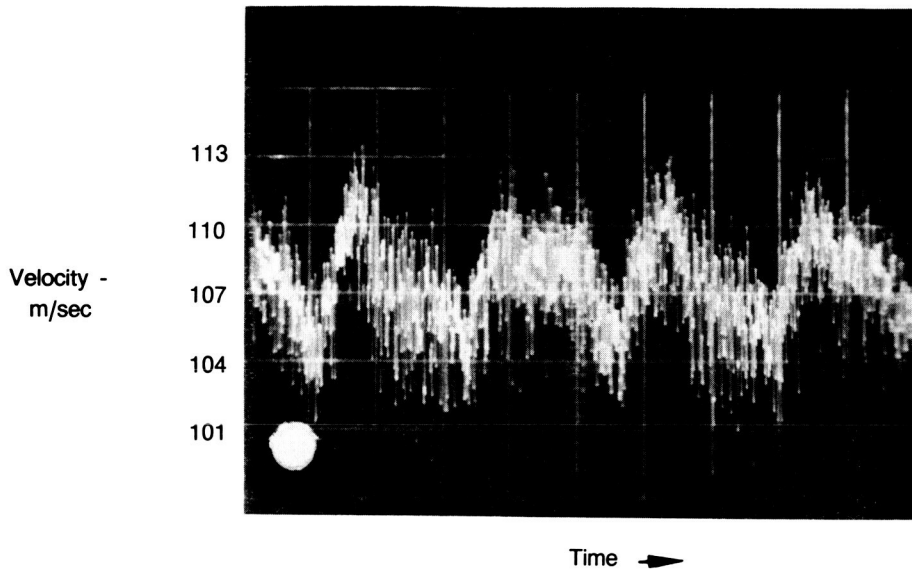
Figure 45. Rotating Wheel Experiment: Narrow Band Frequency Spectrum for the Compensated 9 μm (0.00035 Inch) Resistance Thermometer at the 250 Hz Test Point

(4) *Discussion of Results:* Overall, the results of the rotating wheel test are considered to be very good. The major source of the observed differences between the compensated 76 μm thermocouple and the 6.4 μm resistance thermometer were probably due to an error in the measurement of the thermocouple compensation spectrum (i.e., the aerodynamic parameter Γ). A potential error in the compensation of the resistance thermometer data was observed. The PSD of the compensated 9 μm sensor at 250 Hz was about 17 percent lower in amplitude than the compensated 6.4 μm data at 250 Hz. The calculated corner frequencies were 508 Hz for the 6.4 μm resistance thermometer and 315 Hz for the 9 μm .

Combustor Experiment. — The second experiment consisted of testing three thermocouple wire probes and a resistance thermometer temperature standard in an atmosphere pressure combustor as defined in Tasks 1a and 1b. In addition, an optical fiber thermometer was tested with the above probes for comparison.

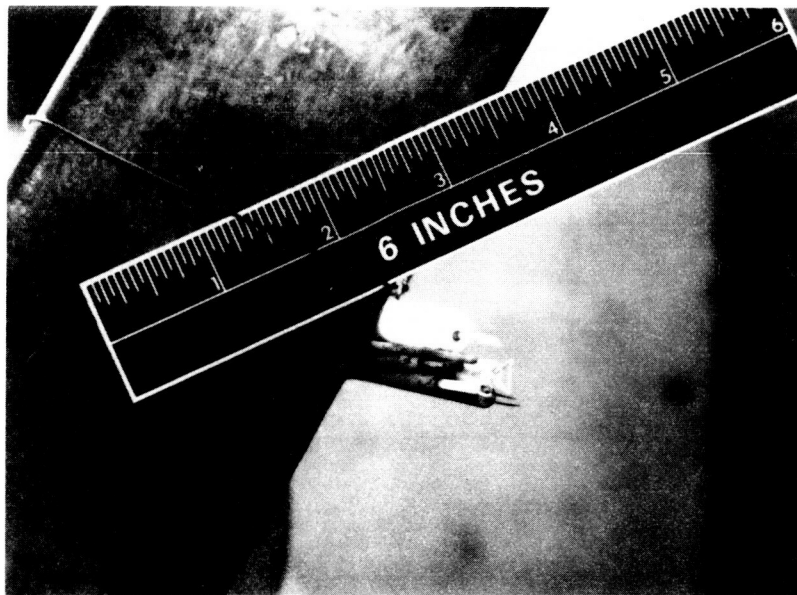
(1) *Hardware and Test Configuration:* The tests were conducted using an existing single element laboratory burner that exhausts to the atmosphere. The burner operates with JP-4 jet fuel and is normally used for high temperature studies of coatings and erosion. The burner can run at temperatures in excess of 1922K (3000°F). The final test configuration of the subscale combustor experiment is shown schematically in Figure 17. The test probes were bundled together to maximize the spatial resolution as shown in Figure 47 and then mounted and tested downstream of the combustor as shown in Figure 48.

ORIGINAL PAGE IS
OF POOR QUALITY



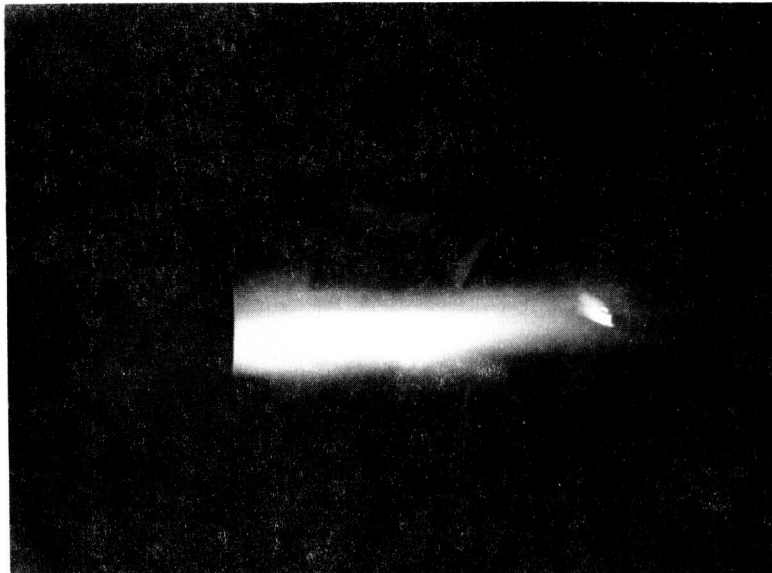
FD 312843

Figure 46. Plot of Velocity Versus Time at the 20 Hz Test Point for the Rotating Wheel Experiment



FD 316118

Figure 47. Test Probe Setup for the Subscale Combustor Experiment



FD 316117

Figure 48. Combustor Test Firing

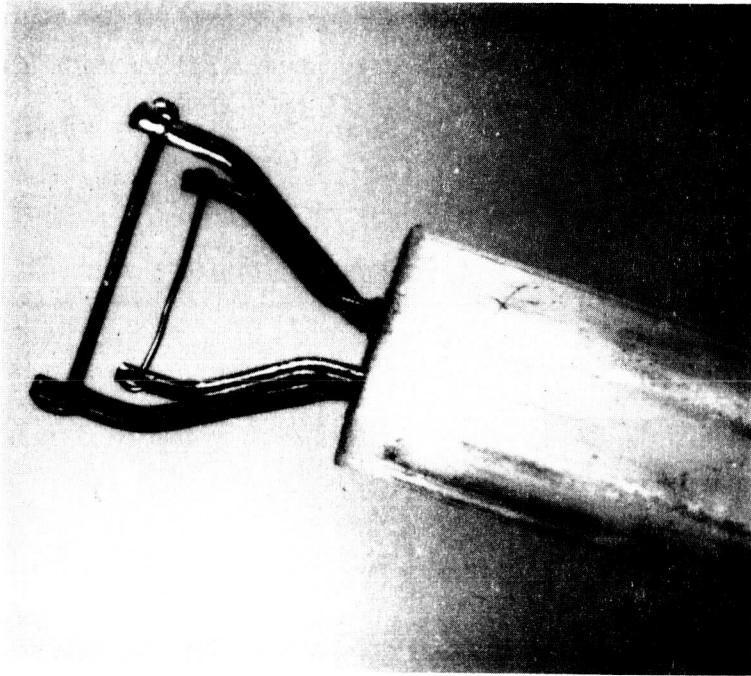
The three-wire thermocouples were fabricated by constructing a two-wire and a separate single element probe as shown in the design in Figure 15. These probes were fabricated from Type B (platinum/6 percent rhodium and platinum/30 percent rhodium) thermocouple material. The two-wire probe had a 127 μm (0.005 inch) and a 254 μm (0.010 inch) diameter element. The single wire probe had a 76 μm (0.003 inch) diameter element. The probes shown in Figure 49 were the probes that were actually tested in the burner. The probes were also pre-test inspected to define the dimensions. The results along with the print dimensions are shown in Figure 50. The inspection was made by taking calibrated photographs through a microscope and measuring the dimensions from the photograph. All of the dimensions were in quite close agreement with the print dimensions except for dimension D which is the element height from the ceramic stick. However, this is not important since the height can be adjusted by changing the relationships between the two separate assemblies.

The temperature standard probe was a commercially available TSI Model 1226 anemometer which was operated as a resistance thermometer. One probe was ordered with a 6.35 μm (0.00025 inch) platinum-iridium resistance element which is the same as used in the rotating wheel tests. However, it was felt that this element would not survive the burner environment so three additional probes were ordered with 12.7 μm (0.0005 inch) elements of the same material.

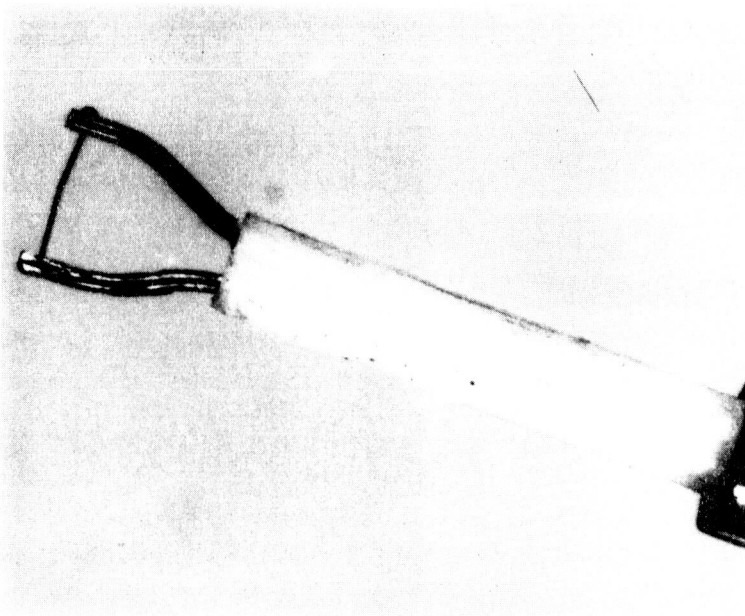
In addition, an Accufiber high temperature optical fiber thermometer sensor (shown in Figure 51) was mounted with the thermocouple and resistance thermometer probes and tested. This probe consists of a 1270 μm (0.050 inch) diameter sapphire fiber with a platinum film on the sensor tip.

ORIGINAL PAGE IS
OF POOR QUALITY

Two-Wire Assembly
as Fabricated

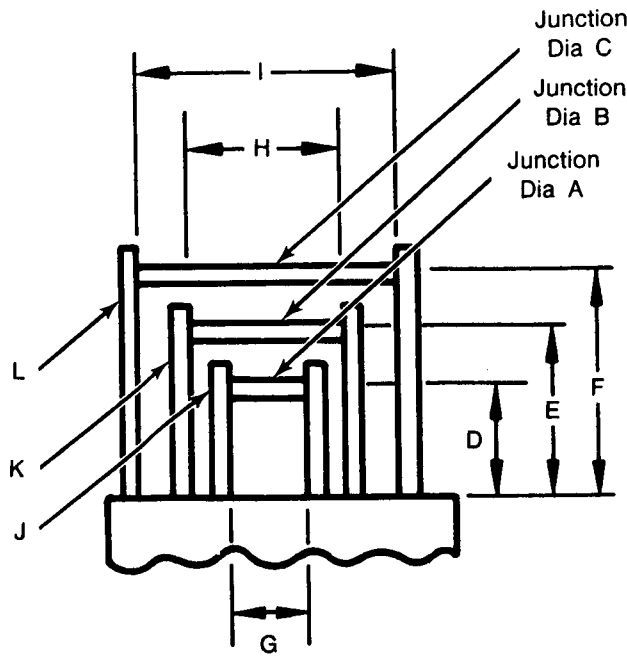


Single Wire Assembly
as Fabricated



FD 312844

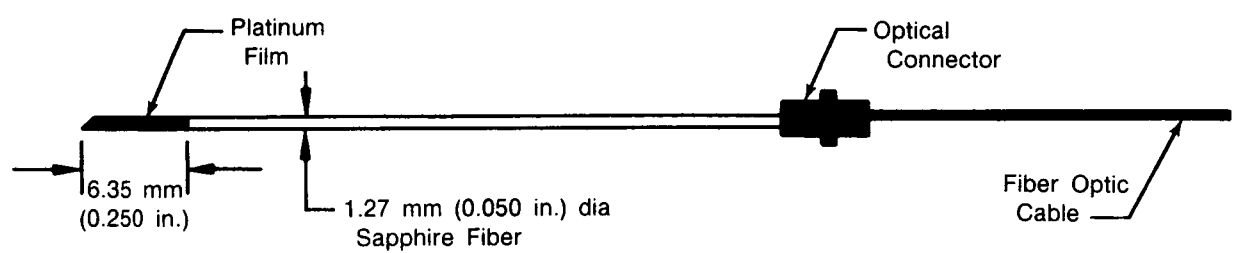
Figure 49. Thermocouple Probes for the Combustor Experiment



Dim	Print μm (in.)	Measured μm (in.)
A	76.2 (0.003)	73.2 (0.0029)
B	127 (0.005)	123.6 (0.0049)
C	254 (0.010)	249.1 (0.0098)
D	2540 (0.100)	3574 (0.1407)
E	3810 (0.150)	3709 (0.146)
F	5080 (0.200)	5055 (0.199)
G	2286 (0.090)	2591 (0.102)
H	3556 (0.140)	3556 (0.140)
I	5080 (0.200)	5131 (0.202)
J	381 (0.015)	381 (0.015)
K	381 (0.015)	381 (0.015)
L	508 (0.020)	508 (0.020)

FD 312845

Figure 50. Combustor Experiment Thermocouple Probe Pre-Test Inspection Summary



FD 312846

Figure 51. Optical Fiber Thermometer Sensor Configuration

A platinum/30 percent rhodium alloy impact tube for measuring the gas stream total pressure was also fabricated and mounted with the probes and was used to evaluate the gas stream local velocity.

The data acquisition system for these tests is shown in Figures 17 and 18. The system consists of an FM tape record system which was previously developed in Reference 1 for the two-wire thermocouples. In addition, TSI anemometer signal conditioning equipment was used and the signal was recorded on FM tape along with the thermocouples. The Accufiber system, shown in Figure 18, was a Model 310 and its signals were also recorded on FM tape.

(2) *Test Program:* The TSI Model 1226 resistance thermometers were checked out and calibrated. The two thermocouple wire probes, the resistance thermometer, the optical fiber thermometer probe, and a platinum impact tube for measuring total pressure were mounted together and positioned downstream of the combustor exit nozzle. After an initial system checkout, 11 tests were conducted as detailed in Table 10.

Test 1 was conducted without the combustor flowing. Data on each channel were recorded on FM tape to establish the background noise signal levels. Test 2 was run with the 6.35 μm (0.00025 inch) resistance thermometer but the element failed prior to insertion into the combustor flow and no FM tape data were recorded. Test 3 consisted of trying again using the larger 12.7 μm (0.0005 inch) resistance thermometer with the combustor conditions set at 1114K (1545°F); however, the resistance element failed at insertion in the flow and no data were again recorded. Test 4 was a repeat of Test 3 and again the resistance element failed. Two minutes of three-wire thermocouple data were recorded. The probes were re-oriented to minimize the spatial size and shading and mounted on the edge of the combustor flow stream for Test 5 where the temperature was 742K (876°F). In addition, the combustor flow rate settings and conditions were changed to reduce the flow velocities. The test was successful with the resistance element surviving and two minutes of FM tape data recorded. For Test 6 the probes were positioned into the center of the combustor flow and the temperatures increased to the desired level of 1159K (1626°F). The resistance element survived for one minute before failing. FM tape data were recorded for all the probes and were used in all the remaining analyses. All of the remaining tests were conducted without a 12.7 μm (0.0005 inch) resistance thermometer since all of these had failed. The remaining tests were conducted at higher temperatures to obtain additional data on the three-wire thermocouples and the optical fiber thermometer probe.

(3) *Data Analyses:* Test point 6 (mean temperature 1159K) and 8 (mean temperature 1655K) were selected for analysis. Ambient events with the burner off and the signal conditioning amplifier gains set to correspond to test run values were processed to establish the SNRs.

The 76 μm (0.003 inch) thermocouple data were compared with the 12.7 μm (0.0005 inch) resistance thermometer at test point 6 and with the 127 μm (0.005 inch) thermocouple at test points 6 and 8. All available resistance thermometer sensors failed prior to the 1655K test point. The 254 μm (0.010 inch) thermocouple was only used in conjunction with the 76 μm thermocouple to obtain an in situ measurement of the aerodynamic parameter Γ for possible use in calculating the compensation spectrum. The combination of 76 μm and 127 μm thermocouples were also used to measure Γ at each test point. The values of Γ measured by the two separate combinations of thermocouples only differed by about 1.2 percent. Differences in the resulting compensation spectra were negligible. All compensated thermocouple data presented in this report were based on Γ values measured from the 76 μm and 127 μm combination.

At each test point, an approximation of the corner frequency for each thermocouple was calculated based on the specific operating conditions outlined below.

- Calculate mean gas velocity as follows:
 - From the total pressure sensor and atmospheric pressure readings calculate mean Mach No.:

$$M = \frac{2 \left[\left(\frac{P_T}{P_s} \right)^{\frac{k-1}{k}} - 1 \right]}{(k-1)} \quad (6)$$

and $V = Mc$

Where: k = Combustor gas ratio of specific heats
 P_T = Combustor gas total pressure
 P_s = Combustor gas static pressure
 c = Combustor gas sonic velocity.

- Calculate local thermocouple wire heat transfer film coefficient:

- Calculate local Reynold's number:

$$Re = \frac{\rho V D}{\mu} \quad (7)$$

Where: ρ = Combustor gas density
 V = Combustor gas velocity
 D = Thermocouple wire diameter
 μ = Combustor gas viscosity.

- Calculate film coefficient using the Hilpert correlation for a cylinder in cross flow:

$$h = 0.615 Re^{0.466} \frac{k}{D} \quad (8)$$

Where: k = Combustor gas thermal conductivity.

- Calculate first order thermocouple time constant:

$$\tau = \frac{\rho_w C_{pw} VOL}{h A} \quad (9)$$

Where: ρ_w = Thermocouple wire density
 C_{pw} = Thermocouple wire specific heat
 VOL = Thermocouple wire junction volume
 A = Thermocouple wire junction surface area.

- Calculate corner frequency:

$$F_c = \frac{1}{2\pi\tau} \quad (10)$$

Estimated values of the thermocouple corner frequencies for both test points are presented in Table 11. The measured values of Γ were extracted from data analyzed over the 6 Hz to 10 Hz bandwidth at the 1159K point and 6 Hz to 12 Hz at the 1655 kHz test point. Note that the measurement of Γ was made by analysis of data within the bandwidth defined by the estimated corner frequencies of the large and small thermocouples. This meets the criteria established in the preceding rotating wheel data analysis. Table 12 lists the measured value of Γ obtained as a function of frequency and the computed average Γ used to generate the compensation spectrum. The values observed appear to increase monotonically with frequency and exhibited a significant 30 percent change over the 6 to 12 Hz bandwidth. However, this observation may simply be due to the fact that the frequencies evaluated all lie in contiguous spectral lines of the Fast Fourier Transform (FFT). Although an appropriate windowing function was used prior to performing the FFT, near spectral neighbors will influence each other (i.e., leakage effects). The spectral line

separation of the FFT analysis performed on the data processed was 2 Hz. To increase the spectral line separation for these data would require re-digitization of the data at a lower sampling frequency. Investigation into a possible frequency dependency of Γ was beyond the scope of the current contract.

TABLE 10. — COMBUSTOR EXPERIMENT TEST CONDITIONS SUMMARY

<i>Test No.</i>	<i>Test Description</i>
1	Burner conditions — No flow Recorded ambient background noise
2	6.4 μm (0.00025 in.) resistance thermometer failed prior to insertion in flow
3	Burner conditions — 1114K (1545°F) 12.7 μm (0.0005 in.) resistance thermometer (S/N 43381) failed at insertion into flow. No data recorded
4	Burner conditions — 1108K (1534°F) and 191 m/sec (625 ft/sec) 12.7 μm (0.0005 in.) resistance thermometer (S/N 43380) failed at insertion into flow. Recorded 2 minutes of three-wire thermocouple data
5	Burner conditions — 742°K (876°F) and 30.7 m/sec (101 ft/sec). Re-oriented probes to decrease spatial size and probe shading, installed 12.7 μm (0.0005 in.) resistance thermometer (S/N 43377), and positioned probes at edge of burner flow. Recorded 2 minutes of data on three-wire thermocouples, resistance thermometer, and optical fiber thermometer probe
6	Burner conditions — 1159°K (1626°F) and 123 m/sec (406 ft/sec). Positioned probes in center of burner flow and recorded 2 minutes of data on three-wire thermocouples, resistance thermometer, and optical fiber thermometer probes before resistance probes failed
7	Same conditions as Test 6 except no resistance thermometer and re-set gains on Accufiber data. Recorded three-wire thermocouples and optical fiber thermometer probes data
8	Burner conditions — 1655K (2519°F) and 205 m/sec (674 ft/sec). No resistance thermometer. Recorded two minutes of three-wire thermocouples and optical fiber thermometer probe (wideload mode)
9	Repeated Test 8 except recorded optical fiber thermometer probe in normal, but signal processor on first stage output
10	Repeated Test 8 except recorded optical fiber thermometer probe in normal, 1 kHz bandwidth
11	Repeated Test 8 except recorded optical fiber thermometer in normal hookup ratio mode

NOTE: All tests conducted using two-wire thermocouple probe S/N 2 (127 μm (0.005 in.)) and 254 μm (0.010 in.) and single thermocouple wire probe S/N 1 (76.2 μm (0.003 in.))

6745C

TABLE 11. — ESTIMATED THERMOCOUPLE CORNER FREQUENCIES —
SUBSCALE COMBUSTOR

<i>Test Point (K)</i>	<i>Thermocouple Diameter (μm)</i>	<i>Corner Frequency (Estimated) (Hz)</i>
1159	76	10.4
1159	127	2.2
1159	254	1.6
1655	76	13.5
1655	127	6.0
1655	254	2.0

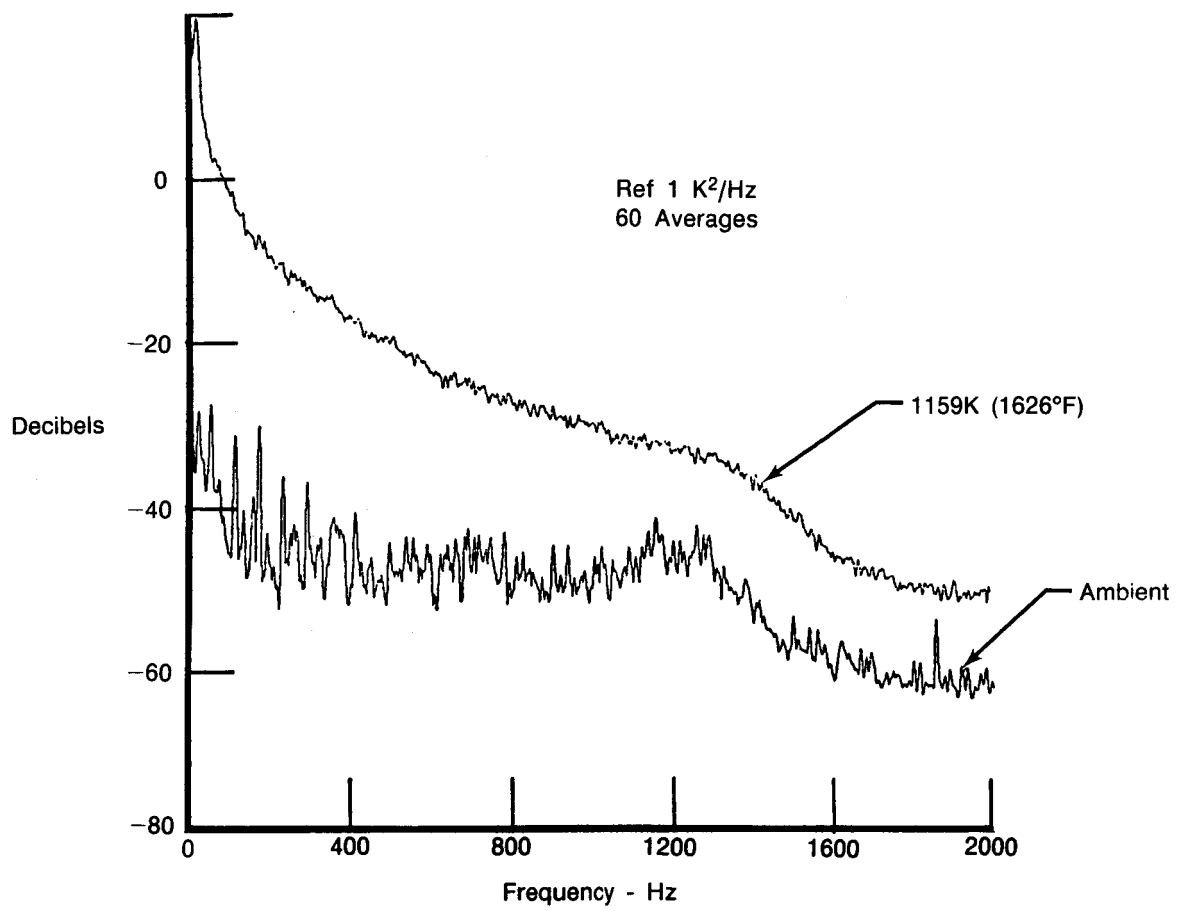
6745C

TABLE 12. — MEASURED VALUES OF Γ AS A FUNCTION OF FREQUENCY FOR COMBUSTOR EXPERIMENT

<i>Test Point (K)</i>	<i>Thermocouple</i>		<i>Measured Gamma ($m^{1.5}/sec$)</i>	<i>Average Gamma ($m^{1.5}/sec$)</i>
	<i>Combination (μm)</i>	<i>Frequency (Hz)</i>		
1159	254/76	6	7.92×10^{-6}	9.42×10^{-6}
		8	9.59×10^{-6}	
		10	10.74×10^{-6}	
1159	127/76	6	8.00×10^{-6}	9.54×10^{-6}
		8	9.71×10^{-6}	
		10	10.90×10^{-6}	
1655	127/76	6	7.32×10^{-6}	9.00×10^{-6}
		8	8.67×10^{-6}	
		10	9.64×10^{-6}	
		12	10.38×10^{-6}	

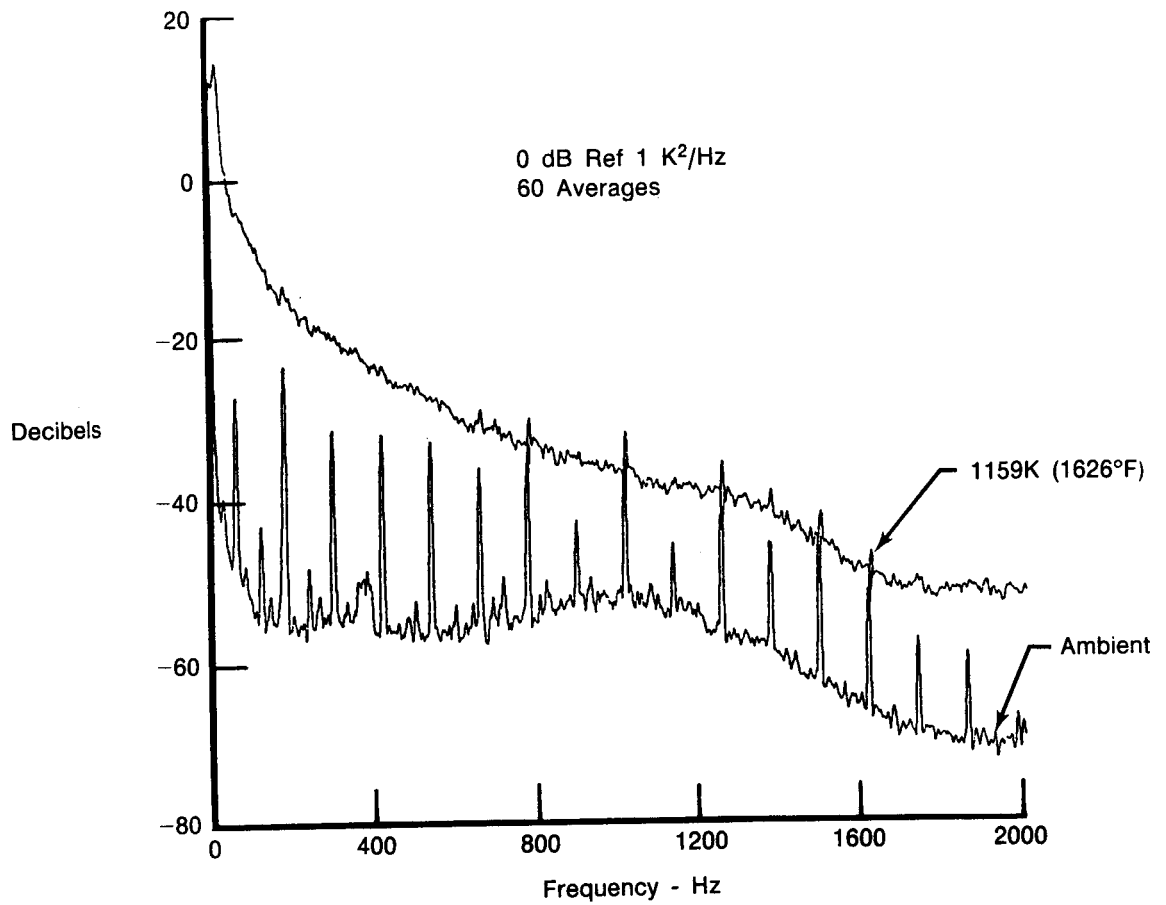
6745C

The signal to noise ratios (SNR) of the uncompensated 76 μm and 127 μm thermocouples for the 1159K test point can be determined from Figures 52 and 53 respectively. The SNRs for both the 76 μm and 127 μm thermocouples (neglecting obvious power line harmonics in the 127 μm data) varied from about 52 dB at 20 Hz to 30 dB at 250 Hz and down to 15 dB at 1000 Hz. The compensated 12.7 μm resistance thermometer SNR is depicted in Figure 54. Its SNR was considerably better than those of the thermocouples.



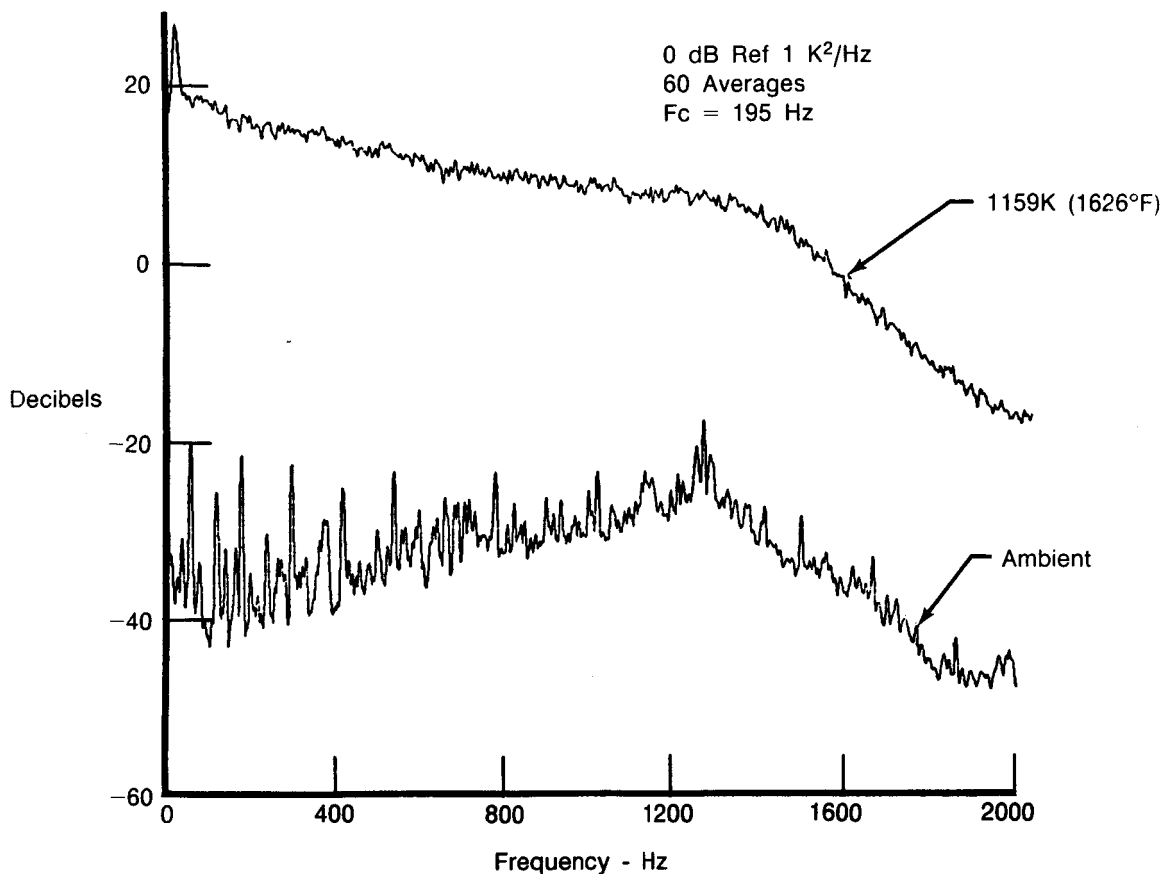
FD 312847

Figure 52. Combustor Experiment: Power Spectral Density Plots for the Uncompensated 76 μm (0.003 Inch) Thermocouple at 1159K (1626°F) and Ambient



FD 312848

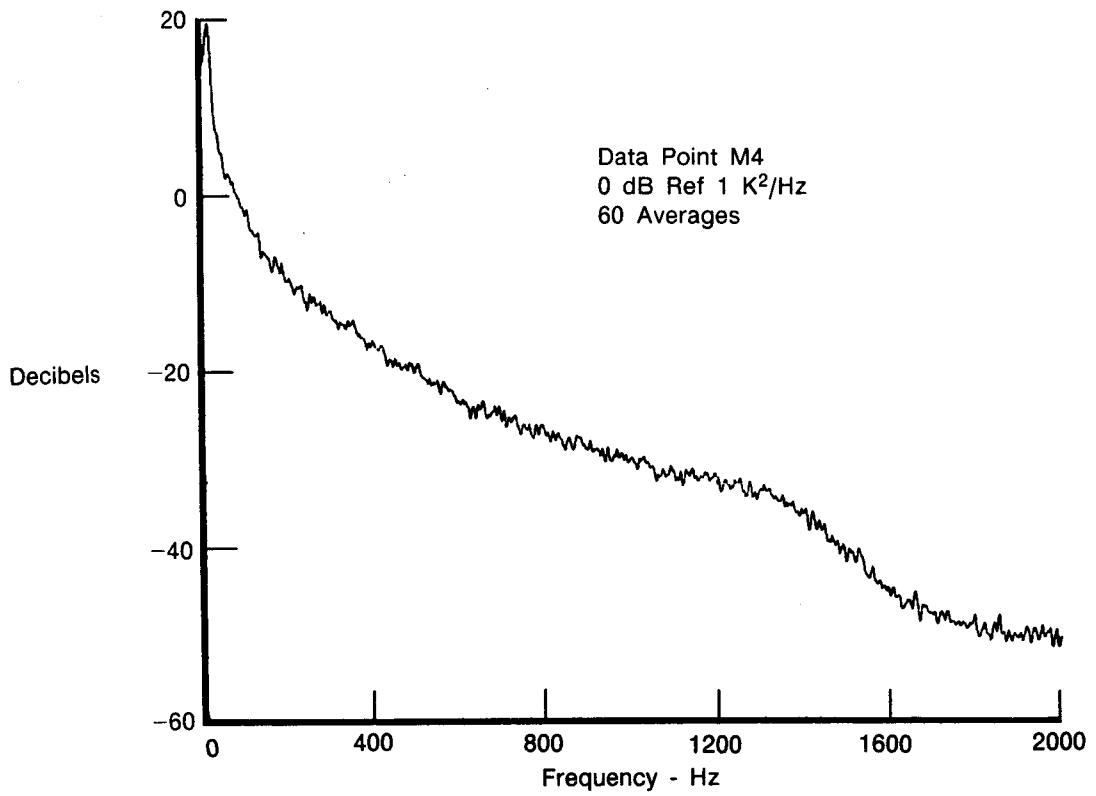
Figure 53. Combustor Experiment: Power Spectral Density Plots for the Uncompensated 127 μ m (0.005 Inch) Thermocouple at 1159K (1626°F) and Ambient



FD 312849

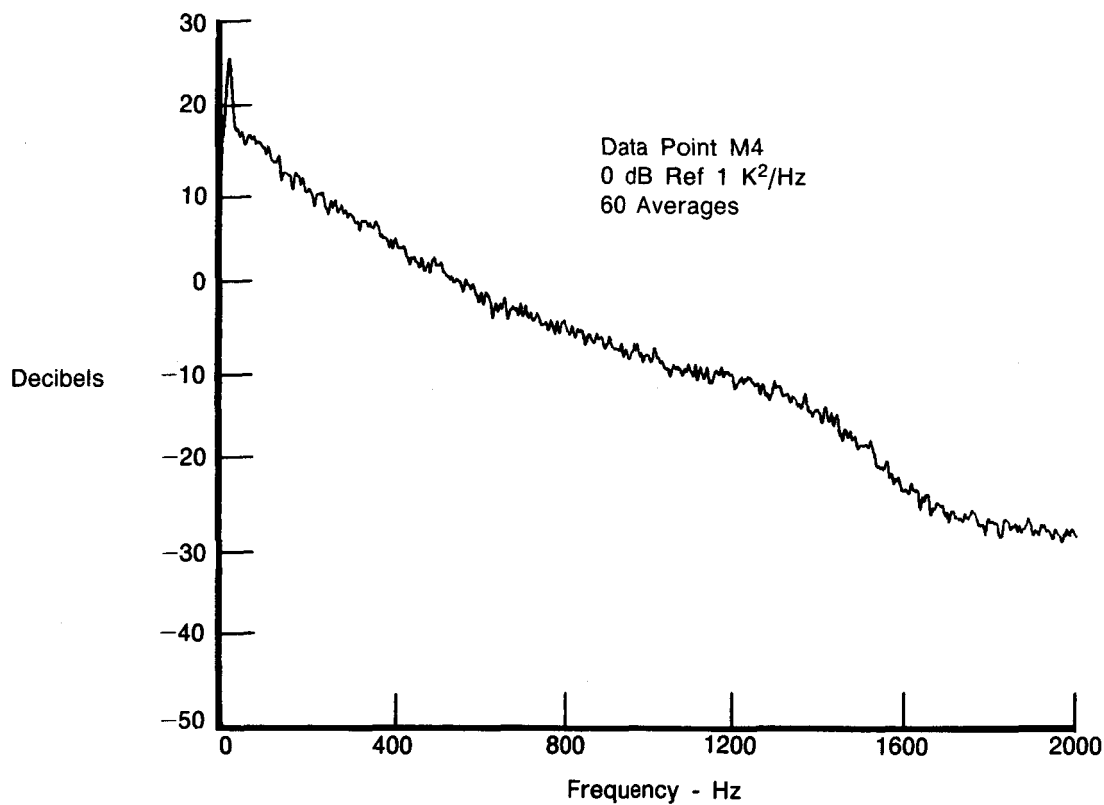
Figure 54. Combustor Experiment: Power Spectral Density Plots for the Uncompensated 12.7 μm (0.0005 Inch) Thermocouple at 1159K (1626°F) and Ambient

As seen by comparison of Figures 55 and 56, the output of the uncompensated 12.7 μm resistance thermometer at the 1159K test point was significantly larger than that of the uncompensated 76 μm thermocouple. The signals were predominantly wideband random. There is a resonance around 20 Hz which was very evident in the resistance thermometer and just discernible in the thermocouple PSD plot. The corner frequency of the resistance thermometer was 195 Hz. The 76 μm thermocouple corner frequency was about 10.4 Hz. Following compensation, their PSD plots are very similar (Figures 57 and 58). At 1000 Hz, the thermocouple output is about 3.4 dB higher than the resistance thermometer. Figures 59 and 60 depict the linear PSD plots of the compensated 76 μm thermocouple and the 12.7 μm resistance thermometer respectively and are included for ease of interpretation. The resonance around 20 Hz is about 23K rms/ $\sqrt{\text{Hz}}$.



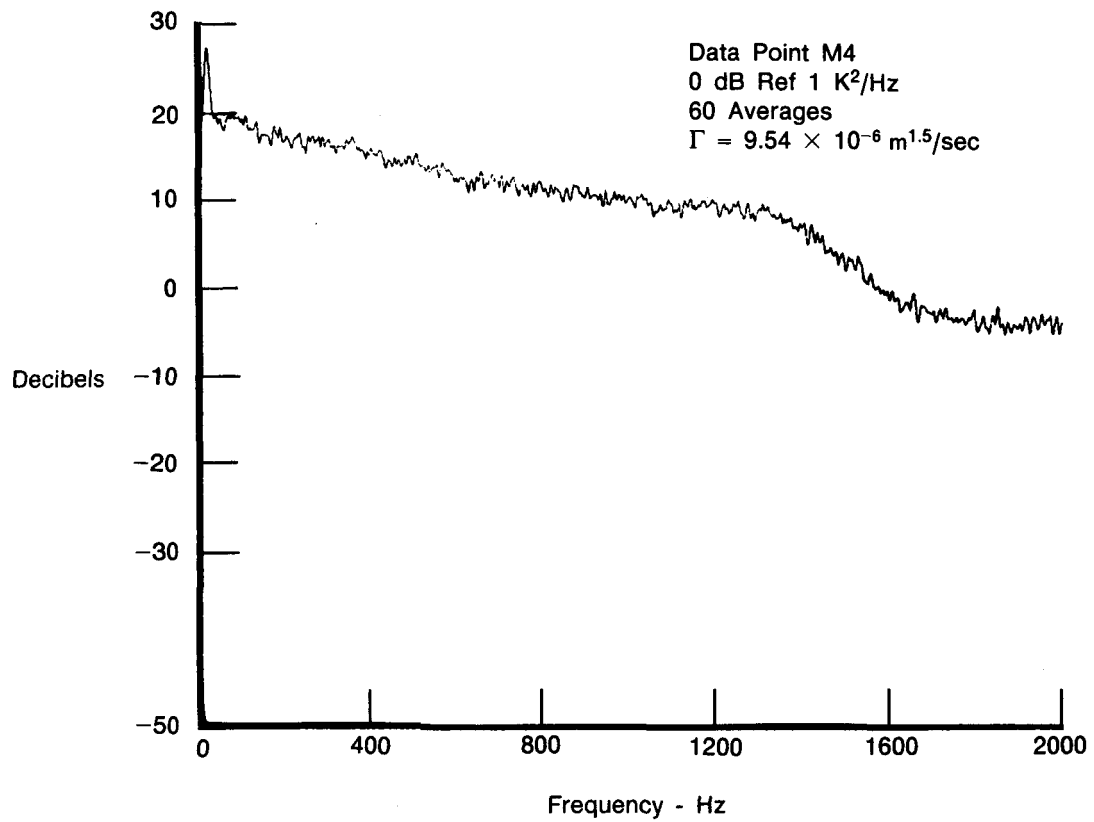
FD 312850

Figure 55. Combustor Experiment: Power Spectral Density Plot for the Uncompensated 76 μm (0.003 Inch) Thermocouple at 1159K (1626°F)



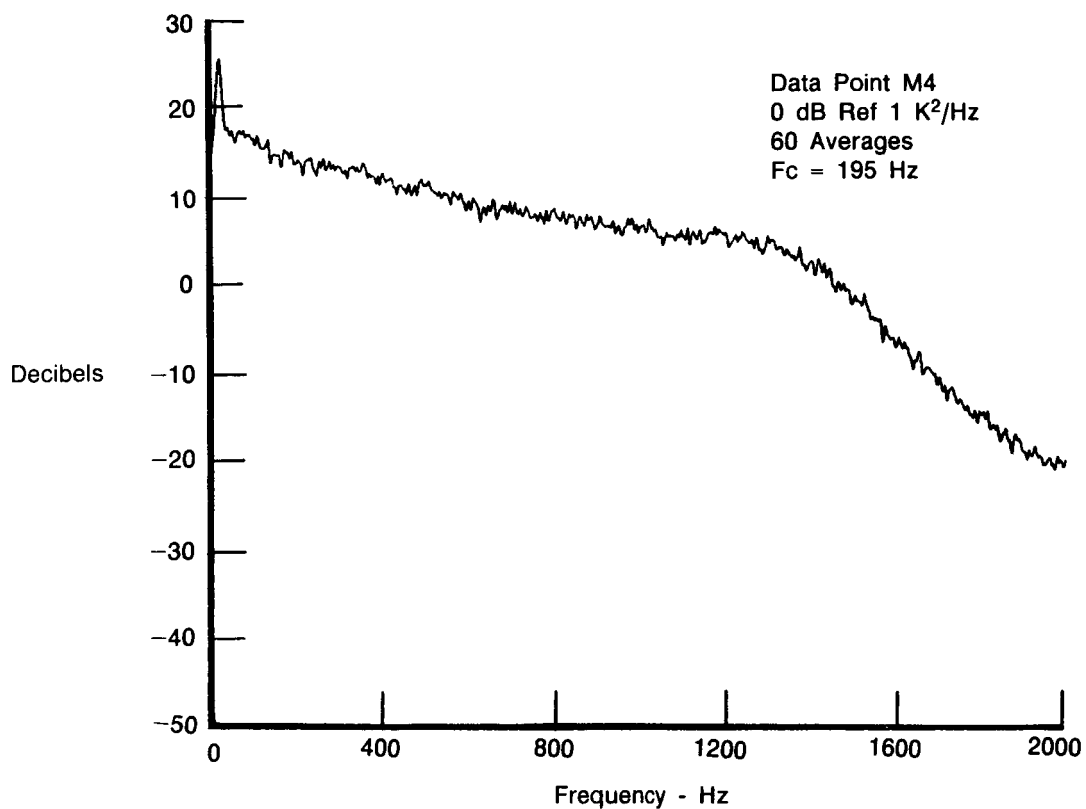
FD 316051

Figure 56. Combustor Experiment: Power Spectral Density Plot for the Uncompensated 12.7 μm (0.0005 Inch) Resistance Thermometer at 1159K (1626°F)



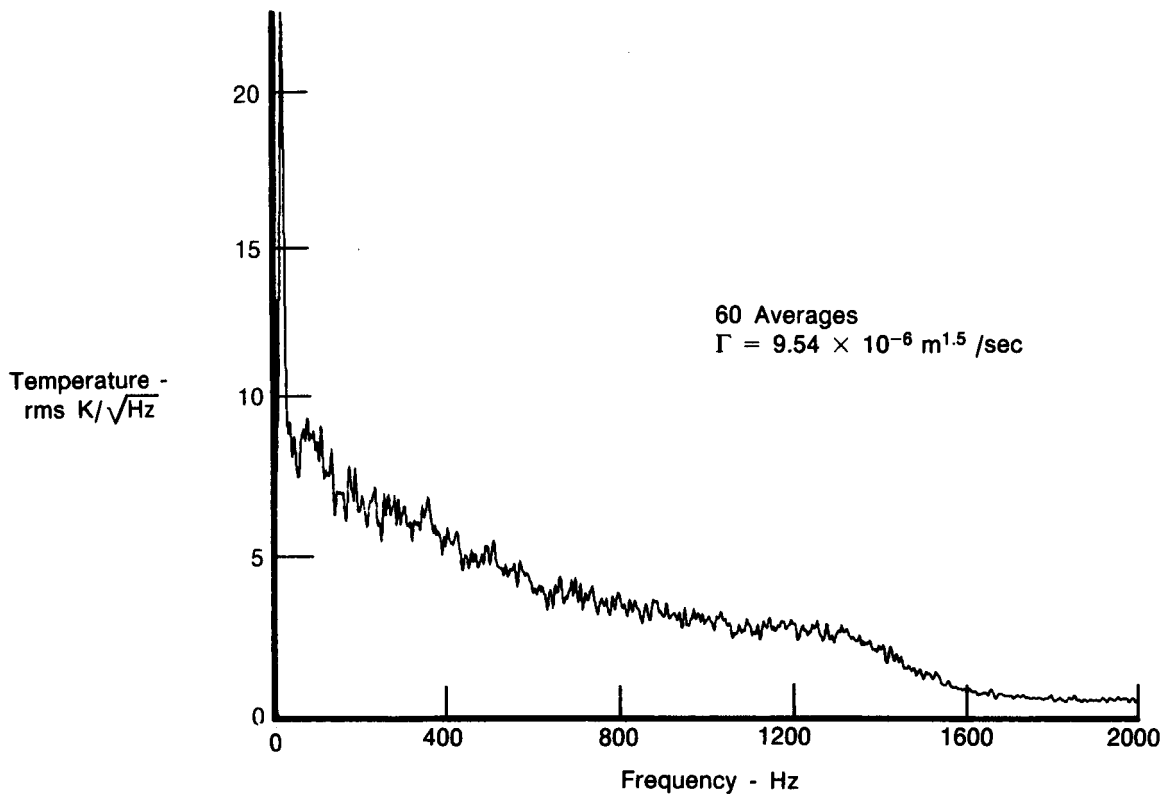
FD 316052

Figure 57. Combustor Experiment: Power Spectral Density Plot for the Compensated 76 μm (0.003 Inch) Thermocouple at 1159K (1626°)



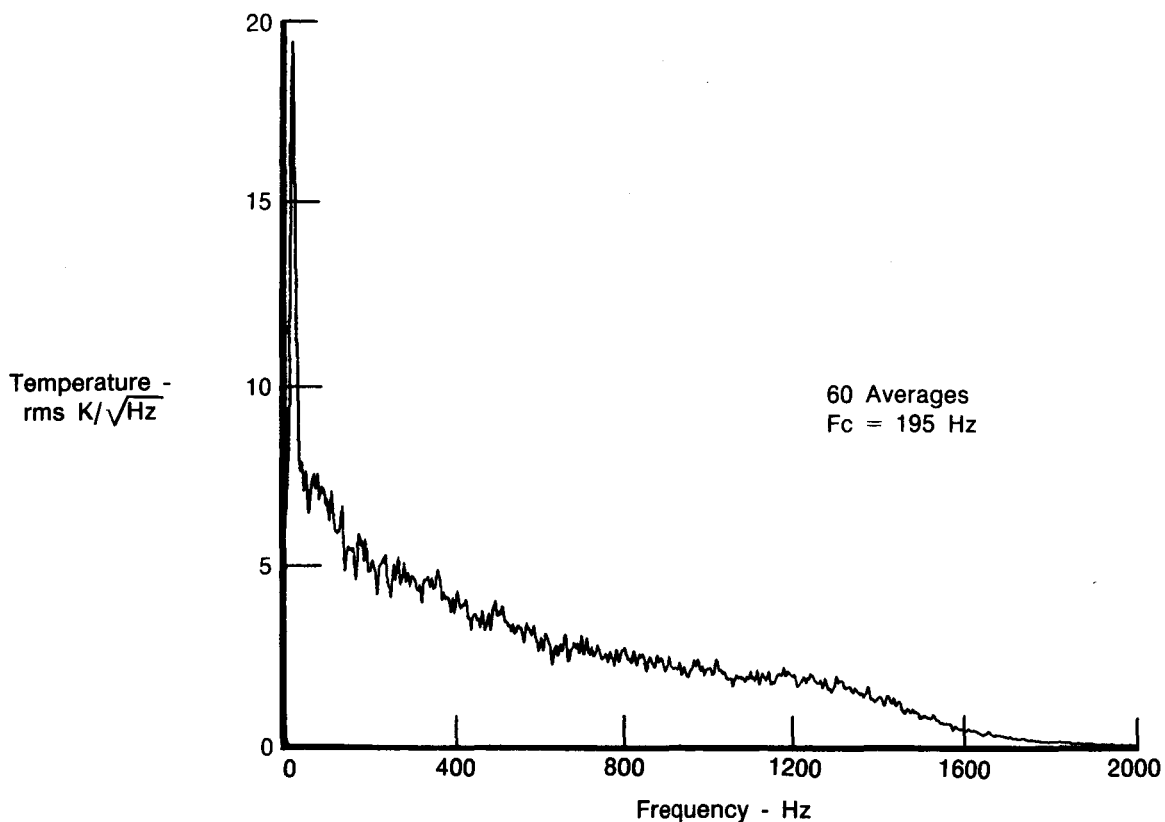
FD 316053

Figure 58. Combustor Experiment: Power Spectral Density Plot for the Compensated 12.7 μm (0.0005 Inch) Resistance Thermometer at 1159K (1626°F)



FD 316054

Figure 59. Combustor Experiment: Linear Power Spectral Density Plot for the Compensated 76 μm (0.003 Inch) Thermocouple at 1159K (1626°F)



FD 316055

Figure 60. Combustor Experiment: Linear Power Spectral Density Plot for the Compensated 12.7 μm (0.0005 inch) Resistance Thermometer at 1159K (1626°)

The amplitude of uncompensated 76 μm thermocouple PSD (Figure 55) is about 7 dB higher than the uncompensated 127 μm thermocouple output at 1000 Hz (Figure 61). The background power line harmonics are evident in the 127 μm PSD plot at frequencies above 540 Hz. Following compensation, the 127 μm and 76 μm thermocouple PSD plots (Figures 62 and 63) are almost identical (neglecting the obvious power line noise present in the 127 μm output). Note that the plot amplitude scalings for these plots are twice as sensitive as the plots used to compare the compensated 12.7 μm resistance thermometer with the 76 μm thermocouple. Neglecting the power line noise, the compensated 76 μm and 127 μm thermocouple PSDs agree within approximately 1 dB up to 1000 Hz. The compensation spectrum for the 76 μm thermocouple at the 1159K test point is given in Figure 64 and that of the 127 μm in Figure 65. Both were generated using the same value of the measured aerodynamic parameter, Γ ($9.54 \times 10^{-6} \text{ m}^{1.5}/\text{sec}$). At 1000 Hz, the compensation required was about 40 dB (i.e., a factor of 100) for the 76 μm thermocouple and about 48 dB for the 127 μm thermocouple. The resistance thermometer required about 14 dB of compensation at 1000 Hz.

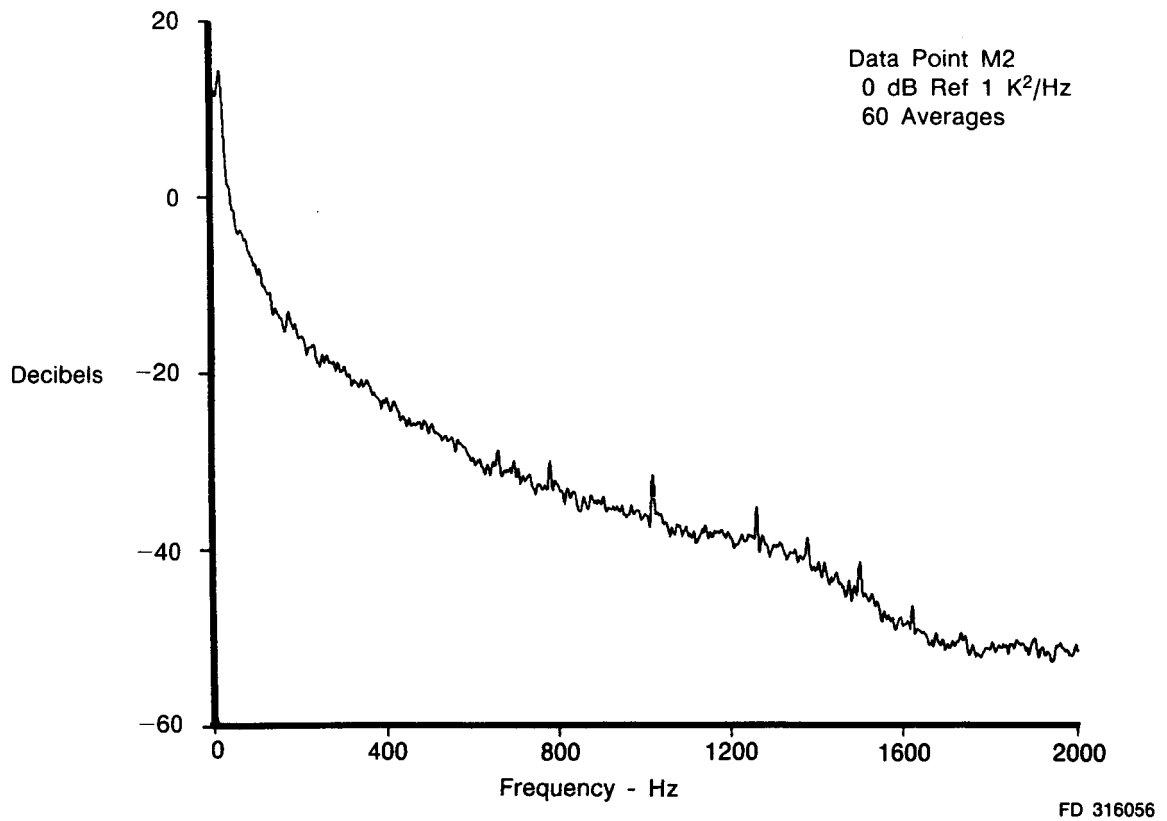
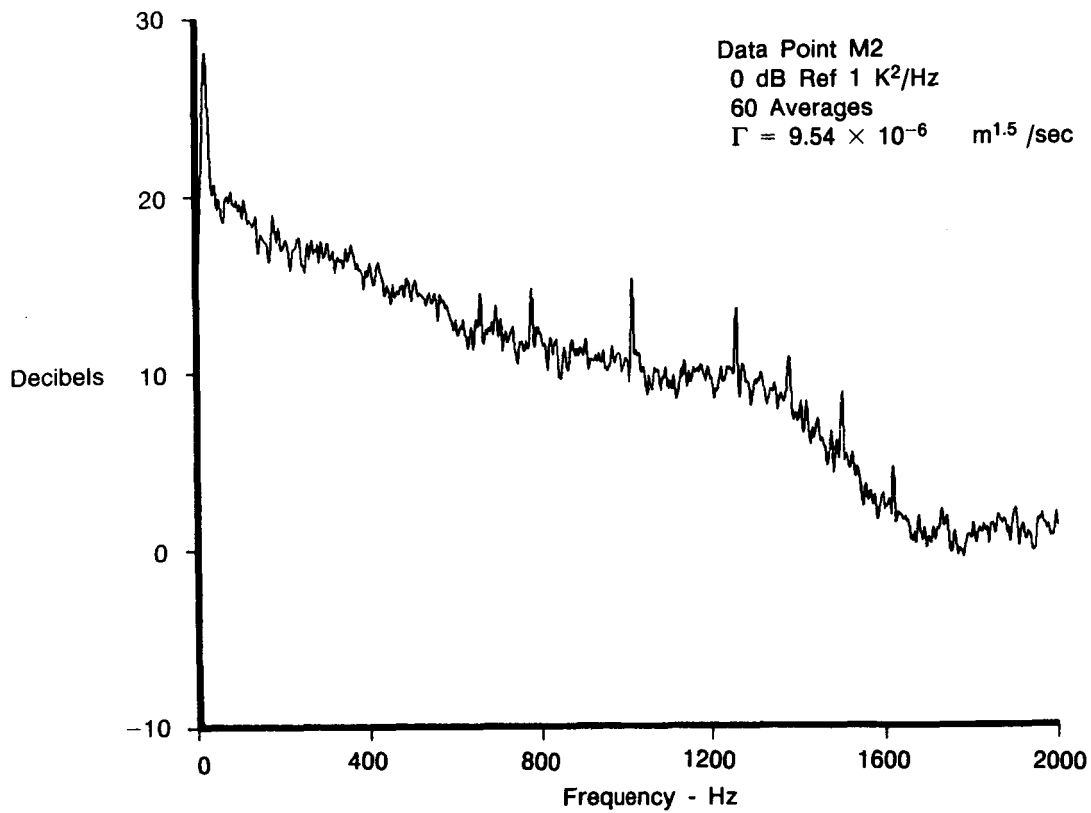
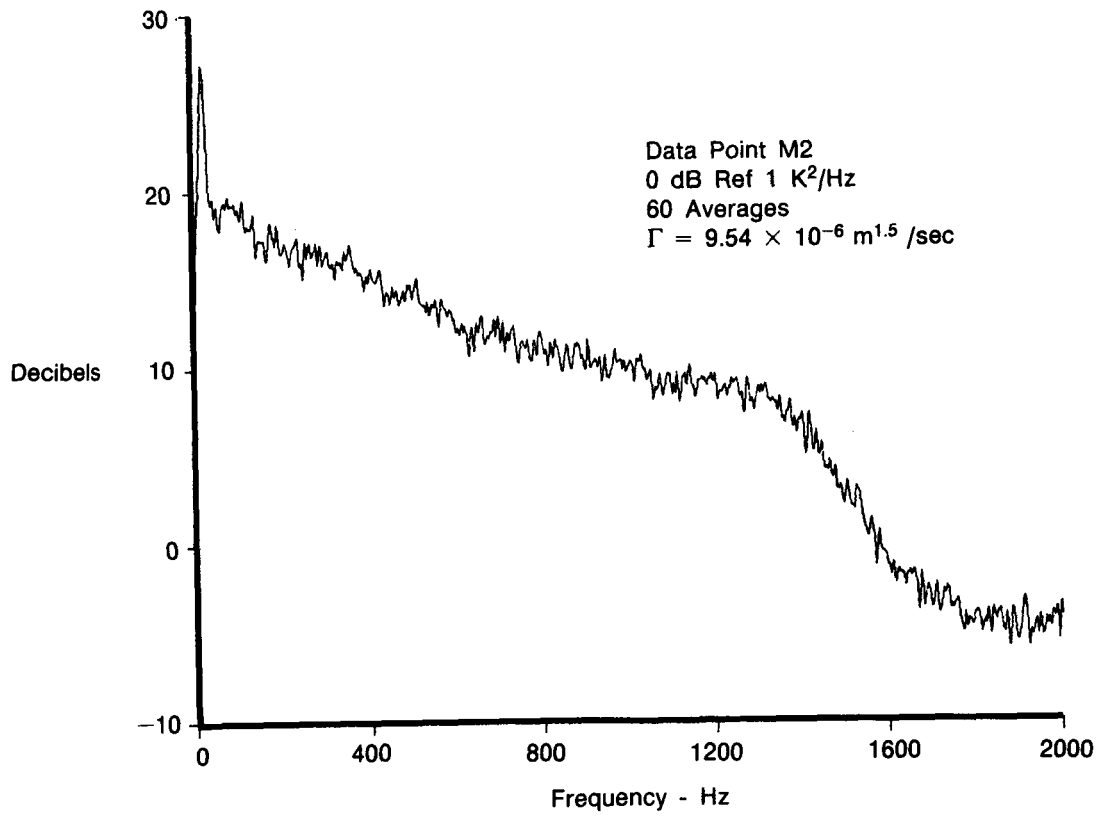


Figure 61. Combustor Experiment: Power Spectral Density Plot of the Uncompensated 12.7 μm (0.005 Inch) Thermocouple at 1159K (1626°F)



FD 316057

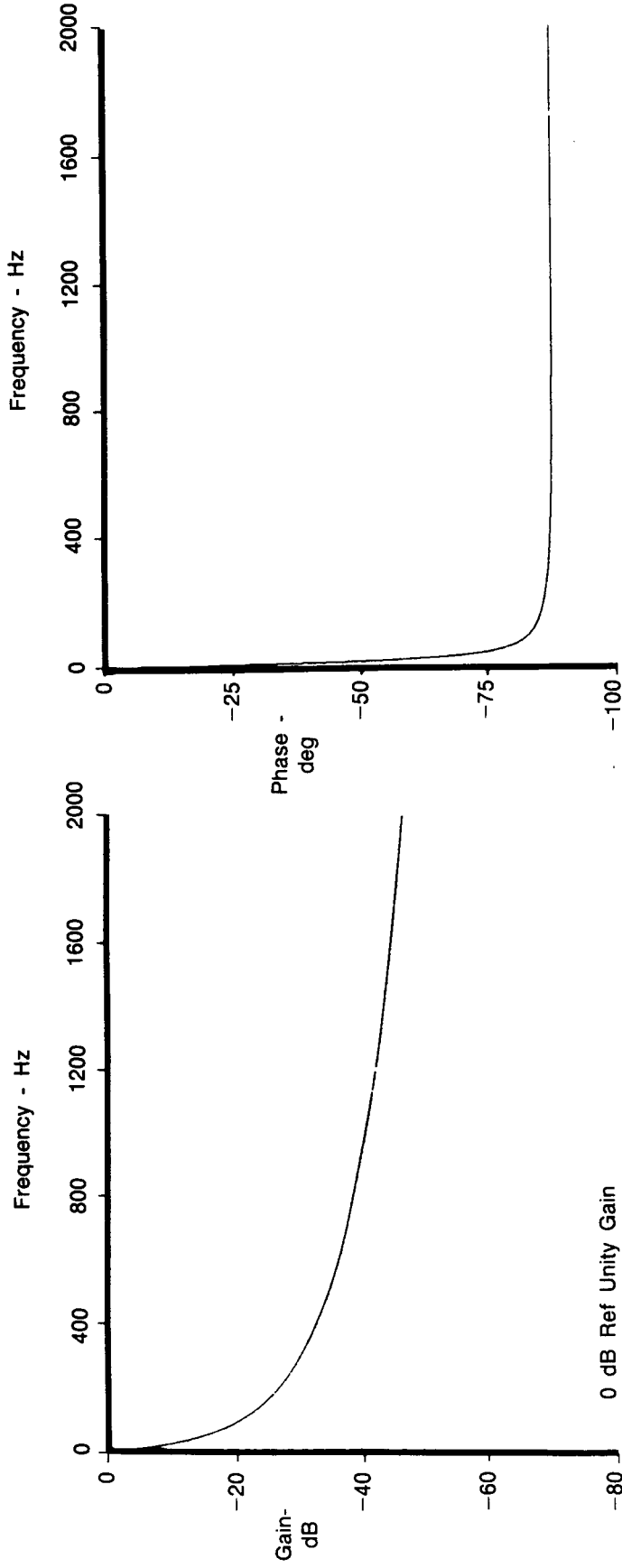
Figure 62. Combustor Experiment: Power Spectral Density Plot of the Compensated 127 μm (0.005 Inch) Thermocouple at 1159K (1626°F)



FD 316058

Figure 63. Combustor Experiment: Power Spectral Density Plot of the Compensated 76 μm (0.003 Inch) Thermocouple at 1159K (1626°F)

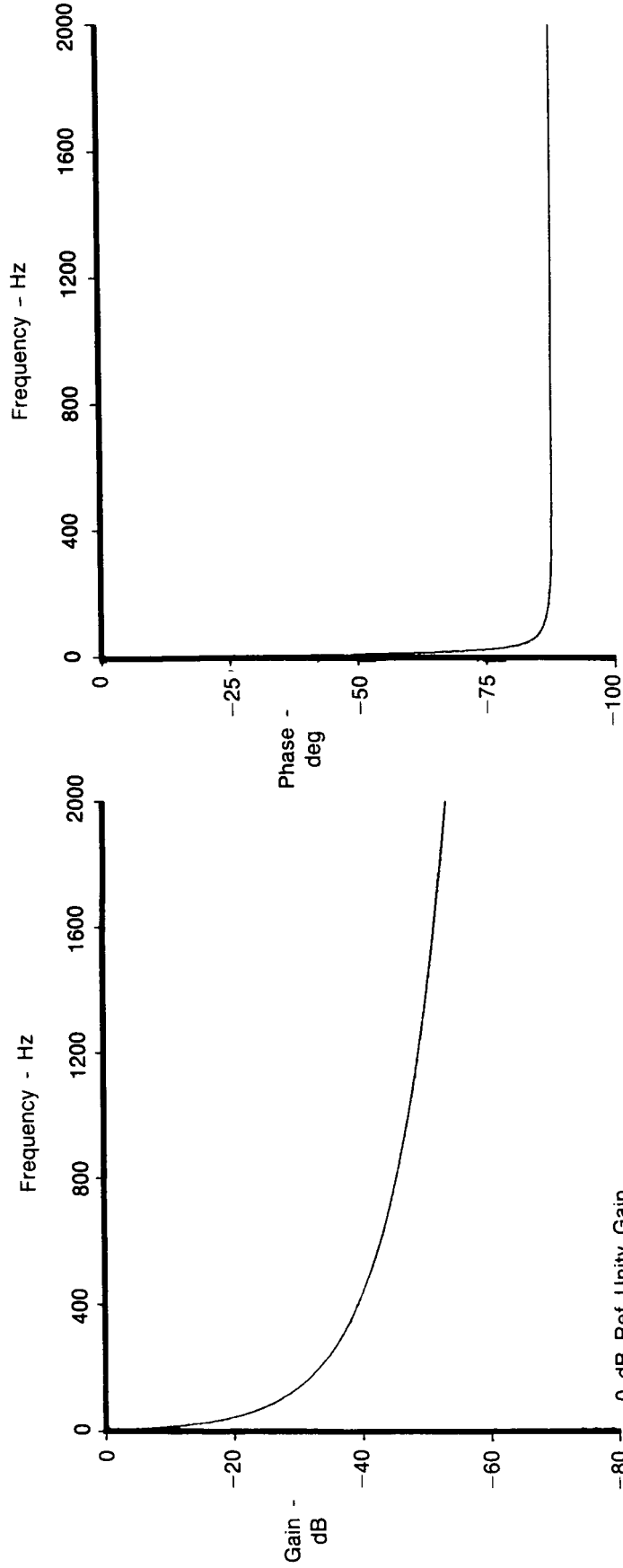
$$\Gamma = 9.54 \times 10^{-6} \text{ m}^{1.5} / \text{sec}$$



FD 316059

Figure 64. Combustor Experiment: Compensation Spectra Plot for the 76 μm (0.003 Inch) Thermocouple at 1159K (1626°F)

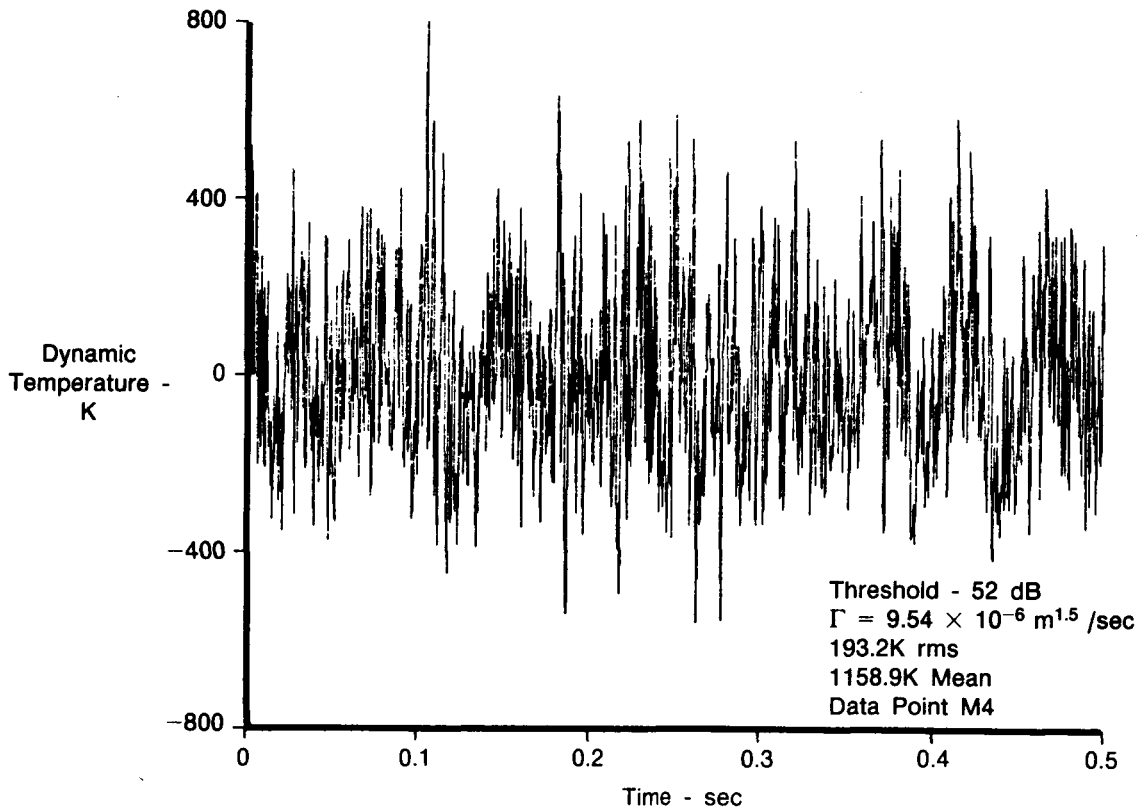
$$\Gamma = 9.54 \times 10^{-6} \text{ m}^{1.5} / \text{sec}$$



FD 316060

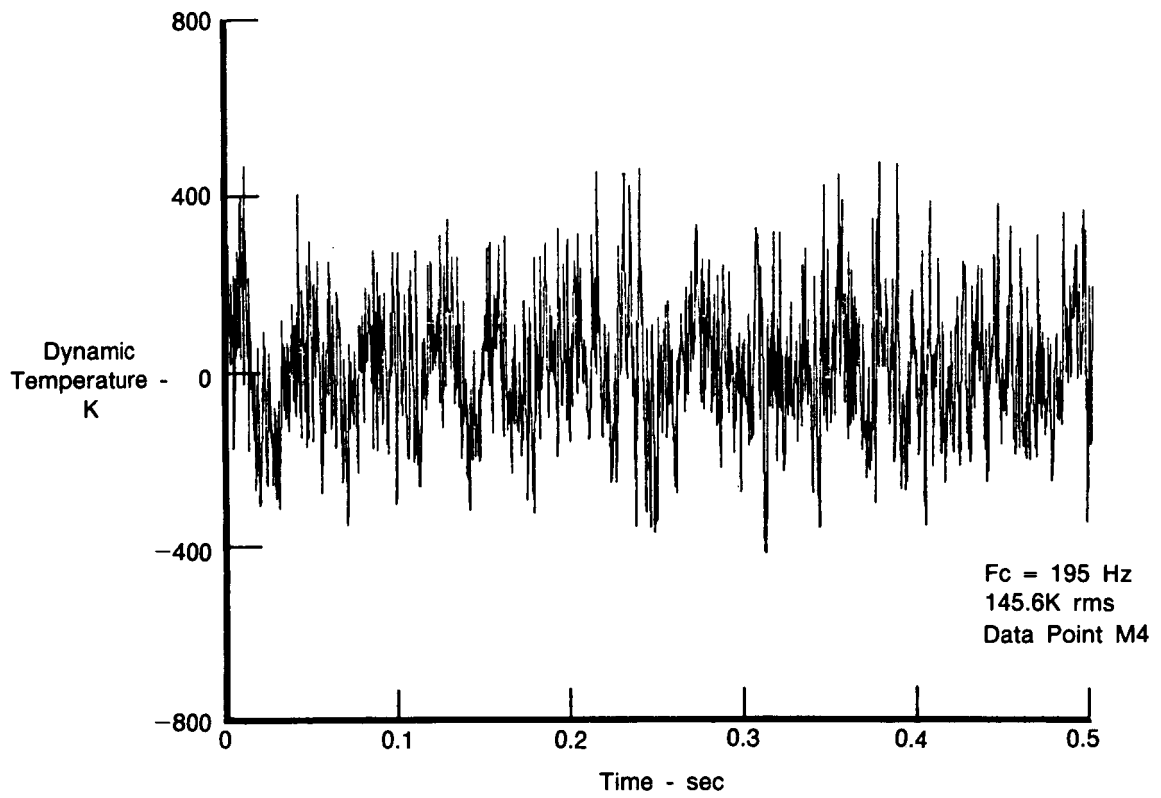
Figure 65. Combustor Experiment: Compensation Spectra Plot for the 127 μm (0.005 Inch) Thermocouple at 1159K (1626°F)

The time records of the compensated 76 μm thermocouple (Figure 66) and the 12.7 μm thermometer (Figure 67) exhibit wideband random characteristics. The overall (p-p) amplitude of the thermocouple (about 1040K p-p, 193K rms) is considerably higher than that of the resistance thermometer (about 776K p-p, 147K rms). Time $t=0$ seconds in the thermocouple plot corresponds to $t=0.125$ second for the resistance thermometer. The similarity of the two waveforms is more readily apparent in the expanded time segments depicted in Figures 68 and 69 where the start times are the same. There is inherently good time phasing between the waveforms. The primary difference is in the relative amplitudes of the various frequency components.



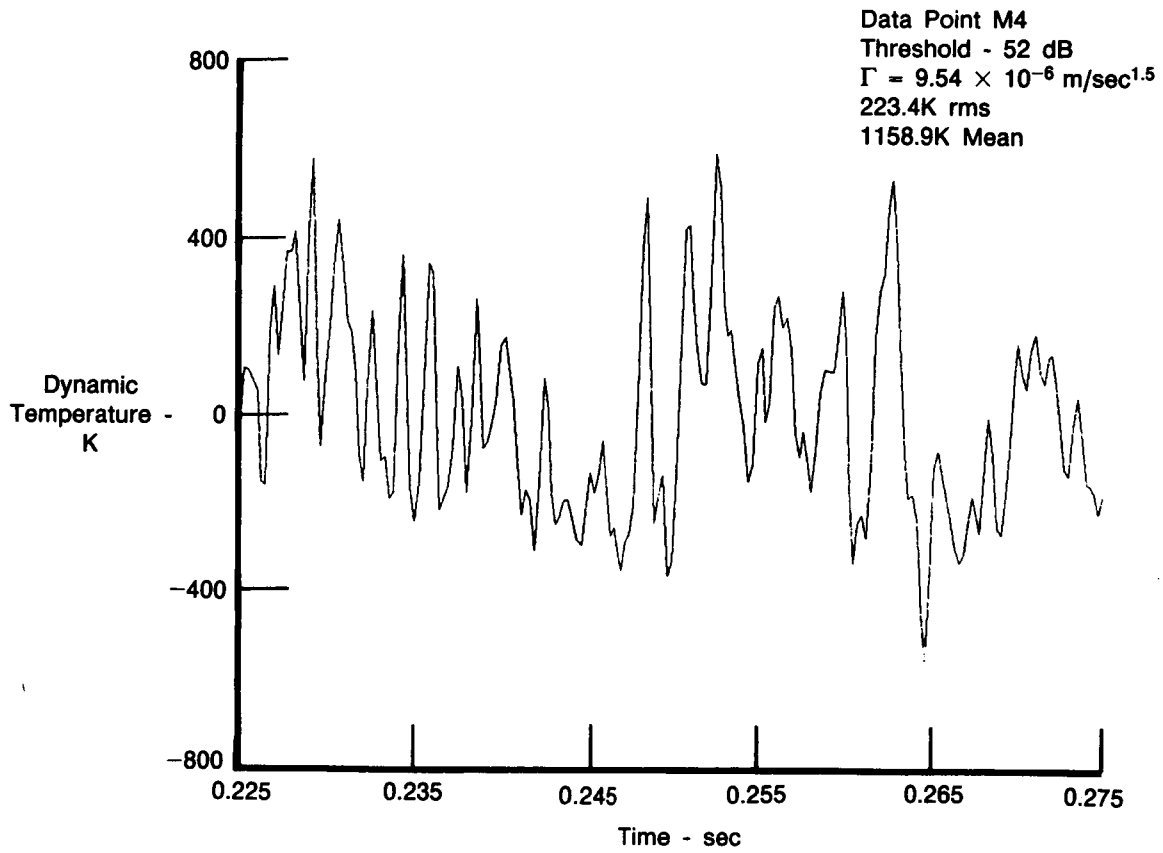
FD 316061

Figure 66. Combustor Experiment: Compensated 76 μm (0.003 Inch) Thermocouple Time Record for 1159K (1626°F)



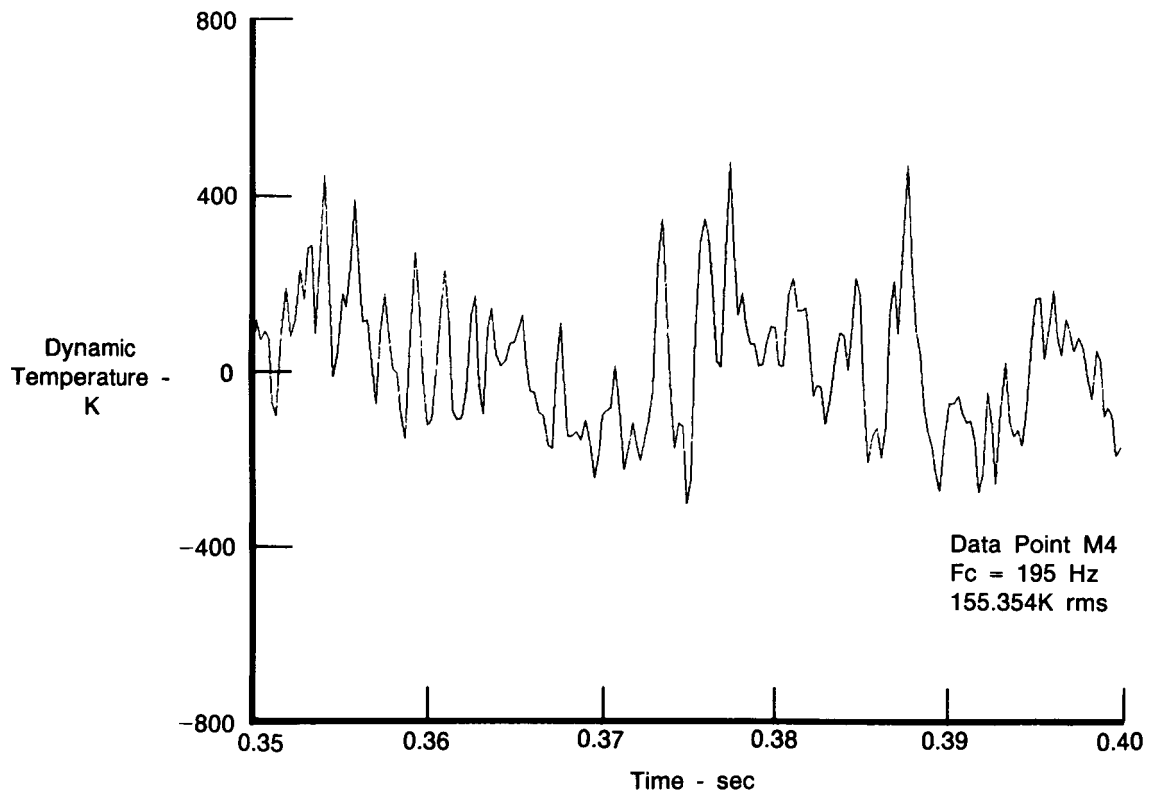
FD 316062

Figure 67. Combustor Experiment: Compensated 12.7 μm (0.0005 Inch) Resistance Thermometer Time Record for 1159K (1626°F)



FD 316063

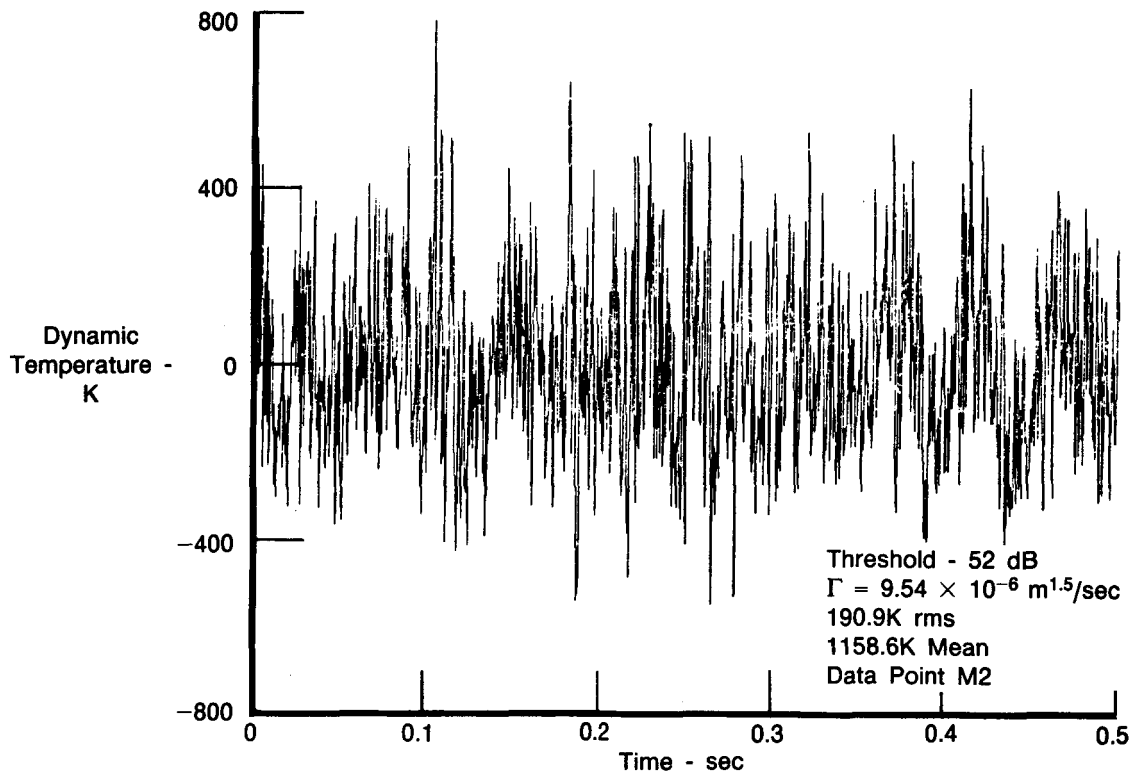
Figure 68. Combustor Experiment: Compensated $76 \mu\text{m}$ (0.003 Inch) Thermocouple Partial Time Record for 1159K (1626°F)



FD 316064

Figure 69. Combustor Experiment: Compensated 12.7 μm (0.0005 Inch) Resistance Thermometer Partial Time Record for 1159K (1626°F)

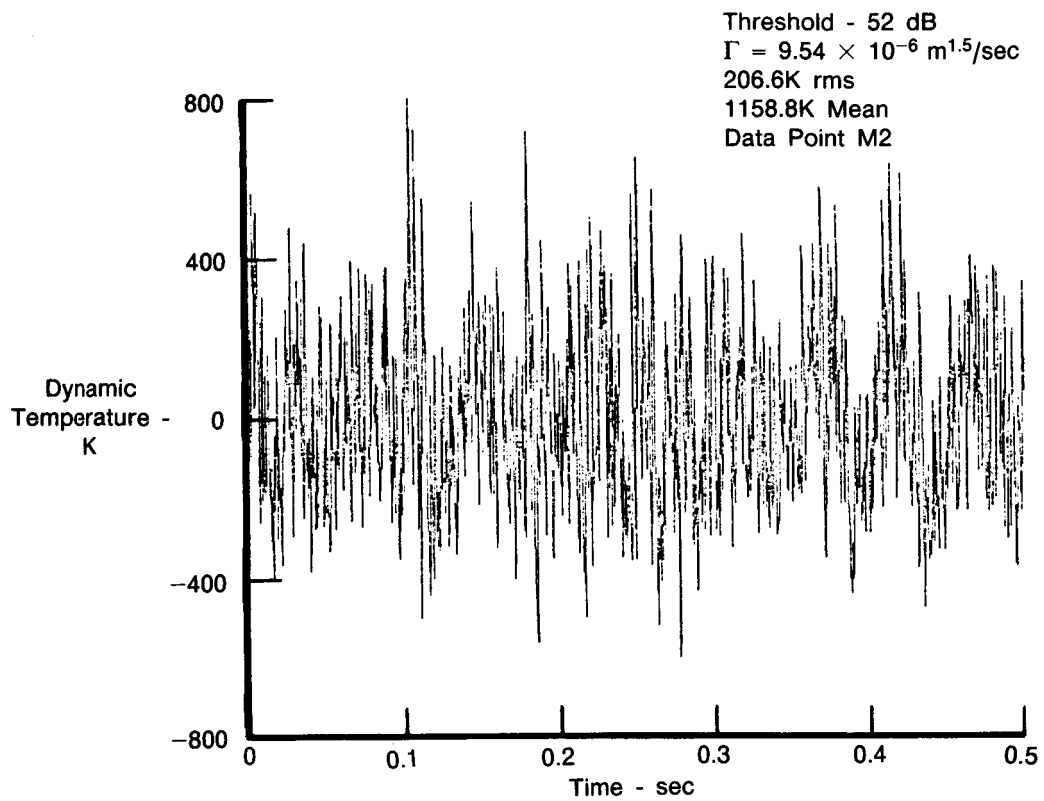
The compensated time records of the 76 μm and 127 μm thermocouples have very similar waveforms which are depicted in Figures 70 and 71. Both records have the same start time. The overall amplitude of the 76 μm thermocouple was about 1028K p-p (191K rms) and the 127 μm was about 1152K p-p (207K rms). The partial time records (Figures 72 and 73) show very good agreement. Differences are primarily at the amplitudes of the higher frequencies.



FD 316065

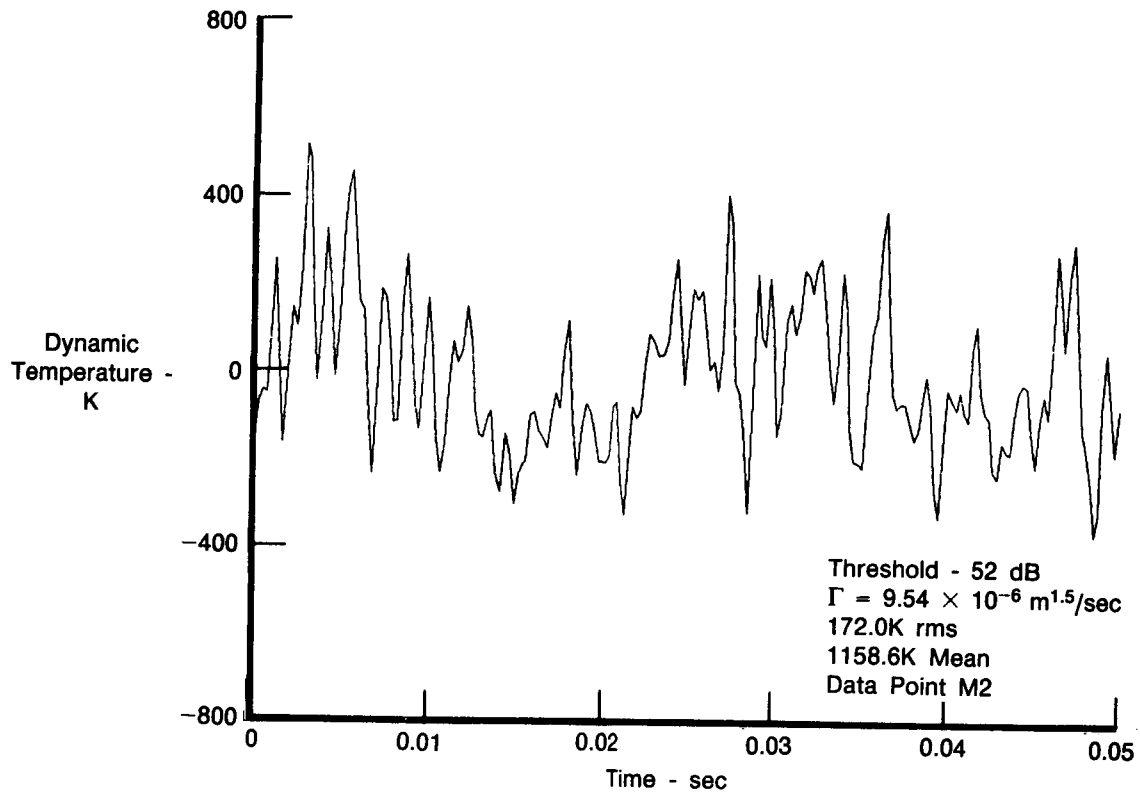
Figure 70. Combustor Experiment: Compensated 76 μm (0.003 Inch) Thermocouple Time Record for 1159K (1626°F)

At the 1655K test point, no resistance thermometer data were available (all sensors had failed). Results of comparing the 76 μm and 127 μm thermocouple data were very similar to those obtained for the 1159K test point discussed above. Overall, the rms values of flowpath dynamic temperature fluctuations increased about 40 percent with the low frequency resonance being less pronounced. The SNR of the data signals improved slightly (3 to 4 dB) to about 17 dB at 1 kHz. The uncompensated 76 μm signal (Figure 74) was about 7 dB higher than the uncompensated 127 μm thermocouple (Figure 75). Following compensation, their PSD plots (Figures 76 and 77) are very similar out beyond 1000 Hz. The measured aerodynamic parameter gamma was slightly lower at the 1655K test point than at 1159K ($\gamma 9.00 \times 10^{-6} \text{ m}^{1.5}/\text{sec}$). This indicates a slightly higher thermocouple frequency response at the 1655K point. The compensation spectra for the 76 μm and 127 μm thermocouples are depicted in Figures 78 and 79. The compensated dynamic temperature time waveforms exhibit very similar characteristics over the entire record length (Figures 80 and 81) and the expanded time segment (Figures 82 and 83).



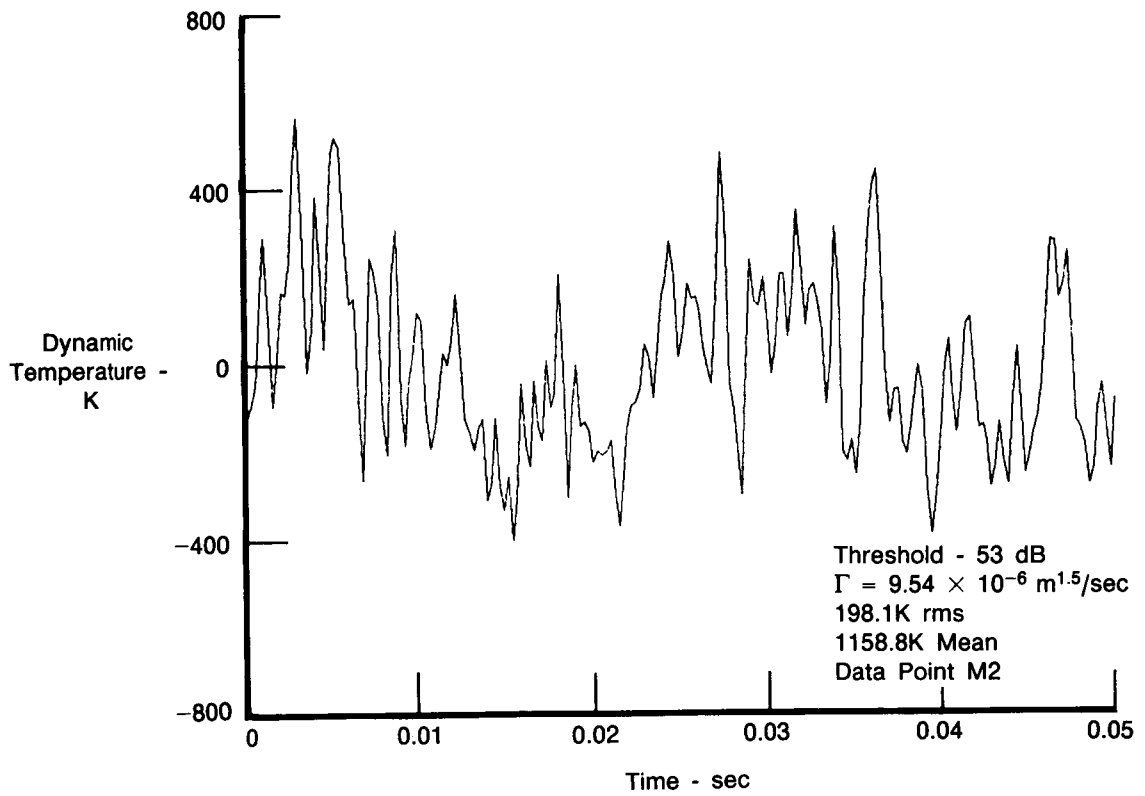
FD 316066

Figure 71. Combustor Experiment: Compensated 127 μm (0.005 Inch) Thermocouple Time Record for 1159K (1626°F)



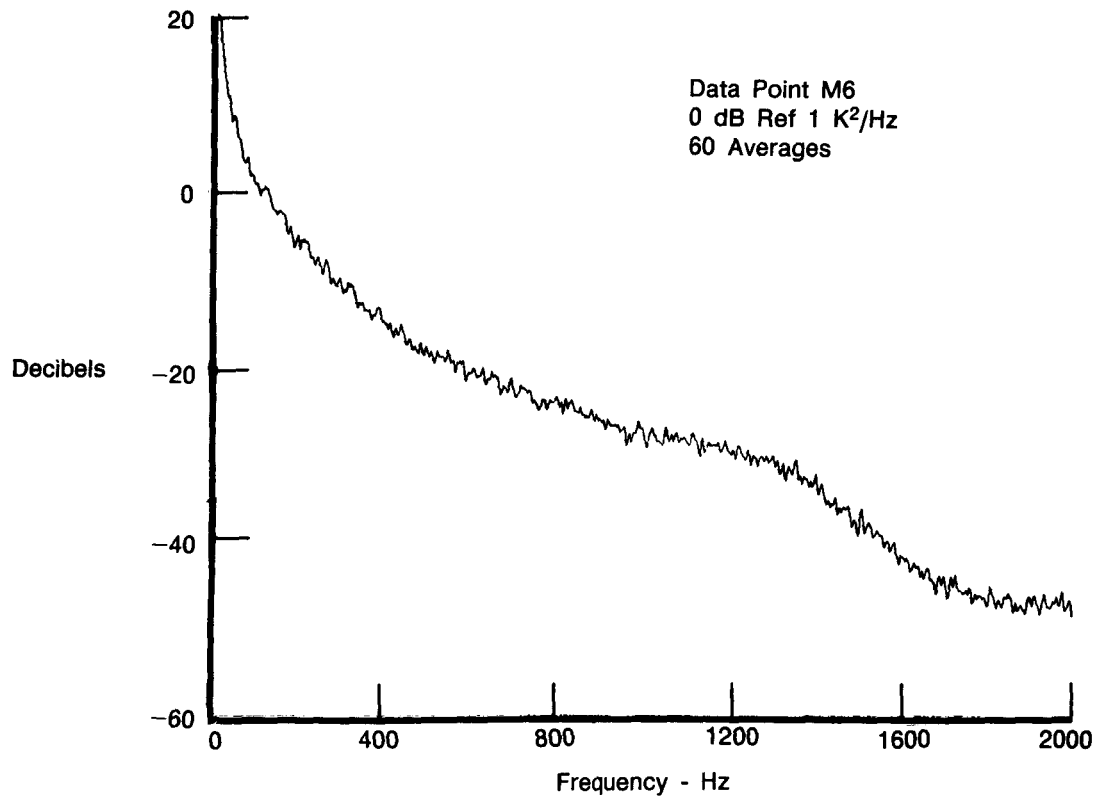
FD 316067

Figure 72. Combustor Experiment: Compensated 76 μm (0.003 Inch) Thermocouple Partial Time Record for 1159K (1626°F)



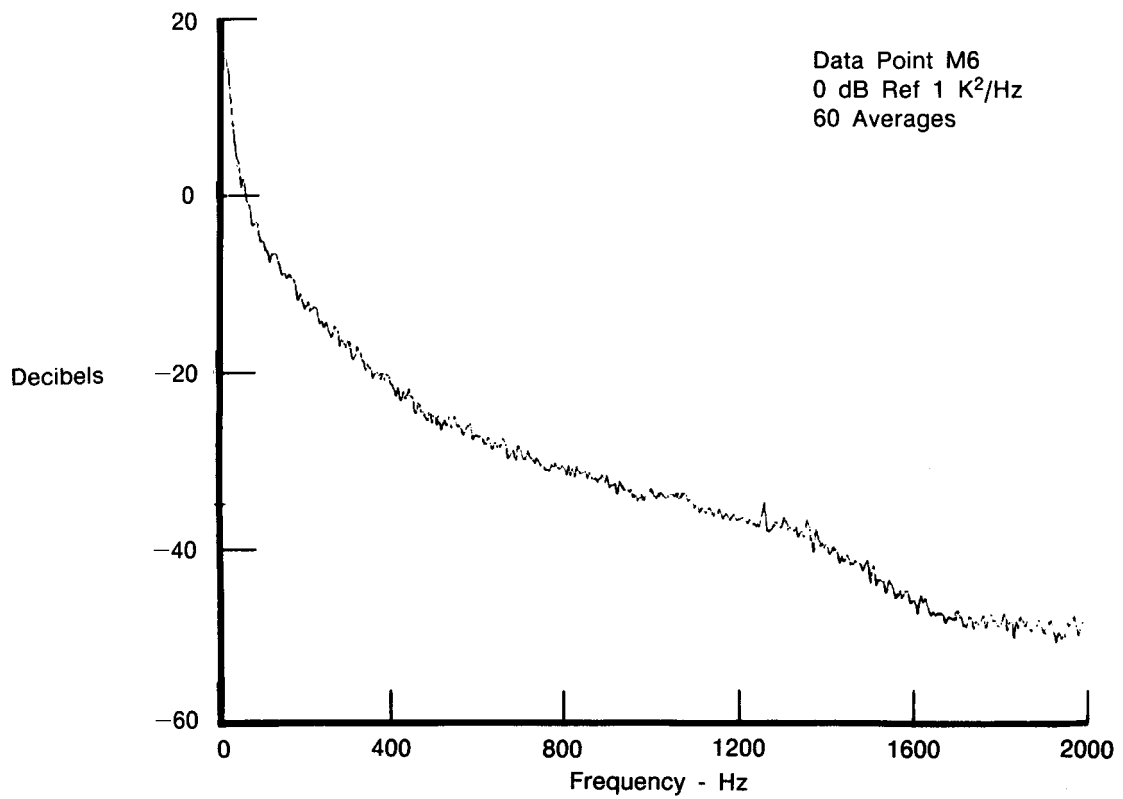
FD 316068

Figure 73. Combustor Experiment: Compensated 127 μm (0.005 Inch) Thermocouple Partial Time Record for 1159K (1626°F)



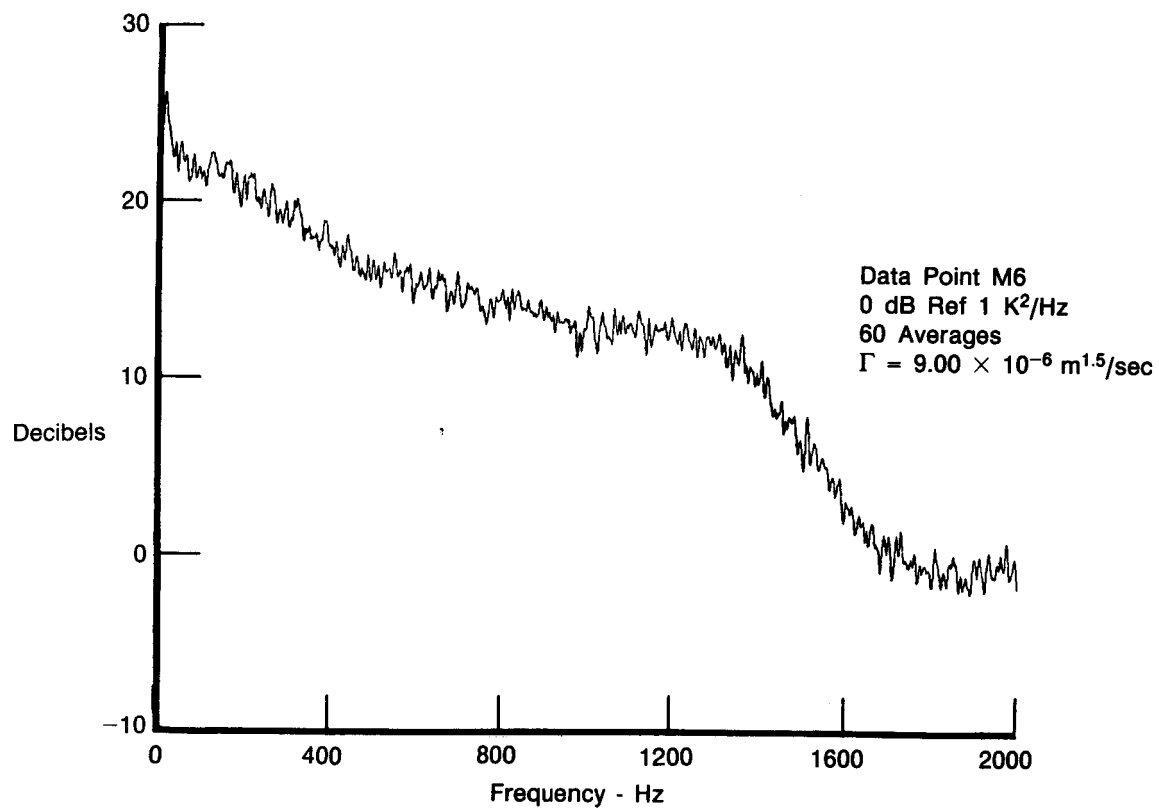
FD 316069

Figure 74. Combustor Experiment: Power Spectral Density Plot of the Uncompensated 76 μm (0.003 Inch) Thermocouple at 1655K (2519°F)



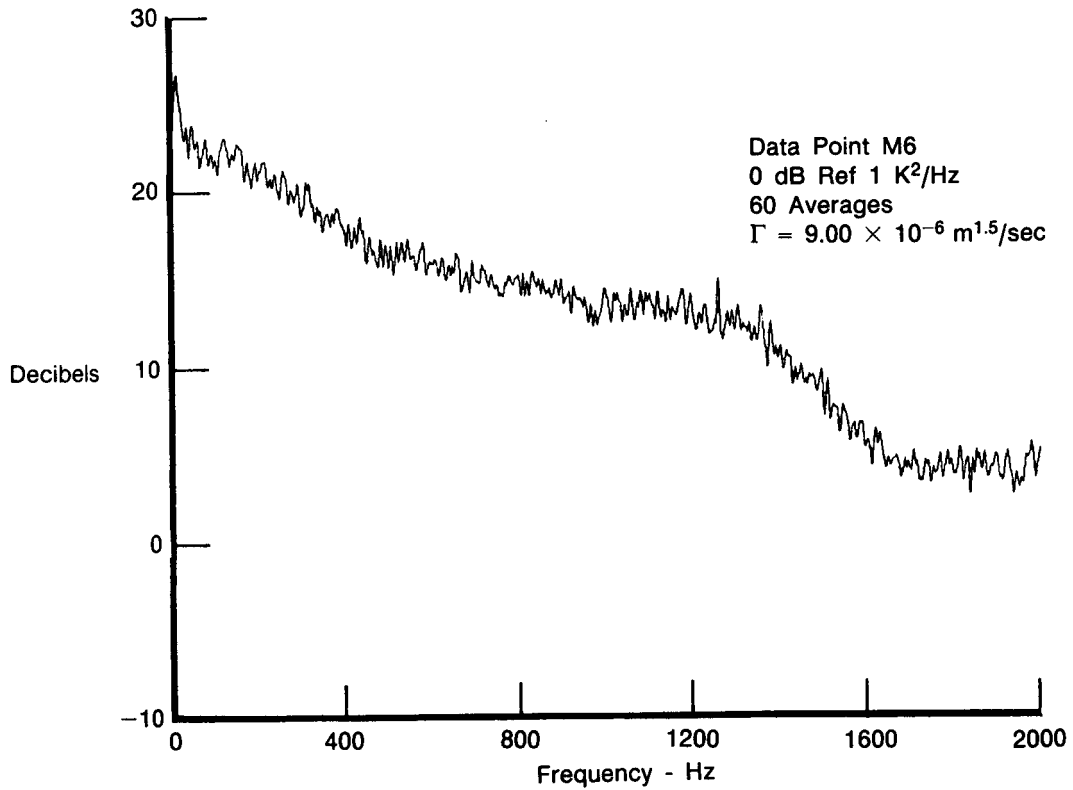
FD 316070

Figure 75. Combustor Experiment: Power Spectral Density Plot of the Uncompensated 127 μm (0.005 Inch) Thermocouple at 1655K (2519°F)



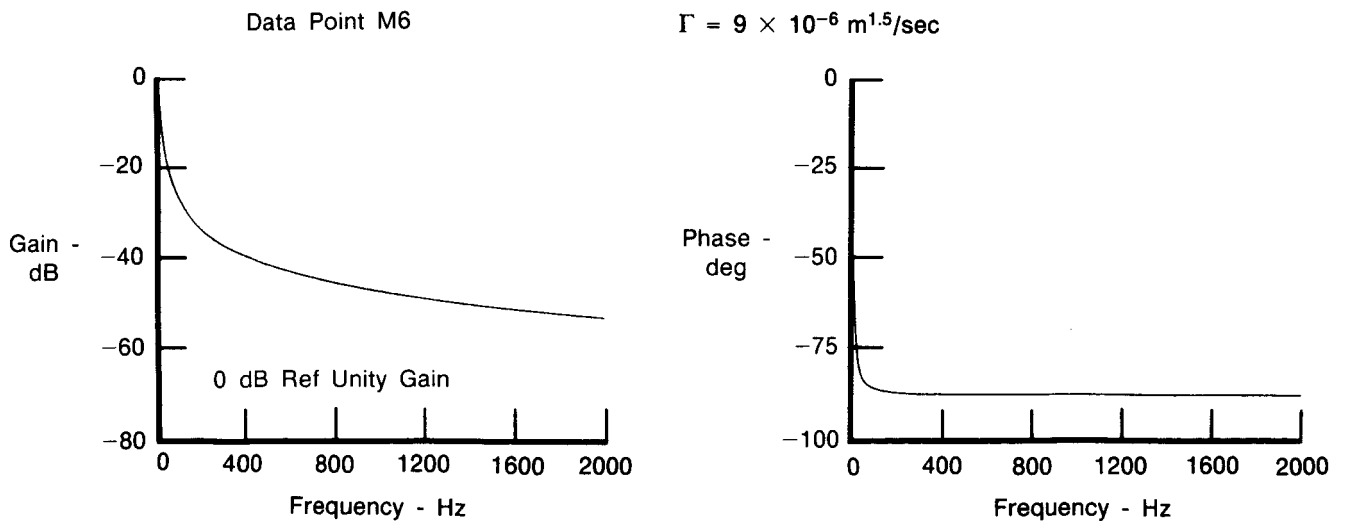
FD 316071

Figure 76. Combustor Experiment: Power Spectral Density Plot of the Compensated 76 μm (0.003 Inch) Thermocouple at 1655K (2519°F)



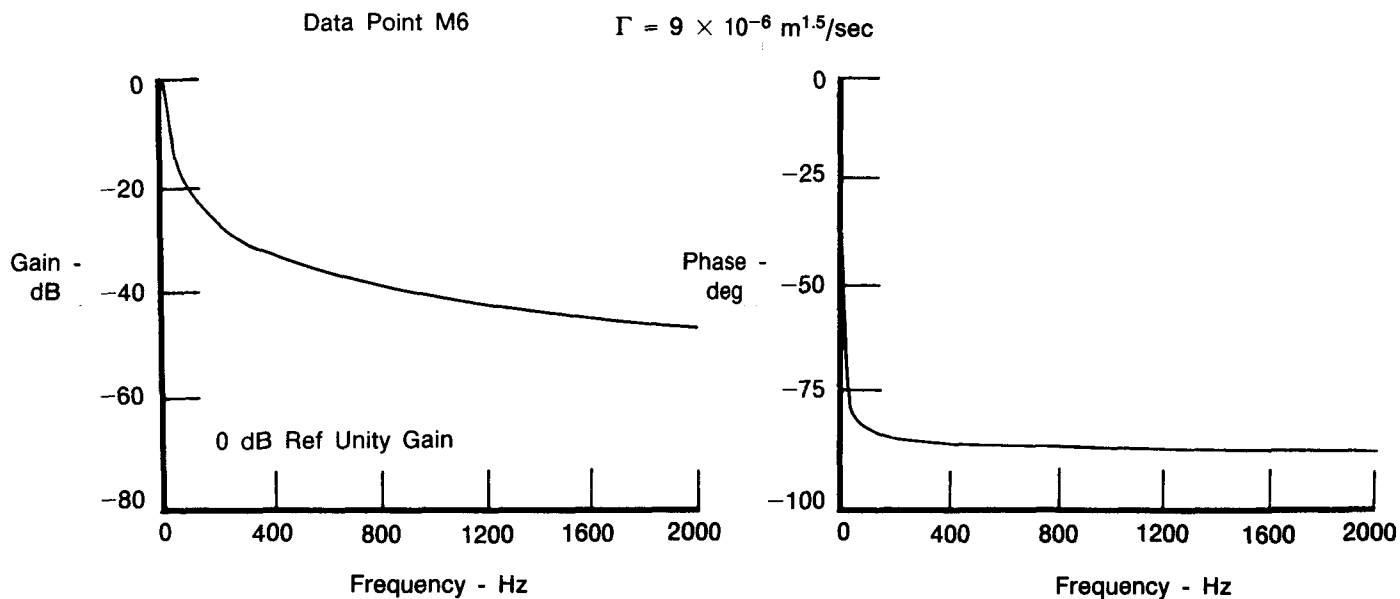
FD 316072

Figure 77. Combustor Experiment: Power Spectral Density Plot of the Compensated 127 μm (0.005 Inch) Thermocouple at 1655K (2519°F)



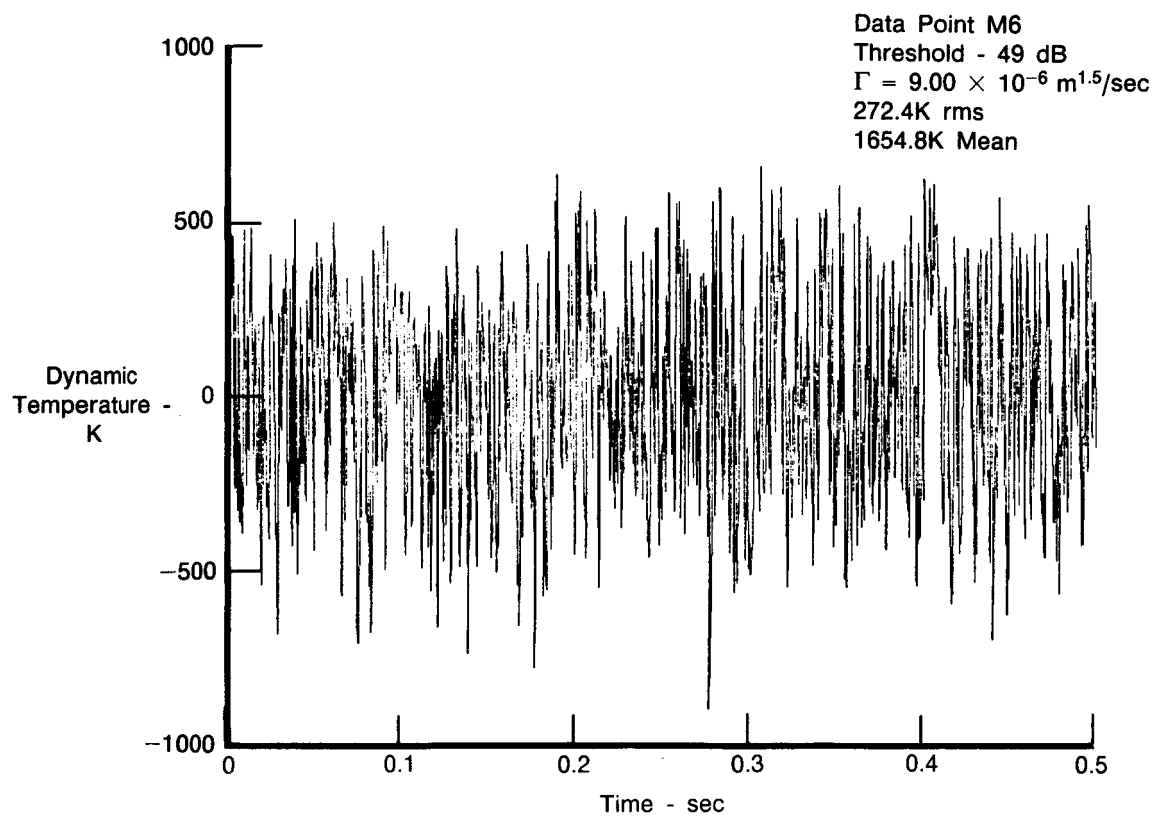
FD 316073

Figure 78. Combustor Experiment: Compensation Spectra for the 127 μm (0.005 Inch) Thermocouple at 1655K (2519°F)



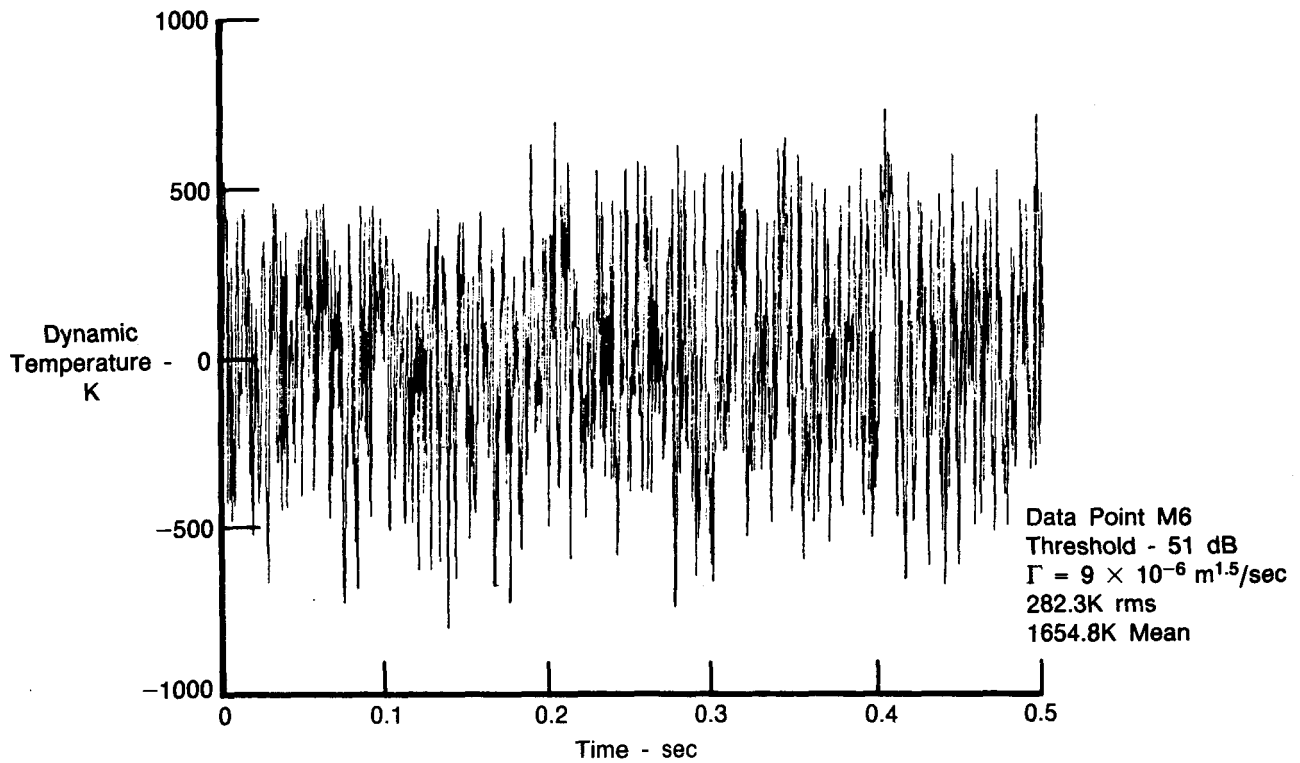
FD 316074

Figure 79. Combustor Experiment: Compensation Spectra for the 76 μm (0.003 Inch) Thermocouple at 1655K (2519°F)



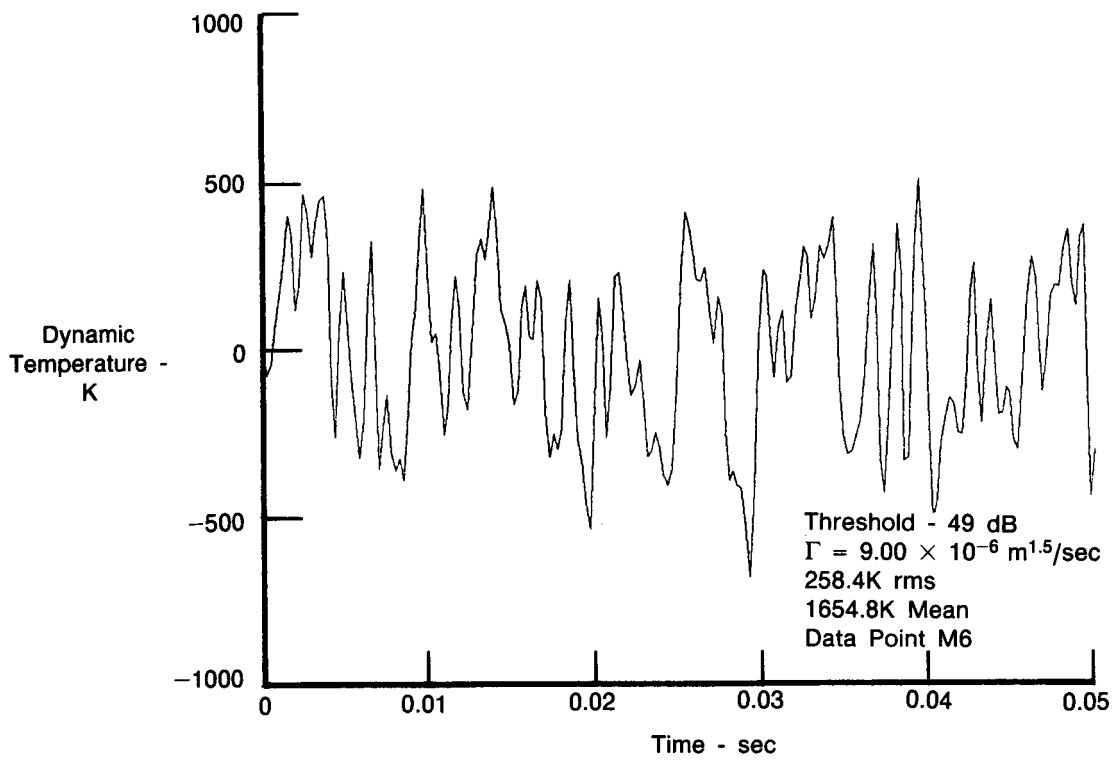
FD 316075

Figure 80. Combustor Experiment: Compensated 76 μm (0.003 Inch) Thermocouple Time Record at 1655K (2519°F)



FD 316076

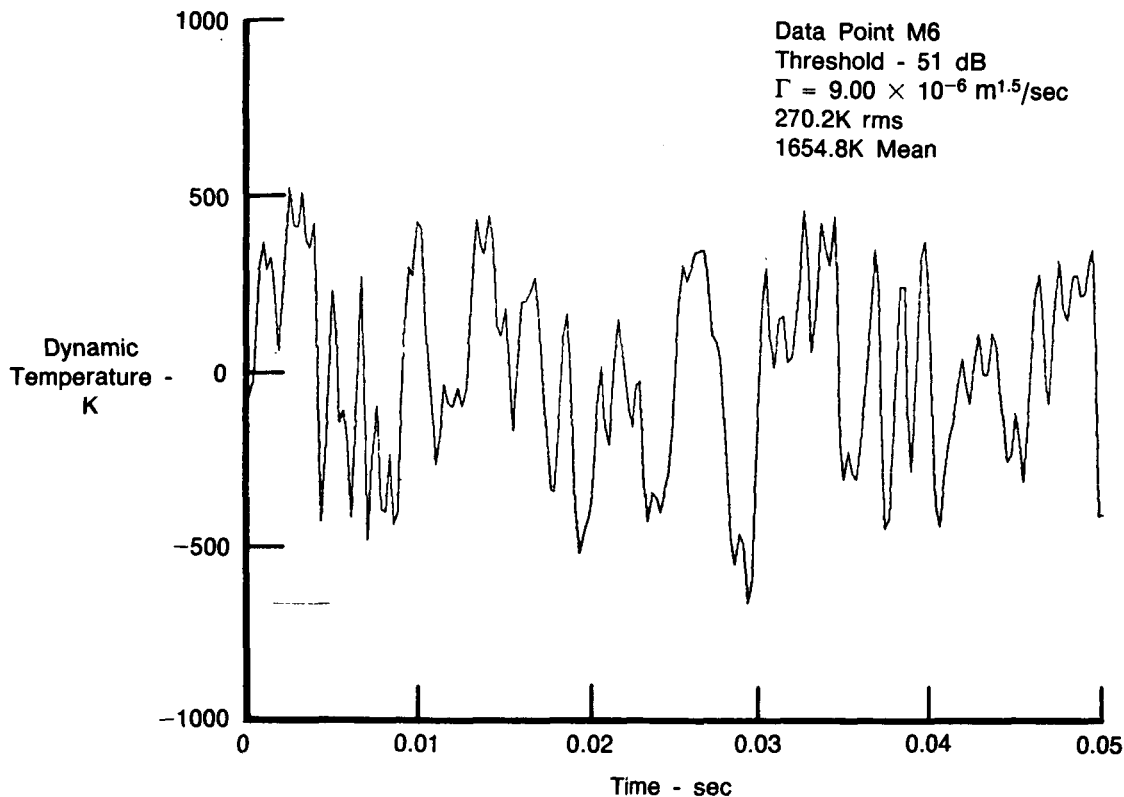
Figure 81. Combustor Experiment: Compensated 127 μm (0.005 Inch) Thermocouple Time Record at 1655K (2519°F)



FD 316077

Figure 82. Combustor Experiment: Compensated 76 μm (0.003 Inch) Thermocouple Partial Time Record at 1655K (2519°F)

C-2



FD 316078

Figure 83. Combustor Experiment: Compensated 127 μm (0.005 Inch) Thermocouple Partial Time Record at 1655K (2519°F)

The dynamic component error (in percent of reading) for the compensated 76 μm thermocouple referenced to the compensated 12.7 μm resistance thermometer at the 1159K test point and the compensated 127 μm thermocouple referenced to the 76 μm thermocouple at both the 1159K and 1655K test points are summarized in Table 13.

The 76 μm thermocouple error referenced to the 12.7 μm resistance thermometer varied from about +18 percent at 20 Hz to +48 percent at 1000 Hz (1159K test point). The error in the rms level of time domain signal (over the entire 1000 Hz bandwidth) was about +33 percent and the peak to peak was about +34 percent. The 76 μm and 127 μm thermocouples exhibited much lower errors when compared to one another. At the 1159K point, the errors were between 8 and 12 percent. At the 1655K point they varied from about 4 to 12 percent (neglecting the 2 percent error value for the p-p time domain levels). The peak to peak time domain error measurements were very subjective. The time resolution of the plots made it difficult to ensure that the 5 highest positive and negative amplitude peaks were being arbitrarily excluded from the measurement (a technique intended to exclude noise spikes). High amplitude time domain noise spikes were primarily due to cumulative error effects in the compensation process. That is, the time domain waveform is the net result of the summation of all frequency components, thus errors in the individual frequency components (amplitude and phase) will have a compounding effect.

TABLE 13. — COMBUSTOR TESTS COMPARISON

Test Point	Sensors	Reference	Dynamic Component Error (% of Reading)				P-P
			20 Hz	20 to 200 Hz	200 Hz to 1 kHz	rms	
1519K (1626°F)	Compensated T/C 3	Compensated RT 0.5	+18.4	+41 (±2)	+48 (±2)	+32.7	+34 (±1)
1159K (1626°F)	Compensated T/C 5	Compensated T/C 3	+11.6	+10 (±1)	+12 (±1)	+8.2	+12 (±1)
1159K (1626°F)	Uncompensated RT 0.5	Compensated RT 0.5	-0.2	-29 (±2)	-80 (±2)	-30.2	-18 (±1)
1655K (2519°F)	Compensated T/C 5	Compensated T/C 3	+7.0	+6 (±1)	+12 (±1)	+3.7	+2 (±1)

Note: (1) Gas stream temperature fluctuations were:
 (a) 1159K (1626°F): ~ 23K rms/Hz at 20 Hz
 ~ 8K rms/Hz 20 Hz to 200 Hz
 ~ 3K rms/Hz 200 Hz to 1 kHz
 (b) 1659K (2519°F): ~ 20 rms/Hz at 20 Hz
 ~ 11K rms/Hz 20 Hz to 200 Hz
 ~ 5K rms/Hz 200 Hz to 1 kHz

(2) (±n): Readability of scaled plots - applicable when noted
 (3) T/C 3 = 76 μm (3 mil) T/C
 T/C 5 = 127 μm (5 mil) T/C
 RT 0.5 = 12.7 μm (0.5 mil) resistance thermometer

Gas path temperature fluctuations in the subscale combustor rig varied from about 23K rms/ $\sqrt{\text{Hz}}$ at 20 Hz to 8K rms at 200 Hz and were only 3K rms at 1000 Hz (1159K test point). Thus, large values of percent of reading errors for the dynamic components represent only a few degrees (Kelvin) of temperature error on a per $\sqrt{\text{Hz}}$ basis.

Differences between the compensated thermocouple data and the resistance thermometer are felt to be mainly due to errors in the measurement of the aerodynamic parameter, Γ (thermocouple), and the calculation of the first order time response of the resistance thermometer. Note that in the rotating wheel experiment the corner frequencies were 308 Hz and 508 Hz. In the combustor experiment, the calculated corner frequency was 195 Hz. Thus, with a lower estimated corner frequency there would be more error in the combustor experiment.

Task 1e — Additional Data Analysis

Summary. — A commercially available high temperature optical fiber thermometer was used in the combustor experiment to provide an additional measurement technique for data comparisons. Per the vendor's literature, the dynamic response of the device is characterized by a -3 dB per octave frequency response function which would greatly extend the frequency measurement range over that of conventional thermocouples. A Pratt & Whitney owned system with a vendor specified bandwidth of 1 kHz for the signal conditioning circuitry was tested, in conjunction with the dual thermocouples and resistance thermometer. The system was originally purchased for a non-dynamic temperature measurement application. Data were obtained from one sensor only and two test points were processed. Post-test inspection revealed deterioration of the sensor's sputtered thin film element had occurred during the test series. Based on its average temperature readings, the deterioration was believed to have occurred during or following processing of the second test point. The uncompensated optical fiber thermometer data from this experiment were observed to exhibit about -3 dB per octave roll off characteristics over only a limited frequency bandwidth relative to the compensated 76 μm thermometer data. At other bandwidths, the roll off rate was about -6 dB per octave. The corner frequency of the optical fiber thermometer was less than 0.04 Hz for the test points processed. Compensated data from the optical fiber thermometer differed from those of the compensated 76 μm thermocouple by as much as +165 percent.

Hardware and Test Configuration. — The optical fiber thermometer system was set up for wideband dynamic temperature operation per the vendor applications note (Reference 3). The maximum sampling rate of the system is 71 samples per second. Thus, wideband (1 to 1000 Hz bandwidth) operation requires external (user provided) data analysis equipment.

The optical fiber probe is an optical pyrometer in which the thermal radiation from a thin film element sputtered on the end of a sapphire rod serves as a thermal radiator per the vendor literature. The key element of the device is that the sapphire fiber remains transparent and non-emitting in the optical and near infrared at temperatures up to its melting point. The thermal radiation from the platinum film is transmitted via the sapphire rod and thence a fiber optic cable to photodetectors. The photodetector signals are digitized and processed in the system computer to yield calibrated temperature readings derived from Planck's equation for blackbody radiators. The system incorporates various calibrations to account for the small but finite emissivity of the probe, transmission losses in the optical path, zero and gain of the photodetectors and other electronic components, etc.

Figure 18 depicts the setup used in the combustor experiment for test stand operation and FM tape recording. The output of the detector was coupled directly to the FM tape for operation in the wideband mode. During the final three test points, the configuration was changed to operate the system: (1) in the single mode with the signal processor still connected to the first stage output and the tape recorder to the detector output; (2) in the single mode with the detector

output connected to the signal processor and to the tape recorder; and, (3) same setup as (2) with system operating in the ratio mode. Checks were made to ensure that the recorder input impedance and grounding were compatible with the optical thermometer detector output. Information on the FM tape recorder setup is contained in Table 2. During testing, the data signal was double recorded on FM tape channels set for different full-scale record levels. The data levels for one of the tape channels was optimized by adjusting the amplification of the optical fiber system via its computer control software at each steady state test point prior to FM tape recording. The system gain settings and linear sensitivity factors for scaling the dynamic signals from voltage to temperature were viewed live on the computer display terminal and hand recorded at each rig test point. Additionally, system diskette recordings were made to provide computer storage of average temperature readings and sensitivity factors for the dynamic data.

Figure 47 depicts the probe installation relative to the other test sensors. Care was taken to ensure that the sensors were not shading one another in the flowpath. The main body of the optical fiber sensor was encased in a ceramic stick to provide mechanical support. The closest edge of the temperature sensing platinum film was about 0.81 cm from the body of the ceramic stick. The probes were grouped within a 0.41 cm diameter plane about 0.28 meter (3.7 L/D) downstream of the 0.076 meter diameter nozzle. Figure 48 depicts the installation. Gas path characteristics within the probe grouping were assumed to be independent of spacial location.

Test Program. — The optical fiber thermometer data were recorded simultaneously with the dual thermocouple and resistance thermometer probes during the combustor rig tests. Table 10 lists the specific test points. At the 1655K test point, the optical fiber thermometer system was operated in four different configurations:

- (1) Wideband mode as depicted in Figure 18.
- (2) Single mode with the signal processor (sampling voltmeter) connected to the detector first gain stage output
- (3) Single mode with the signal processor connected to the detector output
- (4) Ratio mode with the same configuration as in (3).

Configurations (2) through (4) were recorded as a back-up to the wideband mode. The optical fiber system bandwidth was 1000 Hz for all configurations. The concept for processing configurations (2) through (4) was to playback FM tape recorded data at reduced tape drive speed and input the signals into the optical fiber thermometer signal processor (sampling voltmeter) for normal processing at effectively higher sampling rates. However, this technique was not used in the data processing.

Overview of Data Analysis. — The optical fiber thermometer data were recorded on FM tape in conjunction with the dual thermocouple and resistance thermometer signals. Post-test, FM tape data were digitized on a Hewlett Packard model 5451C Fourier Analyzer in an off-line data processing center to generate a digital magnetic tape. The 76 μm thermocouple signals were digitized simultaneously with the optical fiber thermometer data to ensure time correlation. The signals were passed through multiple elliptical anti-aliasing filters set to 1250 Hz corner frequencies (-3 dB) prior to digitizing.

Data were digitized in blocks of 2048 samples. The analog to digital converter (ADC) sampling rate was 4096 Hz. Calibration events for ac and dc signals were reproduced from FM tape and read with a precision digital voltmeter for use in establishing the record/reproduce system calibration.

The digital tapes were read into a mainframe IBM mode 3090 computer for data processing. Temporary utility software routines were written to scale the optical fiber dynamic data to temperature and merge it with the dual thermocouple data processing program to ensure commonality of analysis routines.

Two techniques were used to scale optical fiber thermometer data to temperature. One technique used the linear sensitivity factor provided by the optical fiber thermometer system. The other technique entailed implementing curve fits of tables of nonlinear detector output voltage as a function of temperature and the optical spectral bandwidth (i.e., basic blackbody relationships) which were provided by the vendor. For these conversions, the average temperature readings of the optical fiber thermometer system were used in conjunction with the dynamic signals. The two techniques gave essentially identical results. All data presented in this report were scaled using the curve fits of the basic blackbody relationships.

Data were processed on the IBM computer to yield compensated and uncompensated PSDs and uncompensated dynamic time waveforms scaled to temperature (K). The PSD functions were compensated digitally in the IBM computer using the theoretical frequency response function provided in the vendor applications note (Reference 3).

$$Y(f) = \frac{h}{[6.283k_s \rho_s c_p f]^{0.5}} \quad (11)$$

Where: k_s = Thermal conductivity of sapphire (Btu/hr-ft-°F)
 ρ_s = Density of sapphire (lbm/ft³)
 c_p = Heat capacity of sapphire (Btu/lb_m-°F)
 f = Frequency of oscillations (cycles/hr)
 h = Film coefficient (Btu/hr/ft²-°F).

The value of the film coefficient was calculated based on specific gas path properties at each test point. The properties required were: pressure, velocity, density, and viscosity. The equation for the calculation of h is:

$$\frac{hD}{k_g} = Nu = 0.48Re^{0.51} \quad (12)$$

Where: D = Sensor diameter
 Nu = Nusselt number
 k_g = Thermal conductivity of gas path
 Re = Reynold's number.

To compensate the PSD function, the amplitude of the frequency response function $Y(f)$ was calculated over the bandwidth of the PSD. Then, $Y(f)$ was converted to power by performing a self multiplication. The PSD was then compensated frequency by frequency through division by $Y^2(f)$:

$$\text{Compensated PSD} = \frac{\text{Uncompensated PSD}(f)}{[Y(f) Y(f)]} \quad (13)$$

PSD plots in this report are depicted out to the Nyquist frequency (2048 Hz). Data beyond about 1000 Hz will be noticeably attenuated by the anti-aliasing filters (-3 dB at 1250 Hz) used

during digitization. The entire frequency bandwidth is displayed to provide insight into system noise floors.

In the previous section on data analyses, the compensated 76 μm thermocouple data were compared with the compensated 12.7 μm resistance thermometer. The 76 μm thermocouple power spectra density was between 1.4 and 3.4 dB higher than the resistance thermometer (out to 1000 Hz). The slope (dB/octave) of the thermocouple PSD was generally the same as that of the resistance thermometer. Thus, the compensated 76 μm thermocouple data were judged to provide a good measurement of the relative gas path dynamic characteristics out to 1000 Hz.

Two types of data analyses were made between the thermocouple and the optical fiber thermometer:

- (1) The transfer function between the uncompensated optical fiber thermometer and compensated thermocouple (gas path spectrum).
- (2) The percent of reading difference between the compensated optical fiber thermometer and the compensated thermocouple dynamic components.

The transfer function analysis normalizes the output of the uncompensated fiber optic thermometer to the gas path (as characterized by the compensated thermocouple) to provide insight into its frequency response. The transfer function gain was computed as:

$$\begin{array}{l} \text{Transfer} \\ \text{Function} = 20 \log_{10} \\ \text{Gain} \end{array} \quad \frac{\sqrt{\text{Uncompensated Optical Fiber Thermometer PSD}}}{\sqrt{\text{Compensated Thermocouple PSD}}} \quad (14)$$

The percent of reading difference between the compensated optical fiber thermometer PSD and the compensated thermocouple data provides end results comparison and was calculated as:

$$\% \text{ Difference} = \left(\frac{\sqrt{\text{Compensated Optical Thermometer PSD}}}{\sqrt{\text{Compensated Thermocouple PSD}}} \right) - 1 \times 100 \quad (15)$$

For these analyses, the optical fiber thermometer PSD data were corrected for its 1000 Hz (-3 dB) bandwidth and the thermocouple data for the 5 Hz signal conditioning amplifier ac coupling as follows:

- (a) Optical fiber thermometer (single pole lowpass filter)

$$\text{gain} = 20 \log_{10} \left[\frac{1}{\sqrt{1 + (f/f_c)^2}} \right] \quad (16)$$

Where: $f_c = 1000$ Hz
 $f =$ Frequency.

- (b) Thermocouple ac coupling (single pole highpass filter)

$$\text{gain} = 20 \log_{10} \left[\frac{1}{\sqrt{1 + (f/f_c)^2}} \right] \quad (17)$$

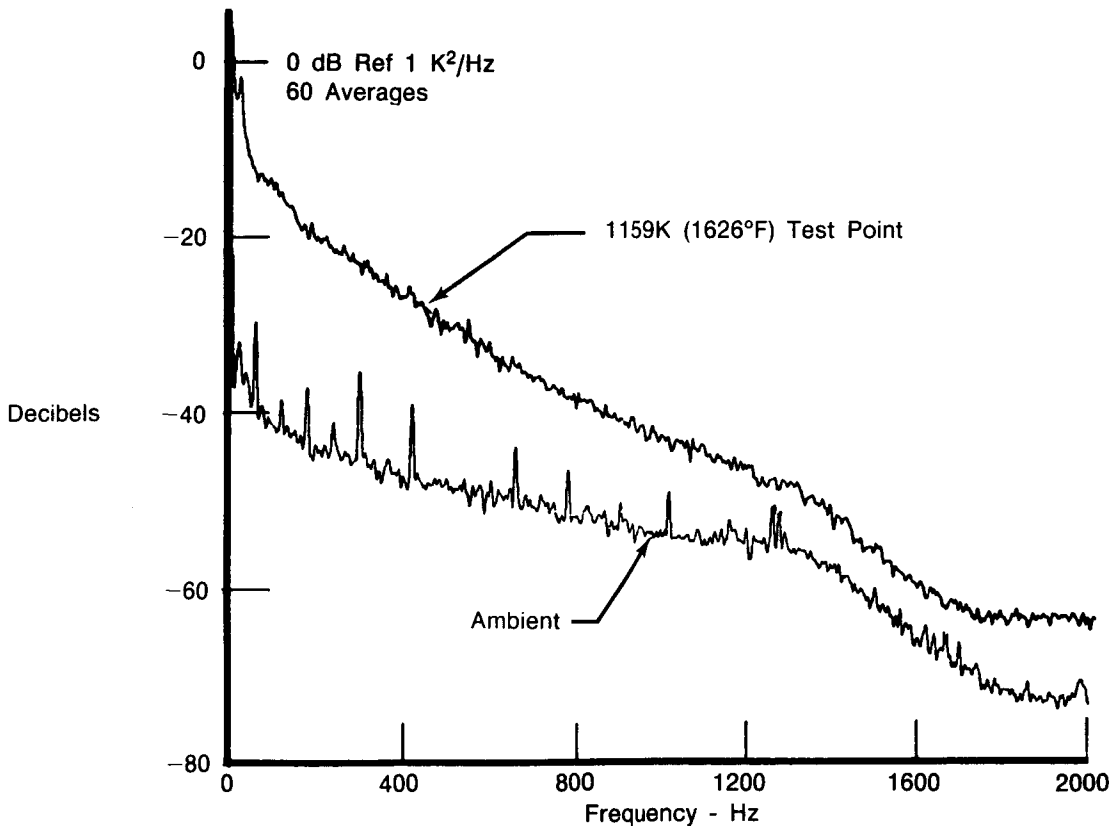
Where: $f_c = 5$ Hz
 $f =$ Frequency.

Data corrections for the optical fiber thermometer bandwidth ranged from 3.01 dB at 1000 Hz down to 0.01 dB at 50 Hz. Corrections for the thermocouple ac coupling ranged 8.60 dB at 2 Hz down to 0.00 dB at 70 Hz.

Data Analysis.

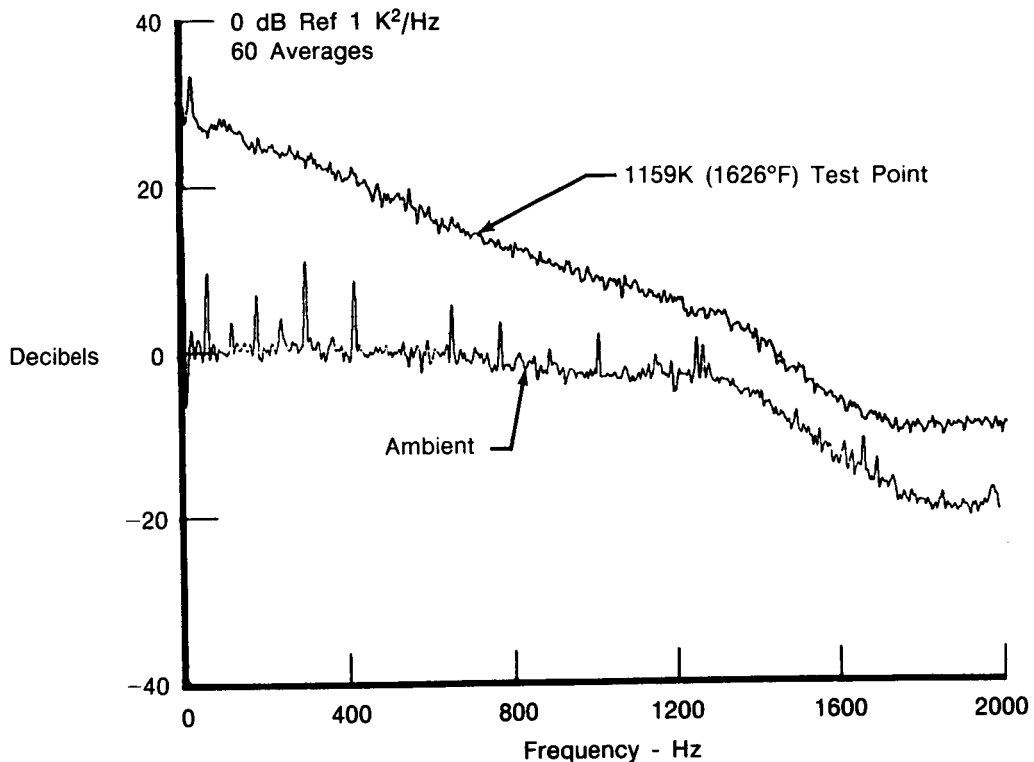
(1) *1159K Test Point:* Figures 84 and 85 depict the SNRs for the uncompensated and compensated optical fiber thermometers. In Figure 85, the ambient background noise was compensated with the same function used for the test point. The SNR typically varied from about 30 dB at 20 Hz to 11 dB at 1000 Hz. The calculated corner frequency of the optical sensor was about 0.014 Hz at the test point conditions and the 76 μm thermocouple corner frequency was about 10.4 Hz.

The uncompensated PSD functions of the optical fiber thermometer and the 76 μm thermocouple are shown in Figures 86 and 87 respectively. The dynamic temperature measured by the thermocouple is considerably larger across the entire frequency bandwidth.



FD 316079

Figure 84. Combustor Experiment: Power Spectral Density Plots of the Uncompensated Optical Fiber Thermometer at 1159K (1626°F) and Ambient



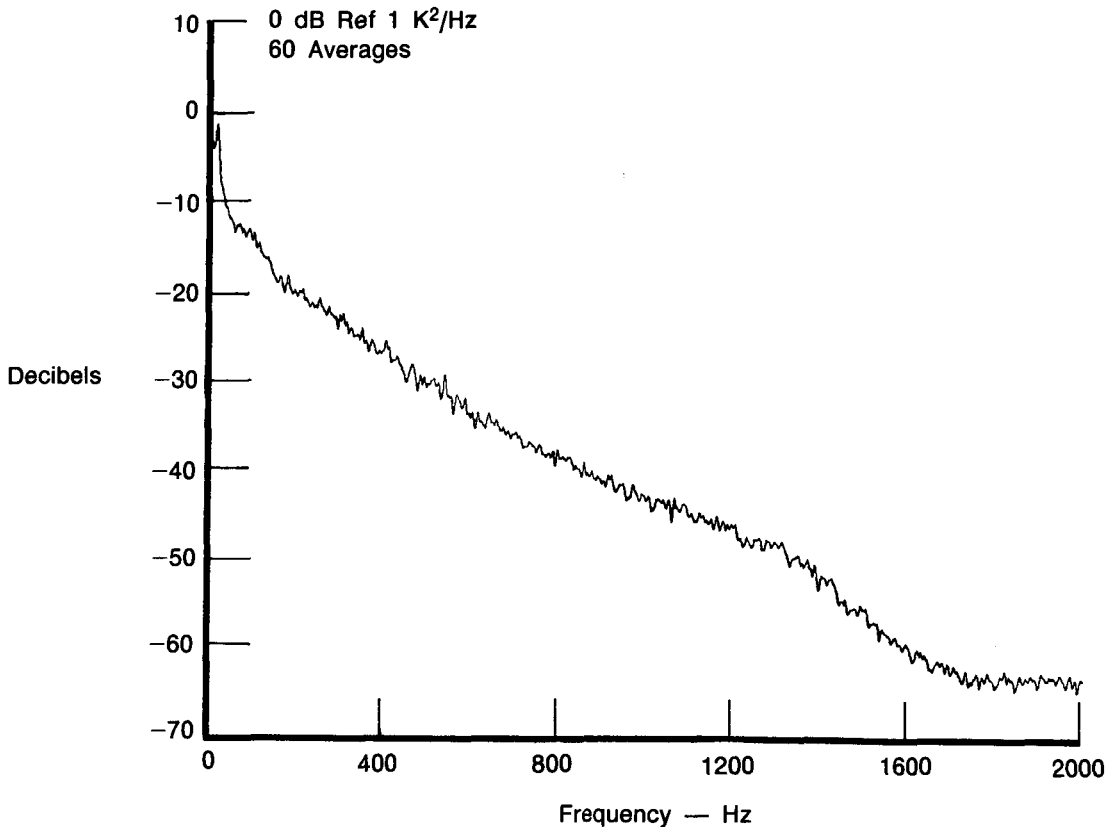
FD 316080

Figure 85. Combustor Experiment: Power Spectral Density Plots of the Compensated Optical Fiber Thermometer at 1159K (1626°F) and Ambient

The transfer function (gain) of the uncompensated optical fiber thermometer to the compensated 76 μm thermocouple is shown in Figure 88. This indicates that the frequency response roll off characteristics for this specific optical thermometer sensor at these test conditions were approximately -6 dB/octave to 12 Hz, -3 dB/octave between 12 and 150 Hz, and -6 dB/octave between 150 Hz and 1000 Hz (the limit of this experiment).

The compensated PSDs for the optical fiber thermometer and the 76 μm thermocouple are given in Figures 89 and 90. The compensation spectrum for the optical thermometer is depicted in Figure 91. At 1000 Hz the compensation is about 52 dB. Figure 92 is a plot of the percent of reading difference between their dynamic components and also indicates the level of temperature fluctuations present in the gas path (as measured by the compensated 76 μm thermocouple). The optical fiber thermometer read a maximum of approximately 200 percent higher than the thermocouple at 4 Hz and a minimum of 30 percent higher at 1000 Hz. The amplitude of dynamic fluctuations in the gas stream varied from about 23K rms/ $\sqrt{\text{Hz}}$ at 20 Hz to 3K rms/ $\sqrt{\text{Hz}}$ at 1000 Hz.

Figures 93 and 94 are the uncompensated time records for the optical fiber thermometer and 76 μm thermocouple respectively. The rms level of the thermocouple was about 41K. The optical fiber thermometer read about 5.9K rms.



FD 316081

Figure 86. Combustor Experiment: Power Spectral Density Plot of the Uncompensated Optical Fiber Thermometer at 1159K (1626°F)

(2) 1655K Test Point: The SNR of the optical fiber was considerably improved at the 1655K point. The energy output of the sensor increased dramatically as the mean temperature increased. At about 20 Hz the SNR (Figure 95) was approximately 45 dB and at 1000 Hz it was about 19 dB. The calculated corner frequency of the optical sensor was about 0.036 Hz. The corner frequency of the 76 μm thermocouple was approximately 13.5 Hz. The calculated compensation spectrum for the optical fiber thermometer is shown in Figure 96. At 1000 Hz, the compensation is about 47 dB.

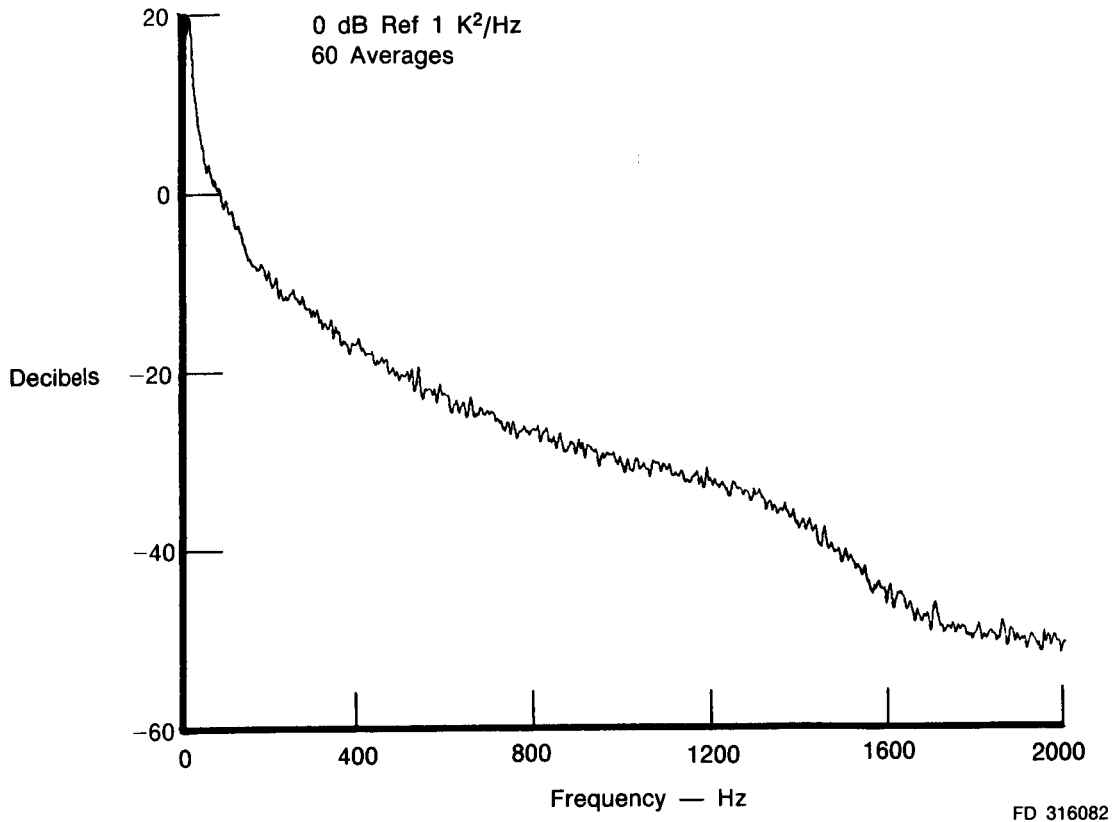
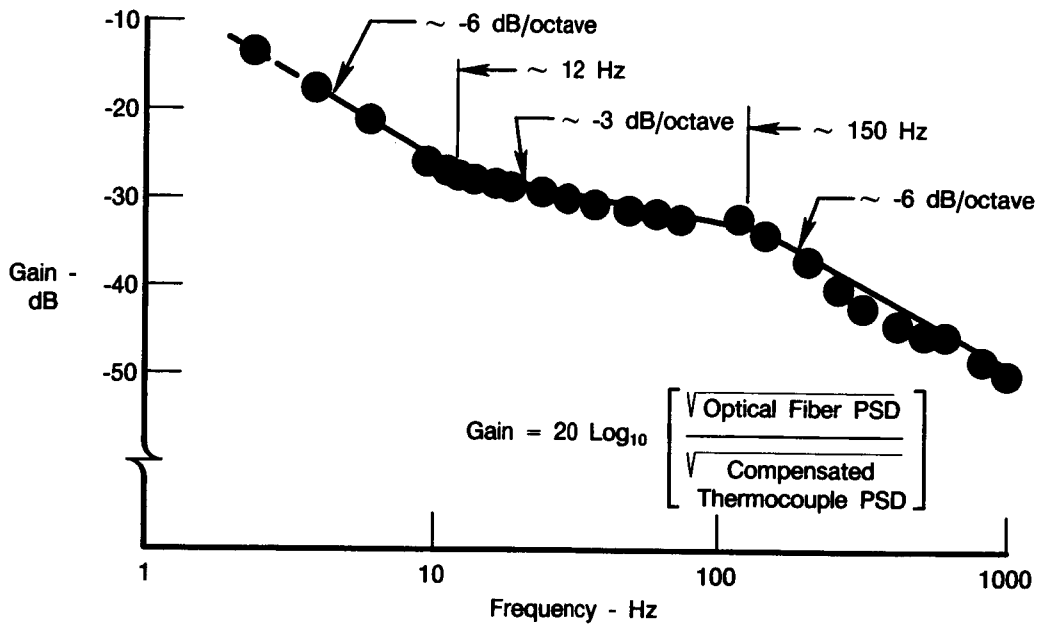
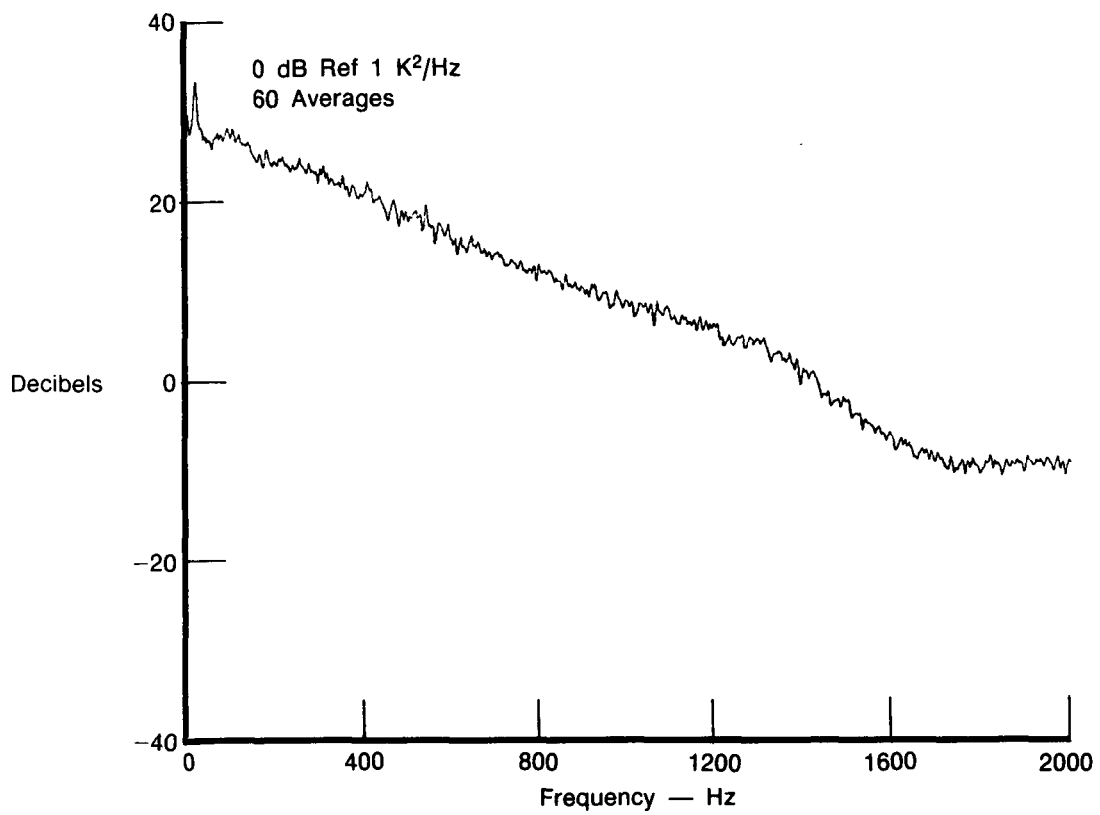


Figure 87. Combustor Experiment: Power Spectral Density Plot of the Uncompensated 76 μm (0.003 Inch) Thermocouple at 1159K (1626°F)



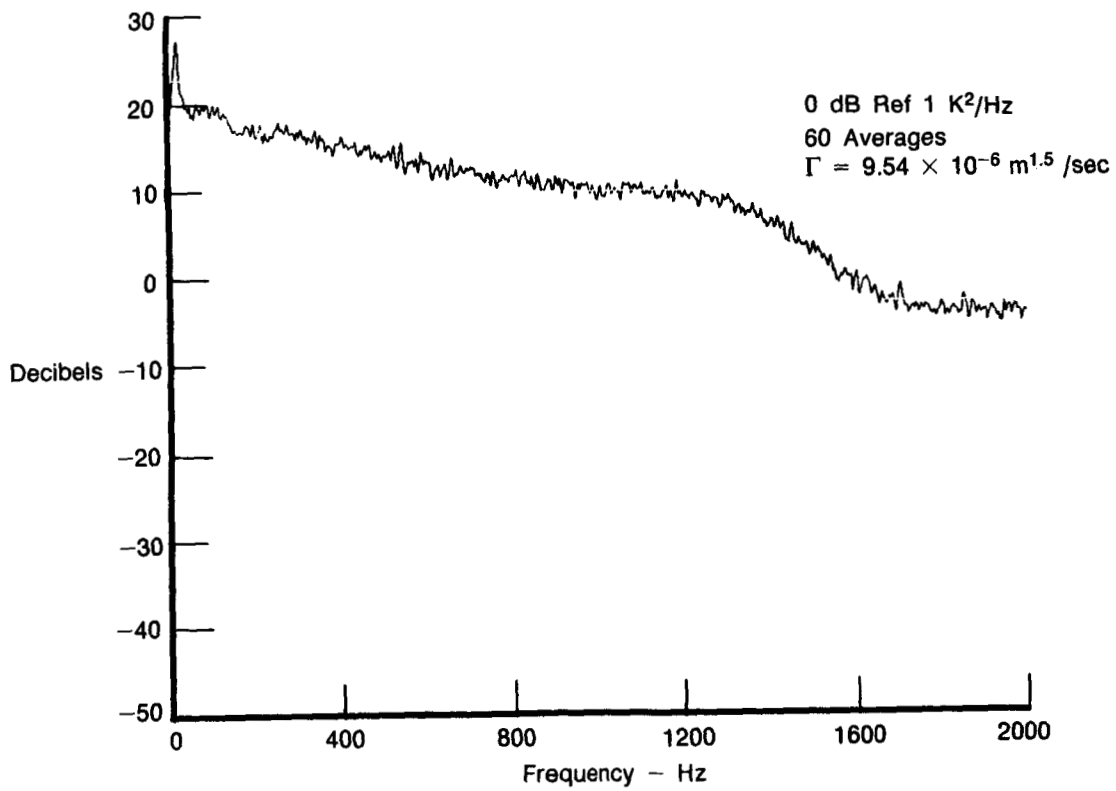
FD 316083

Figure 88. Combustor Experiment: Transfer Function of the Uncompensated Optical Fiber Thermometer to the Compensated $76 \mu\text{m}$ (0.003 Inch) Thermocouple at 1159K (1626°F)



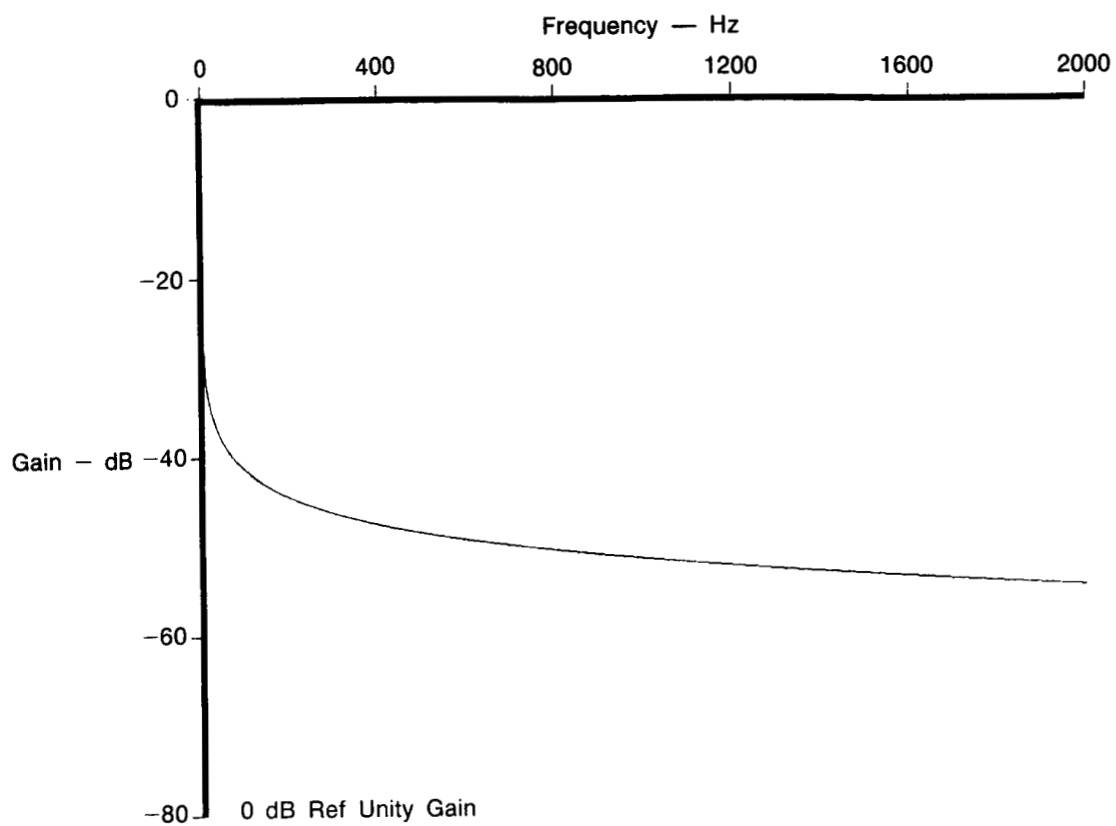
FD 316084

Figure 89. Combustor Experiment: Power Spectral Density Plot of the Compensated Optical Fiber Thermometer at 1159K (1626°F)



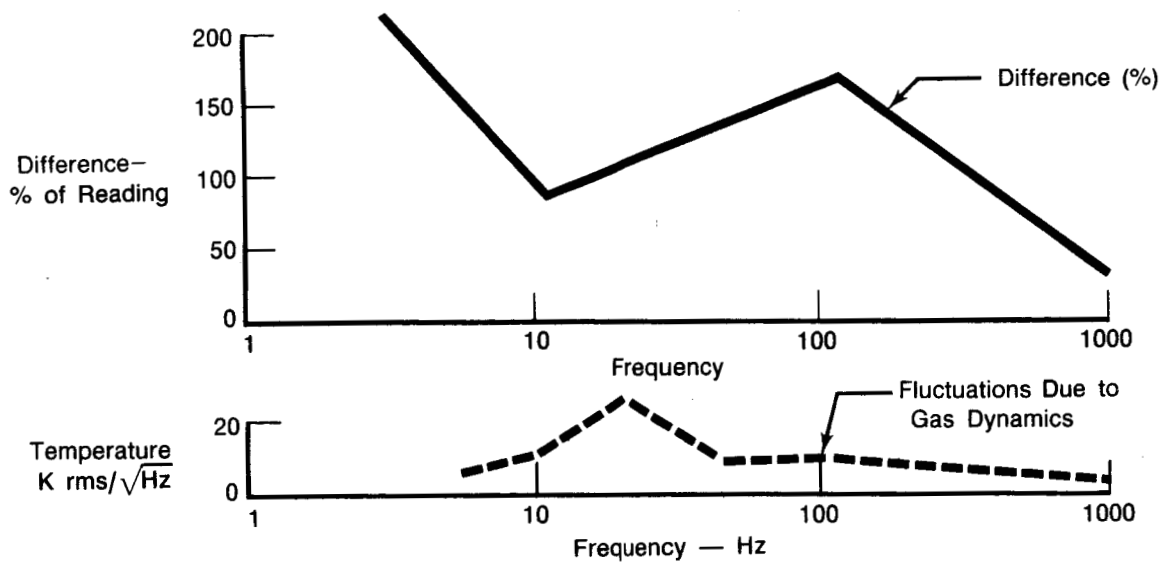
FD 316085

Figure 90. Combustor Experiment: Power Spectral Density Plot of the Compensated 76 μm (0.003 Inch) Thermocouple at 1159K (1626°F)



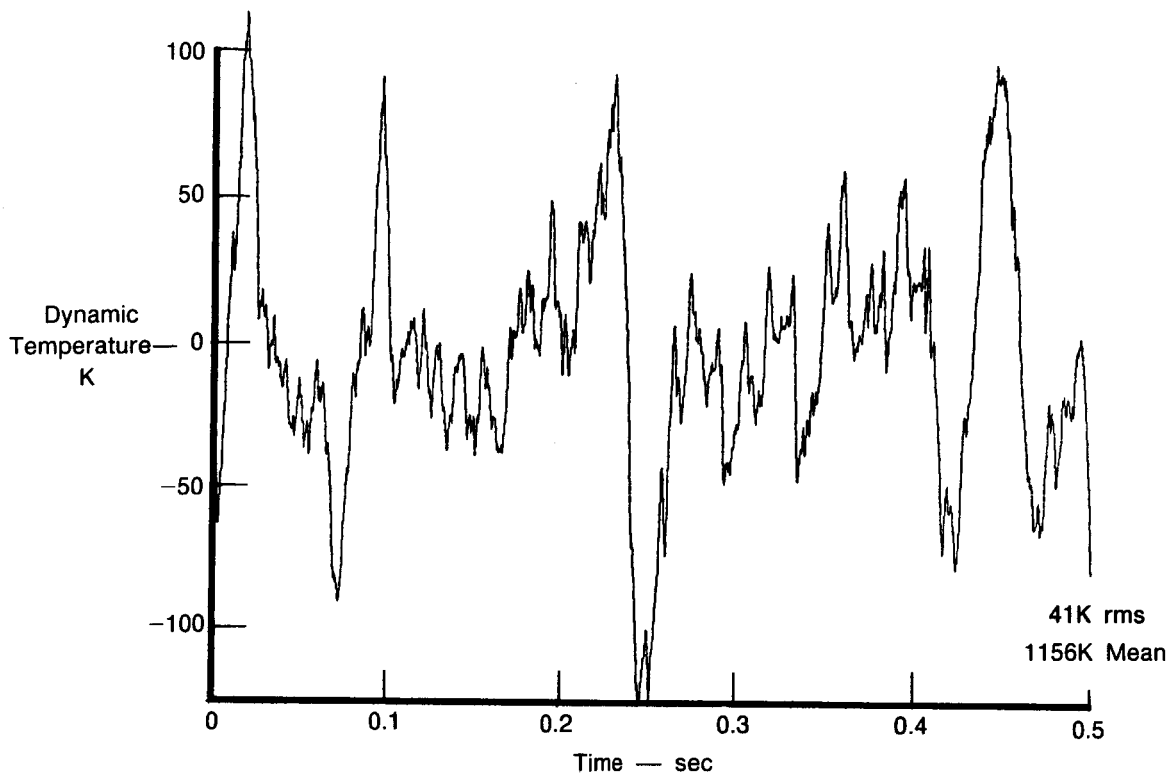
FD 316086

Figure 91. Combustor Experiment: Compensation Spectrum for the Optical Fiber Thermometer at 1159K (1626°F)



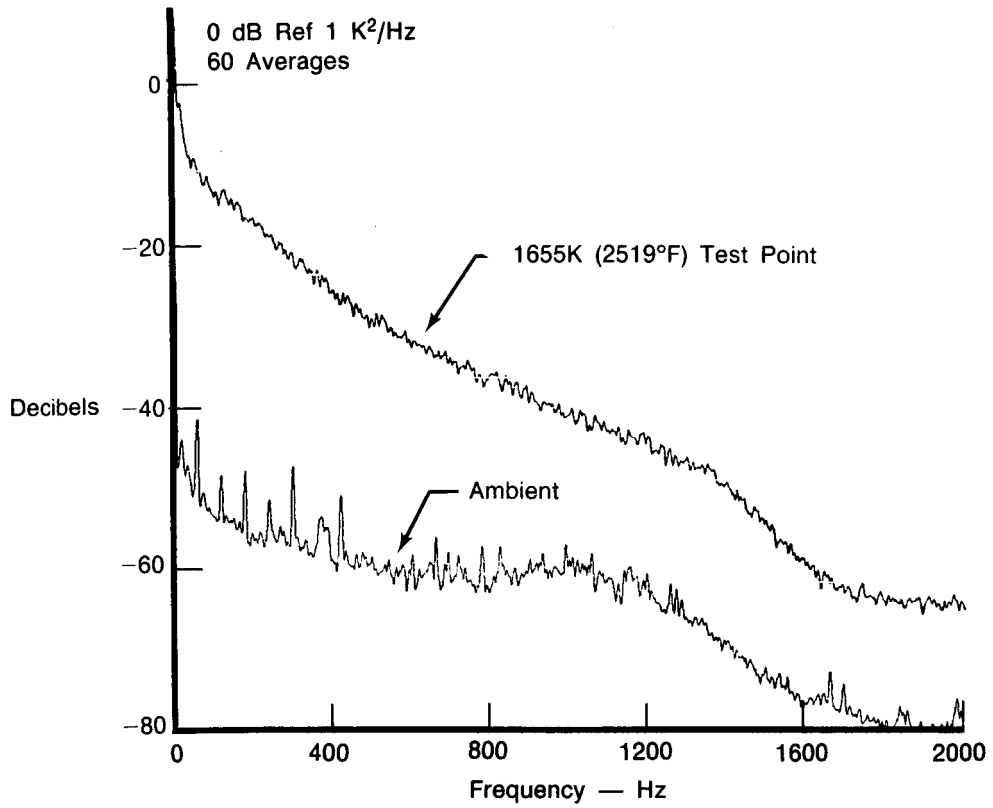
FD 316087

Figure 92. Combustor Experiment: Dynamic Components Comparison of the Compensated Optical Fiber Thermometer Referenced to the Compensated 76 μm (0.003 Inch) Thermocouple at 1159K (1626°F)



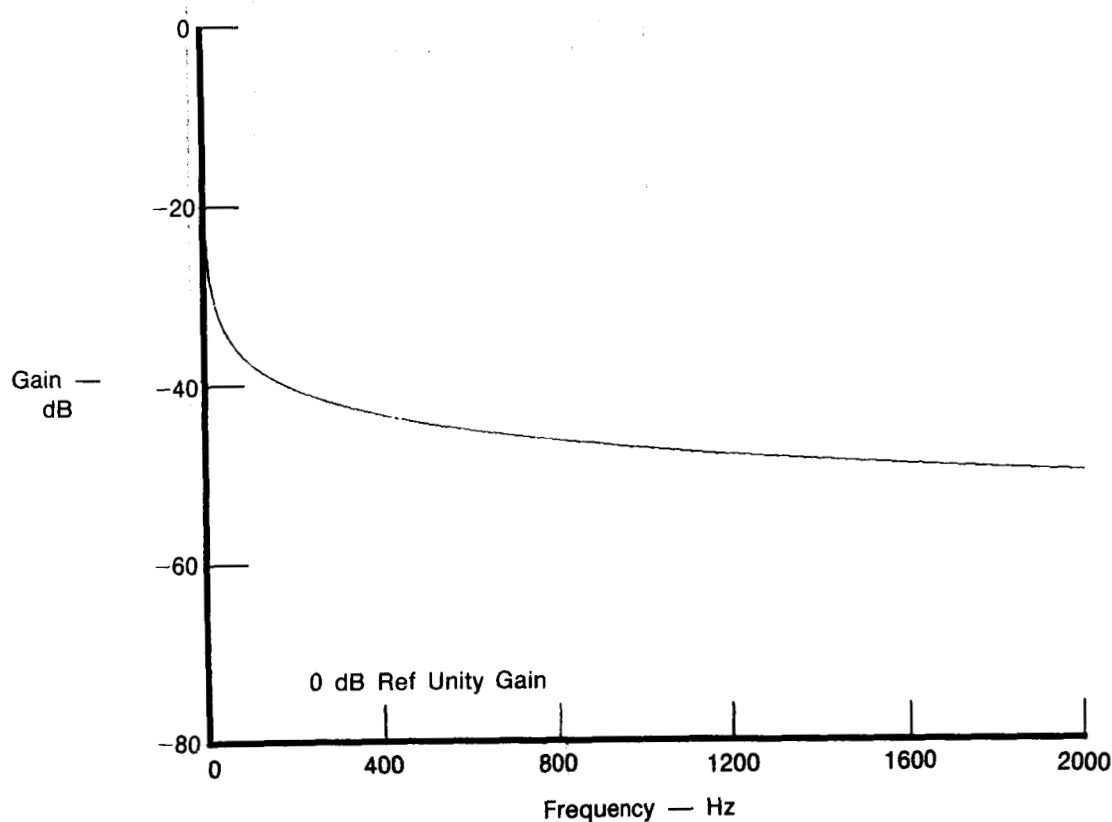
FD 316089

Figure 94. Combustor Experiment: Uncompensated 76 μm (0.003 Inch) Thermocouple Time Record at 1159K (1626°F)



FD 316090

Figure 95. Combustor Experiment: Power Spectral Density Plots of the Uncompensated Optical Fiber Thermometer at 1655K (2519°F) and Ambient



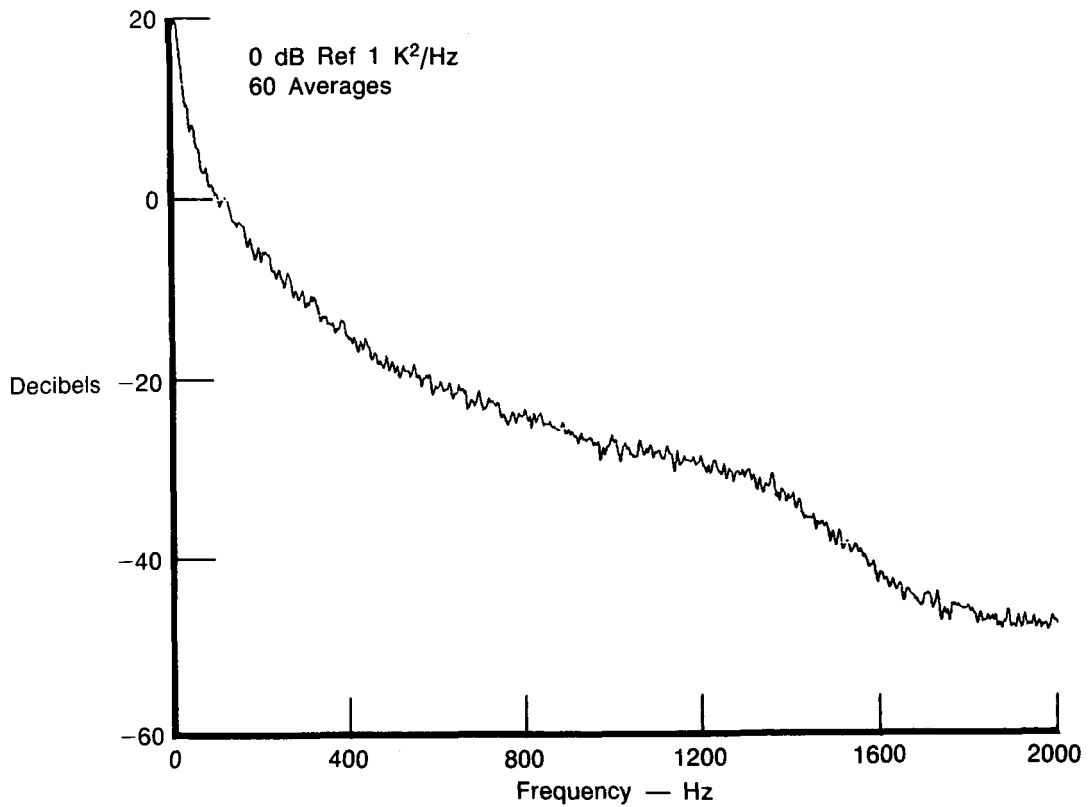
FD 316091

Figure 96. Combustor Experiment: Compensation Spectrum for the Optical Fiber Thermometer at 1655K (2519°F)

The PSD plots of the uncompensated 76 μm thermocouple and the uncompensated optical fiber thermometer are shown in Figures 97 and 98. The amplitude of the thermocouple PSD was considerably greater than the optical fiber thermometer.

Figure 99 is the transfer function (gain) of the uncompensated optical fiber thermometer to the compensated thermocouple. The observed frequency response function roll off rate (for this specific probe and test condition) was very similar to those obtained at the 1159K test point. The slopes were about -6 dB per octave out to 12 Hz, -3 dB per octave between 12 and 250 Hz, and -6 dB per octave between 250 and 1000 Hz.

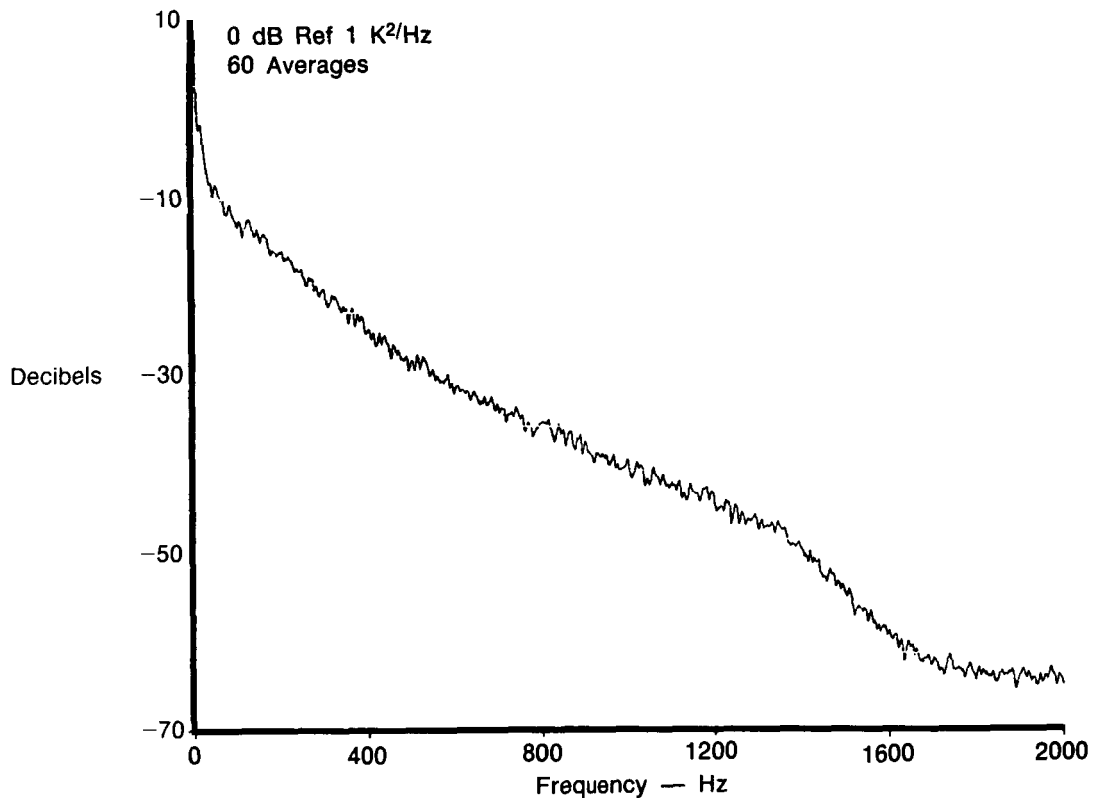
The compensated PSDs are given in Figure 100 (optical thermometer) and 101 (76 μm thermometer). The percent of reading difference between their dynamic components are contained in Figure 102. The compensated optical fiber thermometer data read about 102 percent higher than the thermocouple at 4 Hz and 38 percent lower at 1000 Hz. The gas path temperature fluctuations (as measured by the compensated 76 μm thermocouple) varied from a maximum of about 20K rms/ $\sqrt{\text{Hz}}$ at 20 Hz to 4.5K rms/ $\sqrt{\text{Hz}}$ at 1000 Hz.



FD 316092

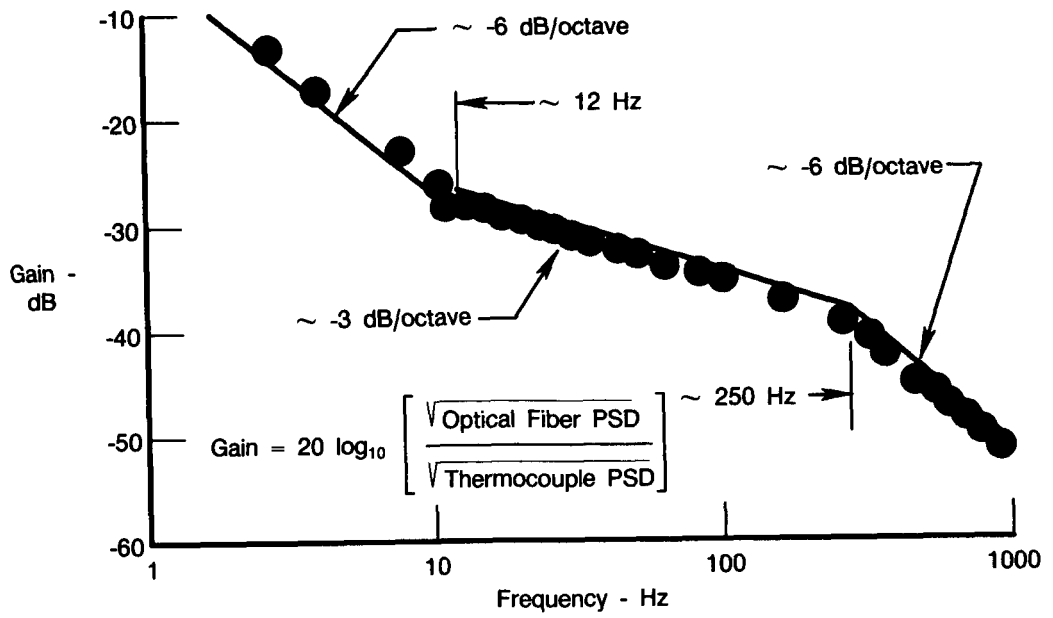
Figure 97. Combustor Experiment: Power Spectral Density Plot for the Uncompensated 76 μm (0.003 Inch) Thermocouple at 1655K (2519°F)

Uncompensated time records for the optical fiber thermometer and thermocouple are depicted in Figures 103 and 104. The rms level of the thermocouple was about 38.5K rms and the optical fiber thermometer was about 10.6K rms.



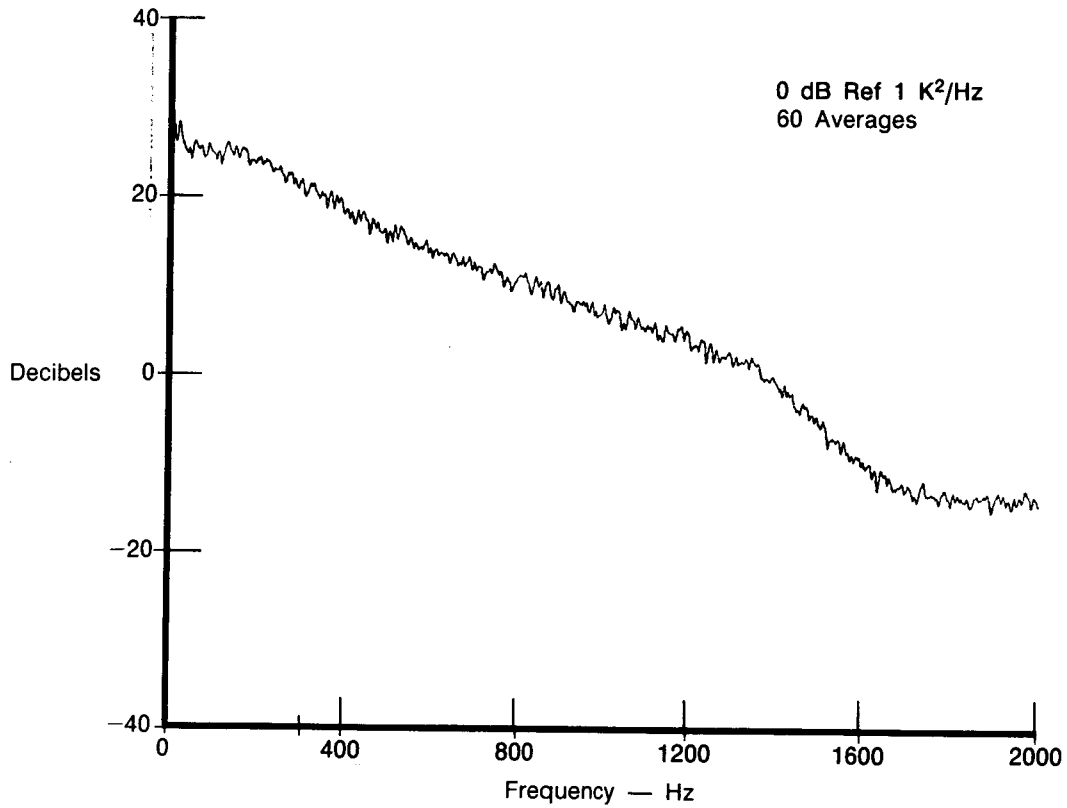
FD 316093

Figure 98. Combustor Experiment: Power Spectral Density Plot for the Uncompensated Optical Fiber Thermometer at 1655K (2519°F)



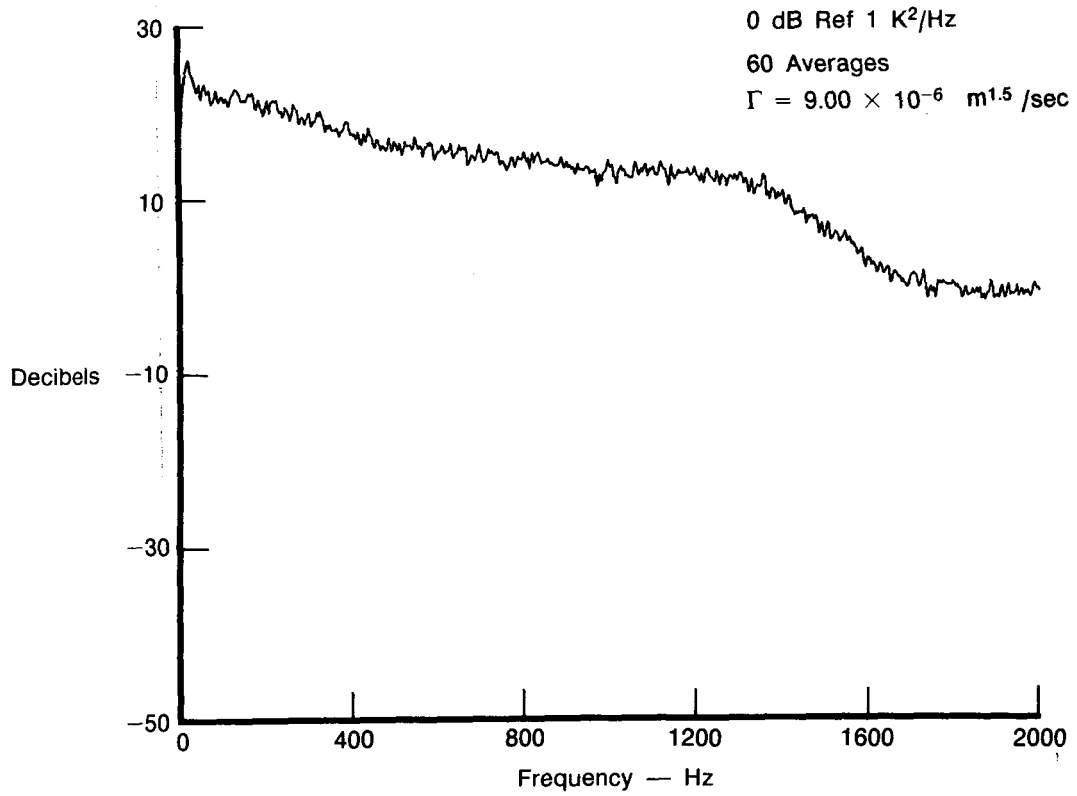
FD 316094

Figure 99. Combustor Experiment: Transfer Function of the Uncompensated Optical Fiber Thermometer to the Compensated 76 μm (0.003 Inch) Thermocouple at 1655K (2519°F)



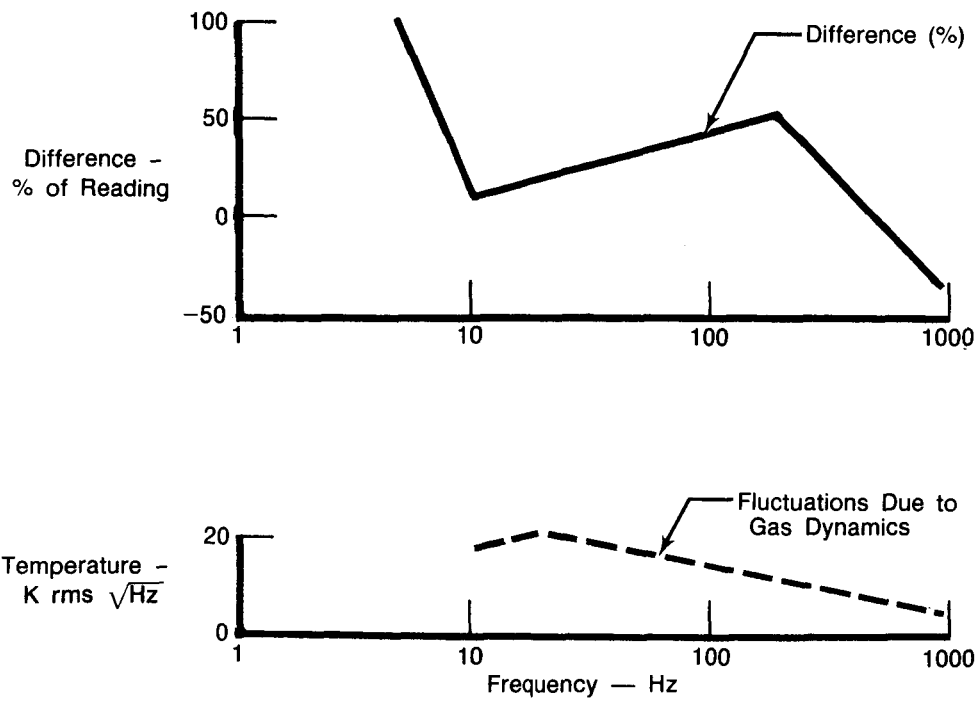
FD 316095

Figure 100. Combustor Experiment: Power Spectral Density Plot for the Compensated Optical Fiber Thermometer at 1655K (2519°F)



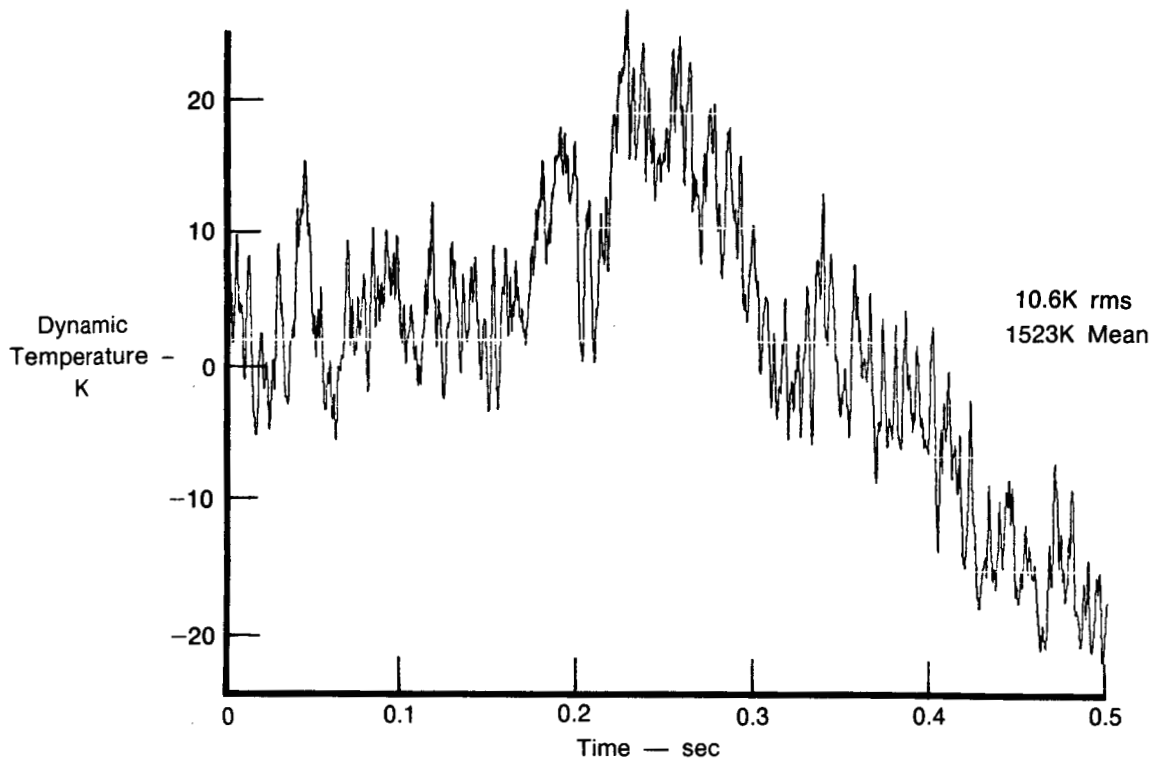
FD 316096

Figure 101. Combustor Experiment: Power Spectral Density Plot for the 76 μm (0.003 Inch) Thermocouple at 1655K (2519°F)



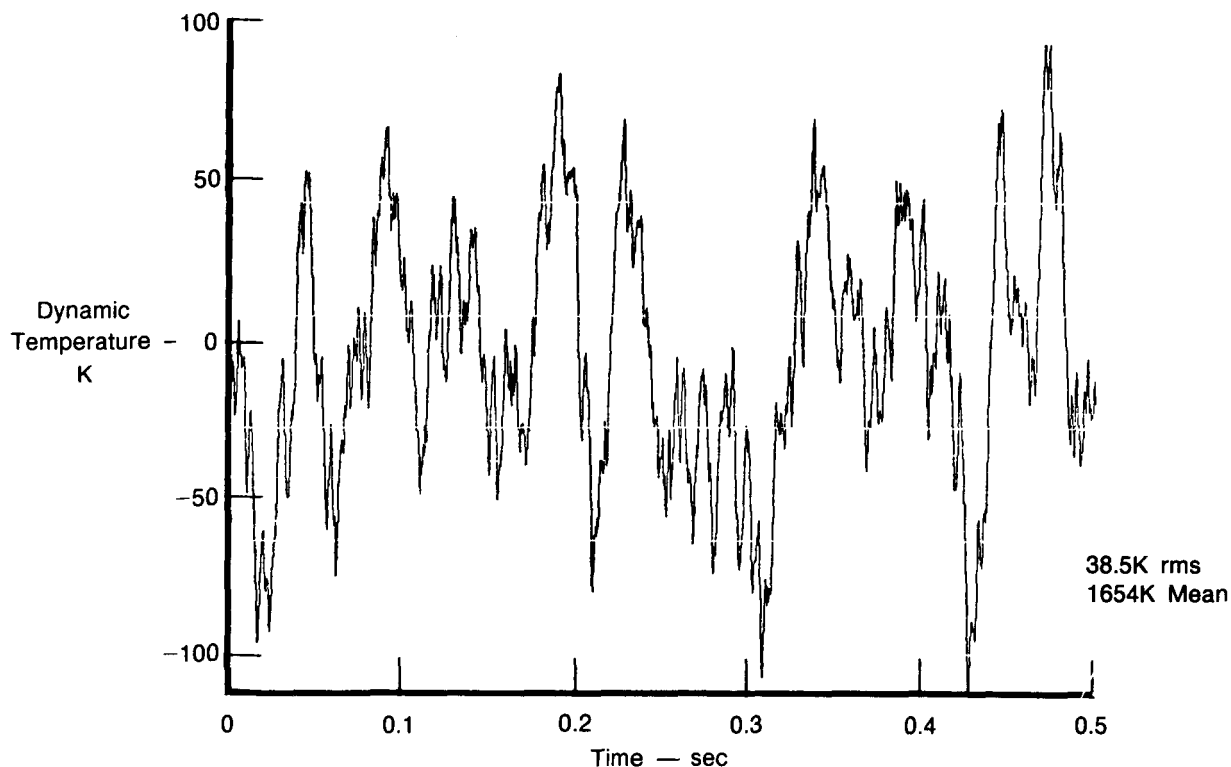
FD 316097

Figure 102. Combustor Experiment: Dynamic Component Comparison of the Compensated Optical Fiber Thermometer Referenced to the Compensated 76 μm (0.003) Thermocouple at 1655K (2519°F)



FD 316098

Figure 103. Combustor Experiment: Uncompensated Optical Fiber Thermometer Time Record at 1655K (2519°F)



FD 316099

Figure 104. Combustor Experiment: Uncompensated 76 μm (0.003 Inch) Thermocouple Time Record at 1655K (2519°F)

Discussion. — Post-test inspection of the optical fiber sensor revealed a general gritty appearance and slight crinkling on the backside of the sputtered thin film temperature radiating element. Table 14 gives the specific sensor test history.

Table 15 lists the mean gas path temperatures measured by the optical fiber thermometer and the 254 μm thermometer as a function of the cumulative test time on the optical sensor. The data analyzed for this report were taken at 65 minutes cumulative test time (1159K test point) and 70 minutes (1655K). Differences between the average temperature readings of the 254 μm thermocouple and the optical thermometer at these two points are primarily due to the difference in radiation losses. At the 1655K point, the radiation loss from the optical fiber was calculated to be 67K greater than the radiation loss of the thermocouple. Between 70 and 87 minutes of cumulative test time (continued steady state operation at 1655K) the average temperature readings of the optical fiber thermometer decreased precipitously. Based on this, the degradation observed in the optical sensor post-test probably occurred between 70 and 87 minutes of cumulative sensor run time. Additionally, analysis of the 1159K and 1655K test points produced very similar results.

TABLE 14. — HIGH TEMPERATURE OPTICAL FIBER THERMOMETER
 SENSOR HISTORY — COMBUSTOR RIG TEST DATA

• Pretest:	New Sensor
• 1159K (1626°F)	65 Min Total Accumulated Time
• 1655K (2519°F)	105 Min Total Accumulated Time
Post-Test Visual Inspection:	• Gritty Appearance
	• Slight Crinkling (Backside)

8746C

Table 16 summarizes the comparisons between the optical fiber thermometer and the 76 μm thermometer. All results were obtained from a single optical thermometer sensor analyzed at two test points.

TABLE 15. — TABLE OF AVERAGE TEMPERATURE READINGS VS CUMULATIVE HIGH TEMPERATURE OPTICAL FIBER THERMOMETER SENSOR RUN TIME IN COMBUSTOR RIG

Cumulative Optical Fiber Thermometer Sensor Test Time (minutes)	10 mil T/C (Type B):		High Temperature Optical Fiber Thermometer Average Temperature
	Average Temperature	Average Temperature	
65	1159K (1626°F)	1083K (1490°F)	
70	1655K (2519°F)	1583K (2282°F)	
87	1655K (2519°F)	1096K (1513°F)	
93	1655K (2519°F)	1102K (1523°F)	
105	1655K (2519°F)	1568K (2363°F)*	

Notes:

- 1) Abrupt shift in average temperature reading at 87 minutes indicates degradation to optical sensor occurred between 70 and 87 minutes.
- 3) At 1655K test conditions, radiation loss from high temperature optical fiber thermometer sensor was calculated to be 67K (120°F) more than T/C.

*Erratic

TABLE 16. — COMPARISON OF OPTICAL FIBER THERMOMETER WITH DUAL WIRE THERMOCOUPLE

•	In 4 Hz to 1 kHz Bandwidth, Required Compensation Is Greater for Optical Fiber Thermometer than 76 μm (3 mil) Thermocouple
	8 Hz: \approx 23 dB More Compensation
	1 kHz: \approx 7 dB More Compensation
•	Observed "Roll-Off" of Uncompensated High Temperature Optical Fiber Thermometer Sensor Compared to Compensated 76 μm (3 mil) Thermocouple Was \approx :
	-6 dB/octave 4 Hz to 12 Hz at 1159K and 1655K Test Point
	-3 dB/octave 12 Hz to 150 Hz at 1159K Test Point
	-3 dB/octave 12 Hz to 250 Hz at 1655K Test Point
	-6 dB/octave 150 Hz to 1 kHz at 1159K Test Point
	-6 dB/octave 250 Hz to 1 kHz at 1655K Test Point
•	Compensated Optical Fiber Thermometer Dynamic Readings Compared to 76 μm (0.003 in.) Dual Wire Thermocouple in 10 Hz to 1 kHz Bandwidth
	1159K Test Point \rightarrow 25 to 165% Higher
	1655K Test Point \rightarrow -30 to 55%

6746C

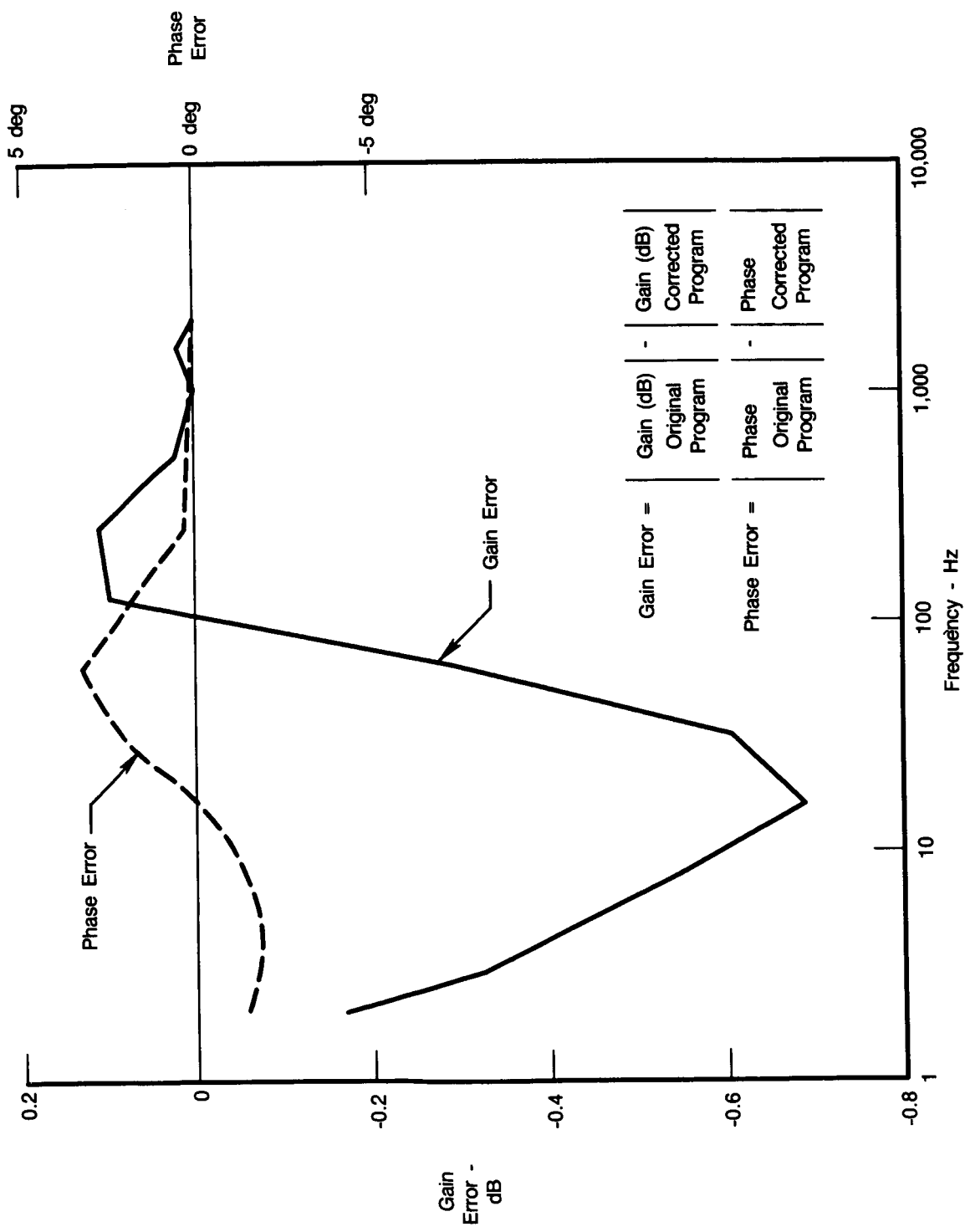
Task II — Reduction of Execution Time of the Dynamic Gas Temperature Measurement Data Reduction Package

Summary. — In Task II, the computer algorithms were reviewed to determine a means of reducing the computer processing times. The use of input waveforms (to the finite difference model) containing multiple frequencies was determined to be a viable technique offering the potential for an order of magnitude (or better) reduction in processing time. Various types of input signals were investigated and evaluated for possible use in computing the theoretical transfer function of the large diameter thermocouple to small diameter thermocouple as a function of the aerodynamic parameter Γ and for computing the compensation spectrum from the measured value of Γ . Finite bandwidth impulse functions were found to be acceptable. The technique consisted of perturbing the model with an impulse time waveform of fixed frequency bandwidth. The resulting output time waveform could then be Fast Fourier Transformed along with the input waveform and the resulting spectra manipulated to yield a specific frequency band of the compensation spectrum. By inputting impulse functions of different bandwidths (typically six) the entire compensation spectrum could be generated. It was estimated that this technique could reduce the nominal 65 minutes of original computer processing time required to compute the transfer functions and compensation spectrum to less than 7 minutes. The compensation spectra generated via the selected finite bandwidth impulse functions were typically within ± 0.1 dB (± 1.1 percent) of the compensation spectra generated using the original program over the frequency band of 0 to 2048 Hz for both the 76 μm (0.003 inch) and the 250 μm (0.010 inch) thermocouple models.

Ultimately, the use of discrete sinusoids for perturbation of the finite differences model as in the original program was retained. In Task III it was determined that the program execution time in the IBM computer was significantly faster than had been estimated. This precipitated the decision to retain use of the discrete sinusoids which is a simpler procedure.

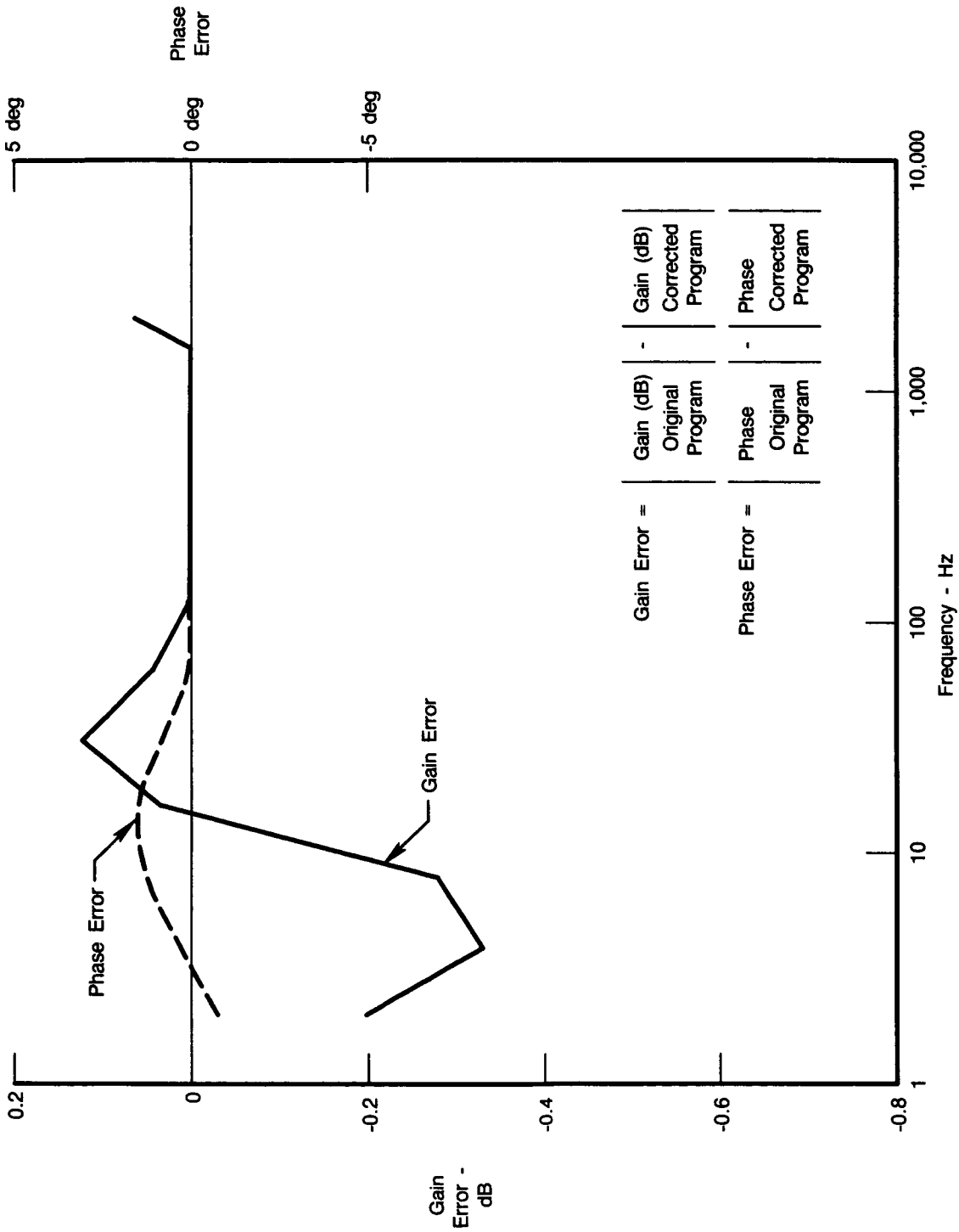
Discussion. — The original algorithm for the finite differences computer model used sinewave gas stream temperature fluctuations as the model boundary condition. To generate the entire compensation spectrum, the model is iterated at various discrete frequencies contained within the compensation spectrum (at each spectral line up to line number 50 and every 10 lines thereafter). This entails evaluation of typically 148 independent frequencies with several thousand iterations of the model required at each frequency. By using an input waveform containing multiple frequencies, the required frequency domain information (gain and phase) could be obtained for many frequencies simultaneously through FFT analysis and manipulation of the input and output waveforms. Thus, the number of independent evaluations of the model could be reduced substantially. The additional time required to perform the FFT analysis would not be a major factor in the overall processing time.

During implementation of the impulse function into the computer code, an error in the original coding for the $\zeta'(7)$ equation was discovered and corrected. The "(TR-T6)" term in the ZP(7) equation on page 93 of Volume II "Operation and Program Manual," NASA CR-168267 (Reference 1) should have been "(TR-T7)." Figures 105 and 106 depict the gain and phase errors for the 76 μm and 254 μm thermocouples due to the erroneous coding. The errors were minimal: 7.6 percent gain error and 3.3 degrees phase error maximum over a portion of the compensation spectra. These errors are inconsequential to results reported in the original contract.



FDA 316100

Figure 105. Errors in Compensation Spectrum of 76 μm (0.003 Inch) Thermocouple Due to Error in ζ (7) in Original Computer Code



FDA 316101

Figure 106. Errors in Compensation Spectrum of 254 μm (0.010 Inch) Thermocouple Due to Error in ζ (7) in Original Computer Code

Both the 76 μm (0.003 inch) and the 254 μm (0.010 inch) thermocouple finite differences models were used in evaluating various types of input functions. The 254 μm (0.010 inch) model was the most severe test due to the larger dynamic range of its frequency dependent gain function and an inherently lower amplitude response to an impulse. The compensation spectra derived from each input function were compared with the corresponding benchmark compensation spectrum generated by use of discrete sinewaves using the original computer program with corrected computer code for computation of ζ '(7). The majority of the tests were run on a Hewlett Packard model 5451C Fourier Analyzer (single precision). Various types of FFT "windowing" functions were evaluated to minimize non-periodicity effects encountered with certain waveforms and lengths of the time records (T_{Rec}).

During initial tests with unit impulse functions, an anomaly in the phase of the compensation spectra was observed. As the frequency was increased from dc, the phase would generally track results obtained with the original program up to a specific channel in the spectrum and then smoothly decrease to 0 degree at the Nyquist frequency. It was first thought that this effect was due to precision or truncation errors in the computations. Investigations were made using double precision computations on the IBM computer with both discrete sinewave and unit impulse input functions. In these tests, the number of incremental time steps per period of the model input waveform (i.e., the effective sampling rate) was varied. It was found that the phase measurement asymptotically approached the correct reading as the number of samples per period was increased. This effect was the same for both discrete sinewaves and the unit impulse. A minimum rate of 128 samples/period was selected for use in Task III. This will limit phase errors to less than 1 degree.

The gain function did not exhibit any similar dependency upon sampling rate. In the original program, the sampling rate for frequencies below 62 Hz was determined from the following expression:

$$\text{Number of samples/period} = \frac{\text{period}}{5 \times 10^{-4}} = \frac{1/\text{frequency}}{5 \times 10^{-4}} \quad (18)$$

Thus the sampling rate ranged from 1000/period at 2 Hz to 33/period at 60 Hz. At all frequencies above 62 Hz, the sampling rate was 32/period. Based on the results of Task II investigations, the maximum phase error in the original program was 4.8 degrees (at 102 Hz for the 76 μm thermocouple).

If an impulse function were used to perturbate the model, the gain and phase information used to generate the compensation spectrum would be extracted by FFT analysis of the input and output from the model. The sampling rate would be determined by the number of elements in the time record (hereafter called block size) and the time length of the record (T_{Rec}). The relations between block size, incremental time step (Δt), FFT frequency line separation (Δf), and sampling frequency (fs) is as follows:

$$\Delta t = \frac{T_{\text{Rec}}}{\text{block size}}$$

$$\Delta f = 1/T_{\text{Rec}}$$

$$f_s = 1/\Delta t = (\Delta f) (\text{block size})$$

As documented in the original contract report (NASA CR-168267), compensating time domain data to 1000 Hz (statement of work frequency range) requires compensation to about 2000 Hz. In the computer coding, a fixed block size (i.e., the record length) would be used and the

sampling rate could be established by selecting either the Δf or Δt parameter. With a fixed block size, a high sampling frequency (to meet the 128 samples/period minimum) results in a correspondingly high value of FFT frequency line separation (i.e., reduced frequency resolution). Proper measurement of Γ requires a frequency resolution of about 2 Hz up to approximately 40 Hz for the 254 $\mu\text{m}/76 \mu\text{m}$ thermocouple pair.

With a block size of 4096, a frequency resolution of 2 Hz would dictate a sampling rate of 8192 Hz. Thus, the highest frequency that would be sampled a minimum of 128/period would be:

$$\frac{8192}{128} = 64 \text{ Hz} \quad (20)$$

To obtain a minimum of 128 samples per period of 2048 Hz would require a sampling rate of;

$$128 \times 2048 = 262,144 \text{ Hz} \quad (21)$$

which would yield a frequency resolution of 64 Hz (block size 4096).

Thus, both criteria, high sampling frequency and small frequency line separation, cannot be met in a single analysis of practical block size (4096). A block size of 131,072 would be required to meet both criteria simultaneously. A technique was developed that would provide reasonable tradeoffs in frequency resolution to meet sampling criteria by performing the analysis in frequency bands (Table 17).

TABLE 17. — COMPENSATION SPECTRUM COMPUTATION BANDS FOR FINITE BANDWIDTH IMPULSE FUNCTION (4096 BLOCK SIZE)

<i>Band No.</i>	<i>Frequency Band</i>	Δf	T_{Rec}
1	0 to 64 Hz	2 Hz	500 ms
2	64 to 128 Hz	4 Hz	250 ms
3	128 to 256 Hz	8 Hz	125 ms
4	256 to 512 Hz	16 Hz	62.5 ms
5	512 to 1029 Hz	32 Hz	31.25 ms
6	1024 to 2048 Hz	64 Hz	15.625 ms

6745C

There are various types of waveforms that possess multiple frequencies. These waveforms are the unit impulse, finite bandwidth impulse, and narrowband and wideband random. Additionally, other types of waveforms with desired frequency content could be generated digitally in the computer (such as a waveform with frequency components of amplitudes generally inverse to the thermocouple response which would yield a smaller dynamic range in the output of the model across the frequency band).

Following extensive tests with various waveforms, use of the finite bandwidth impulse function was determined to be a viable approach. The problem with the pure unit impulse was non-periodicity effects at the higher sampling rates (particularly for the 254 μm thermocouple). As the sampling rate was increased, the time length of the data record decreased. If the output waveform amplitude does not decay to zero by the end of the data block, the frequency components become non-periodic in the FFT and "leak" into near frequency channels producing sizeable errors in the gain and phase functions. The lower spectral lines in the FFT are affected most. However, in severe cases, the effects extend into the higher spectral lines. Attempts to "window" the output function to ensure periodicity and gain accuracy were unsuccessful. For the unit impulse function, various exponential windows were evaluated but the results were too

inaccurate. Attempts to use more conventional FFT windows (the typical bell shaped windows) were also unsuccessful. Use of a windowing function entails application of a scalar amplitude correction factor. The correction factor only produces accurate results when the signal to be analyzed has the same amplitude characteristics over the entire time length of the data record (which the impulse does not).

The narrowband random input function in conjunction with a conventional window appeared to be promising. However, a random signal by nature would require averaging (increasing analysis time) since all frequencies do not exist simultaneously within a given time period. Tests with an input signal whose amplitude vs frequency characteristics were such that the amplitude increased in a ramp fashion as frequency increased did not produce any better results than the unit impulse, again due to non-periodicity effects.

By generating impulse functions through a bandpass (rather than lowpass or allpass) digital filter, it was possible to minimize the effects of non-periodicity. Elimination of the low frequencies within the impulse function minimizes the amplitude of the model's output waveform at time $t = T_{\text{Rec}}$ since the lower the frequency the higher the output from the model. Additionally, by increasing the block size from 2048 (original contract) to 4096, the sampling rate for a fixed time length could be doubled. Thus, a time length of 15.625 ms could provide 128 samples at 2048 Hz at a block size of 4096. It would take a time length of 7.8125 ms to provide the same number of samples at 2048 block size. The longer the time length of the record, the greater the decay of the amplitude of the output signal at time T_{rec} . Logic could be incorporated into the software to warn the operator if non-periodicity was a potential problem. Such logic would key on the dc term from the FFT analysis. The technique described below was arrived at by experimentation. For the low frequency band of the compensation spectrum, a low pass digital filter will be used to generate the impulse function. The sampling requirements (Table 17) are met with time record lengths sufficient to permit complete decay of the impulse function to about zero amplitude at the finite differences model output for both the 254 μm and 76 μm thermocouples. The bandpass filter would be used for all other frequency ranges. Table 17 lists the frequency ranges and the time lengths of the data records for generation of the compensation spectrum and is applicable for both the 254 μm and 76 μm thermocouples.

The procedure for generating the impulse functions is as follows:

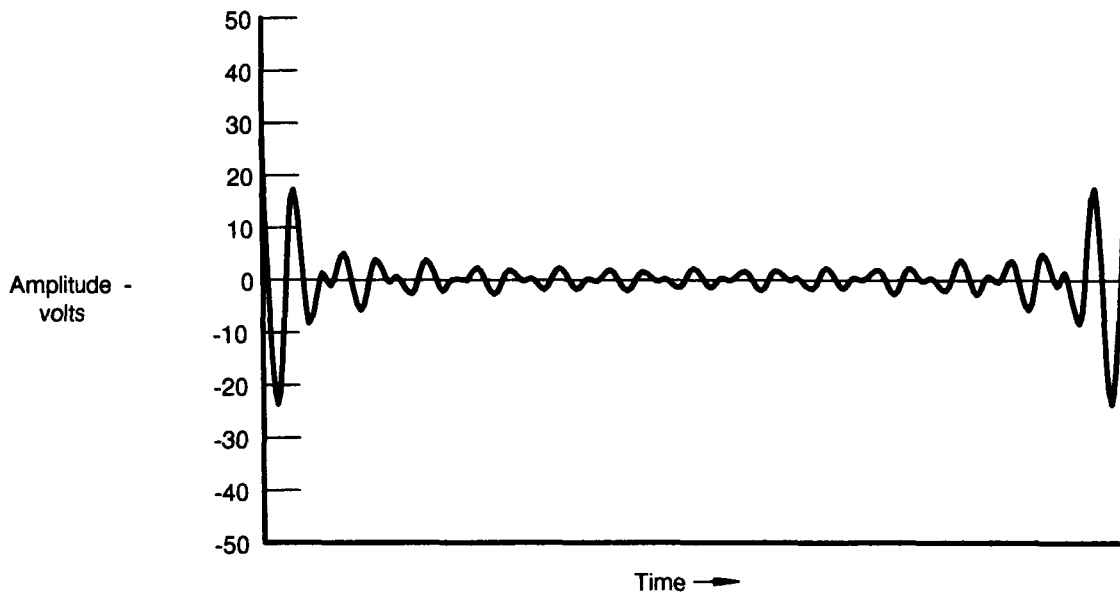
1. Establish two initialized (zero amplitude) rectangular coordinate frequency domain data blocks of 2048 positive frequency elements. In one data block, designated as the lowpass function, enter unity amplitude for the "real" terms of spectral elements 0 through 32. In the other data block, designated as the bandpass function, enter unity amplitude for the real terms of spectral elements 20 through 32.
2. Perform an inverse FFT on each data block to obtain their corresponding time domain waveforms. Note that these waveforms are generic in nature. The amplitude of each element in the time domain data block for the lowpass function (and the bandpass function) is completely independent of any assigned sampling parameters (i.e., Δt , Δf , etc.). Thus, these functions need only be generated once and established as a permanent part of the software in look-up table format. The frequency content of these waveforms is established by assignment of the desired sampling parameters utilized in the iteration of the finite differences model.
3. Shift the data within each datablock by 3840 channels. The data will wrap around producing the waveform (bandpass configuration) depicted in Figure 108. The purpose of this shift is to have the highest amplitude

excursions within the time data record occur early in time within the time data record. The frequency domain effect (of the shift) is simply to modify the phase characteristics.

4. Multiply the elements in each data block by an exponential of the form $e^{-0.0024n}$ (where n = the element number within the data block). Figure 109 depicts the resulting waveform of the bandpass function. This is to force each input function to zero amplitude at a time much less than T_{Rec} to ensure that the output of the model is zero at time $t = T_{Rec}$. If the output of the model is non-zero at $t = T_{Rec}$, errors will be introduced in the analysis due to non-periodicity effects in the FFT analysis to be made.
5. Save the data blocks for the two time domain functions obtained in step 4 for use in perturbing the finite differences model.
6. Perform FFTs on the two data blocks obtained in step 4 above and retain for use in step 9 below to normalize the model's output. Do not apply any windowing function. Note that the frequency content of the impulse functions have been extended by application of the exponential (step 4). The input function now provides frequency content (excitation for input to the model) over a wider range of spectral lines than entered in step 1 above. Figure 110 depicts the extended spectral line content of the bandpass impulse function.
7. Using the sampling parameters specified for band 1 in Table 17, calculate the appropriate time dependent parameters for the finite differences model. Iterate the model using the amplitude values and their corresponding times from each sequential element throughout the range of the data block for the lowpass impulse waveform function obtained in step 5. Establish a time domain data block containing the resultant corresponding output values from the model for each iteration. Figure 111 depicts a typical time waveform at the model output.
8. Perform an FFT on the model output waveform obtained in step 7. Do not use a windowing function.
9. Perform a complex division on the frequency spectrum obtained in step 8 by the corresponding input impulse function frequency spectrum obtained in step 6. This yields the transfer function (gain and phase) of the thermocouple output to the gas path input.
10. Save the transfer function information for the specific frequency band analyzed in steps 7 through 9 for use in generating a composite frequency spectrum.
11. Repeat steps 7 through 10 for each bandpass frequency band in Table 17. Use the generic bandpass input waveform function using the applicable sampling parameters (Table 17).
12. Using the transfer function results from step 10, generate the composite frequency spectrum in a data block containing 1024 positive frequency elements with a spectral line separation of 2 Hz. Use a linear interpolation to compute the phase values at frequencies not evaluated above and a log function interpolation to compute the gain (amplitude) terms. A log

function is recommended for gain interpolation since the log of the gain is approximately linear with log frequency (i.e., the slope of the gain function is typically about -6 db/frequency octave at the higher frequencies where interpolation would be necessary).

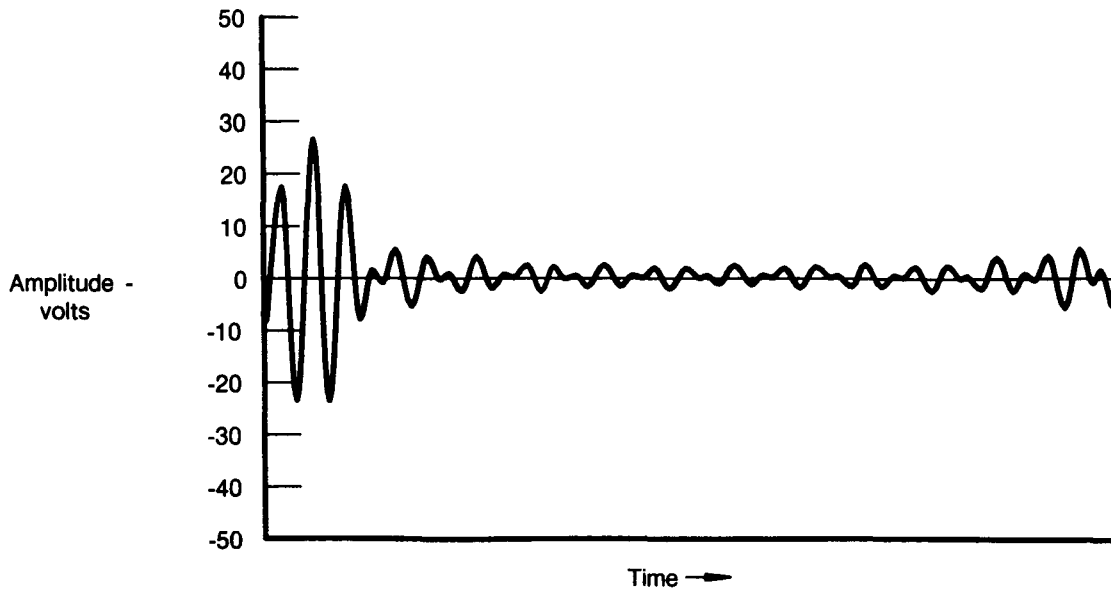
Note that the standard $254 \mu\text{m}/76 \mu\text{m}$ thermocouple analog data would still be acquired using a time domain data block size of 2048 (i.e., 1024 positive frequency elements) and compensated using an FFT spectral line resolution of 2 Hz.



FDA 316102

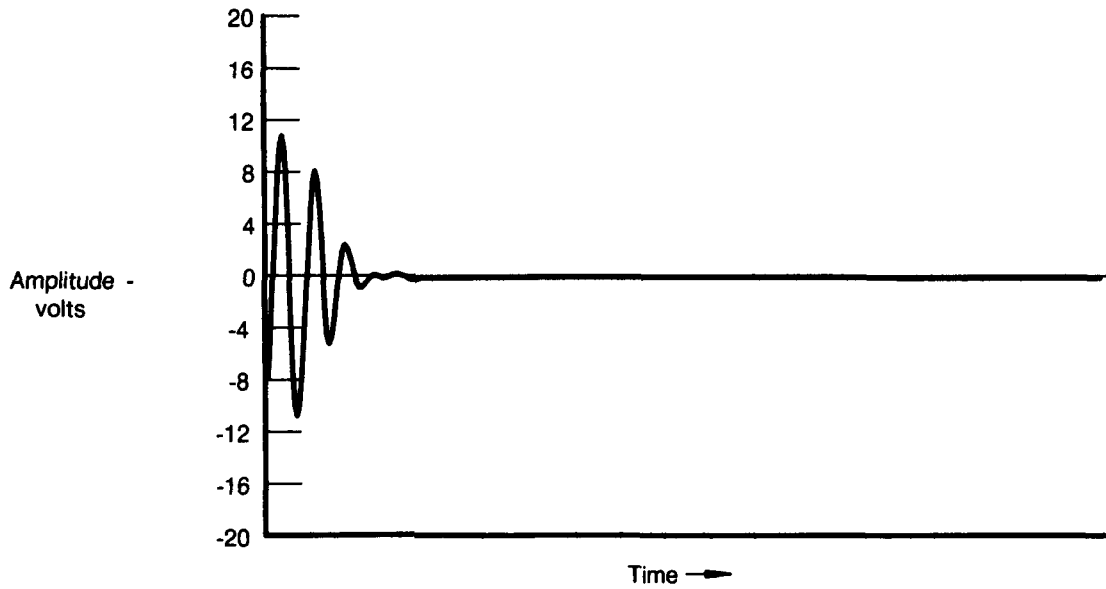
Figure 107. Time Domain of Finite Bandwidth Impulse Function Obtained in Step 2 of Generation Process

For computation of the theoretical transfer functions of the large thermocouple to the small thermocouple as a function of the aerodynamic parameter, Γ , the above technique would be used with the lowpass configuration (spectral lines 0 through 32). Following computation of the transfer function of the large thermocouple to gas stream and small thermocouple to gas stream perform a complex division of these two transfer functions to yield the transfer function of the large diameter to small diameter thermocouples.



FDA 316103

Figure 108. Time Domain Waveform of Finite Bandwidth Impulse Function Obtained in Step 3 of Generation Process



FDA 316104

Figure 109. Time Domain Waveform of Finite Bandwidth Impulse Function Obtained in Step 4 of Generation Process

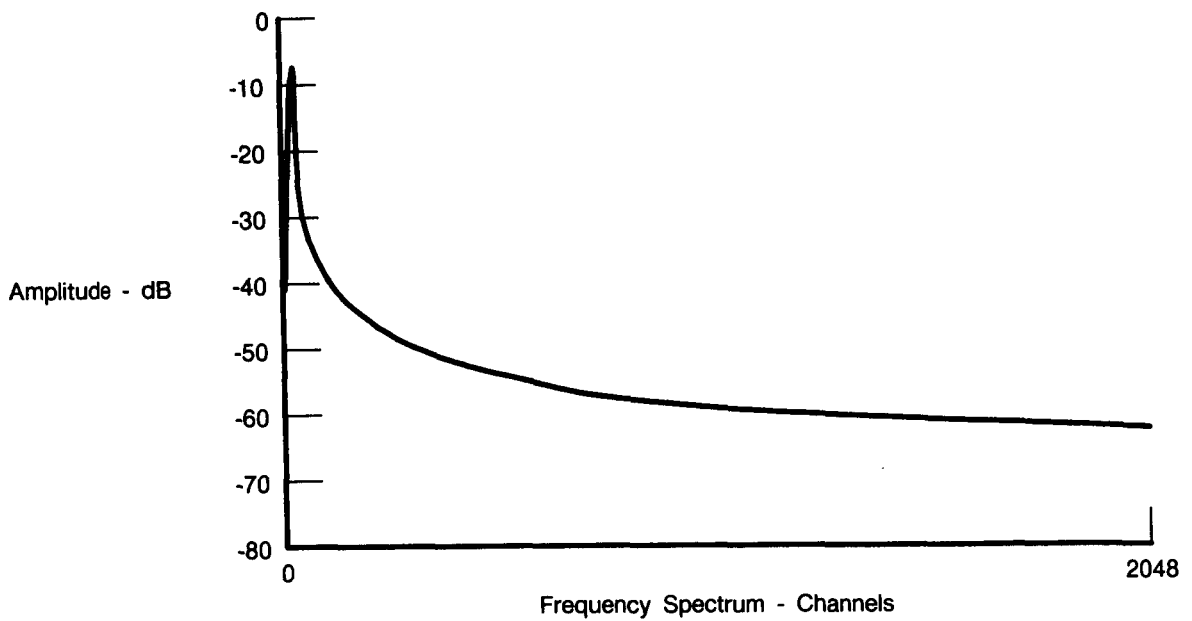


Figure 110. *Frequency Spectrum of Finite Bandwidth Impulse Function*

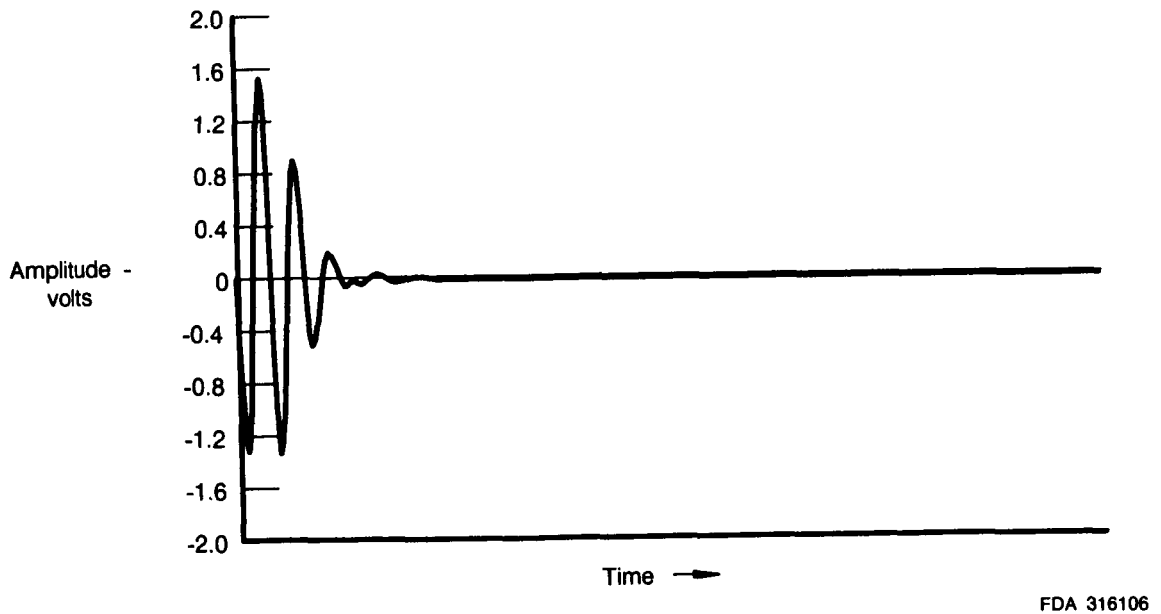
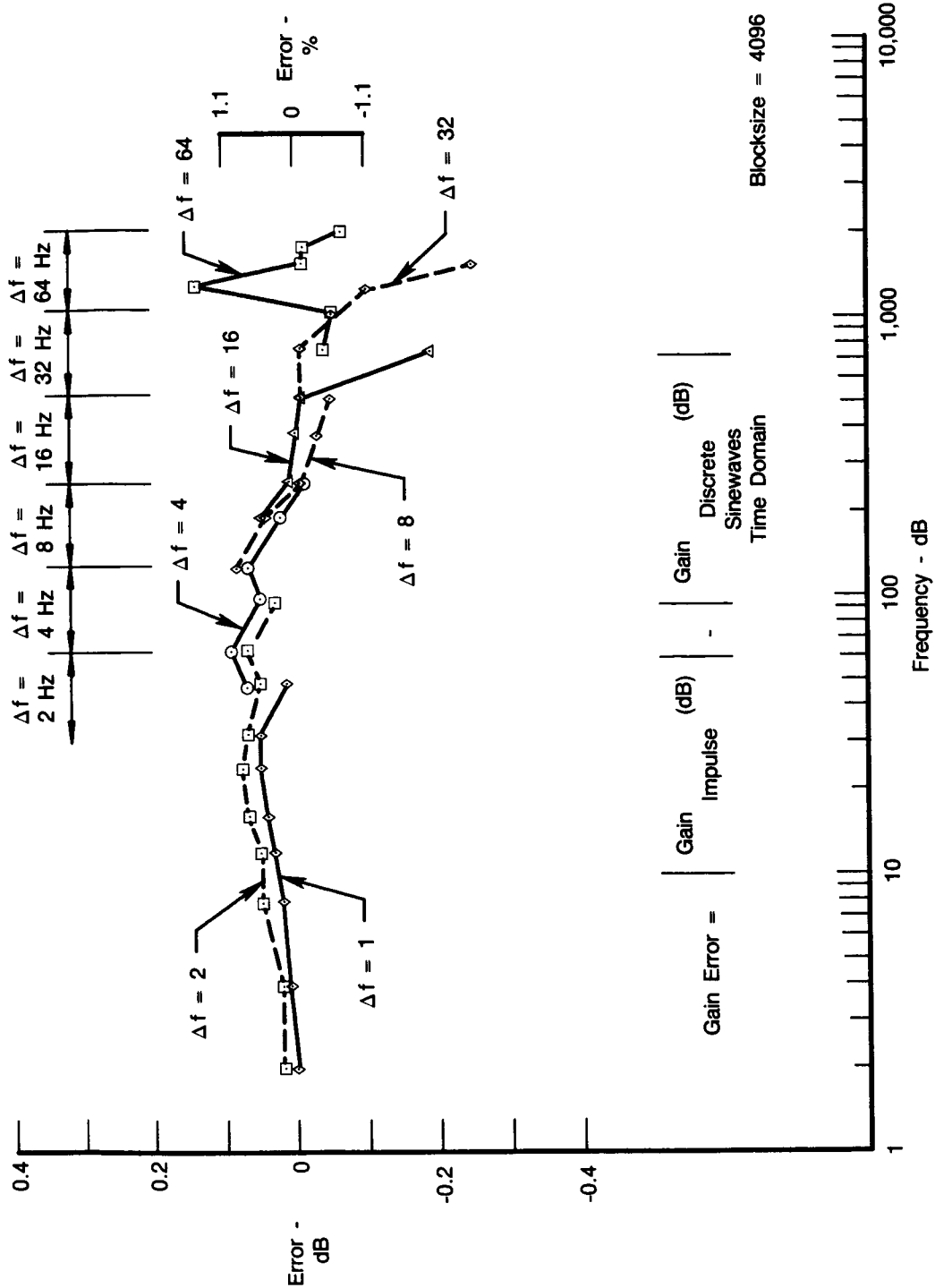


Figure 111. *Typical Time Domain Output of Model Pertubated With Finite Bandwidth Impulse Function*

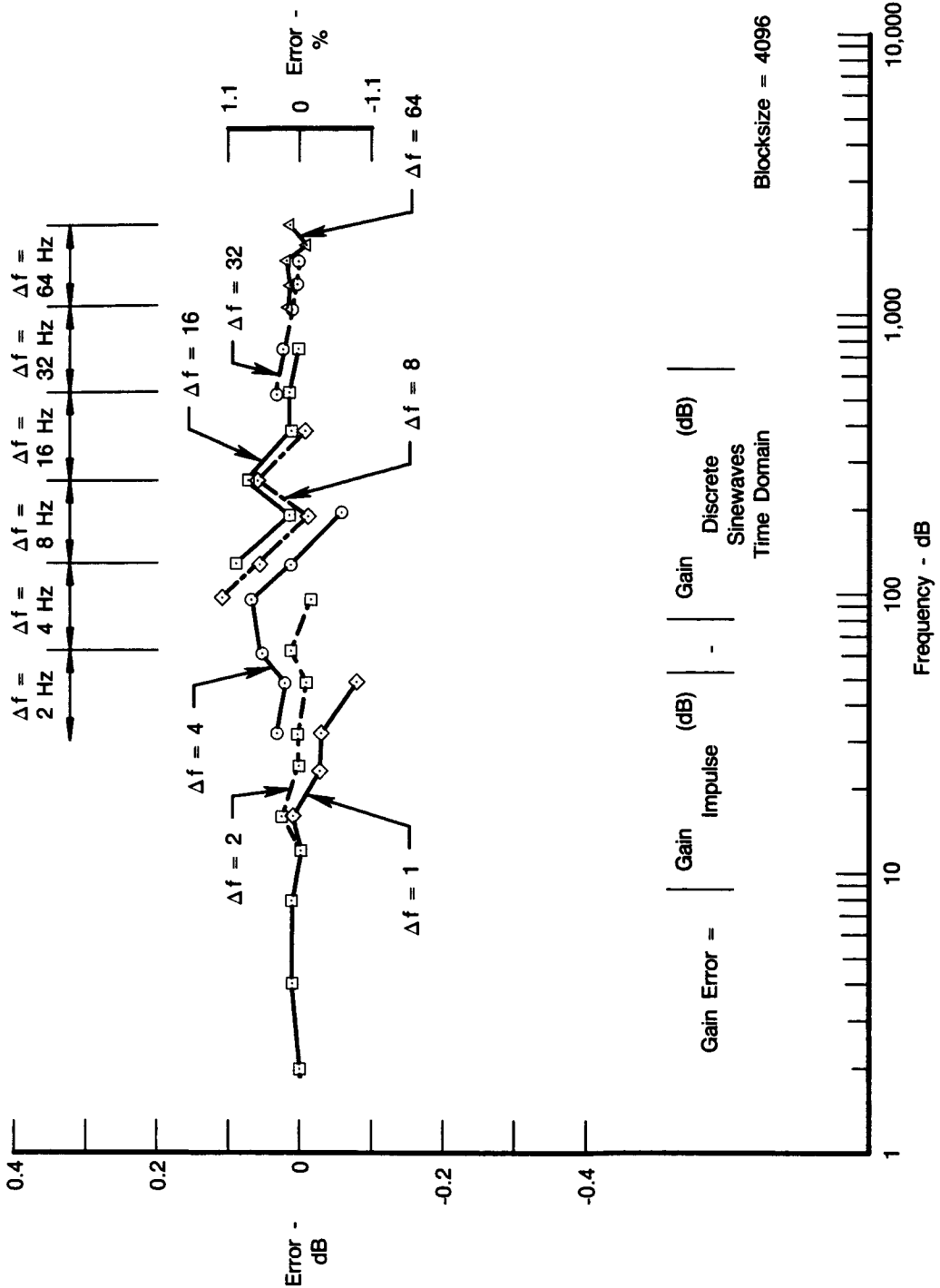
Figures 112 and 113 depict the gain accuracy of the composite compensation spectra for the 254 μm and 76 μm thermocouple models generated by the above procedures. These data were generated on the Hewlett Packard Model 5451C Fourier Analyzer in single precision. Gain errors between the spectra generated from the finite bandwidth impulse functions compared with the compensation spectra generated from discrete sinusoids using the original computer program

were typically less than 1 percent. This is excellent considering the use of single precision computations. Figure 114 depicts the phase function obtained from the finite bandwidth impulse and the original program. The results from the finite bandwidth impulse are the most accurate because sampling in the original program was inadequate.



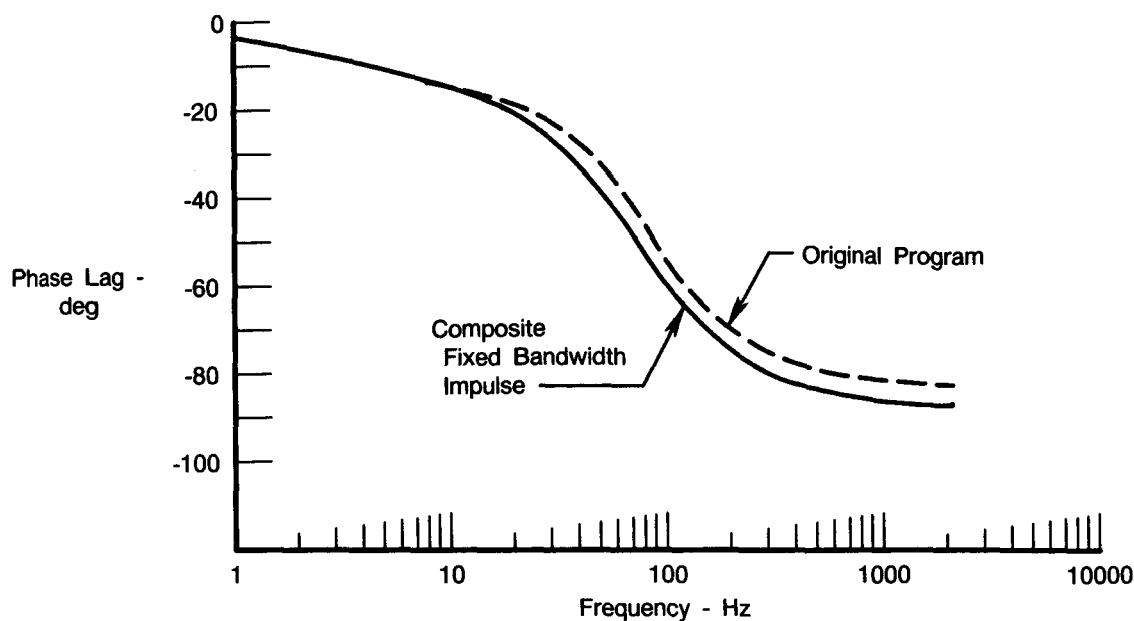
FDA 316107

Figure 112. Bandpass Impulse (ch 16 → 32 Frequency Domain) for 254 μm (0.010 Inch): Gain Error



FDA 316108

Figure 113. Bandpass Impulse (ch 20 → 32 Frequency Domain) for 76 μm (0.003 Inch): Gain Error



FDA 316109

Figure 114. Comparison of Phase Function Computed With Original Program and Fixed Bandwidth Impulse — 76 μm Thermocouple

Task III — Reprogramming of Dynamic Gas Temperature Measurement System Data Package into FORTRAN IV

Summary. — In Task III, the data processing program which was originally written for a Hewlett Packard model 5451C Fourier system was re-written in FORTRAN IV and implemented on IBM computers at Pratt & Whitney and at NASA-Lewis Research Center. Processing time was decreased from about 121 minutes as implemented in the Fourier system to less than 4 minutes in the IBM model 3090 computer (120 records). The finite bandwidth impulse function technique for perturbation of the thermocouple model developed in Task II was rejected in favor of retention of discrete sinusoids as originally implemented when the decrease in processing time on the IBM computer was found to be much greater than estimated.

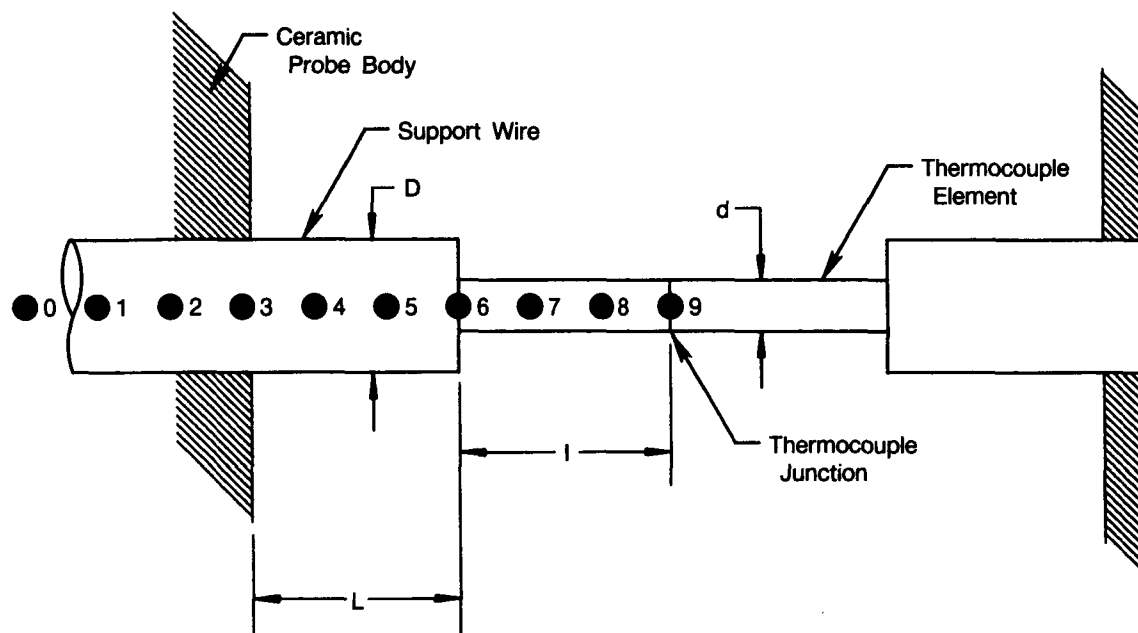
Discussion. — The original data processing program was developed on a Hewlett Packard model 5451C Fourier Analyzer system. The software made extensive use of the analyzer's specific programming features. In Task III, the processing program was written entirely in FORTRAN IV to permit more generalized implementation on other computer systems and to reduce computer processing time.

In Task II, an algorithm to reduce the computer processing time by evaluating the thermocouple model at multiple frequencies simultaneously was developed but was not implemented in the final version of software. Execution of the original algorithm in the IBM computer was much faster than had been predicted.

The merging of high level HP keyboard routines and user written FORTRAN languages in the original program implemented on the HP Fourier system were user friendly but very inefficient in processing speed.

The software to determine the delta time increment for the evaluation of the finite differences model was modified to ensure a minimum of 128 samples per period for each frequency evaluated. This was to ensure adequate sampling necessary for accurate phase measurement. In Task II it was determined that a minimum of 128 samples were required to compute the phase angle to within 1 degree. Additionally, the program was upgraded to process both Type K and Type B thermocouple data.

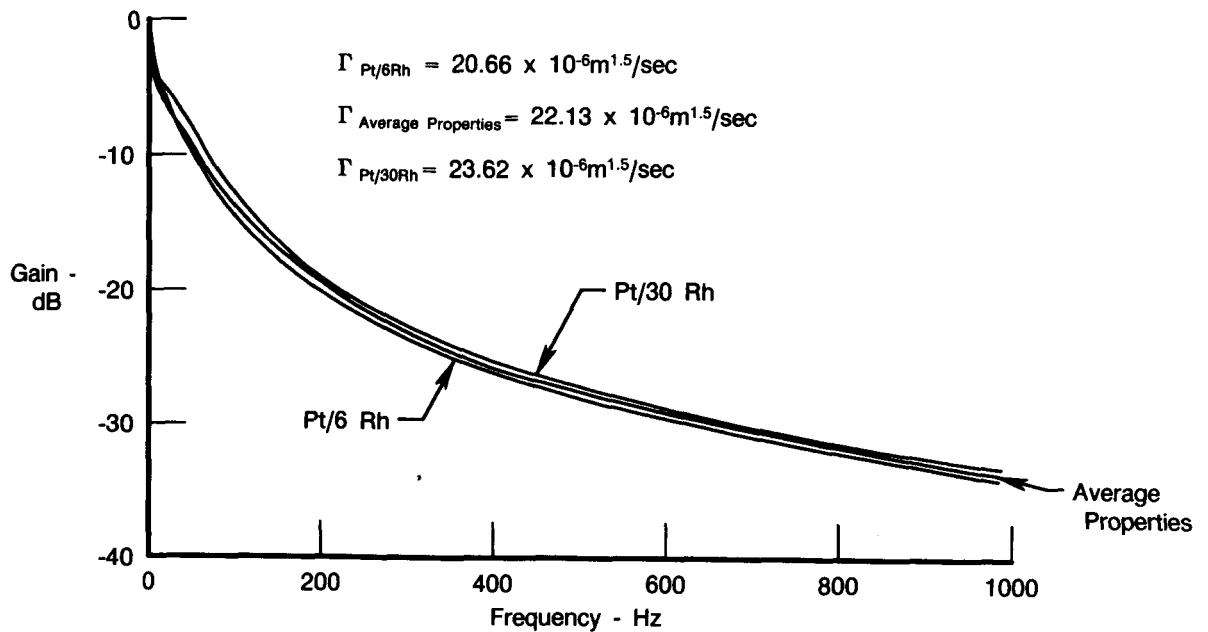
Variations in thermocouple properties (density, heat capacity, and thermal conductivity) were investigated to determine errors incurred due to modelling only one-half of the thermoelement. The nine-node computer model shown in Figure 115 was originally chosen for the simplicity and rapidity of calculation; however, it was recognized that property variations between different legs of the thermoelement would cause differences in calculated compensation spectra. An example of an Instrument Society of America (ISA) Type B (Pt/6Rh-Pt/30Rh) thermocouple was prepared to assess the magnitude of the expected differences. Three compensation cases were run using the same thermocouple experimental data. The first case involved compensating measured data assuming Pt/6Rh properties in the model. The second case used Pt/30Rh properties, and the third case used average properties.



FDA 316110

Figure 115. Nine-Node Finite Difference Model

Results of the calculations are the compensation spectra shown in Figure 116. The Pt/30Rh compensation spectrum is larger than the Pt/6Rh spectrum by about 15 percent over the 0 to 1 kHz bandwidth; the average properties spectrum lies approximately midway between the two. These results indicate the Pt/30Rh material to be more responsive to gas stream dynamic components; its response therefore requires smaller compensation. This is to be expected from comparison of Pt/6Rh and Pt/30Rh properties. Thermal diffusivity, the combination of thermal conductivity, density, and specific heat, is approximately 15 percent lower for Pt/30Rh than Pt/6Rh at 1500°F. Pt/6Rh with higher thermal diffusivity is therefore less responsive to temperature changes. The associated gammas varied approximately ± 7 percent from the $22.13 \times 10^{-6} \text{ m}^{1.5}/\text{sec}$ value based on average material properties. This indicates approximately a one-to-one relationship between an error in the measurement of gamma and error in its compensation frequency spectrum.

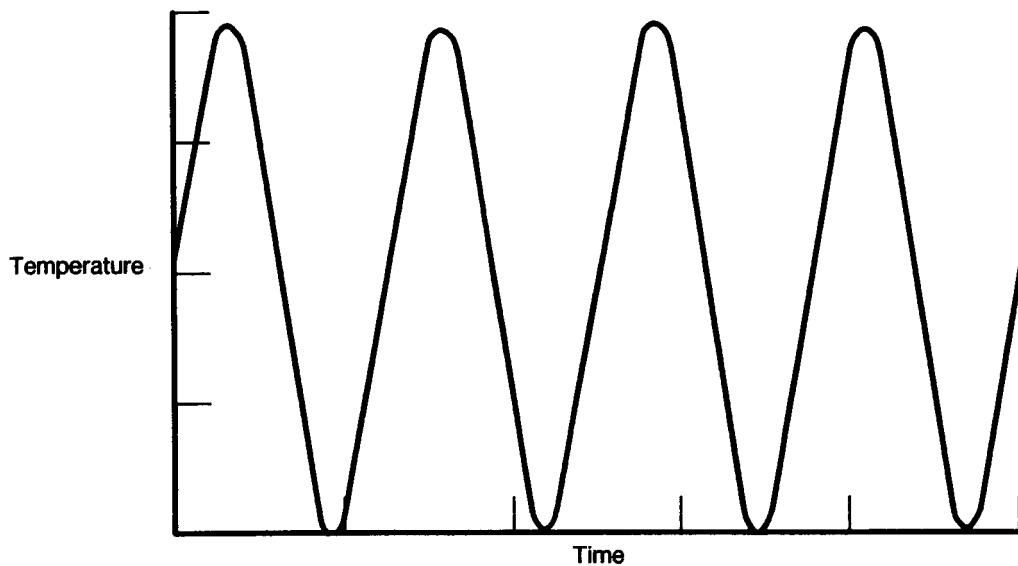


FDA 316111

Figure 116. Calculated Thermocouple Response for Pt/6Rh, Pt/30Rh, and Average Material Properties

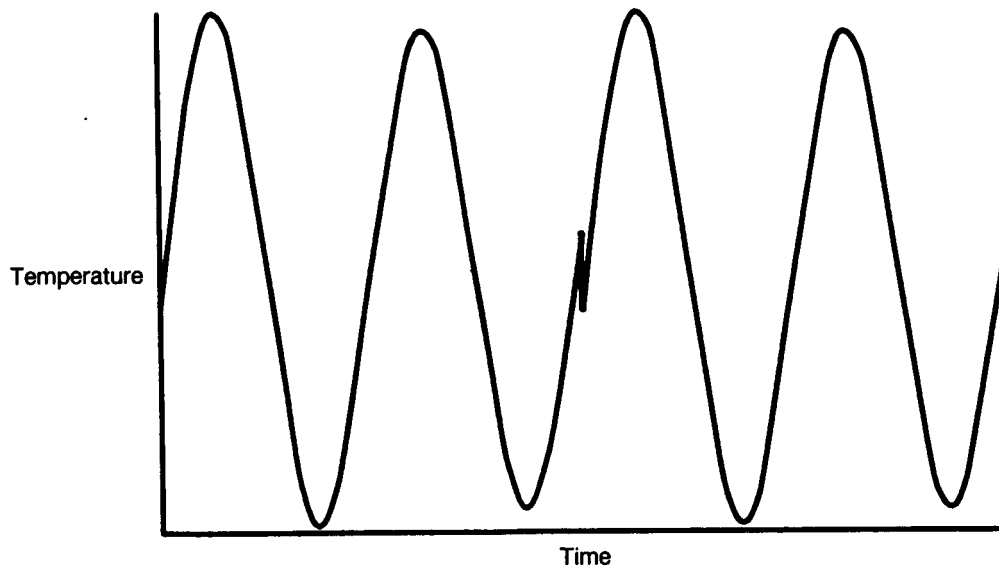
The processing software was modified to use average material properties. This approximation results in additional measurement uncertainty. A more complete model considering both halves of the thermocouple simultaneously, each with individual properties, involves complexity of additional equations and increased computer execution time, and is beyond the scope of this effort. Depending on measurement uncertainty considerations, such a model may be necessary for future programs.

For software checkout, F100 engine FM tape data were digitized and then processed in the mainframe IBM computer (model 3090) at Pratt & Whitney. There were slight differences from the original contract results. These were attributed to the minor error in the original software finite differences model (previously described) and the implementation of average thermocouple properties. Additionally, mathematically generated sinusoidal data records with predetermined parameters (amplitude, system gain, test point conditions, etc.) of 8 Hz and 200 Hz were used to verify proper program execution. Discrete sinusoids (narrowband signals) such as the 8 Hz and 200 Hz test cases will exhibit a discontinuity in the compensated time record and a small amplitude modulation. Figures 117 and 118 depict the compensated time records for 76 μm and 254 μm thermocouples at 8 Hz. The effect is most noticeable in the frequency band near the corner frequency of the thermocouple where the change in the gain function per spectral line of the compensation spectrum is highest. The effect is inherent in the use of discrete Fourier Transforms. The FFT of the sinusoid will indicate significant energy in the first couple of spectral lines above and below the true frequency. These components should be compensated by the same gain and phase as the true frequency. However, they are compensated as if they were the true frequency. For the 8 Hz sinusoid, the effects are more pronounced in the 254 μm thermocouple (Figure 118) with a corner frequency of about 4 Hz than the 76 μm (Figure 117) with a corner frequency of about 23 Hz. At higher frequencies (relative to the thermocouple corner frequency and the spectral line frequency separation) the effect will be negligible.



FDA 316969

Figure 117. Compensated Time Waveform for 76 μm Thermocouple for an 8 Hz Sinusoid



FDA 316113

Figure 118. Compensated Time Waveform for 254 μm Thermocouple for an 8 Hz Sinusoid

The software was implemented at the NASA-Lewis Research Center on an IBM computer. On-site support was provided to interface the thermocouple data processing software with NASA's front end digitization system. The 8 Hz sinusoidal data case was run to ensure proper program execution. The F100 FM tape data from Reference 1 were digitized at NASA and processed in their computer to provide an end to end checkout. These results were compared with those obtained at Pratt & Whitney to ensure common results.

Task IV — Data Acquisition

P&W personnel provided on-site support at NASA-Lewis Research Center to review and assist in the setup for data acquisition of dual wire thermocouple data during the testing of a high pressure burner rig. This effort involved reviewing the setup in terms of equipment, amplifiers, filters, and scaling. The task was completed with the successful acquisition of data having a sufficient signal-to-noise ratio to achieve the required accuracy.

DISCUSSION OF RESULTS

The results of the two experiments (rotating wheel and subscale combustor) of Task I were effective in verifying the accuracy and frequency response of the dynamic gas temperature measurement system previously developed in Reference 1. Detailed discussions of the compensated data from the two-wire thermocouple probes and fine wire resistance thermometer temperature probe standards are presented in the Task 1d and 1e technical discussion sections. However, a brief review of these results can be summarized as follows.

Rotating Wheel Experiment

At the 250 Hz test condition (the primary analysis point) the 76 μm (0.003 inch) thermocouple compensated data were approximately 23 percent lower than the compensated 6.4 μm (0.00025 inch) resistance thermometer temperature standard. This variation is greater than originally predicted for this experiment; however, these results are not unreasonable when the uncertainties associated with the detail components of the rotating wheel apparatus are considered. A large amount of the observed difference may be attributed to the fact that the aerodynamic parameter, Γ , used for compensating 250 Hz data was extrapolated from lower frequency data at 20 Hz. During the data analysis it was determined that temperature fluctuations of sufficient magnitude were not present in the 250 Hz test data spectrum. It has been demonstrated that the data must contain temperature fluctuations at frequencies generally lying between the corner frequencies of the large and small diameter thermocouples to ensure adequate sensitivity for the measurement of Γ .

Subscale Combustor Experiment

Results from the subscale combustor tests were good, especially when considering the level of the gas path temperature fluctuations. In the region of 20 Hz, where the temperature fluctuations were approximately 23K rms/ $\sqrt{\text{Hz}}$, the compensated 76 μm thermocouple read approximately 18 percent greater than the compensated 12.7 μm (0.0005 inch) resistance thermocouple temperature standard. At all higher frequencies, where the dynamic temperature amplitudes ranged from approximately 8K rms/ $\sqrt{\text{Hz}}$ down to 3K rms/ $\sqrt{\text{Hz}}$, the compensated 76 μm thermocouple was 41 to 48 percent higher than the 12.7 μm resistance thermometer. Although the percent of reading errors for the dynamic components appear high, they are relatively low in actual temperature differences.

The compensated 76 μm (0.003 inch) and 127 μm (0.005 inch) thermocouples produced much closer results when compared. The maximum error between the two was only 12 percent of reading.

Comparison of the high temperature optical fiber thermometer (compensated and uncompensated) with the compensated 76 μm (0.003 inch) thermocouple showed larger differences than the comparison of the 76 μm (0.003 inch) thermocouple to the 12.7 μm (0.005 inch) resistance thermometer. Compensated optical fiber thermometer data varied from 38 percent lower to 199 percent higher than the corresponding compensated 76 μm thermocouple data.

Using the compensated 76 μm thermocouple to represent the true gas path frequency characteristics, the transfer function of the uncompensated optical fiber thermometer to the compensated thermocouple exhibited a gain function roll-off rate of approximately -3 dB per octave over a limited frequency range. For the average test point conditions this frequency range was from approximately 12 to 150 Hz. For the second test condition this range was approximately 12 to 250 Hz. At all other frequencies out to the range of the analysis (1 kHz), the roll-off rate was approximately -6 dB per octave. These results however, were obtained using a

single optical fiber thermometer sensor which was observed to have deteriorated during testing. Post-test inspection of the sensor revealed that the platinum coating on the tip had deteriorated sometime during the test and may have affected the sensor performance.

Computer Programming Efforts

The results of the computing program software development have similarly been discussed in detail in these Tasks; however, a brief review of these results can be summarized as follows.

In Task II, the computer algorithms originally developed for the Hewlett-Packard Fourier Analyzer System used in Reference 1 were reviewed to determine a means of reducing the processing time. The result of these efforts were the development of an input function for use in the IBM computer program developed in Task III. Ultimately the original program's use of discrete sinusoids for perturbation of the finite element model was retained. It was determined in Task III that the program execution time of the IBM computer was significantly faster than anticipated.

In Task III, the original program of Reference 1 was rewritten in FORTRAN IV and implemented on IBM computers at P&W and NASA-Lewis. Processing time was decreased from approximately 121 minutes for the original program to less than 4 minutes on the IBM computer. Detailed descriptions of the program developed are presented in Volume II of this report.

Recommendations

Directions for further work in this measurement technique fall into two general categories: 1) fine tuning and optimization of the measurement method, and 2) fundamental aspects of heat transfer. These are outlined below:

1. Measurement uncertainty contribution, both precision and bias, should be determined for each source in the experiment and compensation method. The need for the dynamic temperature sensor is to optimize thermoelement diameter ratio and frequency range for determining Γ , and to improve the experimental setup and other factors to minimize uncertainty in the compensated gas stream measurement. Such an uncertainty analysis would involve propagation of uncertainties for time-dependent quantities, and would require combining measurement uncertainties in both time and frequency domains. The physical significance of uncertainty of a given spectral line in the temperature spectrum merits careful consideration. Lastly, the uncertainty of the resistance thermometer data needs to be determined for meaningful comparisons with dynamic temperature sensor data.
2. The finite-difference model should be extended to include material properties for both halves of the thermoelement. Use of average properties simplifies the model but compromises uncertainty in the compensation method. The average properties vs individual properties change would determine the corresponding measurement uncertainty contribution, and allow cost vs complexity tradeoffs to be made for the compensation scheme.
3. The variation of Γ with frequency should be investigated. The Γ values used in this work were averaged over the practical working bandwidth. Investigation of frequency dependent effects were beyond the scope of this work.

4. Values of h_g implicit in Γ should be determined explicitly. The measurement technique developed here offers a novel possibility for measuring h_g for a cylinder in crossflow in a combustion stream.

CONCLUSIONS

The accuracy of the dynamic gas temperature measurement system has been demonstrated in laboratory experiments. Differences between reference sensor and compensated dynamic gas temperature sensor data were small in comparison with experimental mean gas temperatures. The compensation technique developed is among the first available for correcting transient effects of both conduction and convection.

The dynamic gas temperature measurement system offers measurement capabilities previously unavailable for gas turbine engines. Structural adequacy of the probes demonstrated in previous work is now more meaningful in combination with measurement fidelity verification. The method can potentially be adapted to transient engine acceleration combustor exit temperature measurements, associated blade and vane cooling flow temperature measurements during transients, as well as used for measurement of steady-state engine dynamic gas temperature signals.

LIST OF SYMBOLS

<u>Symbol</u>	<u>Description</u>	<u>Units</u>
A	Constant in finite-difference transfer function equations = $D^2 \Delta/8 \alpha \Delta T$	Meters-sec/K
a_n	Amplitude of the gas temperature at frequency f_n	K
$a_n(f)$	a_n as a function of frequency	K
a_1	Amplitude of the small 76 μm (0.003 in.) thermocouple element	K
a_2	Amplitude of the large 254 μm (0.010 in.) thermocouple element	K
B	Constant in finite-difference transfer function equation = $d^2 \delta/8 \alpha \Delta T$	Meters-sec/K
C	Constant in finite-difference transfer function equation = $D^2/4 \Delta$	Meters
C_n	Radian frequency = $2 \pi f_n$	Radians/sec
C_{pw}	Specific heat of thermocouple wire	Cal/grams-K
D	Large thermocouple element diameter at junction	Meters
d	Small thermocouple element diameter at junction	Meters
E	Constant in finite-difference transfer function equations = $d^2/4 \delta$	Meters
E	Young's Modulus	Newton/Meters ²
F	Constant in finite-difference transfer function equations = $\Gamma D^{1/2} \Delta/2 \alpha$	Meters
F/A	Free stream gas fuel-air ratio	Dim-less
f	Frequency	Hz
f_n	nth frequency window in frequency space	Hz
G	Constant in finite-difference transfer function equations = $\Gamma d^{1/2} \delta/2 \tau$	Meters
G	Thermocouple signal gain	Dim-less
G_a	Design safety factor for vibrational stress	Dim-less
$S_1(f)$	Measured FFT spectrum of smaller diameter thermocouple	K Phase — degrees
H	Probe ceramic height	Meters
H(f)	Measured transfer function (FFT frequency response function) of larger diameter thermocouple with respect to smaller diameter thermocouple	Gain — dim-less Phase — degrees
h^+ , h_g	Convective film coefficient of thermocouple element	Watt/m ² K
h^-	Convective film coefficient of thermocouple support wire	Watt/m ² K

j	Time index	Seconds
k_c	Thermal conductivity of the probe ceramic	Cal/sec-Meter-K
k_g	Thermal conductivity of the gas	Cal/sec-Meter-K
k_w	Thermal conductivity of the thermocouple wire	Cal/sec-Meter-K
L	Length of the probe thermocouple support wire	Meters
l	One half of the length of the probe thermocouple element wire	Meters
M or M_n	Free stream gas Mach number	Dim-less
n	Cyclic frequency — subscript	Hz
N	Number of ensemble averages	Dim-less
Nu	Convective heat transfer Nusselt number for the thermocouple wire	Dim-less
P or P_T	Gas total pressure	Newton/Meter ²
P_{rg}	Gas Prandtl number	Dim-less
S	Probe stress	Newton/Meters ²
SNR	Thermocouple signal-to-noise ratio	Dim-less
T, T_g , T_T	Gas total temperature	K
T_B	Probe ceramic base temperature	K
T_n	Instantaneous temperature of thermocouple wire at frequency n	K
T_p	Probe ceramic tip temperature	K
T_{Xpeak}	Maximum peak in instantaneous temperature of thermocouple wire at spacial location X	K
t_0	Arbitrary time reference	Seconds
U_g or V	Gas free stream velocity	Meters/sec
X	Spacial index — subscript	Dim-less

<u>Symbol</u>	<u>Greek Symbols</u>	<u>Units</u>
α	Thermal diffusivity of the thermocouple wire	Meters ² /sec
Γ	Aerodynamic parameter which is defined as = $0.48 k_g P_{rg}^{1/2} U_g^{1/2} / (\mu_g / \rho_g)^{1/2} \rho_w C_{pw}$	Meters ^{3/2} /sec
γ	Gas stream ratio of specific heats	Dim-less
γ^2	Coherence function	Dim-less
Δ	Finite difference model spacing of the thermocouple support wire	Meters

ΔT	Temperature difference	K
Δt	Time step	sec
δ	Finite difference model spacing of thermocouple element wire	Meters
ϵ_{error}	Transfer function error	%
ζ	Transfer function (gain and phase) of the thermocouple wire with respect to the gas temperature at frequency f_n	Gain — dim-less Phase — degrees
η	Fin efficiency function = $\sqrt{4 \text{Nu Kg}/D^2 \text{kc}}$	1/Meters
η_{1n}	Phase shift of the 76 μm (0.003 in.) thermocouple with respect to gas temperature at frequency f_n	Degrees
η_{2n}	Phase shift of the larger diameter thermocouple with respect to gas temperature at frequency f_n	Degrees
θ_{1n}	Peak amplitude of the smaller diameter thermocouple at frequency f_n	K
$\theta_1(f)$	θ_{1n} as a function of frequency	K
θ_{2n}	Peak amplitude of the larger diameter thermocouple at frequency f_n	K
$\theta_2(f)$	θ_{2n} as a function of frequency	K
λ_i	Stress constant for cantilever beam	Dim-less
λ_{1n}	Phase shift of smaller diameter thermocouple at frequency f_n with respect to arbitrary time t_0	Degrees
$\lambda_1(f)$	λ_{1n} as a function of frequency	Degrees
λ_{2n}	Phase shift of larger diameter thermocouple at frequency f_n with respect to arbitrary time t_0	Degrees
$\lambda_2(f)$	λ_{2n} as a function of frequency	Degrees
σ	Boltzmann constant	J/K
μ_g	Gas stream viscosity	Grams/Meter-sec
ρ_w	Density of the thermocouple wire	Grams/Meter ³
ρ_g	Density of the gas stream	Grams/Meter ³
φ_n	Phase shift of the gas temperature with respect to arbitrary time t_0 at frequency f_n	Degrees
$\varphi(f)$	φ_n as function of frequency	Degrees
ψ	Fin efficiency	Dim-less

REFERENCES

1. Elmore, D. L., Robinson, W. W., and Watkins, R. B., "Dynamic Gas Temperature Measurement System Final Report, Vol. I, Technical Efforts," prepared for NASA-Lewis Research Center by Pratt & Whitney, Government Products Division, Contract NAS3-23154, Report NASA CR-168267, 10 May 1983.
2. Dils, R. R., and P. S. Follansbee, "Wide Bandwidth Gas Temperature Measurements in Combustor and Combustor Exhaust Gases," 1976, ISA ASI 76245 (307-328).
3. Accufiber Model 310 Application Note - Wideband Temperature Measurement.

BIBLIOGRAPHY

Schultz, D. L., Jones, T. V., and Oldfield, M. L. G., "A New Transient Cascade Facility for the Measurement of Heat Transfer Rates," University of Oxford, Department of Engineering Sciences, Report OUEL Prt. 1207/77.

Bednarek, K. and Niedzialek, B., "Construction and Calibration of Measuring Probes for the Testing of Combustion Chambers of Jet Engines," Warsaw, Instytut Lotnictwa, Prace (Warsaw, Aviation Institute, Papers) No.37, 1969, pp. 11-18.

McDearman, J. R., Googe, J. M., and Shepherd, R. L., "A Three-Wire Insulator Shunting Model for High-Temperature Thermocouple Errors," IEEE Trans. on Industrial Electronics and Control Instrumentation, Vol. IEC1-18, No. 4, November 1971, pp. 137-144.

Steward, W. F. and Edwards, S. F., "Calibration of Small Gage Thermocouples," The Review of Scientific Instruments, Vol. 43, No. 1, January 1972, pp. 169-170.

Venkatramani, N., Satyamurthy, P., Dixit, N. S., Lancelot, J. P., and Rohatzi, V. K., "Measurement of High Gas-Stream Temperature Using Dynamic Thermocouples," Int. J. Heat Mass Transfer, Vol. 26, No. 5, pp. 663-669.

Kretschmer, D., Odgers, J., and Schlader, A. F., "The Pulsed Thermocouple for Gas Turbine Application," Journal of Engines for Power, January 1977.

Ching Jen Chen and Peter Li, "Minimization of Temperature Distortion in Thermocouple Cavities," AIAA Journal, Vol. 15, No. 6, June 1977, pp. 869-871.

Keltner, N. R. and Beck, J. V., "Surface Temperature Measurement Errors," Trans. of the ASME, Vol. 105, May 1983, pp. 312-318.

Larson, M. B. and Nelson, E., "Variables Affecting the Dynamic Response of Thermocouples Attached to Thin Skinned Models," Trans. of the ASME, February 1969, pp. 166-168

Carrol, R. M. and Shepherd, R. L., "Measurement of the Transient Response of Thermocouples and Resistance Thermometers Using an in Situ Method," Oak Ridge National Laboratory, Contract No. W-7405-eng-26, Report No. ORNL/TM-4573, June 1977.

Keltner, N. B., "Intrinsic Thermocouple Response," Sandia Laboratory, ISA ASI 74223, 1974, Aerospace Instr. Symp., International-Fundamentals of Aerospace 20th Proc., Vol. 11.

Gat, R., Kammer, D. S., and Hahn, O. J., "The Effect of Temperature Dependent Properties on Transients Measurement With Intrinsic Thermocouple," Int. J. of Heat and Mass Transfer, Vol. 18, pp. 1337-1342, 1975.

Donaldson, I. S. and Haslett, R. A., "A Fast Response Surface Thermocouple," Journal of Mechanical Engineering Science, Vol. 16, pp. 174-177, June 1974.

Wing-fai, Ng, "Time-Resolved Stagnation Temperature Measurement in a Transonic Compressor Stage," MIT, Gas Turbine and Plasma Dynamics Laboratory, GTL Report No. 177, October 1983.

Giedt, W. H. and Chambers, J. T., "A Dual Element Transducer for Measuring High Gasstream Temperatures," Journal of Heat Transfer, ASME Transactions, August 1965, pp. 397-402.

Neuhoff, F., "Calibration and Application of a Combination Temperature-Pneumatic Probe of Velocity and Rotor Loss Distribution Measurements in a Compressor," BDM Corp., Naval Postgraduate School, Report No. NPS67-81-03CR, December 1981.

Moffat, R. J., "Gas Temperature Measurement," Temperature, Its Measurement and Control in Science and Industry, Vol. 3, Part 2 of Applied Methods and Instruments, No. 52, pp. 553-571, Krieger Pub. Co., 1972.

Warshawsky, I. and Kukns, P. W., "Review of the Pneumatic-Probe Thermometer," Temperature, Its Measurement and Control in Science and Industry, Vol. 3, Part 2 of Applied Methods and Instruments, No. 53, pp. 573-586, Krieger Pub. Co., 1972.

Krause, L. N., Glawe, G. E., and Johnson, R. C., "Heat-Transfer Devices for Determining the Temperature of Flowing Gases," Temperature, Its Measurement and Control in Science and Industry, Vol. 3, Part 2 of Applied Methods and Instruments, No. 54, pp. 587-593, Krieger Pub. Co., 1972.

Terbush, R. K., "Improved Sonic Pyrometer," Temperature, Its Measurement and Control in Science and Industry, Vol. Three, Part 2 of Applied Methods and Instruments, No. 55, pp. 595-600, Krieger Pub. Co., 1972.

Glawe, G. E., Johnson, R. C., and Krause, L. N., "Intercomparison of Several Pyrometers in a High Temperature Gas Stream," Temperature, Its Measurement and Control In Science and Industry, Vol. 3, Part 2 of Applied Methods and Instruments, No. 56, pp. 601-695, Krieger Pub. Co., 1972.

Stein, Peter, "Estimating the Necessity of a High Recovery Factor Thermocouple for Particular Operating Conditions," Temperature, Its Measurement and Control in Science and Industry, Vol. 3, Part 2 of Applied Methods and Instruments, No. 57, pp. 607-613, Krieger Pub. Co., 1972.

Benson, R.S., "Development of a Resistance Wire Thermometer for Measuring Transient Temperatures in Exhaust Systems of Internal Combustive Engines," Temperature, Its Measurement and Control in Science and Industry, Vol. 3, Part 2 of Applied Methods and Instruments, No. 60, pp. 631-653, Krieger Pub. Co., 1972.

Fingerson, L. M. and Blackshear, P. O., "Heat Flux Probes for Dynamic Measurements in High Temperature Gases," Temperature, Its Measurement and Control in Science and Industry, Vol. 3, Part 2 of Applied Methods and Instruments, No. 61, pp. 655-663, Krieger Pub. Co., 1972.

Bloomquist, D. D., Duval, G. E., and Dick, J. J., "Electrical Response of a Bimetallic Junction to Shock Compression," Washington State University, Dept. of Physics, Final Report F4620-77-C-0034, March 1978.

Kairser, F. B., "Performance and Evaluation of an X Hot Wire Sensor in a Two Dimensional Free Jet in the Presence of Cross Flow Component," Thesis, Air Force Inst. of Tech, Air University, 1976.

Collis, D. C. and Williams, M. J., "Two Dimensional Convection from Heated Wires at Low Reynolds Numbers," Journal of Fluid Mechanics, Vol. 6, pp. 367-384, 1959.

Eklund, T. I. and Dobbins, R. A., "Application of the Hot Wire Anemometer to Temperature Measurement in Transient Gas Flows," Int. Journal of Heat and Mass Transfer, Vol. 20, pp. 1051-1058, 1977.

Temme, M. J. and Geidt, W. H., "Dual Probe for High-Temperature - Gas Measurements," Advanced Tech Labs, Report No. ARL-174, December 1961.

Keshock, E. G., "Investigation of Factors Affecting the Heater Wire Method of Calibrating Fine Wire Thermocouples," Final Report, NASA CR-112041, 1972.

Moffat, R. J., "The Gradient Approach to Thermocouple Circuitry," Temperature, Its Measurement and Control in Science, and Industry, Vol. 3, Part 2 of Applied Methods and Instruments, No. 2, pp. 33-38, Reinhold Pub. Co., 1962.

Schroder, R., "The Response Time of Miniature Shielded Thermocouples," Argonne National Laboratory, Report No. ANL-Trans-554, December 1967.

Adamson, T. C., Jr., Messiter, A. F., and Liow, M. S., "Large Amplitude Shock Wave Motion in Two-Dimensional Transonic Channel Flow," AIAA 16th Aerospace Science Meeting, Huntsville, Ala., January 16-18, 1978, Paper No. 78-247.

Giedt, W. H. and Corallo, R. A., "Determination of High Gas-Stream Temperatures from Short-Exposure Probe Responses," "Advances in Test Measurement," Vol. 5, Proceedings of the 5th Annual ISA Test Measurement Symposium, New York, October 28-31, 1968, No. 68-509.

Parker, R., "Response of Thermocouples to a Rapid Temperature Rise," Advances in Test Measurement, Vol. 5, Proceedings of the 5th Annual ISA Test Measurement Symp., New York, October 28-31, 1968, No. 68-512.

Oldfield, M. L. G., Jones, T. V., and Schultz, D. L., "An On-Line Interaction Mini-Computer System for Heat Transfer Measurements in a Transient Turbine Cascade," University of Oxford, Department of Engineering Science, Report No. 1215/77, September 1977.

DISTRIBUTION LIST
FOR CONTRACT NAS3-24228
Instrumentation and Control Technology Office
(Each addressee will receive one copy of Volume I only, unless otherwise indicated)

*NASA Lewis Research Center
Attn: G. C. Fralick
Mail Stop 77/1
Cleveland, OH 44135
(50 copies)

*NASA Lewis Research Center
Attn: Gerald A. Boulanger
Cleveland, OH 44135
Mail Stop 500/305

*NASA Scientific and Technical
Information Facility
Attn: Acquisitions Branch
P.O. Box 8757
B.W.I. Airport, MD 21240
(22 copies)

*NASA Lewis Research Center
Attn: Library
Mail Stop 60/3
21000 Brookpart Road
Cleveland, OH 44135
(2 copies)

*NASA Lewis Research Center
Attn: Report Control Office
Mail Stop 60/1
21000 Brookpart Road
Cleveland, OH 44135

General Electric Company
Aircraft Engine Group
Evendale, OH 45215
Attn: Wayne Shaffernocker, MSH-78
Ronald Weise, MSH-78
William Stowell

Stanford University
Attn: Dr. R. J. Moffatt
Asst. Prof., Mech. Engr.
Dir. Thermoscience
Measurement Center
Stanford, CA 94305

Hitec Products, Inc.
Attn: Steve Wnuk
P.O. Box 790
87 Fitchburg Rd.
Ayer, MA 01432

*Air Force Wright Aeronautical
Laboratory
Attn: R. Cox/POTC
Wright Patterson AFB, OH 45433

*Air Force Wright Aeronautical
Laboratory
Attn: William Stange, POTC
Wright Patterson AFB, OH 45433

*Air Force Wright Aeronautical
Laboratory
Attn: M. Roquemore/POSF
Wright Patterson AFB, OH 45433

UTRC/OATL
Attn: John T. Carroll
Bldg. 30, MS R-23
Palm Beach Gardens Facility
West Palm Beach, FL 33402

Lewis Engineering Company
Attn: C. B. Stegner
238 Wate Street
Naugatuck, CT 06770

FluiDyne Engr. Corporation
Attn: I. Matsuura
5900 Olson Memorial Highway
Minneapolis, MN 55422

General Electric Company
Attn: George Leperch, A129dD
Aircraft Engine Group
1000 Western Avenue
Lynn, MA 01910

* Volumes I and II

Rocketdyne
Attn: Dr. John C. Lee
6633 Canoga Avenue
Canoga Park, CA 91304

Combustion Engineering
Attn: John Fishburn
Dept 9005-03D1
Windsor, CT 06095

RdF Corporation
Attn: Frank Hines
23 Elm Avenue
Hudson, NH 03051

***NASA Langley Research Center**
Attn: R. E. Wright, Jr. (MS-234)
Hampton, VA 23665

NASA Langley Research Center
Attn: S. L. Ocheltree (MS-235A)
Hampton, VA 23665

Babcock & Wilcox R&D Division
Attn: John Berthold
P.O. Box 835
Alliance, OH 44601

Applied Sensors International
Attn: Richard Stillmaker
7834 Palace Drive
Cincinnati, OH 45242

Carnegie-Mellon University
Attn: Dr. Norman Chigier
Dept of Mechanical Engineering
Pittsburgh, PA 15213

* Volumes I and II

Arnold Engineering Development Ctr.
Attn: Marshall Kingery
Arnold Air Force Station, TN 37389

Calspan Field Services, Inc.
AEDC Division
Attn: C. T. Kidd
Arnold Air Force Station, TN 37389

Physical Sciences Dept
Attn: M. G. Dunn
Arvin/Calspan Adv Tech Center
Buffalo, NY 14225

Eaton Corporation
Attn: Howard K. Cooper
Electronic Instrumentation Div.
(Altech Strain Sensors)
5340 Alla Road
Los Angeles, CA 90066

Naval Air Propulsion Test Center
Attn: Guy Mangano/Code PE42
Trenton, NJ 08628

Naval Air Propulsion Test Center
Attn: James Zidzik
Trenton, NJ 08628

Accufiber
Attn: Dr. R. R. Dils
2000 E. Columbia Way, Bldg. No. 7
Vancouver, WA 98661

Virginia Polytechnic Institute
and State University
Attn: W. F. O'Brien, Jr.
Mechanical Engineering Dept
Blacksburg, VA 24061

*Naval Post Graduate School
Attn: Prof. R. P. Shreeve
Department of Aeronautics (Code 67)
Monterey, CA 93940

Pennsylvania State University
Attn: Prof. B. Lakshminarayana
233 Hammond Bldg.
University Park, PA 16802

Kulite Semiconductor Products, Inc.
Attn: John R. Hayer
1039 Hoyt Avenue
Ridgefield, NJ 07657

Bolt Beranek and Newman, Inc.
Attn: Richard E. Hayden
50 Moulton Street
Cambridge, MA 02138

*Air Force Wright Aeronautical
Laboratory
Attn: Mr. Charles Bentz/POTC
Hot Section Technology
Wright Patterson AFB, OH 45433

AVCO Corporation
Attn: Mr. K. Collinge
Director of Research
IRAD Mechanical Projects Manager
Lycoming Division
550 South Main Street
Stratford, CT 06497

Massachusetts Inst of Technology
Attn: Dr. Alan Epstein
Room 31-266
Cambridge, MA 02139

Public Service Elect & Gas Co.
Attn: Dr. Melvin L. Zwillenberg
Research & Development Dept
80 Park Plaza
Newark, NJ 07101

Xerox Electro-Optical Systems
Attn: Mr. Clifford I. Cummings
Manager
Intelligence & Reconnaissance
1616 North Fort Myer Dr., 16th Floor
Arlington, VA 22209

Construction Materials Support Group
Attn: Mr. J. W. Scott
Owens/Corning Fiberglas
CMG Process Technology Lab.
Granville, OH 43023

Babcock & Wilcox R&D Division
Attn: Harold Wahle
P.O. Box 835
Alliance, OH 44601

Caterpillar Tractor Company
Attn: Mr. Donald Wilson
Technical Center, Building F
100 Northeast Adams Street
Peoria, IL 61629

NASA Headquarters
Attn: M/Paul N. Herr
Washington, D.C. 20546

Sverdrup (AEDC)
Attn: Paul McCarty
Arnold, AFB, TN 37389

Rosemont, Inc.
Attn: Mr. Larry N. Wolfe
Mail Stop F-15
P.O. Box 959
Burnsville, MN 55337

Thermogage, Inc.
Attn: Charles E. Brookley
330 Allegany Street
Frostburg, MD 21534

Hycal Engineering
Attn: William Clayton
9650 Telstar Avenue
El Monte, CA 91731

Medtherm Corporation
Attn: Larry Jones
P.O. Box 412
Huntsville, AL 35804

* Volumes I and II

General Electric Company
Attn: Ronald J. Casagrande
Aircraft Equipment Division
50 Fordham Road
Wilmington, MA 01887

Allison Gas Turbine Operations
Attn: John Custer, W-16
General Motors Corporation
P.O. Box 894
Indianapolis, IN 46206

Allison Gas Turbine Operations
Attn: Ken Cross
General Motors Corporation
P.O. Box 894
Indianapolis, IN 46206

Allison Gas Turbine Operations
Attn: David Willis
General Motors Corporation
P.O. Box 894
Indianapolis, IN 46206

Pratt & Whitney - Main Plant
P.O. Box 109600
West Palm Beach, FL 33410-9600
Attn: William Watkins (MS 731-36)
H. R. Przirembel (MS 713-37)
D. P. Harrold (MS 713-13)

Allison Gas Turbine Operations
Attn: Ralph Fox
General Motors Corporation
P.O. Box 894
Indianapolis, IN 46206

Battelle Columbus Laboratories
Attn: Ross G. Luce
Energy & Thermal Tech Section
Columbus, OH 43201

Teledyne CAE
1350 Laskey Road
Toledo, OH 43612
Attn: R. Hugh Gaylord
Joseph Pacholec

AVCO Corporation
Attn: E. Twarog, Manager
Electronics and Instr
Lycoming Division
550 South Main Street
Stratford, CT 06497

Thermonetics Corporation
Attn: H. J. Poppendiek
1028 Garnet Avenue
San Diego, CA 92109

National Bureau of Standards
Attn: Ken Kreider
Washington, D.C. 20234

*National Bureau of Standards
Attn: George Burns
Inst for Basic Research
Washington, D.C. 20234

General Electric Company
Attn: Dr. David Skelley
Bldg. K-1, Room 3B24
P.O. Box 8
Schnectady, NY 12301

Mechanical Technology, Inc.
Attn: R. Hohenberg
968 Albany-Shaker Road
Latham, NY 12110

Garrett Turbine Engine Company
Attn: N. Fred Pratt
P.O. Box 5217
Phoenix, AZ 85010

Boeing Aerospace Company
Attn: Darrell R. Harting
Engineering Laboratories
Seattle, WA 98124

Williams International
2280 West Maple Road
Walled Lake, MI 48088
Attn: Henry Moore, Head Instr Dept
J. H. Johnston

Eaton Corporation
Attn: Mr. Lamont Eltinge
P.O. Box 766
Southfield, MI 48037

* Volumes I and II